## *Chemically Modified Hydroxyethyl Cellulose*

JOUBERT, FANNY

DEPARTMENT OF CHEMISTRY

# Chemically Modified Hydroxyethyl Cellulose

Fanny Joubert

A thesis submitted for the degree of Doctor of Philosophy


2014

# Statement of copyright

# Declaration

The work in this thesis was conducted in the Department of Chemistry at Durham University, England from October 2011 to October 2014. Unless stated, the described work was performed by the author and has not been submitted for any qualification/degree at this or other universities. Parts of the work, however, have been published in, or are in preparation for submission to academic journals.

- ✓ F. Joubert, O. M. Musa, D. R. W. Hodgson, N. R. Cameron, "The preparation of graft copolymers of cellulose and cellulose derivatives using ATRP under homogeneous reaction conditions", *Chem. Soc. Rev.*, 2014, 43, 7217-7235. (Chapter 1 & Chapter 4)

- ✓ F. Joubert, G. J. Sharples, O. M. Musa, D. R. W. Hodgson, N. R. Cameron, "Preparation, properties and antibacterial behaviour of a novel cellulose derivative containing lactam groups", *J. Polym. Sci. Part A: Polym. Chem.*, 2015, 53, 68-78. (Chapter 3)

- ✓ F. Joubert, O. M. Musa, D. R. W. Hodgson, N. R. Cameron, "Graft copolymers of hydroxyethyl cellulose by a "grafting to" method: $^{15}N$ labelling as a powerful characterisation tool in "click" polymer chemistry", *Polym. Chem.*, 2015, 6, 1567-1575. (Chapter 5)

- ✓ F. Joubert, P. Yeo, G. J. Sharples, O. M. Musa, D. R. W. Hodgson, N. R. Cameron, "Preparation of an antibacterial graft-copolymer of hydroxyethyl cellulose", in preparation. (Chapter 5)

# Acknowledgments

First and foremost, I must thank my supervisors, Neil Cameron and David Hodgson, Professors at Durham University, and Osama Musa, my industrial partner, for their support during the last three years. Our meetings and discussions have been a constant source of ideas and inspiration in order to bring the projects forward.

I must thank Gary Sharples and Paul Yeo, with whom we collaborated on the biological assays part. I would like also to thank those responsible for the solution state NMR service, Alan Kenwright for his help interpreting spectra and for his various suggestions which were useful to solve analytical problems. I want also to thank David Apperley and Fraser Markwell, who are in charge of the solid state NMR service, for their fast, amazing work and useful advice. I must also thank Lian Hutching for letting me use SEC instruments with some of my "cellulosic compounds".

Furthermore, I must thank the NRC group for providing a gorgeous environment to work in, especially the fantastic post-doc team constituting of David Johnson, Paul Thornton and Sarah Hehir for taking the time to help me, but not only… and Artur Kubulis who has been the best "colleague" through the three years. I would like to thank all people that I had the pleasure to meet at Durham University and outside with a special mention to my "Frenchies", Charlène, M. C. and Céline, the adopted French one, Anne, and my "Italian" Brunella for listening to me to complain ALL the time about almost everything. All made my PhD experience in Durham incredible and unforgettable!

To finish, I want to thank my friends in France, especially Julie alias "RG" and my family for supporting and encouraging me throughout the three years of my PhD. And I have also to thank the two organisations Ashland and EPSRC for funding.

# Abstract

Synthetic, man-made polymers are produced from petroleum, however this activity may well decrease as a function of time because of the non-renewability of the oil. This will result in the decreased production of synthetic polymers with consequent problems to our everyday life because of their ubiquity (food, furniture, containers, electronics…). An alternative could be the use of biopolymers such as cellulose, starch, proteins, amylose and chitin which are extracted from renewable sources. Cellulose is the most abundant biopolymer on earth and is principally found in the cell walls of plants. Cellulose presents interesting properties such as a high thermal stability and high strength, however the principal drawback is its insolubility in both organic and aqueous solvents limiting considerably its use in industry. Chemical modification of the hydroxyl groups of cellulose overcomes some of this problem. In fact, hydroxyethyl cellulose (HEC), where the hydroxyl groups have been modified with ethylene oxide, shows good solubility in aqueous solvents (dimethyl sulfoxide, water) due to the interruption of the cellulose H-bonding networks. Although the chemical modification of cellulose has improved considerably the physical properties of cellulose, the derivatives are usually not competitive against synthetic polymers.

Due to its solubility and the presence of the three hydroxyl groups, HEC was chosen as a substrate for chemical modification, with the aim of mimicking the properties of synthetic polymers. The synthetic polymer of reference in our work was poly(N-vinylpyrrolidone) (PVP) because of its solubility in organic and aqueous solvents and sorption properties. The introduction of lactam groups onto HEC could produce a material with properties similar to PVP and this was the goal of our work. Three methods for modifying HEC with lactam groups are reported. The first was the functionalization of HEC with 1-

(hydroxymethyl)-2-pyrrolidone (HMP) with degrees of functionalization up to ~0.9 on the primary alcohol functionality of HEC. The functionalized HECs showed markedly different properties to unfunctionalized HEC, such as increased the thermal stability and reduced viscosity. The two others methods led to the preparation of well-defined HEC-g-PVPs using a "grafting from" strategy combined with Atom Transfer Radical Polymerisation (ATRP) and "grafting to" combined with Reversible Addition-Fragmentation Chain-Transfer (RAFT) polymerisation. The ATRP of N-vinylpyrrolidone (NVP) from a prior-synthesised macro-initiator, Br-HEC, did not work efficiently; however, RAFT polymerisation of NVP using an alkyne-terminated xanthate as transfer agent produced an 80% monomer conversion with a 1.4 $Đ_M$. The alkyne-terminated PVP was coupled successfully to partially $^{15}$N-labelled $N_3$-HEC and the copper-catalyzed azide-alkyne cycloaddition (CuAAC) was confirmed by $^{15}$N NMR spectroscopy. The versatility of the method was demonstrated using poly(N-isopropyl acrylamide) (PNIPAAM) which was synthesised using an alkyne-terminated trithiocarbonate as transfer agent with a 90% monomer conversion and a 1.2 $Đ_M$. Subsequently, this straightforward method was used to prepare anti-microbial graft-copolymers of HEC from an ionic liquid (IL) monomer, 1-(11-acryloyloxyundecyl)-3-methylimidazolium bromide which was polymerised in high monomer conversion (70-80%) with some evidence of control over molecular weight distribution ($Đ_M$ =1.5). The influence of the chain length of the grafts on the antibacterial effects was minor with a 20 and 39 µg/mL minimum inhibition concentration (MIC) for *E. coli* and for *S. aureus* respectively. The MICs were comparable to those measured for ampicillin, which is known as an antibiotic, indicating the strong effect of our HEC-g-P(IL) on bacteria.

# Table of contents

# List of abbreviations

AA: Acrylic acid

AIBN: 2,2′-Azobis(2-methylpropionitrile)

AgOAc: Silver acetate

AGU: β-D-anhydroglucopyranose

ATRP: Atom Transfer Radical Polymerisation

BMIMCl: 1-Butyl-3-methylimidazolium chloride

cfu: Colony-forming unit

CMA: Cholesteryl methacrylate

CMC: Carboxymethyl cellulose

CTA: Chain Transfer Agent

CuAAC: Copper Catalysed Azide-Alkyne Cycloaddition

$Đ_M$: Dispersity

DCM: Dichloromethane

DLS: Dynamic Light Scattering

DMAc: N,N-Dimethylacetamide

DMAP: 4-Dimethylaminopyridine

DMEM: Dulbecco's Modified Eagle Medium

DMF: N,N-Dimethylformamide

DMSO: Dimethyl sulfoxide

DP: Degree of Polymerisation

DS: Degree of Substitution

EC: Ethyl cellulose

EDC: N-(3-Dimethylaminopropyl)-N′-ethylcarbodiimide hydrochloride

EtOH: Ethanol

FCS: Fetal Calf Serum

FT-IR: Fourier tansform infrared

HEC: Hydroxyethyl cellulose

HPC: Hydroxypropyl cellulose

HMP: 1-(Hydroxymethyl)-2-pyrrolidone

HMBC: Heteronuclear Multiple-Bond Correlation spectroscopy

HSQC: Heteronuclear Single Quantum Coherence spectroscopy

HEP: Hydroxyethylol-pyrrolidone

IL: Ionic Liquid

LAM: Less Activated Monomer

LB: Luria-Bertani

$LD_{50}$: Lethal Dose that kills 50% of cells

LCST: Lower Critical Temperature Solution

$M_n$: Number average molecular weight

MWCO: Molecular weight cut-off

MAM: More Activated Monomer

MEHQ: Mono methyl ether of hydroquinone

MIC: Minimum Inhibition Concentration

MMA: Methyl methacrylate

MS: Molar Substitution

NIPAAM: N-Isopropylacrylamine

NMP: N-Methyl-pyrrolidone

NMR: Nuclear Magnetic Resonance

NVP: N-Vinylpyrrolidone

PAA: Poly(acrylic acid)

PBA: Poly(n-butyl acrylate)

PCL: Poly(ε-caprolactone)

PDEAEMA: Poly(2-(diethylamino)ethyl methacrylate)

PDEGMA: Poly(2-(hydroxyethoxy)ethyl methacrylate)

PDMAA: Poly(N,N-dimethylacrylamide)

PDMAEMA: Poly(2-(dimethylamino)ethyl methacrylate)

PDMDEGMA: Poly(methyl diethylene glycol methacrylate)

PEG: Poly(ethylene glycol)

PEGMA: Poly(ethylene glycol) methyl ether methacrylate

PEMO: Poly(3-ethyl-3-methacryloyloxy-methyloxetane)

PHEMA: Poly(2-hydroxyethyl methacrylate)

PLLA: Poly(L-lactide)

PMMA: Poly(methyl methacylate)

PMMAzo: Poly(azobenzene-containing methacrylate)

PNIPAAM: Poly(N-isopropylacrylamine)

POEGMA: Poly(oligo(ethylene glycol) methacrylate)

PSt: Polystyrene

PVP: Poly(N-vinylpyrrolidone)

P4VP: Poly(4-N-vinylpyridine)

QPDMAEMA: Quaternized poly(2-(dimethylamino)ethyl methacrylate)

RAFT: Reversible Addition-Fragmentation Chain-Transfer

RDRP: Reversible-Deactivation Radical Polymerisation

rpm: Revolutions Per Minute

SEC: Size Exclusion Chromatography

SEM: Scanning Electron Microscope

TEA: Triethylamine

TGA: Thermo Gravimetric Analysis

TMEDA: N,N,N′,N′-Tetramethylethylenediamine

THF: Tetrahydrofuran

XPS: X-ray photoelectron spectroscopy

# List of Schemes

# List of Tables

# List of Figures

# Chapter 1: Introduction

## 1.1. POLYMERISATION METHODS

### 1.1.1. Introduction

Polymerisations produce macromolecules from repeat units called monomer residues which are often constituted of carbon and hydrogen atoms. Polymerisation methods can be divided into two main categories depending on the nature of the reaction mechanism. Step-growth polymerisation consists of the reaction of monomers containing bi-functional or multifunctional groups such as carboxylic acid, alcohol and amino groups, and thus leads to the progressive formation of dimer, trimer, oligomer molecules and thus polymer chains. Figure 1-1 displays the schematic plot of the evolution of the average degree of polymerisation (DP) as a function of the monomer conversion (p) in a step-growth polymerisation (orange curve) and shows that the average molecular weight increases slowly while the consumption of monomer is relatively fast. This results in polymers with low to moderate average degree of polymerisation. Chain-growth polymerisation consists of the successive addition of monomers through a minimum two-step mechanism (initiation and propagation) leading potentially to a high degree of polymerisation. Unlike step-growth polymerisation, the monomers are consumed slowly while the molecular weight increases rapidly and this is shown in Figure 1-1 with the blue curve which exemplifies one chain-growth polymerisation named free radical polymerisation[1]. Other chain-growth polymerisations include anionic, cationic,

coordination and group transfer polymerisations, however our interest was is in free radical polymerisation.

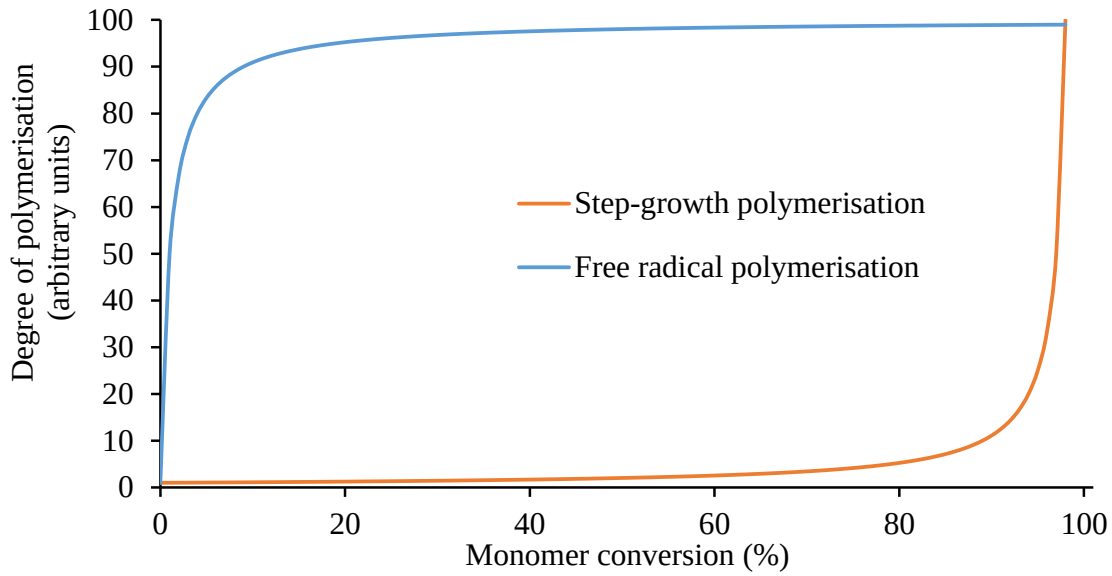


**Figure 1-1:** Schematic plots respresenting the evolution of the degree of polymerisation (DP) as a function of the monomer conversion (p); for the step-growth polymerisation (orange), the plot follows Carathors equation (i.e. DP = 1/(1-p)); for free radical polymerisation (blue), the plot is a sketch showing the theoretical relationship between DP and p.

## 1.1.2. Free radical polymerisation

Free radical polymerisation is extensively used to synthesise vinyl polymers such as polystyrene, polyacrylonitrile and polyacrylamide. The mechanism which is summarised in Figure 1-2 is defined by three steps: initiation, propagation and termination. The initiation step consists of the formation of radical species which can sometimes be produced by heating the monomer itself, but more commonly, free radical initiators are

used which are divided into four classes: (hydro)peroxides, azo compounds, redox initiators and others that produce radical species under light. The radical species activates the carbon-carbon double bond of the monomer species *via* an addition mechanism which processes with *head-to-tail* orientation because of steric and electronic effects. In the second step named chain-propagation, the radical derived from the monomer reacts with other monomers leading to the formation of a propagating chain radical. Subsequently, this can react with another propagating chain radical *via* a recombination or disproportionation process, which defines the termination step of the free radical polymerisation mechanism. The recombination process consists of the radical-radical coupling of two propagating chains leading to the formation of one dead chain having higher molecular weight. Unlike the recombination process, the disproportionation process, which consists of the abstraction of a hydrogen atom from the methylene group next to the radical of another propagating chain, leads to the formation of two distinct dead chains with lower molecular weight. The predominant termination mechanism depends on the steric hindrance at the active centre.

Initiation:

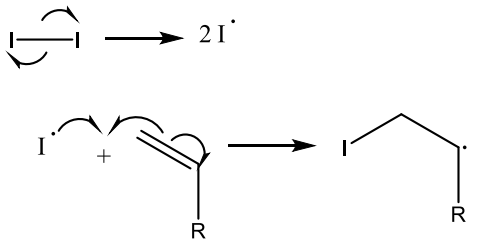


Propagation:

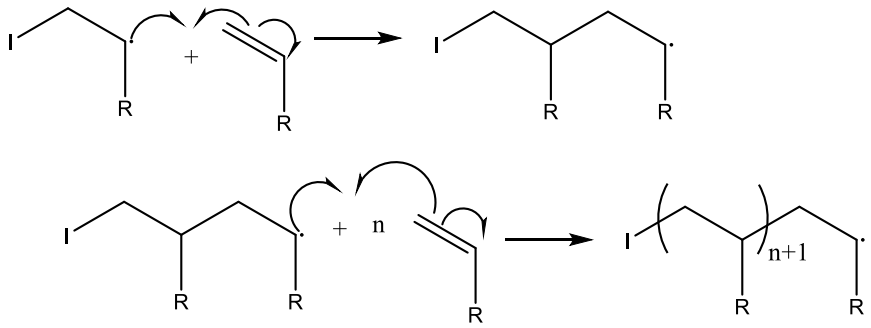


Termination:

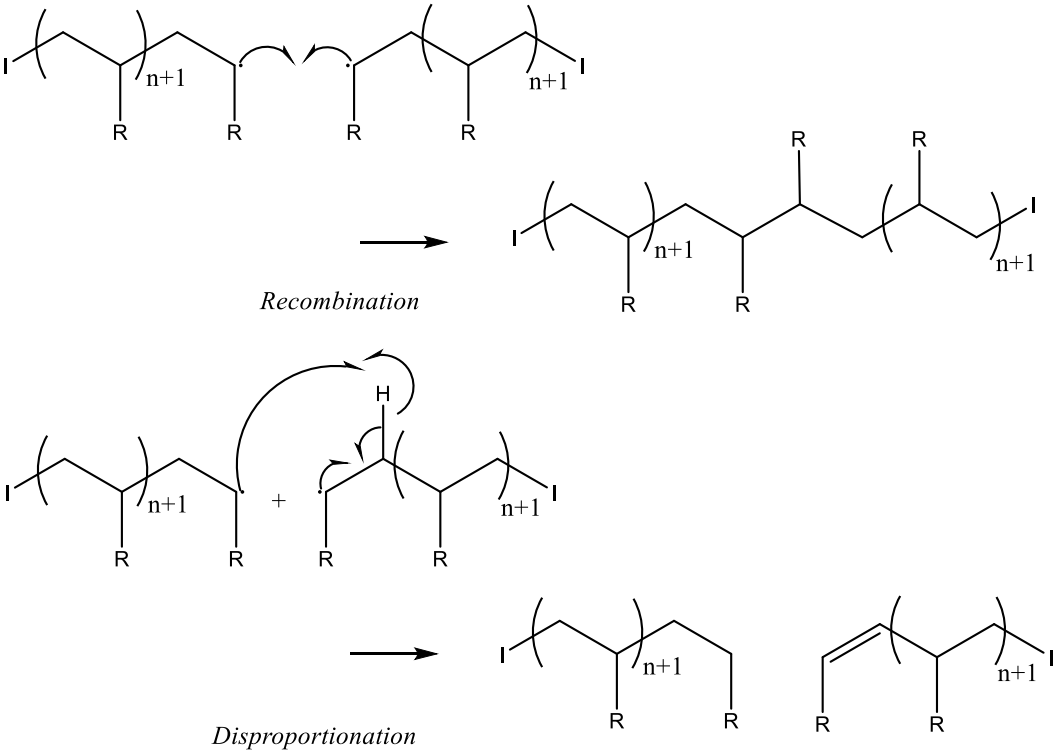


**Figure 1-2:** Mechanism of free radical polymerisation

The average number of monomers polymerised per initiated chain ($\nu$) is defined by the following equation 1-1.

$$\nu = \frac{k_p\,[M]}{2\,(f\,k_d k_t [I])^{1/2}} \qquad \textbf{(1-1)}$$

where $k_p$, $k_d$ and $k_t$ are the rate constants of propagation, initiator dissociation and termination; *f* defines the efficiency of the initiation; and [M] and [I] corresponds to the concentration of monomer and initiator respectively.

The average chain-length can be optimised by varying the monomer and/or initiator concentrations. A decrease of initiator concentration results in a decrease of the number of growing chains. This leads to longer chain length which subsequently increases the molecular weight. Free radical polymerisation can be used to produce polymers with controlled molecular weight (see section 1.1.3). However, the molecular weight distribution represented by the dispersity value $Đ_M$ which is the ratio of the weight-average molar mass ($M_w$) to number-average molar mass ($M_n$) is relatively broad with $Đ_M$ value ranging from about 1.5 to 50 depending on the level of monomer conversion and side effects such as gelation effects and chain transfer occurring during the polymerisation process.

## 1.1.3. Reversible-deactivation radical polymerisations

Over the last two decades, reversible-deactivation radical polymerisation (RDRP), previously known as controlled radical polymerisation (CRP) techniques, have been extensively developed in order to reduce the molecular weight distribution and achieve control of the molecular architecture in terms of topology, functionalities and composition

compared to conventional free radical polymerisation. The main features of RDRP are well-described by Matyjaszewski and co-workers[2]. One feature is the linear evolution of the rate of polymerisation as the function of the polymerisation time when the concentration of the propagating radical species is kept constant over time. This is obtained *via* the introduction of a dynamic equilibrium between propagating species and dormant species which can be achieved by either a reversible termination mechanism as developed in Atom Transfer Radical Polymerisation and Stable Free-Radical Polymerisation (SFRP) or a reversible transfer process as demonstrated in Reversible Addition-Fragmentation Chain-Transfer (RAFT) polymerisation. However, the concentration of propagating radical species is influenced by the rate of the initiation step and termination step. In fact, increasing the rate of the initiation step increases the concentration of propagating radical species whereas the presence of the termination step results in the decrease of the concentration of propagating radical species. Another feature of RDRPs is the linear evolution of the degree of polymerisation as a function of the monomer conversion as shown schematically in Figure 1-3 (green curve). This is due to a fast rate of initiation compared to that of the propagation and the suppression of radical transfer reactions.

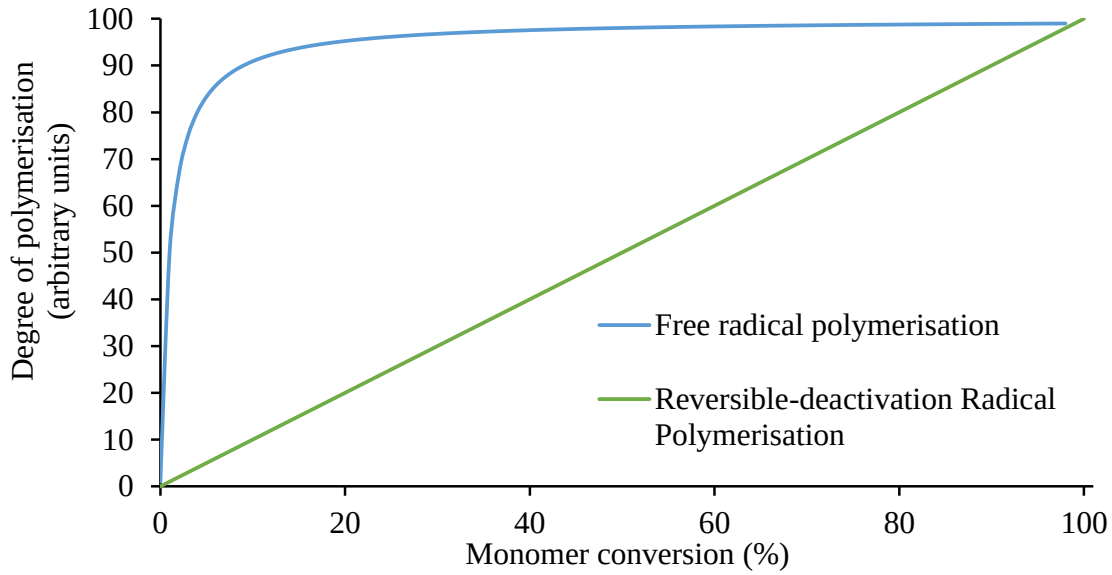


**Figure 1-3:** A sketch representing the evolution of the degree of polymerisation as a function of the monomer conversion for Reversible-Deactivation Radical Polymerisation (green)

Furthermore, the rate of initiation is one of the criteria responsible for the molecular weight distribution. In fact, the production of a narrow molecular weight distribution (i.e. a $Đ_M \leq 1.2$) requires that the rate of the initiation rate is faster or comparable to that of propagation and this results in a simultaneous growth of the chains. The presence of the dynamic equilibrium reduces the overall concentration of radical species, suppressing the termination step, which decreases the dispersity to a value below 1.2. In fact, a decreased radical concentration ($[M^{\bullet}]$) decreases the rate of termination ($v_t$) and propagation ($v_p$), however $v_t$ is reduced more than $v_p$ because of its square dependence on the radical species concentration ($v_t = 2k_t[M^{\bullet}]^2$) compared to the rate of propagation ($v_p = k_p [M][M^{\bullet}]$)[1]. The supression of the termination step also leads to an additional feature of RDRPs: the possible chain extension due to the conservation of the active centre after the

total consumption of the monomer species. This results in the possibility of propagating other monomer species which leads to the formation of block copolymers.

### 1.1.3.1. Atom Transfer Radical Polymerisation

Atom Transfer Radical Polymerisation (ATRP) was discovered independently by Sawamoto and Matyjaszewski in 1995 and is currently the most investigated RDRP technique with over 11,000 publications[3]. The dynamic equilibrium is established between the dormant species which is the initiator (R-X) and the propagating chain (R) shown in Figure 1-4. The dormant species, typically an alkyl halide, reacts with the transition metal ($Mt^m$) which is prior-complexed with a ligand in order to solubilise the transition metal and this reaction proceeds with a rate constant of activation ($k_{act}$). The transition metal complex is then oxidised to a higher level ($X\text{-}Mt^{m+1}$) and the formed radical species R can then react with the monomer (M) at a rate constant of propagation, $k_p$. The reversible mechanism, where the dormant species and the transition metal complexes with a lower oxidation state are reformed, proceeds with a rate constant of deactivation $k_{deact}$. The ratio of $k_{act}$ to $k_{deact}$ determines the equilibrium constant of ATRP ($K_{ATRP}$).

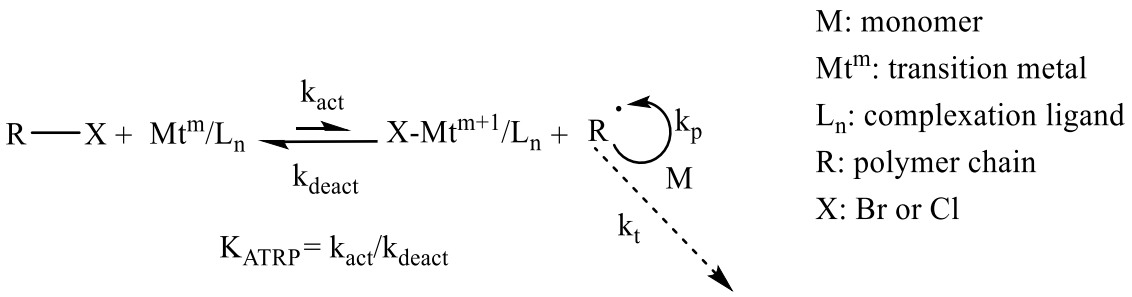


**Figure 1-4:** Mechanism of Atom Transfer Radical Polymerisation

The rate of polymerisation ($R_p$) depends on the propagation ($k_p$) and ATRP equilibrium ($K_{ATRP}$) constants and the concentration of monomer ([M]), initiator ([R-X]) and transition metal complexes ([$Mt^m/L_n$] and [$X\text{-}Mt^{m+1}/L_n$]) and is shown in Equation 1-2.

$$R_p = k_p \times K_{ATRP} \times \frac{[\mathrm{R{-}X}][Mt^m/L_n][\mathrm{M}]}{[X{-}Mt^{m+1}/L_n]} \qquad \textbf{(1-2)}$$

In the total absence of termination and chain transfer processes, the dipersity $Đ_M$ (Equation 1-3) can be estimated as a function of the constant of propagation, deactivation, monomer conversion and concentration of initiator and transition metal complex at higher level of oxidation.

$$Đ_M = 1 + \frac{1}{DP} + \left(\frac{k_p[R{-}X]}{k_{deact}\,[X{-}Mt^{m+1}/L_n]}\right)\left(\frac{2}{p} - 1\right) \qquad \textbf{(1-3)}$$

with p the monomer conversion and DP the average degree of polymerisation.

The structure of the ligand ($L_n$) and the alkyl halide (R-X) and reaction conditions (temperature, solvent and pressure) influence $k_{act}$, $k_{deact}$ and thus $K_{ATRP}$. In fact, the denticity and the bite angle characteristics of the ligand influence strongly its binding with the transition metal and this results in different values of $k_{act}$ for each ligand. For instance, the use of tetradentate ligands provides a larger $k_{act}$ compared to bidentate ligands due to the formation of a more stable complex between ligand and transition metal resulting in a higher rate of polymerisation. Furthermore, $k_{act}$ depends on the reactivity of the initiator,

the alkyl halide which varies with the choice of alkyl group and the transferable halogen. A fast homolytic bond cleavage and a relatively good stabilisation of the radical species increases $k_{act}$. For instance, bromide is a better leaving group compared to chloride resulting in a faster rate of polymerisation when using an alkyl bromide and the rate of the polymerisation increases also with the stability of the alkyl group. Furthermore, $K_{ATRP}$ increases with both the temperature and the solvent polarity. However, the rate of polymerisation has to be balanced with the dispersity $Đ_{M.}$ In fact, an increase of the rate can result in a loss of the control of the polymerisation. For instance, the use of a tetradentate ligand results in both a high rate of polymerisation and high value of $Đ_M$ compared to the use of a bidentate ligand. For each monomer, an appropriate set of parameters (i.e., choice of ligand, catalyst, initiator and reaction conditions) must be defined to have a relatively good comprise between the rate and the control of polymerisation.

### 1.1.3.2. Stable Free-Radical polymerisation

Stable Free-Radical polymerisation is similar to ATRP because the dynamic equilibrium resides in a reversible termination process between growing chains and stable radicals such as nitroxides. The most used stable radical is 2,2,6,6-tetramethyl-1-piperidinoxyl (TEMPO) which lends its name to the best known SFRP technique, Nitroxide-Mediated polymerisation (NMP). The stable radical can be either produced from the thermal decomposition of the initiator such as an alkoxyamine (Figure 1-5) or added together with a conventional initiator such as AIBN.

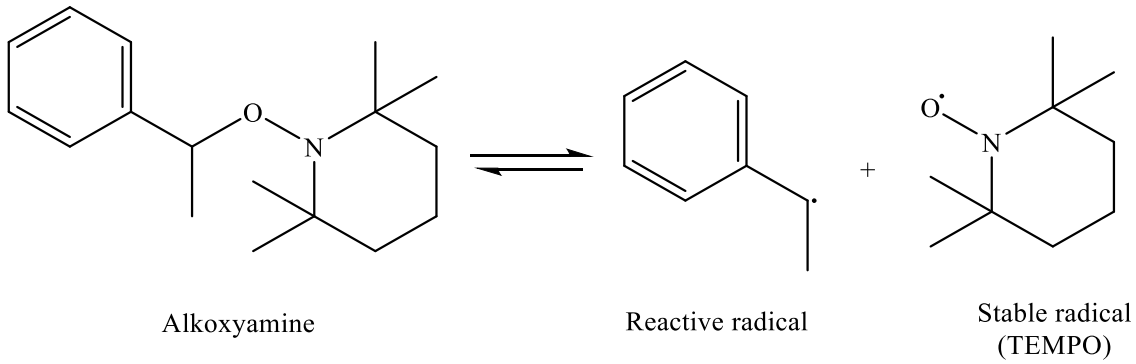


**Figure 1-5:** Thermal decomposition of an alkoxyamine

The reactive radical initiates the polymerisation while the stable radical decreases the overall concentration of radical species thus limiting the termination step. The mechanism is summarised in Figure 1-6.

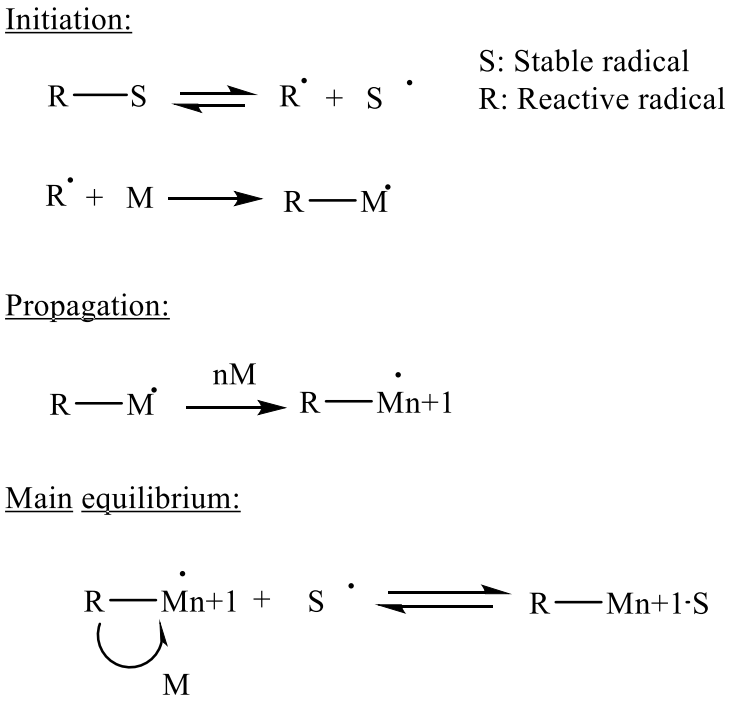


**Figure 1-6:** Mechanism of Nitroxide-Mediated Polymerisation

Compared to ATRP, NMP needs to proceed at higher temperatures and for longer reaction times and dipersity $Đ_M$ values down to 1.1-1.2 can be difficult to reach. Furthermore, the rate of polymerisation is usually slower than that of ATRP and initiators are often not commercially available. However NMP processes do not require the use of a transition metal which needs to be removed from polymers produced from ATRP[4] (although more recent variants of ATRP employ very low levels of metal).

#### 1.1.3.3. Reversible Addition-Fragmentation Chain-Transfer polymerisation

Unlike ATRP and SFRP, the reversible equilibrium in Reversible Addition-Fragmentation Chain-Transfer (RAFT) polymerisation consists of a degenerative chain-transfer process between dormant species and growing chains using a chain-transfer agent (CTA) which contains a thiocarbonylthio functional group. The mechanism of the RAFT polymerisation is shown in Figure 1-7. The initiation, as for the conventional free radical polymerisation, consists of the decomposition of the initiator into radicals which subsequently react with monomers forming polymeric radicals. These growing chains react with the thiocarbonylthio group leading then to the liberation of a new radical species from the CTA (pre-equilibrium step) which initiates the growth of another chain (reinitiation step). The new polymeric chain can then react with the CTA through the thiocarbonylthio-function liberating the other polymeric chain which can then grow. This latter step is reversible and is known as the main-equilibrium of the RAFT polymerisation.

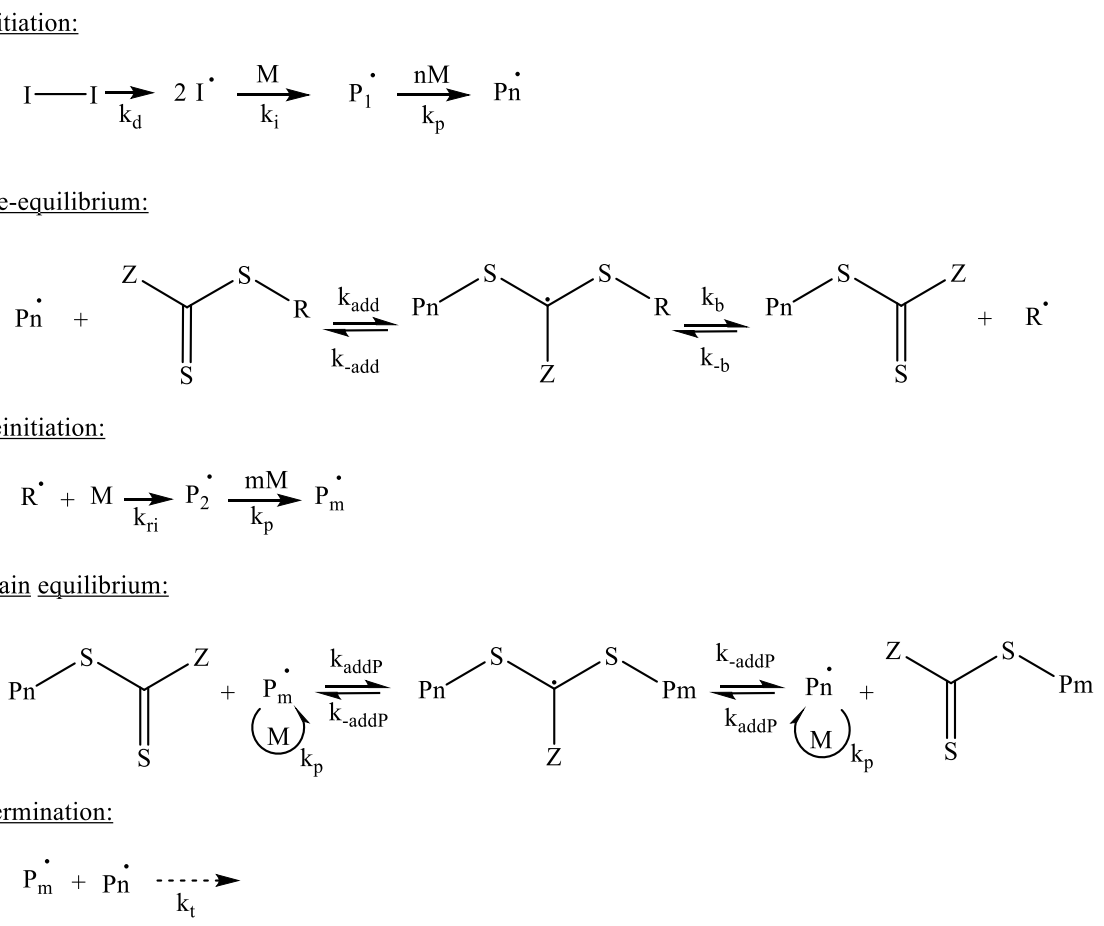


**Figure 1-7:** Mechanism of Reversible Addition-Fragmentation Chain-Transfer polymerisation

The pre-equilibrium can be defined with the partition coefficient ($\Phi$) which is the ratio of rate constant of the fragmentation ($k_\beta$) to the sum of the rate constants of fragmentation and addition ($k_{-add}$). To promote the fragmentation process, the R group of the CTA structure (Figure 1-7) should be a good homolytic group leading to a $\Phi$ value superior to 0.5. Furthermore, the R group structure should be different to that of the monomer species to promote the liability of the R group. The rate of the main-equilibrium can be determined using the chain transfer coefficient ($C_{tr}$) which is the ratio between the rate constant of chain transfer ($k_{tr}$) to rate constant of propagation ($k_p$) and $C_{tr}$ is determined by the reactivity of the CTA. Four main classes of CTA including trithiocarbonate,

dithiocarbonate, dithiocarbamate and xanthate (Figure 1-8) were developed with different value of $C_{tr}$ enhancing the versatility of RAFT polymerisation toward monomer structures[5, 6].

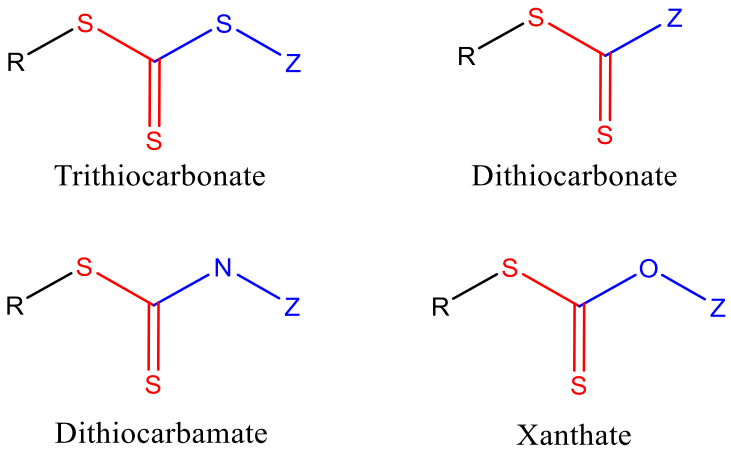


**Figure 1-8:** Structures of CTAs

In fact, monomers can be classified into either less activated monomers (LAMs) or more active monomers (MAMs) categories depending on their reactivity and radical stabilisation. MAMs form more stable radicals enhancing the propagation step but are less reactive towards chain-transfer because MAMs contain carbonyl, nitrile or aromatic groups adjacent to the vinyl group engendering resonance stabilisation effects. Methyl methacrylate, acrylamide, acrylonitrile are examples of MAMs. To ensure the control of the polymerisation of MAMs, a CTA with a high transfer constant such as trithiocarbonate and dithiocarbonate has to be used. LAMs are monomers such as N-vinylpyrrolidone, vinyl acetate and N-vinylcarbazole that have a hydrogen or nitrogen lone pair, a saturated carbon or a heteroatom of a heteroaromatic group adjacent to the carbon-carbon double bond. Their radical forms are then less stabilised limiting then the

chain-propagation but are more reactive towards chain-transfer processes. For polymerising LAMs in a controlled manner and/or supressing retardation processes, a CTA with a low transfer constant due to the resonance effect such as a xanthate or dithiocarbamate has to be used.

Compared to ATRP and SFRP, RAFT polymerisation is more versatile towards monomers and less sensitive to air which simplifies the procedure. However, the use of a CTA containing sulphur compounds can lead to the formation of coloured polymers which can be an important issue for some applications.

## 1.2. A BIO-POLYMER: CELLULOSE

### 1.2.1. Definition

Cellulose is the most abundant biopolymer on Earth as it represents about fifty per cent of biomass, with an annual production estimated to be $10^{11}$ tons per year[7-9]. Cellulose is synthesised by some plants, animals, bacteria and also algae. In plants, cellulose is a major component of the rigid cell walls[10-12].

### 1.2.2. Structural aspects

The molecular structure of cellulose is shown in Figure 1-9 and is defined as long polymer chains of β-D-anhydroglucopyranose units (AGU units). The β-D-glucoses are covalently bonded together by the linkage between the C1 anomeric carbon and the C4 oxygen atom,

providing β-1,4-glycosidic bonds[13]. The structural aspect of cellulose defines its properties.

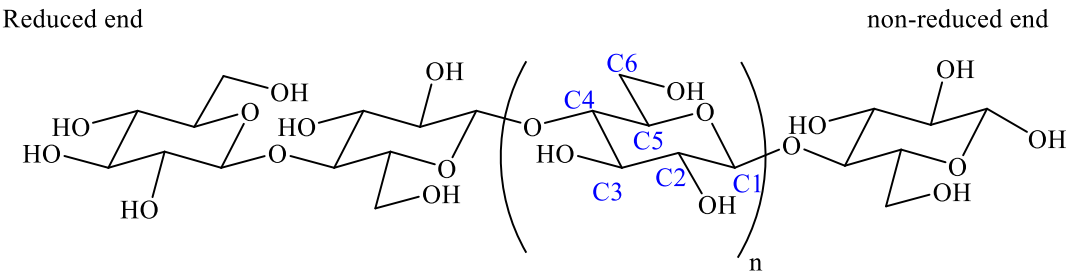


**Figure 1-9:** Molecular structure of cellulose

The supramolecular aspect is mainly characterised by two hydrogen-bonding networks: the intramolecular (Figure 1-10) and intermolecular (Figure 1-11) H-bonding networks which are respectively within and between chains. These networks are responsible for the insolubility of cellulose in common solvents[7, 14-16].

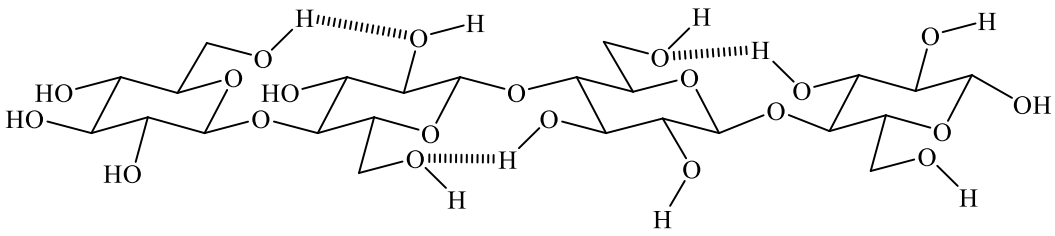

**Figure 1-10:** Intramolecular H-bonding network of cellulose

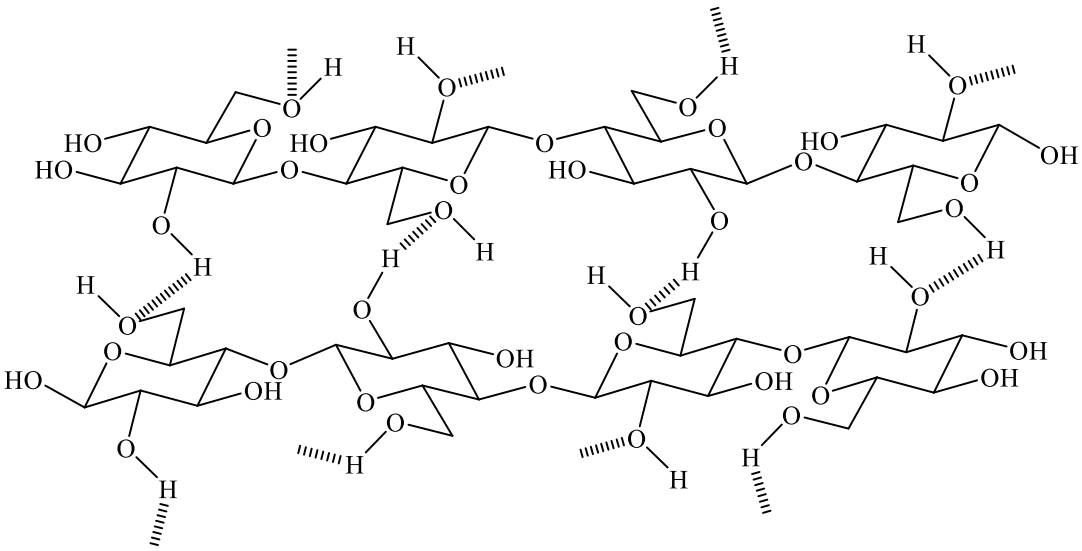

**Figure 1-11:** Intermolecular H-bonding network of cellulose

## 1.2.3. Chemically modified cellulose

### 1.2.3.1. Introduction

Although cellulose is a low cost material with low density (in its unpurified state), biodegradability, high strength and high thermal stability, its applications have been mainly limited to the paper and textile industries due to its poor solubility. Cellulose has been chemically modified to impart new properties such as solubility in organic solvents, crease resistance, dimensional stability, thermoplasticity and antimicrobial properties[12, 15, 17].

#### 1.2.3.1.1. Reactivity

The reactivity of cellulose arises from the presence of hydroxyl groups. Two secondary alcohols are present at the C2 and C3 positions and one primary alcohol at the C6 position, where the -OH reactivity follows the order: $-OH_{C6} >> -OH_{C2} > -OH_{C3}$[18, 19]. The degree of substitution (DS) defining the number of hydroxyl groups that have been modified ranges from 0 to 3. Different methods using NMR spectroscopy[20, 21] and elemental analysis[22] have been established for measuring DS. For instance, DS is directly calculated as the ratio of integrals of protons defining the functional group that have been added to cellulose to protons defining the cellulose backbone in the $^{1}H$ spectrum. Meanwhile, the content of carbon, hydrogen, nitrogen or any other halogens present in the newly prepared derivatives can be measured using elemental analysis and the resulting data permit the estimation of the DS in some cases.

#### 1.2.3.1.2. Homogeneous vs heterogeneous reactions

The chemical modification of cellulose and its derivatives has been performed under both heterogeneous and homogeneous conditions. Heterogeneous conditions refer to situations where cellulose is not dissolved in the solvent so the reaction occurs at the interface between the solid and liquid phases resulting in modification only at the surface. Cellulose fibers[23, 24], membranes[25, 26] and nano-whiskers[27, 28] have all been modified under heterogeneous conditions. Homogeneous conditions are defined by the dissolution or, at least, by the swelling of cellulose in the solvent resulting in modification of the entire cellulose molecular structure. This remains extremely challenging because of both the high molecular weight of cellulose and the intra/inter-H bonding networks which define

the cellulose solid-state structure and limit considerably its solubility in common solvents. Recently, Olsson and Westman[29] reviewed advances in methods for the dissolution of cellulose. Water swells cellulose because the water molecules interact with the cellulose backbone but do not break fully the H-bonding interactions. Cellulose is partially soluble in alkali solution where a maximum of 10% w/w of cellulose was dissolved in $NaOH/H_2O$ solution. The addition of species including PEG, urea or thiourea enhances the solubility of cellulose in alkali solution at low temperature by limiting the aggregation of cellulose chains. Furthermore, the DMAc/LiCl system has been used commonly to dissolve cellulose. It involves interaction between the hydroxyl groups of cellulose and the Cl anion, resulting in the formation of "bridges" between cellulose and the macro-cation $[DMAc\text{-}Li]^+$. However, this process requires the prior-elimination of water which prevents its use in industry. Ionic liquids (IL) such as 1-butyl-3-methylimidazolium chloride (BMIMCl) dissolve cellulose due to the penetration of the anion into the cellulose structure, breaking the H-bonding networks.

#### 1.2.3.1.3. Commercial cellulose derivatives

Etherification, esterification and oxidation reactions of the hydroxyl groups have been used to create ranges of new cellulosic materials. These commercial derivatives include hydroxyethyl cellulose (HEC), carboxymethyl cellulose (CMC), ethyl cellulose (EC), hydroxypropyl cellulose (HPC) and others (Figure 1-12).

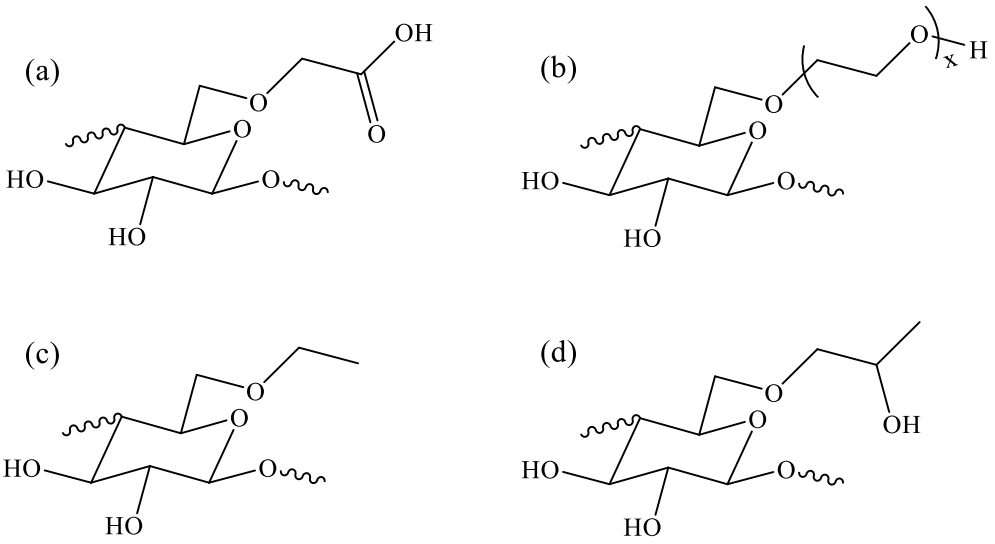


**Figure 1-12:** Molecular structure of cellulose derivatives (considering a DS of 1 at the C6 position); (a) CMC, (b) HEC, (c) EC, and (d) HPC

For instance, HEC (Figure 1-12 b) is obtained by etherification with ethylene oxide and is defined by both the DS and the molecular substitution (MS) which represents the length of the ethylene oxide side chain. This addition to the cellulose backbone disrupts the H-bonding networks resulting in solubilisation in polar solvents such as dimethylsulfoxide (DMSO) and water. HEC has been used extensively as an emulsifier, stabiliser, thickener and as a cosmetic film-former in the formulation of hair and skin products[30-32].

## 1.2.3.2. Grafting approaches

### 1.2.3.2.1. Definitions

Recently, chemical modification of cellulose by polymer grafting has generated much interest because it combines two polymers, one of which is a bio-polymer, and the other a unique material, combination of which is expected to produce new materials properties. Different grafting approaches are described in the literature[19, 33, 34]: the "grafting through" approach is characterised by the polymerisation of a macro-monomer in the presence of a low molecular weight monomer; the "grafting to" approach involves attaching a pre-synthesised polymer chain to the cellulose backbone; the "grafting from" approach involves the polymerisation of monomeric species from the backbone.

### 1.2.3.2.2. "Grafting from"

The "grafting from" approach is the most popular for modifying cellulose. Free radical polymerisation is the main method used to graft synthetic polymers from cellulose, where the backbone has been initiated by hydrogen abstraction[35, 36], single electron transfer[37], irradiation[38, 39] or other methods[19, 33, 40]. However, these methods also result in the formation of ungrafted homopolymer chains and give no control over the density or the length of the grafts. In recent years, Reversible-deactivation radical polymerisation (RDRP) processes have been used to create cellulose-based graft-copolymers producing a narrow molecular weight distribution of the grafts. The most commonly used RDRP process is Atom Transfer Radical Polymerisation (ATRP)[41, 42] because of the straightforward preparation of cellulose macro-initiators from the reaction between one

of the hydroxyl groups present on the cellulose backbone and commercially available acyl chlorides or bromides. However, Reversible Addition-Fragmentation Chain-Transfer (RAFT) polymerisation is another reported way for producing well-defined graft-copolymer cellulose. Semsarilar *et al.*[43] were the first to report the use of the RAFT method in combination with cellulosic material and they highlighted the preparation of a macro-CTA from an HPC backbone which acted as a chain-transfer agent (CTA) in the RAFT polymerisation of N-isopropylacrylamide (NIPAAM) and ethyl acrylate.

Compared to other RDRP techniques, ATRP produces polymers with the narrowest molecular weight distribution, and the required reagents such as catalysts and ligands are commercially available at low cost. On the other hand, commercially available transfer agents for Reversible Addition-Fragmentation Chain-Transfer (RAFT) polymerisation[44] can be quite expensive and may have to be synthesised for specific targets, which adds steps to the fabrication process. Furthermore, the use of RAFT polymerisation produces polymers with possibly undesirable colour and odour due to the presence of sulphur in the transfer agent[45] which can be a constraint in some applications. This problem could potentially be solved by cleaving RAFT agents, and recently, Willcock *et al.*[46] reviewed different approaches, including for instance thermal elimination, aminolysis and hetero-Diels-Alder reactions. It should be pointed out that ATRP also has some inherent disadvantages; it has to be conducted in a rigorously oxygen-free environment and the use of copper may be a problem as it can be difficult to remove. Furthermore, some solvents and vinyl monomers deactivate the catalyst resulting in unsuccessful or uncontrolled polymerisation.

#### 1.2.3.2.3. "Grafting to"

The conjugation between cellulose or cellulose derivatives with synthetic polymers is possible *via* the presence of functional groups on each polymer which undertake reactions such as thiol-ene chemistry[47], hetero Diels-Alder chemistry[48, 49] or azide-alkyne cycloaddition chemistry (CuAAC)[50-52]. In order to prepare well-defined cellulose-based graft-copolymers, RDRP techniques such as RAFT and ATRP have been used. Recently, Hansson *et al.*[53] combined an ATRP process and click chemistry to prepare graft-copolymers, Cell-g-PMMA. Their method consisted of using an alkyne-terminated initiator for ATRP of methyl methacrylate (MMA) and PMMA was thus clicked to cellulose, which was prior-functionalized with sodium azide. Subsquently, Goldmann *et al.*[48] used RAFT polymerisation to graft poly(isobornyl acrylate) to a cellulose substrate using Diels-Alder cycloaddition and Xiao *et al.*[54] used RAFT polymerisation in combination with thiol-ene click reaction for preparing methyl cellulose-g-poly(vinylacetate).

# Chapter 2: Aims and objectives

The work presented in this thesis was partially funded by Ashland Inc. which is an American chemical company. Ashland is known as being one of the worldwide leaders in the preparation of hydroxyethyl cellulose (HEC) and merged three years ago with ISP an international company which was well-known for producing poly(N-vinylpyrrolidone) (PVP). Ashland decided to focus on the development of novel cellulosic materials which will combine the properties of both the parent cellulosic material and synthetic polymers such as PVP. This fusion inspired the work described in this thesis with the broad aim to chemically modify HEC which was chosen because of its solubility in polar solvents and water, and the presence of the three hydroxyl groups, capable of undertaking chemical reactions. Thus, the preparation of HEC derivatives and HEC-based graft-copolymers will alter the properties of the parent HEC and thereby potentially mimic synthetic polymers properties. This could lead to potential alternatives to synthetic polymers derived from the petrochemical industry which will lose its prevalence, in the future. For this, three different strategies were pursued for modifying HEC and each approach corresponds to a chapter in this thesis. The first approach (Chapter 3) was based on the functionalization of the hydroxyl groups of HEC with functional groups, whereas the two other methods described in Chapters 4 and 5 refer to the grafting approaches in order to prepare well-defined graft-copolymers of HEC. Chapter 4 explores the "grafting from" approach combined with Atom transfer Polymerisation (ATRP) for the preparation of synthetic polymers, whereas Chapter 5 discusses the "grafting to" approach where synthetic polymers were produced from Reversible Addition-Fragmentation Chain-Transfer (RAFT) polymerisation. The physical properties of HEC derivatives prepared in

Chapter 3 were evaluated and compared to the parent HEC, however the preparation of well-defined graft-copolymers, explored in both Chapter 4 and 5, led to new HEC properties such as antibacterial action.

# Chapter 3: HEC modification via functionalization reactions

## 3.1. INTRODUCTION

This chapter was developed from one of the requirements of our industrial sponsor, Ashland, which was the preparation of cellulose derivatives containing lactam groups. In the literature, lactam groups were introduced onto cellulose/cellulose derivatives using a "grafting from" approach and this consists of polymerising synthetic monomers from a cellulose backbone to form graft-copolymers. The polymer containing lactam groups that has been grafted from cellulose and cellulose derivatives was poly(N-vinylpyrrolidone) (shown in Figure 3-1) which is a biocompatible polymer and, commonly prepared *via* radical polymerisation of N-vinylpyrrolidone (NVP)[55]. The key property of poly(N-vinylpyrrolidone) (PVP) is its solubility in both organic and aqueous solvents. Its solubility is due to the presence of the lactam amide group which provides both hydrophobic and polar characteristics. In addition, polar methylene and methine define the backbone and a ring engenders further hydrophobicity. PVPs are mostly used as vesicle transporters[56, 57], film formers[58, 59], binders[60] and detoxifiers[61] in the pharmaceutical, cosmetic, food and adhesive industries.

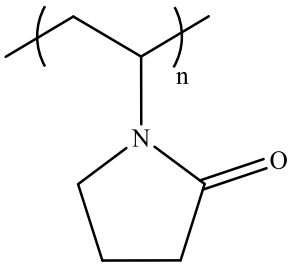


**Figure 3-1:** Structure of poly(N-vinylpyrrolidone) (PVP)

The most widely used technique for polymerising NVP onto cellulose and cellulose derivatives is conventional free radical polymerisation where radicals are generated from either a hydrogen abstraction or a single electron transfer. To abstract a hydrogen of one alcohol group of a cellulose backbone, Mustafa Yigitoglu *et al.*[36] used AIBN resulting in the formation of CMC-g-PVP whereas Flefel *et al.*[35] used persulfate ion in their study on the graft-copolymerisation of both NVP and acrylamide (AA) onto a mixture of CMC and HEC. Furthermore, direct oxidation allows the production of radical species due to a single electron transfer and this was used in the work of Ibrahim *et al.*[37] who described the use of a Ce(IV) system for grafting PVP to a cellulosic membrane, defined as a mixture of CMC-Na and HEC. As an alternative to the use of chemicals for initiating the graft-copolymerisation of NVP onto cellulose/cellulose derivatives, γ-radiation was used in two different approaches[38, 39]. The first was pre-irradiation where the NVP was added after irradiating the cellulose backbone which minimized NVP homopolymerisation. However, the second approach, called mutual irradiation, which consisted of irradiating the mixture containing both monomer and cellulose, afforded both the grafting of NVP to cellulose and the homopolymerisation of NVP. The use of γ-rays risks the degradation of cellulosic material by breaking down the glycosidic linkage[19, 33], and this can be mitigated in the mutual irradiation approach because of the presence of the monomer

which acts as a stabilizer. Inagaki and Katsuura[40] used a small amount of sodium ethoxide in order to activate the graft-polymerisation of NVP onto cellulose phosphonate via the reaction of the P-H bond with the vinyl groups. The reactivity of P-H was estimated to be up to 96%, however only a short chain length of PVP (5 repeated units of NVP) was grafted from cellulose phosphonate.

The graft-copolymerisation of NVP onto cellulose or onto cellulose derivatives has significantly improved some of the properties of these materials. Takacs *et al.*[39] showed that 30% grafting of NVP onto cotton-cellulose increased the water uptake by a factor of 2-3 and this was due to the opening of the cellulose structure. Furthermore, Ghanshyam *et al.*[38] reported the improvement of the sorption of metal ions such as $Fe^{2+}$, $Cu^{2+}$ and iodine of a cellulose-based graft-copolymer. Flefel *et al.*[35], who modified a mixture of CMC-Na and HEC with both PVP and poly(acrylic acid) (PAA), showed considerably increased biodegradability resistance and significant activity against fungi that are responsible for plant diseases. The modification of cellulose phosphonate with NVP produced flame-retardant properties because of the increase of thermal stability resulting in a reduction of the flammability. Furthermore, Ibrahim *et al.*[37] grafted NVP onto a mixture of CMC-Na and HEC (ratio of 3:1) to increase membrane affinity for water, increasing the solute permeability through the membranes. To conclude, the modification of cellulose and cellulose derivatives with lactam groups extends the use of cellulosic material into waste water purification, metal ion enrichment, separation and effluent remediation technologies, increasing the range of applications from fungicidal agents to absorbent agents.

The motivation of our work was the coupling of the cellulose derivative, HEC, with lactam groups in order to mimic the properties of PVP, leading to applications in new areas of advanced materials science for cellulosic materials. We aimed to lactam-

functionalize HEC to give a unique bio-based polymer, rather than graft-copolymerise NVP onto HEC. Our functionalization strategy is based on a low cost reaction centered on short reaction times under solvent-free conditions. Furthermore, our lactam-functionalized material has a well-defined cellulose-based polymer backbone, which facilitates characterisation using standard equipment platforms. Consequently, the lactam-functionalized HEC may compete favorably with a grafted copolymer equivalent from an industrial point of view. Like the graft copolymer, our lactam-functionalized HEC displayed significantly improved stability, swelling, solubility and bacterial anti-adhesive properties over unfunctionalized HEC. These enhancements, combined with straightforward synthesis, provide a new type of cellulose hybrid material that could be produced economically on an industrial scale.

## 3.2. EXPERIMENTAL

### 3.2.1. Materials

2-Pyrrolidone, paraformaldehyde, 2-hydroxyethyl cellulose ($M_w$ =250 kDa, DS =1, MS =2), 2-amino-2-methyl-1-propanol hydrochloride, potassium hydroxide, dimethyl sulfoxide (DMSO), N-methyl-pyrrolidone (NMP), dimethylformamide (DMF) 1,4-dioxane, Luria broth and ampicillin sodium salt were purchased from Sigma. 1-(Hydroxyethyl)-2-pyrrolidone (HEP) was obtained from Ashland. Cyclohexane, acetone, butanone, ethanol, dichloromethane (DCM), propan-2-ol, chloroform, toluene and diethyl ether were purchased from Fisher Scientific. Deuterated solvent, DMSO-$d_6$ was purchased from Apollo Scientific. Bacteria *Escherichia coli* K-12 wild-type strain

(W3110 / ATCC27325, F-, λ-, rpoS(Am), rph-1, Inv(rrnD-rrnE)) and *Staphylococcus aureus* (3R7089 strain Oxford / ATCC9144) were grown in the laboratory.

## 3.2.2. Characterisation techniques

Solution state NMR spectroscopy was performed using either a Varian VNMR-700 spectrometer at 699.73 MHz ($^{1}$H) and 174.93 MHz ($^{13}$C), or a Bruker Advance 400 spectrometer at 400.13 MHz ($^{1}$H) and 100.60 MHz ($^{13}$C). For solid state $^{13}$C NMR spectroscopy, a Varian VNMRS spectrometer with a 9.4 T magnet was used at 100.56 MHz employing the cross polarisation method. Elemental analyses were performed using an ULTIMA 2ICP optical emission spectrometer. Size exclusion chromatography (SEC) was under taken with DMF as solvent at 70 $^{o}$C, where 100 µL of solution, agitated overnight, to ensure complete dissolution was injected at a flow rate of 1.00 mL.min$^{-1}$ by a Viscotek SEC autochanger model. A Viscotek TDA 301 unit with triple detection (right angle laser scattering at 670 nm, differential refractometer and viscometer) was used. Analyses were undertaken using OmniSEC 4.0 software. A Perkin Elmer Pyris 1 system was used for thermogravimetric analysis (TGA). A Brookfield Digital Viscometer model DV-I+ was used for measuring dynamic viscosities. A PowerWave™ XS Microplate Spectrophotometer was used for measuring absorbance in 96-well microplates.

## 3.2.3. Synthesis and characterisation of modified HECs

### 3.2.3.1. Functionalizing agent: 1-(hydroxymethyl)-2-pyrrolidone

In a one-necked round-bottomed flask carrying a condenser, 2-pyrrolidone **1** (10.62 g, 0.125 mol, 1eq.) and potassium hydroxide (0.03 g, 0.534 mmol) were mixed and heated at 80 ºC. Paraformaldehyde (3.78 g, 0.125 mol, 1 eq.) was added slowly and the mixture was stirred for 30 min at 80 ºC. After the mixture was allowed to cool to room temperature, toluene was added, and the mixture was heated to 80 ºC until complete dissolution occurred. The solution was allowed to cool to room temperature and filtered. The solid product was then recrystallized from toluene, filtered and dried under vacuum at 40 ºC overnight to afford 1-(hydroxymethyl)-2-pyrrolidone (11.78 g, 82%) as a white powder; mp. 78-80 ºC. $^{1}$H NMR (400 MHz, DMSO-$d_6$): $\boldsymbol{\delta}_H$ (ppm) 5.75 (s, 1H, $CH_2$-O**H**); 4.57 (s, 2H, C**H**$_2$-OH); 3.40 (t, J =7.2 Hz, 2H, $CH_2$-C**H**$_2$-N); 2.22 (t, J =8.0 Hz, 2H, C**H**$_2$-CO); 1.91 (app qn, J =7.6 Hz, 2H, $CH_2$-C**H**$_2$-$CH_2$); $^{13}$C NMR (100 MHz, DMSO-$d_6$): $\boldsymbol{\delta}_C$ (ppm) 174.2(**C**=O); 65.0(**C**$H_2$-OH); 45.1 ($CH_2$-**C**$H_2$-N); 31.1 (**C**$H_2$-CO); 17.6 ($CH_2$-**C**$H_2$-$CH_2$); EA (calculated): 51.9 %C; 7.8 %H; 12.0 %N; EA (found): 52.0 %C; 7.8 %H; 11.9 %N.

### 3.2.3.2. Functionalization of HEC with 1-(hydroxymethyl)-2-pyrrolidone

2-Hydroxyethyl cellulose (HEC) **3** ($M_w$ =250,000 g/mol, DS =1, MS =2, 1.0 g, 4 mmol, 1 eq), 1-(hydroxymethyl)-2-pyrrolidone (HMP) **2** (1.5 or 10 eq.) and 2-amino-2-methyl-1-propanol hydrochloride (0.116 g, 0.923 mmol, 0.25 eq.) were mixed and the mixture was heated for a defined reaction time. Temperatures and reaction times are summarised

in Table 3-1. Once the mixture had cooled to room temperature, the product **4** was precipitated with acetone (200 mL) and collected by filtration. Due to the presence of unreacted HMP in the $^{1}$H NMR spectrum, polymer was dissolved in water (10 mL) and precipitated in acetone (100 mL) and these processes were repeated until the total disappearance of signals of starting material HMP by $^{1}$H NMR spectroscopy. This resulted in a relatively low yield (20-50%). Increased yields were achieved by dialysis of the reaction mixture for 2 days using a 3,500 Da MWCO membrane against milli-Q water and product **4** isolated by lyophilization. The precipitate was collected by filtration and dried under vacuum at 50 ºC overnight to afford the modified HEC as a pale yellow powder in yields ranging from 30% to 100% based on the estimation of DS by $^{13}$C NMR spectroscopy. Samples from each reaction were characterised by solid state $^{13}$C NMR spectroscopy using the cross polarization method. Samples were also dissolved in DMSO-$d_6$ and were characterised using $^{1}$H (700 MHz), $^{13}$C (176 MHz), HMBC and HSQC NMR experiments. A sample of experiment FJ-73 was characterised using size exclusion chromatography (SEC) in DMF.

#### 3.2.3.3. Functionalization reaction of HEC with 1-(hydroxyethyl)-2-pyrrolidone

In a three necked reactor fitted with an overhead stirrer, 2-hydroxyethyl cellulose **3** (1 g, 4 mmol, 1 eq.), 1-(hydroxyethyl)-2-pyrrolidone **5** (5.16 g, 40 mmol, 10 eq.) and 2-amino-2-methyl-1-propanol hydrochloride (0.116 g, 0.923 mmol, 0.25 eq.) were heated at 155 ºC for 2 h. Once the mixture had cooled at room temperature, the product **6** was dialysed for 2 days through a 3,500 Da MWCO membrane against milli-Q water. The aqueous solution was lyophilised and the polymer was obtained as a pale yellow powder in yield

of 0% (1 g) based on the estimation of DS by $^{13}C$ NMR spectroscopy. The samples were characterised using solution state NMR spectroscopy. Samples were dissolved in DMSO-$d_6$ and $^{1}H$ NMR (400 MHz) and $^{13}C$ NMR (150 MHz) experiments were run.

## 3.2.4. Evaluation of physical properties of HMP-functionalized HEC

### 3.2.4.1. Assessment of solubility

The solubilities of HEC and HMP-functionalized HEC ($DS_{primary\ alcohol}$ ~0.9) were evaluated. Solvent (1 mL) (see Table 3-4) was added to cellulosic material (10 mg) in a vial. The vials were allowed to stand overnight at room temperature then the solutions were vortexed before determining visually the solubility.

### 3.2.4.2. Dye release study

HMP-functionalized HEC ($DS_{primary\ alcohol}$ ~0.9) and HEC were both tested for comparison purposes. Cellulosic material (0.1 g) and rhodamine B (3 mg) were ground to a powder using a pestle and mortar. The powder was then pressed at a force of 10 tonnes for 5 min using a KBr press, normally used for preparing IR samples. Each disc was placed in a vial with distilled water (20 mL). The samples were then left at 25 ºC for 7 h, and the dye release from the discs was monitored visually, with photographs being taken every 10 min for the first hour and then every hour.

### 3.2.4.3. Measurement of single point viscosity

Solutions of 3% w/w in water were prepared using HMP-functionalized HEC ($DS_{primary\ alcohol}$ ~0.9) and HEC. Defining a measure of internal resistance, the dynamic (absolute) viscosity of each solution was measured in mPa.s using a Brookfield instrument which measured the force required for the torque to rotate the spindle in the immersing solution. In our experiment, the rotational speed of the torque and temperature was kept constant, i.e., at 96 rpm and 25 ºC respectively.

### 3.2.4.4. Assessment of thermal stability

The thermal stabilities of HMP-functionalized HEC ($DS_{primary\ alcohol}$ ~0.9) and HEC were compared using thermogravimetric analyses under nitrogen with a temperature ramp of 30 ºC to 300 ºC at a rate of 10 ºC/min.

### 3.2.4.5. Bacteriological studies

*Escherichia coli* K-12 wild-type strain (W3110, $F^-$, $\lambda^-$, *rpoS(Am), rph-1, Inv*(*rrnD-rrnE*))[62] and *Staphylococcus aureus* (3R7089 strain Oxford)[63] were selected for bacteriological studies as representative Gram-negative (*E. coli*) and Gram-positive (*S. aureus*) species. The following two experiments aimed to evaluate bacterial anti-adhesion properties and monitor their viability and growth following exposure to materials treated with either HEC or HMP-functionalized HEC ($DS_{primary\ alcohol}$ ~0.9).

#### 3.2.4.5.1. Anti-adhesion testing

Bacterial adhesion properties were assessed using the procedure of Wood *et al.*[64]. Aqueous solutions containing 3% w/w of HEC and HMP-functionalized HEC ($DS_{primary\ alcohol}$ ~0.9) were prepared. Squares (18 mm×18 mm) of Whatman 3MM filter paper were submerged in each cellulosic solution and also in distilled water, as a control, for 40 min at room temperature. Each paper was then placed in a separate flask and dried overnight under vacuum at 50 ºC. On each paper, bacterial culture (100 µL) grown to an $A_{650nm}$ of 0.4 was applied. Sterile squares of polymer film (Saran wrap) were placed over each paper square to limit evaporation, then the squares were incubated at 37 ºC for 24 h in a humid environment. The film was removed and 56/2 minimal salts buffer (150 µL) was added to each filter paper. Excess culture and the filter paper were placed in a 2 mL spin column vial and centrifuged to recover the bacterial culture. The resulting bacterial pellet was re-suspended in Luria-Bertani (LB) broth and serial 10-fold dilutions from $10^{-1}$ to $10^{-5}$ were prepared using LB as diluent. Dilutions (10 µL) were spotted onto an LB agar plate, the plates were incubated for 18-20 h at 30 °C and the number of colonies was visually counted.

#### 3.2.4.5.2. Bacterial growth and viability testing

Aqueous solutions containing 0.04 g/mL of HEC and HMP-functionalized HEC ($DS_{primary\ alcohol}$ ~0.9) were prepared. *E. coli* and *S. aureus* were grown to an $A_{650nm}$ of approximately 0.25 in a 96-well microplate, then a solution (10 µL) containing either HEC or HMP-functionalized HEC ($DS_{primary\ alcohol}$ ~0.9) was added. Appropriate controls using water (10 µL) or ampicillin solution (10 µL) were added to bacteria growing on the same plate.

Bacterial growth at 37 °C was monitored at $A_{650nm}$ as a function of time using a Biotek Synergy HT Multi-Mode Microplate Reader.

# 3.3. RESULTS AND DISCUSSION

## 3.3.1. Synthesis

### 3.3.1.1. 1-(hydroxymethyl)-2-pyrrolidone

The preparation of 1-(hydroxymethyl)-2-pyrrolidone **2** followed a literature procedure[65]: Paraformaladehyde was reacted with 2-pyrrolidone **1** in the presence of potassium hydroxide for 30 min at 80 ºC (Scheme 3-1) to obtain 1-(hydroxymethyl)-2-pyrrolidone **2** in a yield of 82%.

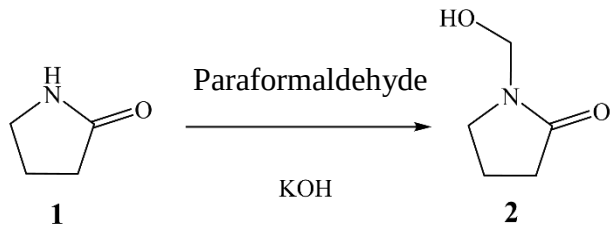


**1** **2**

**Scheme 3-1:** Preparation of 1-(hydroxymethyl)-2-pyrrolidone **2** (HMP)

### 3.3.1.2. Functionalization of HEC with 1-(hydroxymethyl)-2-pyrrolidone

The functionalization reaction was inspired by the modification of textiles with methylolated lactams[66]. The modification of HEC **3** with 1-(hydroxymethyl)-2-

pyrrolidone (HMP) **2** (Scheme 3-2) was investigated with different reaction conditions which are summarised in Table 3-1.

**Table 3-1:** Reaction conditions used for the functionalization reaction of HEC with 1-(hydroxymethyl)-2-pyrrolidone

| **Exp. N°** | **Reaction conditions** | | | | | **Yield (%)** |
|---|---|---|---|---|---|---|
| | Solvent | Time (h) | Temperature (ºC) | Ratio (mol) HEC:HMP | Catalyst* | |
| **FJ-13** | DMSO[*1] | 17 | 90 | 1:1.5 | Y | 67 |
| **FJ-10** | | 17 | 110 | 1:1.5 | Y | 46 |
| **FJ-8** | | 17 | 155 | 1:1.5 | Y | 60 |
| **FJ-27** | NMP[*1] | 17 | 155 | 1:1.5 | Y | 80 |
| **FJ-73** | | 17 | 155 | 1:0 | Y | 100 |
| **FJ-23** | | 5 | 155 | 1:1.5 | Y | 45 |
| **FJ-36** | | 5 | 155 | 1:10 | Y | 45 |
| **FJ-35** | | 2 | 155 | 1:1.5 | Y | 62 |
| **FJ-40** | | 0.5 | 155 | 1:1.5 | Y | 50 |
| **FJ-41** | No solvent[*2] | 0.5 | 155 | 1:10 | Y | 33 |
| **FJ-49** | | 1 | 155 | 1:10 | Y | 90 |
| **FJ-251** | | 1.5 | 155 | 1:10 | Y | 94 |
| **FJ-45** | | 2 | 155 | 1:10 | Y | 66 |
| **FJ-21** | | 5 | 155 | 1:10 | Y | 64 |
| **FJ-29** | | 5 | 155 | 1:10 | N | 26 |
| **FJ-213** | | 17 | 155 | 1:10 | Y | 99 |

[*] "Y"=yes, "N"=no

[*1] in one neck round bottom flask with a magnetic stirrer with 20 mL of solvent

[*2] in a three necked reactor fitted with an overhead stirrer

Our investigation was divided into three parts depending on the solvent used. Dimethyl sulfoxide (DMSO) was first used and permitted the determination of the minimum required temperature for initiating the functionalization of HEC with HMP. The second

solvent used was N-methyl-pyrrolidone (NMP) which probed the influence of both the reaction time and ratio of AGU:HMP on the degree of substitution (DS) of the hydroxyl groups of HEC with HMP. Furthermore, the integrity of the polymer chains under acidic conditions was investigated in NMP. Finally, HMP acting as both functionalizing agent and solvent was explored. The importance of the catalyst on the DS was also investigated and the absence of degradation of the HEC backbone was confirmed.

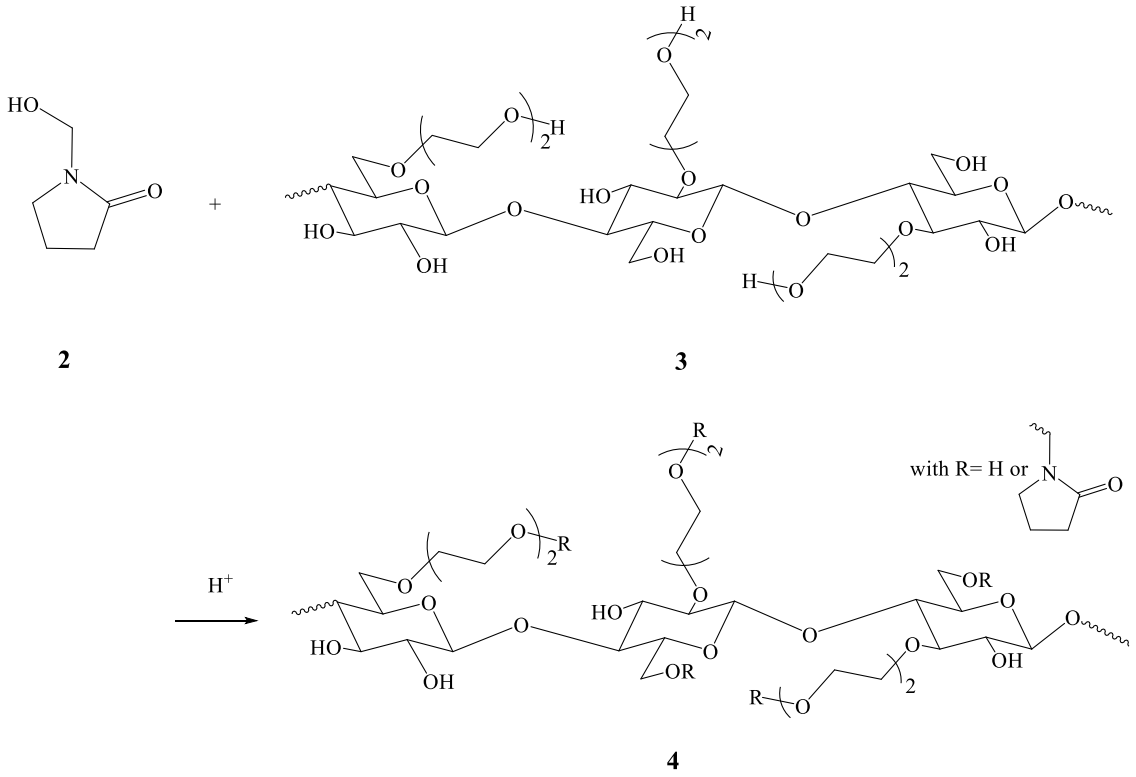


**Scheme 3-2:** Functionalization reaction of HEC **3** with HMP **2**

### 3.3.1.2.1. Functionalization reactions using dimethyl sulfoxide

The functionalization reactions where DMSO was used as solvent proceeded for 17 h with a ratio 1:1.5 of AGU:HMP in the presence of 2-amino-2-methyl-1-propanol hydrochloride. The temperature was set at 90, 110 and 155 ºC for the experiment FJ-13,

FJ-10 and FJ-8 respectively in order to determine the temperature necessary for functionalizing HEC with HMP. Each sample was characterised using NMR spectroscopy and the structure of HMP-functionalized HEC was numbered as shown in Figure 3-2.

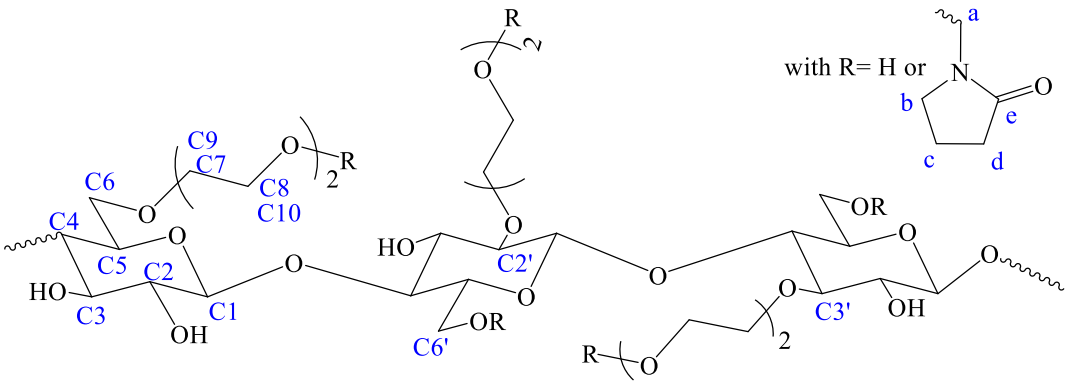


**Figure 3-2:** Numbering structure of HMP-functionalized HEC **4**

The solid state $^{13}C$ CP-MAS NMR spectrum (Figure 3-3) of a sample of experiment FJ-13 shows signals correlating with the presence of the HEC backbone. The signal $\delta_C$ ~61.8 is assigned to the primary alcohols at C10 (R=H) and C6' (R=H) position and the broad signal $\delta_C$ ~71.0 ppm is assigned to the set of carbons from positions C6 to C9, defining the ethylene oxide side-chain. The signal $\delta_C$ ~75.2 ppm is assigned to the set of carbons at C2, C2', C3, C3' and C5 positions, $\delta_C$ ~83.0 ppm is assigned to the carbon at C4 position and $\delta_C$ ~103.6 ppm is assigned to the carbon defining the anomeric centre C1.

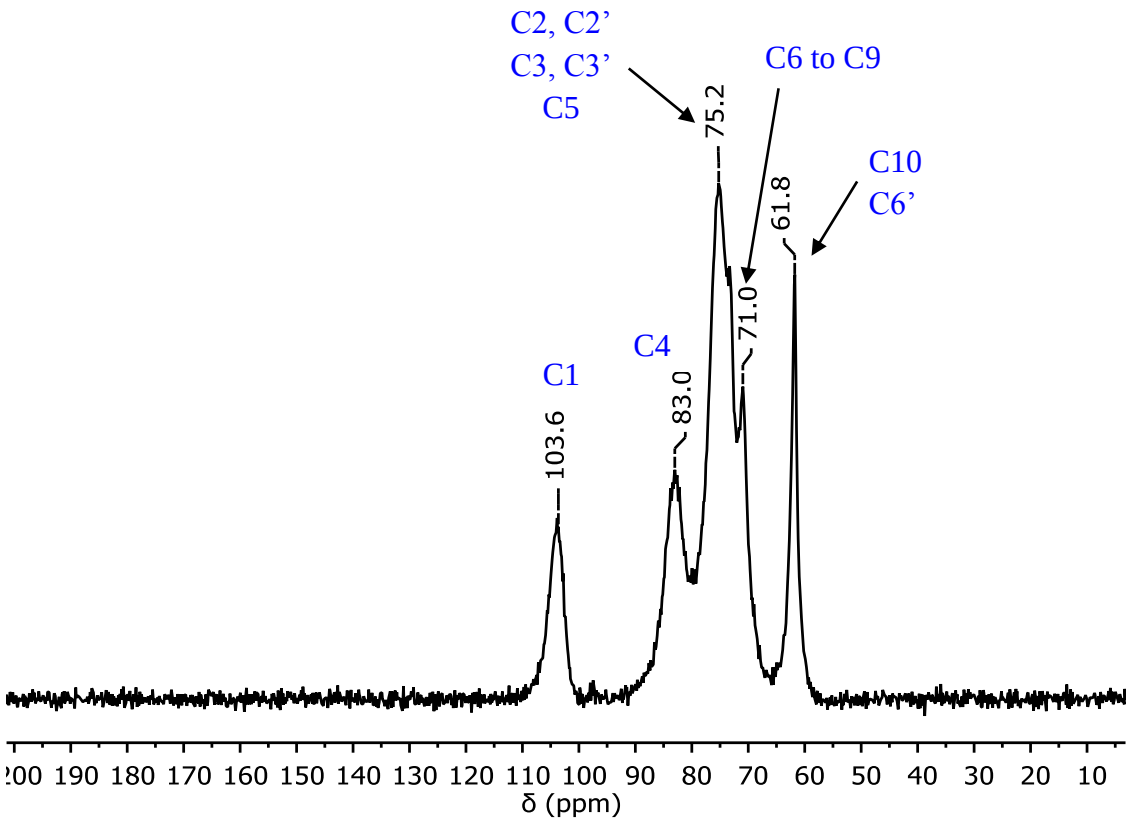


**Figure 3-3:** Solid state $^{13}C$ CP-MAS NMR spectrum of sample of exp. FJ-13 (17 h at 90 ºC in DMSO)

The solution state $^{1}H$ NMR spectrum (Figure 3-4) of a sample of experiment FJ-13 showed only two signals $\boldsymbol{\delta}_H$ ~3.4 ppm and ~3.5 ppm which are assigned to the protons defining the ethylene oxide side-chain. However, the broad signals across the baseline are assigned to the rigid cellulose backbone whereas the sharper signals are due to the more mobile side-groups.

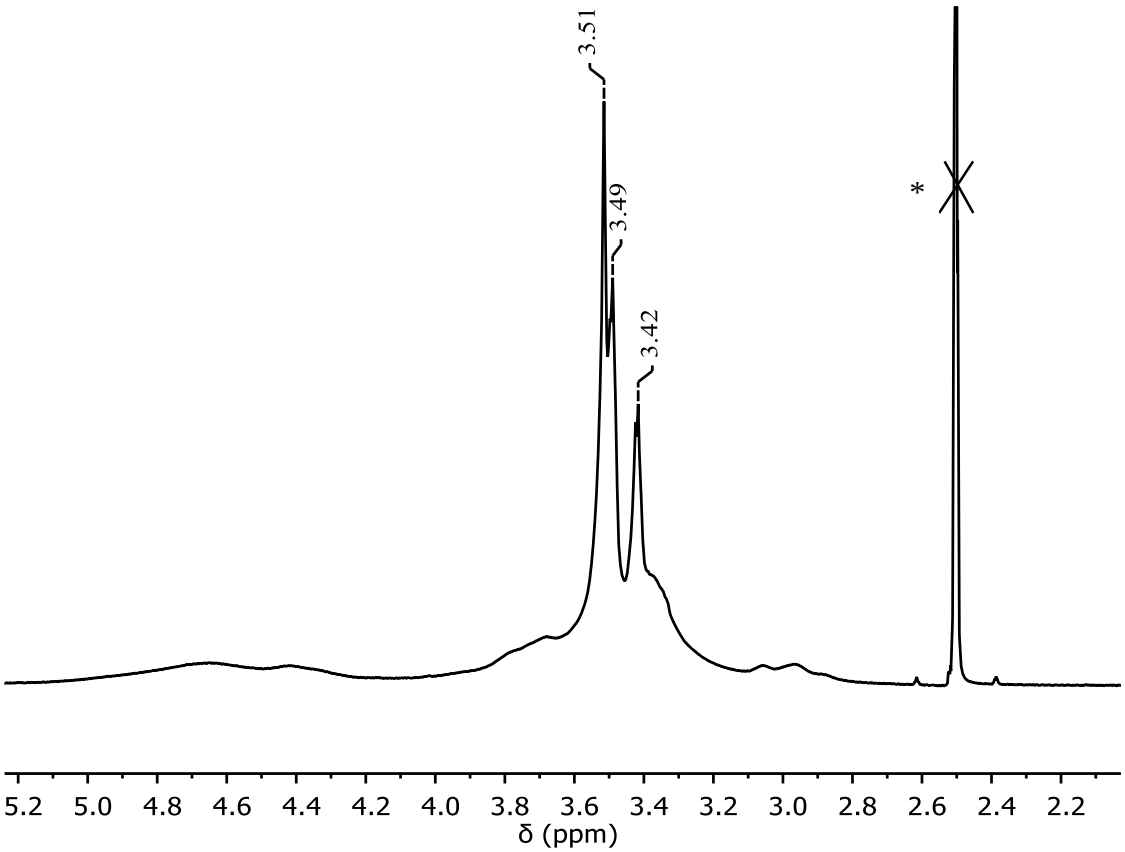


*NMR solvent and/or solvent residues

**Figure 3-4:** Solution state $^{1}$H NMR (700 MHz, DMSO-$d_6$) spectrum of sample of exp. FJ-13 (17 h at 90 ºC in DMSO)

The solution state $^{13}$C NMR spectrum (Figure 3-5) of a sample of experiment FJ-13 showed signals characteristic of the HEC backbone and better resolved spectrum compared to the solid state spectrum (Figure 3-3). The peak $\boldsymbol{\delta}_C$ ~60.6 ppm is assigned to the carbons of the primary alcohols at C10 and C6' position where R=H. The peak $\boldsymbol{\delta}_C$ ~70.2 ppm is assigned to the set of carbons at C7, C8 and C6 (R=H) position that define the ethylene oxide side-chain. The peak $\boldsymbol{\delta}_C$ ~72.7 ppm is assigned to the carbon at the C9 position whereas the signal $\boldsymbol{\delta}_C$ ~74.6 ppm is assigned to the carbon at the C5 position. The peak $\boldsymbol{\delta}_C$ ~77.3 ppm is assigned to the carbon at C2 position and the peak $\boldsymbol{\delta}_C$ ~80.2 ppm is assigned to the carbons at C3 and C2' (R=H) position. The signal at 82.1 ppm is assigned

to the carbons at C4 and C3' (R=H) position and the signal 102.0 ppm is assigned to the anomeric carbon at the C1 position.

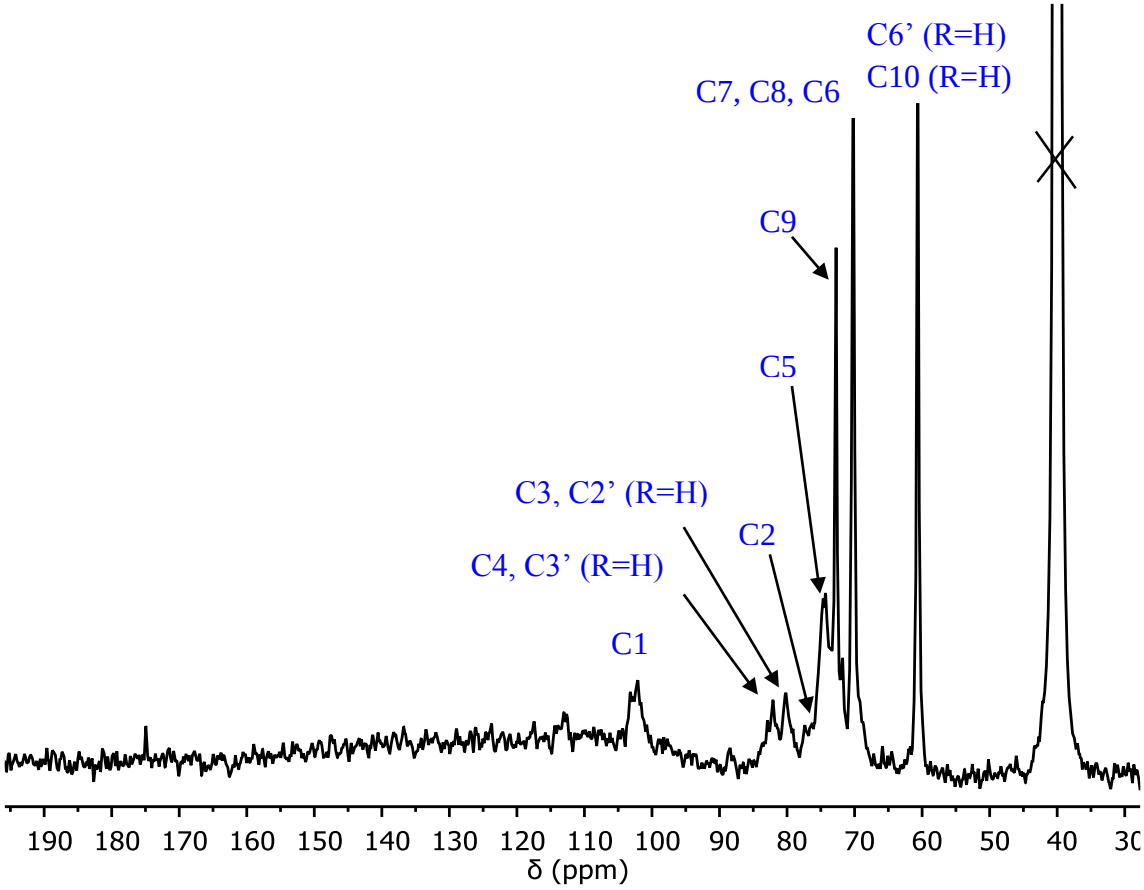


**Figure 3-5:** Solution state $^{13}C$ NMR (176 MHz, DMSO-$d_6$) spectrum of sample of exp. FJ-13 (17 h at 90 ºC in DMSO)

The results of the NMR spectroscopy for sample of experiment FJ-13 did not show the presence of the functionalizing agent, HMP, but only those of HEC were detected indicating the unsuccessful derivatization of HEC backbone with HMP. For the following experiment FJ-10, the ratio AGU:HMP and reaction time was the same as for experiment FJ-13, however, the reaction temperature was increased from 90 to 110 ºC. The characterisation of the sample of experiment FJ-10 using NMR spectroscopy showed the

non-functionalization of HEC with HMP as the sample of experiment FJ-13. The temperature was increased from 110 to 155 ºC for the experiment FJ-8 and the analysis of the sample using NMR spectroscopy revealed spectra containing some differences.

The solid state $^{13}C$ CP-MAS NMR spectrum (Figure 3-6) of a sample of experiment FJ-8 showed the appearance of new signals characteristic of HMP moiety. The set of signals $\boldsymbol{\delta}_C$ ~18.3, 31.7 and 47.2 ppm is assigned to the carbons defining the pyrrolidone ring with $\boldsymbol{\delta}_C$ ~18.3 ppm to the -$CH_2$-**C**$H_2$-$CH_2$, $\boldsymbol{\delta}_C$ ~31.7 ppm to the -**C**$H_2$-C=O and $\boldsymbol{\delta}_C$ ~47.2 ppm to the -N-**C**$H_2$- and the signal $\boldsymbol{\delta}_C$ ~178.6 ppm is assigned the carbonyl group. In comparison with the spectrum in Figure 3-3, a decrease of the intensity of the signal $\boldsymbol{\delta}_C$ ~60 ppm suggested that the modification takes place preferentially at the primary alcohol(s) of HEC. The newly formed methylene group of HEC is likely to appear in the range of $\boldsymbol{\delta}_C$ ~70-75 ppm, resulting in an increase in the broadness of the bands in this range. In addition, the -**C**$H_2$O- signal of HMP is also likely to be obscured by these signals.

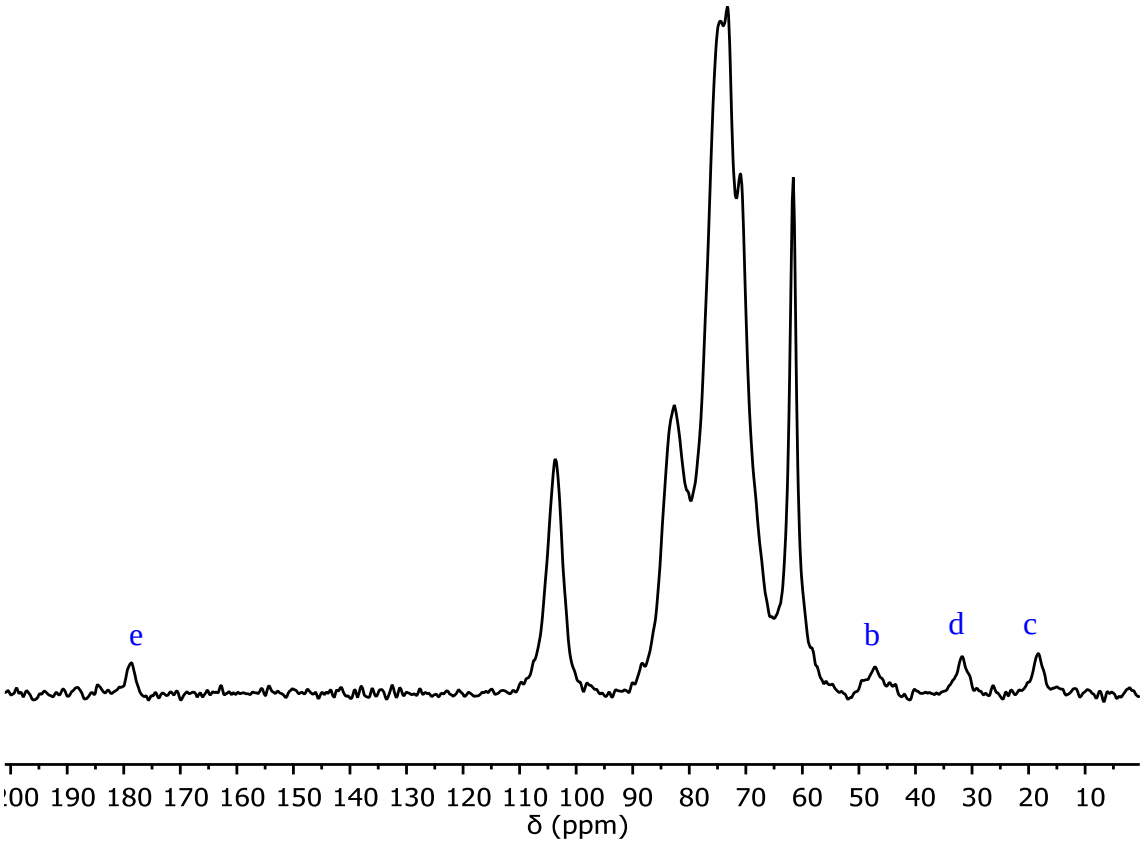


**Figure 3-6:** Solid state $^{13}C$ CP-MAS NMR spectrum of sample of exp. FJ-8 (17 h at 155 ºC in DMSO)

The solution state $^{1}H$ NMR spectrum (Figure 3-7) of a sample of experiment FJ-8 shows signals at $\boldsymbol{\delta}_H$ ~1.93 ppm and 2.27 ppm corresponding to the protons of -$CH_2$-C**H**$_2$-$CH_2$- and -C**H**$_2$-C=O group respectively of the pyrrolidone ring. The signal of the -C**H**$_2$-N- is probably overlapping with the signal $\boldsymbol{\delta}_H$ ~3.42 ppm which is in line with that expected for an HEC derivatives as well as the signal $\boldsymbol{\delta}_H$ ~3.50 ppm (Figure 3-4). Most importantly, however, the signal $\boldsymbol{\delta}_H$ ~4.61 ppm appears to be consistent with the pendent -C**H**$_2$- group of HMP attached to a hydroxyl group of HEC. The chemical shift, although similar to the functionalizing agent HMP, is distinct ($\boldsymbol{\delta}_H$ ~4.57 ppm), which supports the idea of the OH of HMP being exchanged with an O-alkyl fragment from HEC.

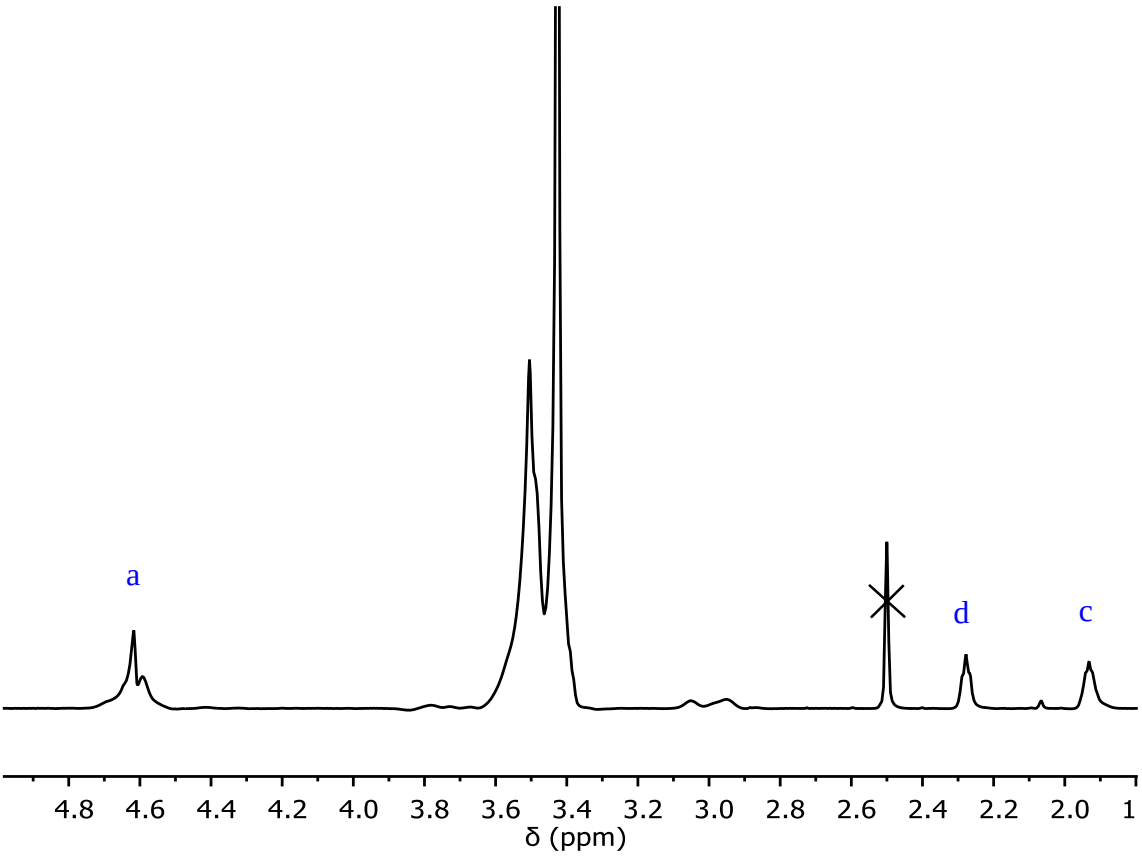


**Figure 3-7:** Solution state $^{1}$H NMR (700 MHz, DMSO-$d_6$) spectrum of sample of exp. FJ-8 (17 h at 155 ºC in DMSO)

In order to demonstrate the attachment of HMP to HEC, HMBC and HSQC solution NMR experiments were performed (Figure 3-8). The HSQC experiment (Figure 3-8 a) permits the assignment of the solution state $^{13}$C NMR spectrum (Figure 3-9). Critically, a signal consistent with the pendent -**C**$H_2$- group of HMP lies at $\boldsymbol{\delta}_C$ ~72.5 ppm. Signals between $\boldsymbol{\delta}_C$ ~60 ppm to $\boldsymbol{\delta}_C$ ~70 ppm correlate to the HEC backbone and the signals $\boldsymbol{\delta}_C$ ~18, 31 and 46 ppm correspond to the pyrrolidone group, which further supports the presence of both HEC- and HMP-like species within the isolated material[67, 68]. Furthermore, the correlation of the signal $\boldsymbol{\delta}_C$ ~46 ppm with the signal $\boldsymbol{\delta}_H$ ~3.37 ppm permits the assignment of the protons -C**H**$_2$-N- in the solution state $^{1}$H NMR spectrum (Figure 3-7).

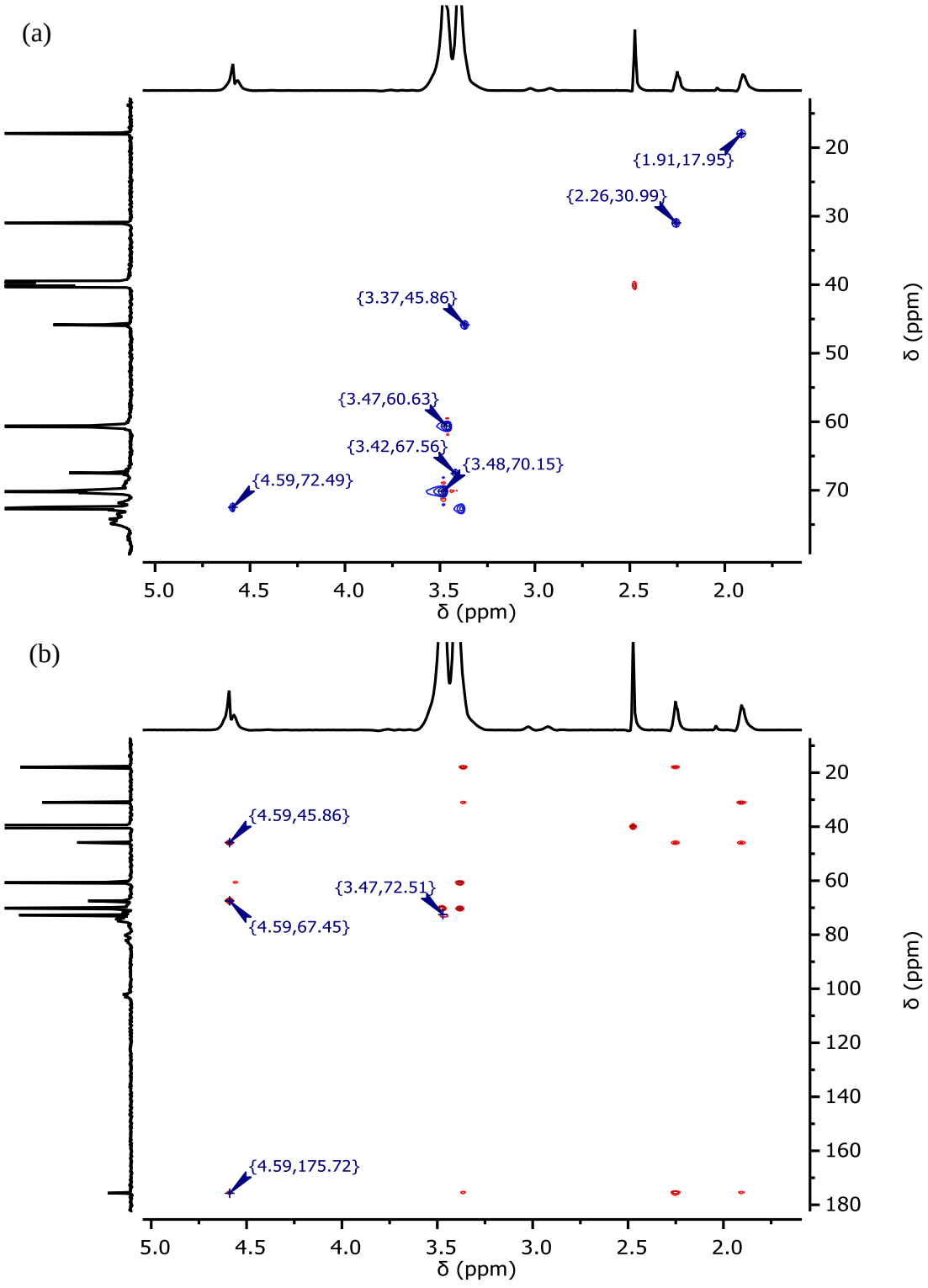


**Figure 3-8:** $^{1}H$-$^{13}C$ NMR correlation spectra of the sample of exp. FJ-8 (17 h at 155 ºC in DMSO) (a) HSQC and (b) HMBC

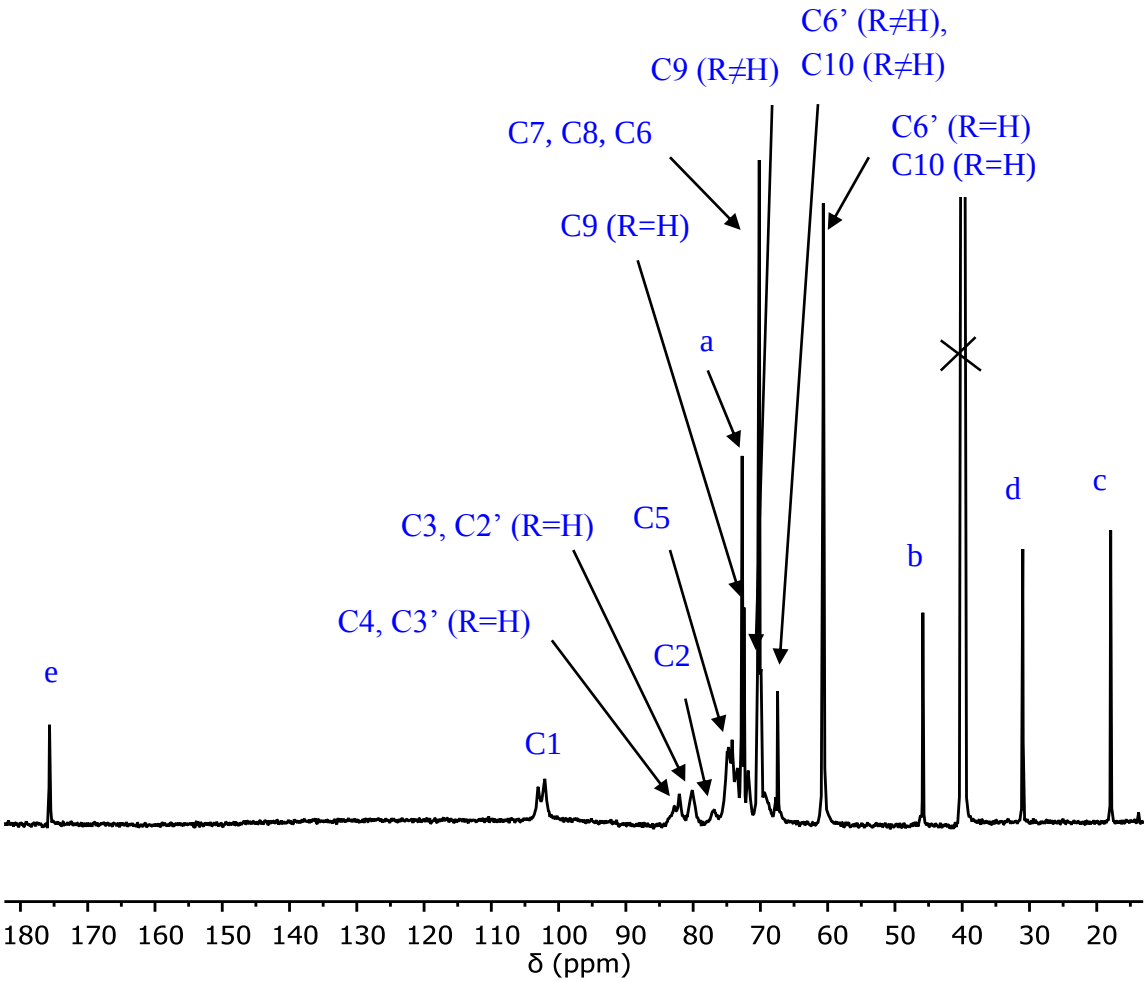


**Figure 3-9:** Solution state $^{13}C$ NMR (176 MHz, DMSO-$d_6$) spectrum of sample of exp. FJ-8 (17 h at 155 ºC in DMSO)

The HMBC experiment (Figure 3-8 b) highlights the covalent bonding between HMP and HEC. The $\boldsymbol{\delta}_H$ ~4.61 ppm signal, which is assigned to the pendent -C**H₂**- group of HMP, correlates with $\boldsymbol{\delta}_C$ ~45.8 ppm, 67.5 ppm and 175.7 ppm. The signals $\boldsymbol{\delta}_C$ ~45.8 ppm and 175.7 ppm are respectively assigned to -**C**$H_2$-N- and the carbonyl -C=O group of the pyrrolidone. The presence of correlation between $\boldsymbol{\delta}_C$ ~ 67.5 ppm and $\boldsymbol{\delta}_H$ ~4.61 ppm suggests covalent bonding between the pendent -C**H₂**- group of HMP and the primary alcohol group(s) of HEC. This is consistent with the primary C6' (R=H) / C10 -methylene-

hydroxyl group being the most nucleophilic hydroxyl on HEC, in agreement with the established order of hydroxyl group nucleophilicities of HEC (C10 ≥ C6' (R=H) >> C2 > C3)[12]. The signal $\boldsymbol{\delta}_C$ ~72.5 ppm of the pendent -**C**$H_2$- group of HMP correlates to $\boldsymbol{\delta}_H$ ~3.47 ppm. The $\boldsymbol{\delta}_H$ ~3.47 ppm can be assigned to the protons at the C10 and C6' position where R≠H which serves to provide a second confirmation of the ligation between HMP and HEC. For reference purposes, the solution state $^{13}C$ NMR spectrum of HEC is shown in Figure 3-5.

The $^{13}C$ NMR assignment of the functionalized HEC (Figure 3-9) also permits quantification of functionalization through integration of methylene signals, which are expected to relax at similar rates. The signals $\boldsymbol{\delta}_C$ ~60.6 ppm and 67.5 ppm have been assigned to the carbons at C6'/C10 positions where R=H and R≠H respectively. Using the relative integrals of these C6'/C10 signals, the $DS_{primary\ alcohol}$ value for the sample of experiment FJ-8 was estimated to be ~0.1.

To summarise, the functionalization of HEC with HMP in DMSO did not take place at temperatures of 90 and 110 ºC, but when the reaction temperature was increased to 155 ºC, the presence of HMP was detected using NMR spectroscopy. The attachment of HMP to HEC backbone was proven using the 2D NMR spectroscopy and a $DS_{primary\ alcohol}$ of ~0.1 was calculated using the solution state $^{13}C$ NMR spectrum. DMSO decomposes at 155 ºC because of the detection of the characteristic smell at the end of the reaction. For this reason, the solvent was changed to N-methyl-pyrrolidone (NMP) for subsequent investigations.

#### 3.3.1.2.2. Functionalization reactions using N-methyl-pyrrolidone

NMP was used as the solvent for investigating the influence of both the reaction time and the ratio of AGU:HMP on the $DS_{primary\ alcohol}$. For each experiment, the temperature was set at 155 ºC and a 1:1.5 ratio of AGU:HMP was chosen for experiment FJ-27, FJ-23, FJ-35 and FJ-40 whereas the ratio AGU:HMP was decreased markedly to 1:10 for the experiment FJ-36. The functionalization reactions were allowed to proceed for 17, 5, 2 and 0.5 h for FJ-27, FJ-23, FJ-35 and FJ-40 respectively. For the experiment FJ-36 where the influence of the amount of HMP was evaluated, 5 h of reaction time was chosen. Each sample of experiment was characterised using NMR spectroscopy.

From analyses of the $^{1}H$, $^{13}C$, HMBC and HSQC spectra, the successful functionalization of HEC is demonstrated. Based on the $^{13}C$ NMR spectra, the $DS_{primary\ alcohol}$ values estimated from the ratio between the integrals of the signal $\boldsymbol{\delta}_C$ ~67 ppm of the modified HEC primary alcohol(s) to that of the unmodified cellulose primary alcohols at $\boldsymbol{\delta}_C$ ~61 ppm are reported in Table 3-2 for each experiment. For the sample of experiment FJ-27, the $DS_{primary\ alcohol}$ was the same as that for sample of experiment FJ-8 where DMSO was used as solvent. With a $DS_{primary\ alcohol}$ of 0.1, the change of solvent from DMSO to NMP did not affect the level of the derivatization, however the decrease of the reaction time increased the $DS_{primary\ alcohol}$ up to a value of 0.2. This can be explained by side reactions which break down the linkage between HEC and HMP after a certain reaction time.

**Table 3-2:** DS result for each experiment using NMP as solvent

| Exp. Nº | Reaction time (h) | Ratio AGU:HMP | $DS_{primary\ alcohol}$ |
|---|---|---|---|
| FJ-27 | 17 | 1:1.5 | 0.1 |
| FJ-23 | 5 | 1:1.5 | 0.2 |
| FJ-36 | 5 | 1:10 | 0.2 |
| FJ-35 | 2 | 1:1.5 | 0.2 |
| FJ-40 | 0.5 | 1:1.5 | 0.2 |

The decrease of the reaction time resulted in minor changes in the NMR spectra of samples compared to those of HMP-functionalised HEC ($DS_{primary\ alcohol}$ ~0.1) (Figure 3-6, Figure 3-7 and Figure 3-9) which suggested an increase of the $DS_{primary\ alcohol}$. Because of the same value of $DS_{primary\ alcohol}$ for others samples (exp. FJ-23, FJ-36 and FJ-40), only NMR spectra of sample of experiment FJ-35 were discussed.

In the solid state $^{13}C$ NMR spectra (Figure 3-10) of HMP-functionalized HEC ($DS_{primary\ alcohol}$ ~0.2), increases in the signals $\boldsymbol{\delta}_C$ ~18.3, 31.7 and 47.2 ppm assigned to the pyrrolidone ring were observed, the signal $\boldsymbol{\delta}_C$ ~71ppm overlapped with the signal $\boldsymbol{\delta}_C$ ~75 ppm and the signal $\boldsymbol{\delta}_C$ ~60.6 ppm, assigned to primary alcohol(s) of HEC, decreased compared to those of the HEC backbone.

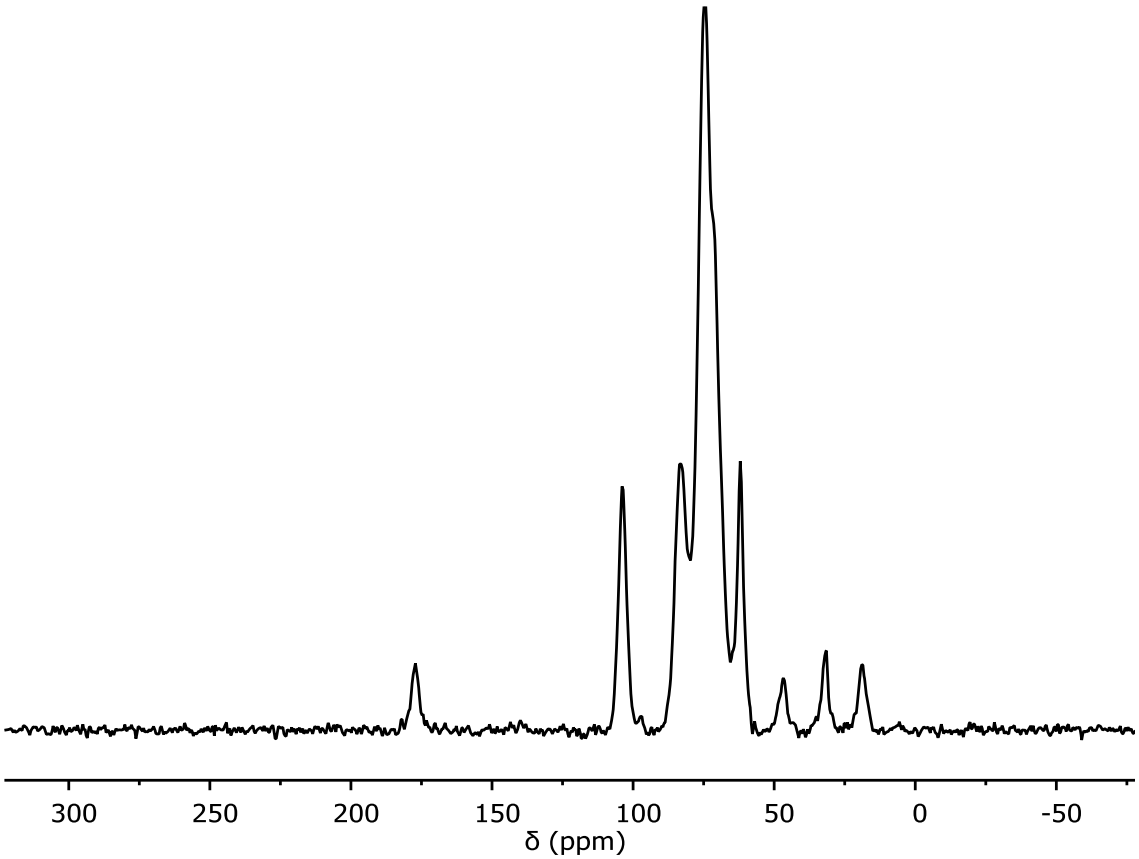


**Figure 3-10:** Solid state $^{13}C$ CP-MAS NMR spectrum of HMP-functionalized HEC (DS ~0.2)

The solution state $^{1}H$ NMR spectrum (Figure 3-11 a) of HMP-functionalized HEC ($DS_{primary\ alcohol}$ ~0.2) showed a signal $\boldsymbol{\delta}_H$ ~3.47 ppm which was not detected in the $^{1}H$ NMR spectrum of HMP-functionalized HEC ($DS_{primary\ alcohol}$ ~0.1) (Figure 3-7). This is assigned to the protons of primary alcohol(s) (i.e, at C6 (R ≠H) and C10 (R ≠H) positions) which reacted with HMP. The intensities of HMP signals $\boldsymbol{\delta}_H$ ~1.93, 2.27 and 4.61 ppm were increased compared to those in Figure 3-7. In the solution state $^{13}C$ NMR (Figure 3-11 b) of HMP-functionalized HEC ($DS_{primary\ alcohol}$ ~0.2), the intensities of signals assigned to HMP moiety were also increased and the intensity of the signal $\boldsymbol{\delta}_C$ ~61 ppm assigned to the primary alcohols of HEC decreased compared to those in the spectrum of HMP-functionalized HEC ($DS_{primary\ alcohol}$ ~0.1) (Figure 3-9). In addition, the ratio of the

integrals of the signals $\boldsymbol{\delta}_C$ ~67 ppm to $\boldsymbol{\delta}_C$ ~61 ppm was used to estimate a $DS_{primary\ alcohol}$ of being 0.2 which correlated with the changes observed in the NMR spectroscopy analysis.

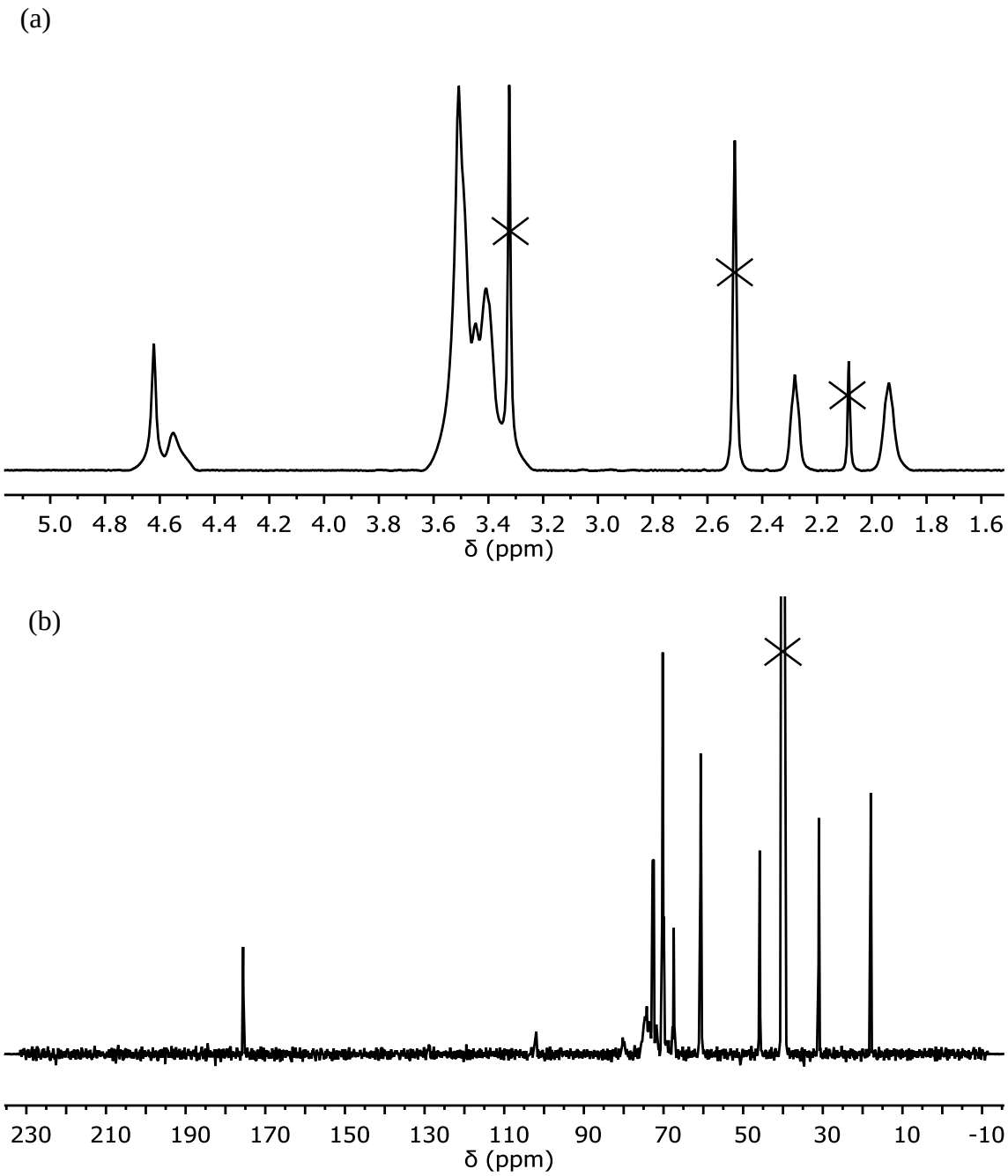


**Figure 3-11:** Solution state NMR spectra of HMP-functionalized HEC (DS ~0.2); (a) $^{1}H$ (700 MHz, DMSO-$d_6$) and (b) $^{13}C$ (176 MHz, DMSO-$d_6$).

With the objective of increasing the $DS_{primary\ alcohol}$, the number of equivalents of HMP per glucose unit was greatly increased in reaction FJ-36 and reaction time was increased to 5 h. However, the calculated DS was again ~0.2 and this implied that the number of equivalents of HMP per glucose unit did not influence the DS in reactions using NMP as solvent. This ceiling in the $DS_{primary\ alcohol}$ can be explained by the presence of two hydrogen bonding networks, where the presence of intramolecular and intermolecular H-bonding in HEC structure could limit the functionalization reaction of HMP to HEC in this solvent.

In order to investigate the integrity of HEC chains under the reaction conditions, HEC was dissolved in the presence of the catalyst in NMP during 17 h at 155 ºC (exp. FJ-73). The samples were characterised using SEC alongside the starting HEC material. The resulting curves are display in Figure 3-12 and both were found to overlay, indicating little or no change to the HEC backbone, containing the stability of the polymers chains of HEC over 17 h at 155 ºC in the presence of catalyst.

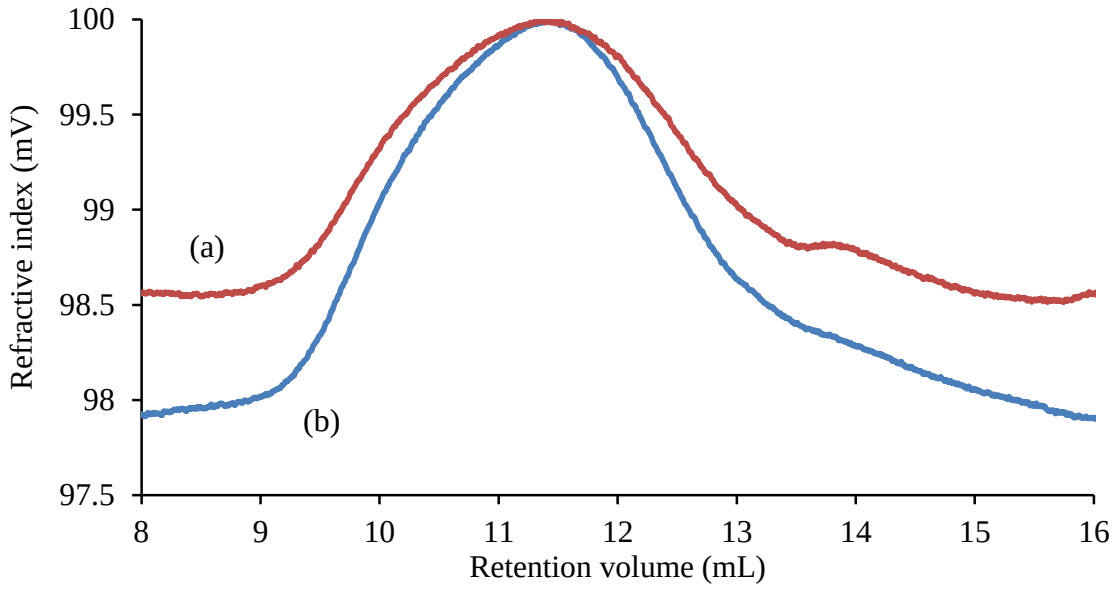


**Figure 3-12:** Results of SEC analysis of (a) HEC and (b) HEC treated at 155 ºC overnight in the presence of 2-amino-2-methyl-1-propanol hydrochloride; plot shown is from RI detection.

To summarise, the influence of the reaction time and the ratio AGU:HMP was evaluated when NMP was used as solvent. The decrease of the reaction time from 17 h to 5 h afforded increased $DS_{primary\ alcohol}$ from 0.1 to 0.2 respectively. However, a further decrease in reaction time to 0.5 h with a $DS_{primary\ alcohol}$ of ~0.2 being achieved after only 30 min. On the other hand, a decreased ratio AGU:HMP did not lead to an increase of the $DS_{primary\ alcohol}$ demonstrating a poor influence of the ratio AGU:HMP over the degree of functionalization of HEC with HMP. The stability of the polymer chains under these conditions was questioned because of the combination of high reaction temperature and the use of a mild acid catalyst. The SEC analysis of HEC before and after being heated in presence of the catalyst at 155 ºC confirmed a lack of degradation. Subsequent investigations were carried out to increase the $DS_{primary\ alcohol}$, where our strategy was based on the use of HMP as both functionalizing agent and solvent.

#### 3.3.1.2.3. Functionalization reaction using 1-(hydroxymethyl)-2-pyrrolidone

HMP is liquid at the reaction temperature of 155 ºC and served as both solvent and functionalizing agent. An AGU:HMP ratio of 1:10 was chosen to provide a less viscous, and eventually homogeneous, reaction system. A series of reactions were performed with varying reaction times of 0.5, 1, 1.5, 2, 5 and 17 h in the presence of the catalyst to determine the influence of reaction time on the degree of functionalization of the primary alcohol group(s) of the HEC backbone. Furthermore, an extra experiment FJ-29 where the catalyst was omitted was performed to evaluate the influence of the catalyst on $DS_{primary\ alcohol}$.

Each sample was characterised using NMR spectroscopy where 2D experiments confirmed the attachment between the HMP moiety and HEC backbone. $DS_{primary\ alcohol}$ were calculated using solution state $^{13}C$ NMR spectra and are summarised in Table 3-3.

**Table 3-3:** DS results for each experiment in a solvent-free reaction

| Exp. Nº | Reaction time (h) | $DS_{primary\ alcohol}$ |
|---|---|---|
| **FJ-41** | 0.5 | 0.1 |
| **FJ-49** | 1 | 0.9 |
| **FJ-251** | 1.5 | 0.9 |
| **FJ-45** | 2 | 0.9 |
| **FJ-21** | 5 | 0.8 |
| **FJ-213** | 17 | 0.3 |

For a reaction time of 30 min, the calculated $DS_{primary\ alcohol}$ was 0.1. This low value is explained by the heterogeneous nature of the reaction mixture. HMP was used as the solvent and its incomplete melting after 30 min created a heterogeneous system. For

reaction times of 1, 1.5 and 2 h, $DS_{primary\ alcohol}$ values of 0.9 were calculated using the solution state $^{13}C$ NMR spectra (Figure 3-13 b) which showed the near-complete disappearance of the signal $\boldsymbol{\delta}_C$ ~61 ppm assigned to the primary alcohols of HEC. In addition, the solid state $^{13}C$ NMR spectrum (Figure 3-13 a) highlighted the near-complete functionalization of HEC with HMP. However, a $DS_{primary\ alcohol}$ value less than 1 indicates either limited accessibility of HMP to the HEC backbone because of H-bonding in the HEC, or the presence of side reactions.

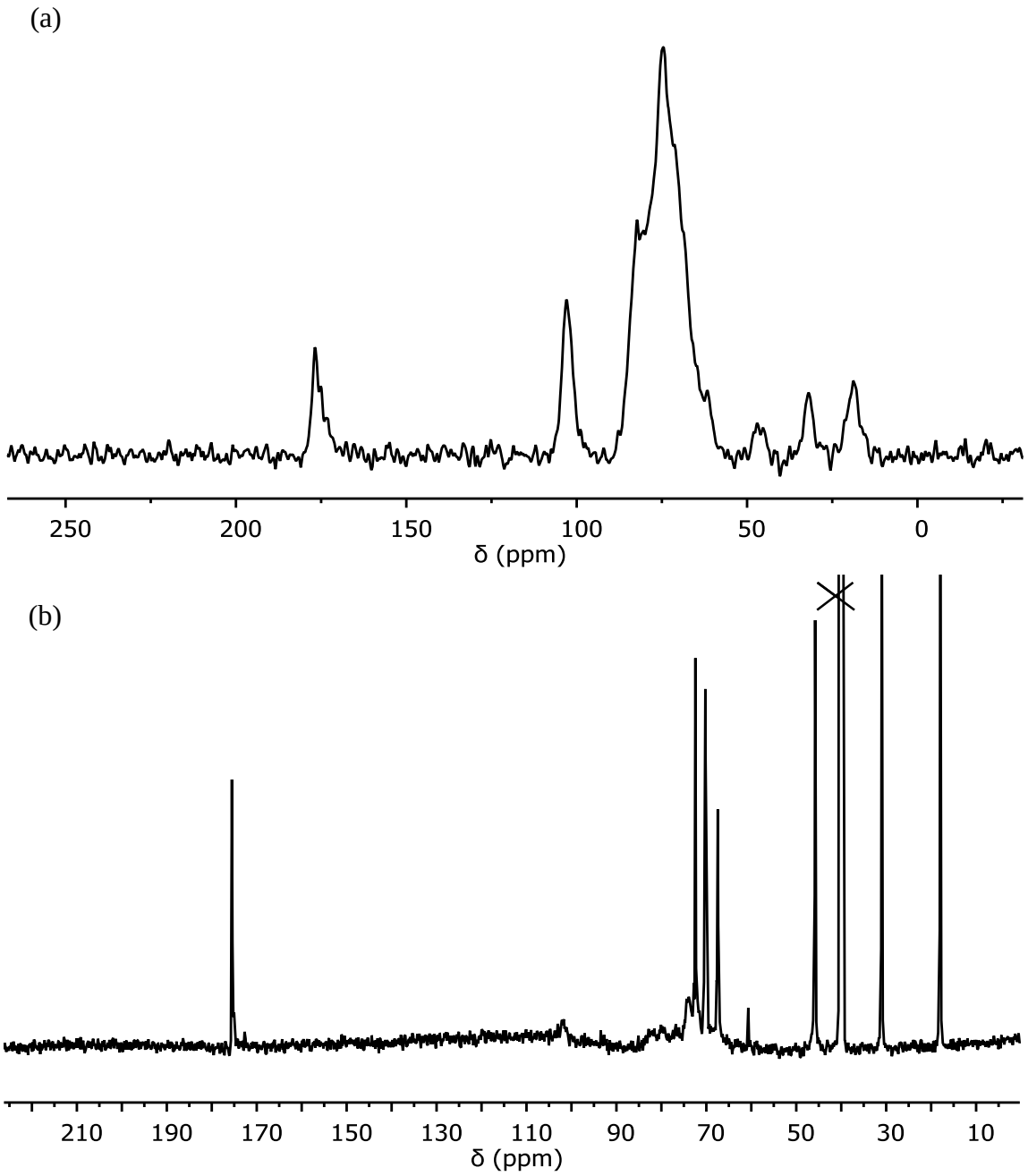


**Figure 3-13:** $^{13}C$ NMR spectra of HMP-functionalized HEC (DS ~0.9); (a) solid state CP-MAS and (b) solution state (176 MHz, DMSO-$d_6$).

For a reaction time of 5 h, a decreased $DS_{primary\ alcohol}$ value of 0.8 was determined and a $DS_{primary\ alcohol}$ of 0.3 was estimated after 17 h. A possible reason of this reduction is the presence of side reactions resulting in the breakage of the linkage between HMP and

HEC. This liberates HMP **2** from the functionalized-HEC material which could decompose into formaldehyde and 2-pyrrolidone **1**. This decomposition reaction is essentially irreversible given that formaldehyde can be lost as a gas from the system (Scheme 3-3) and could be verified, for instance, using NMR spectroscopy proving the presence of 2-pyrrolidone.

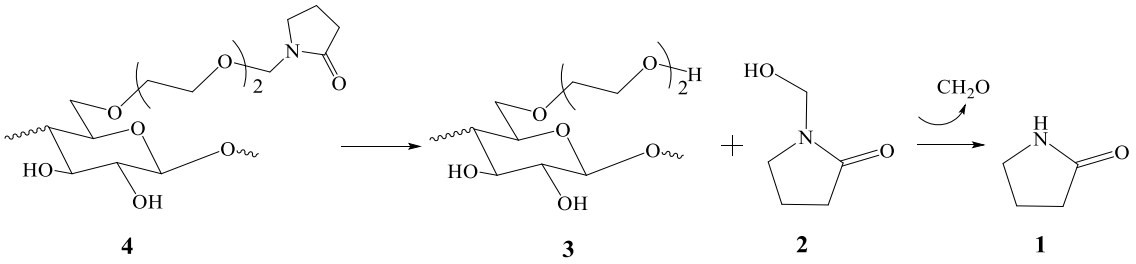


**Scheme 3-3:** Scheme of degradation of HMP-functionalized HEC **4** (DS =1 at C10 position)

Furthermore, the side reactions could potentially lead to the alteration of the integrity of the HEC chains, however the breadth of the HEC backbone NMR signals (Figure 3-13) is a strong indication of the high molecular weight of HMP-functionalized HEC, nonetheless further analysis was performed to probe the integrity of the cellulose backbone following reaction with HMP. HEC of 90 kDa (1 g) after reacting with HMP was dialysed against a 50 kDa membrane and near quantitative mass recovery (~1.5 g) was obtained after lyophilisation. This indicates that the average molecular weight of the recovered HEC is higher than 50 kDa but this experiment did not supress the degradation hypothesis because chains could be effectively degraded to lower average molecular weight from 90 kDa to 50 kDa. However the results of SEC experiments showed in Figure

3-12 demonstrated no major loss of molecular weight after HEC was treated under mild acidic conditions for overnight. Thus we conclude that reaction with HMP did not cause significant degradation of the HEC backbone.

To determine the influence of the catalyst on the efficiency of the reaction, the catalyst was removed for the experiment FJ-29, the ratio AGU:HEC was kept the same as in others experiments and the reaction was performed for 5 h at 155 ºC. A $DS_{primary\ alcohol}$ of 0.1 was calculated whereas a $DS_{primary\ alcohol}$ of 0.8 was reached when using 2-amino-2-methyl-1-propanol hydrochloride. This confirmed the reliance on the catalyst.

To summarise, solvent free reactions enhanced the level of functionalization of primary alcohol(s) with HMP ($DS_{primary\ alcohol}$ ~0.9) after only 1 h of reaction. However, a strong decrease of the $DS_{primary\ alcohol}$ was observed after a reaction time of 3 h suggesting a degradation of HMP-functionalized HEC in HMP and this suggested the reversibility of the functionalization reaction. In addition, the importance of the catalyst was proven because of significant reduction of the $DS_{primary\ alcohol}$ in absence of catalyst and the evidence of the stability of HEC chain under these reaction conditions was further confirmed via a dialysis experiment.

#### 3.3.1.2.4. Conclusion

Our preliminary investigation of the functionalization reaction of HEC with HMP was performed in DMSO permitting the optimisation of the reaction temperature. The reaction takes place at a minimum temperature of 155 ºC, and a $DS_{primary\ alcohol}$ of 0.1 was obtained

after 17 h with a 1:1.5 ratio of AGU:HMP in presence of 2-amino-2-methyl-1-propanol hydrochloride. Owing to the decomposition of DMSO at 155 ºC, NMP was subsequently used as solvent and a $DS_{primary\ alcohol}$ value of ~0.2 was reached after only 0.5 h. The decreased ratio AGU:HMP did not affect DS, however, the use of HMP as solvent and reagent increased considerably the $DS_{primary\ alcohol}$ to a value up to 0.9. The use of the catalyst permitted a near-complete functionalization of the primary alcohol(s) whereas its absence decreased the $DS_{primary\ alcohol}$ to 0.1. Furthermore, the use of an ammonium salt mitigates against the possibility of acid-catalysed polysaccharide chain degradation. HMP, as a formaldehyde-derived system, is more reactive than the sugar-derived glycosidic acetals, where the oxocarbenium ions formed on glycosidic bond cleavage are significantly destabilised by the 2-hydroxy group[69, 70]. More reactive acetal-derived systems are generally susceptible to transformations mediated by weaker general acid species, whereas polysaccharides are unreactive. This idea is borne out in our observation that polysaccharide degradation is not evident from SEC and dialysis experiments.

#### 3.3.1.3. Functionalization reaction of HEC with hydroxyethylol-pyrrolidone

The aim of this experiment was to investigate the functionalization reaction mechanism by attempting to couple hydroxyethylol-pyrrolidone (HEP) **5** to HEC **3** (Scheme 3-4). In term of structure, an ethylene group in HEP replaces a methylene in HMP. The presence of the two methylene groups on the side chain of HEP provides a different reactivity due to the absence of resonance effects between the nitrogen and alcohol. The reaction between HEP and HEC was based on the same procedure for that of HMP-functionalized

HEC ($DS_{primary\ alcohol}$ ~0.9). The product **6** was further characterised using solution state NMR spectroscopy.

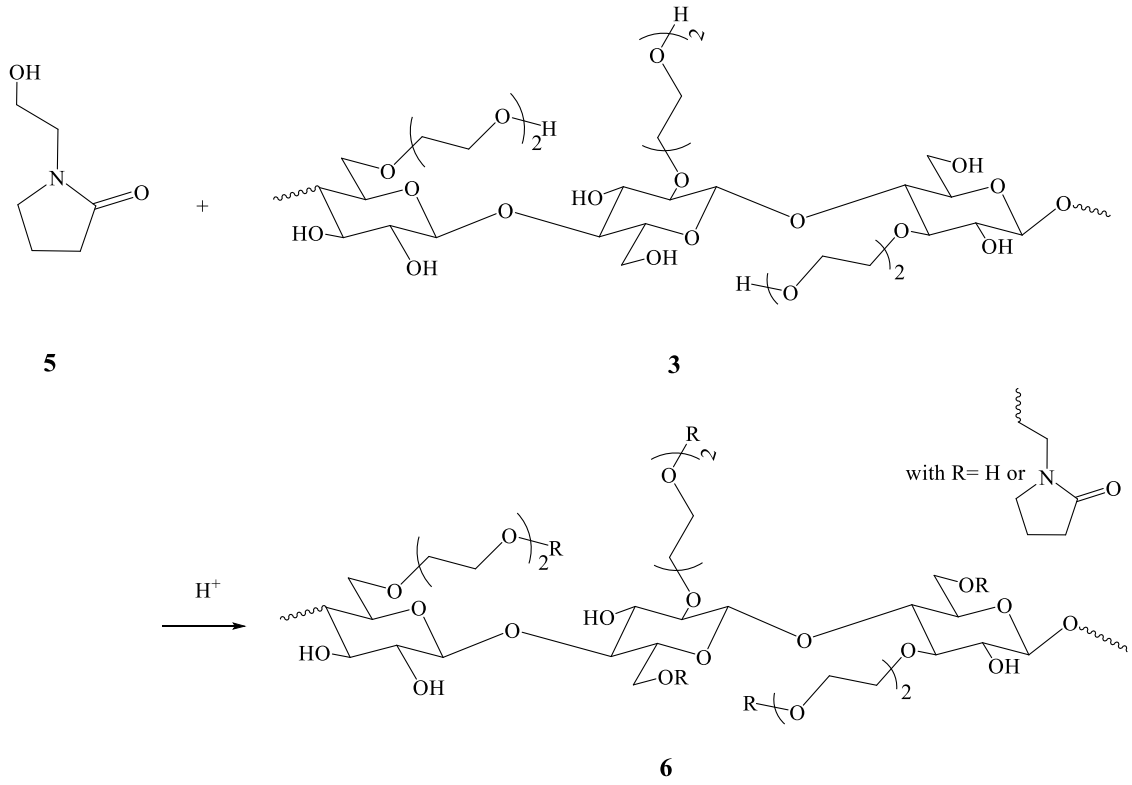


**Scheme 3-4:** Functionalization of HEC **3** with hydroxyethylol-pyrrolidone **5**

An $^{1}H$ NMR spectrum (Figure 3-14 a) demonstrated the presence of HEC with signals $\delta_H$ ~3.4-3.5 ppm assigned to the ethylene oxide side chain of HEC, but did not show signals characteristic of HEP leading us to conclude that functionalization of HEC with HEP was unsuccessful. This was also confirmed with the $^{13}C$ NMR spectrum (Figure 3-14 (b)) which does not contain signals of HEP, but only those of HEC were detected. The absence of reactivity between HEC and HEP suggested a reaction mechanism for preparing HMP-functionalized HEC which relies on the resonance effects of HMP. The catalyst, 2-amino-2-methyl-1-propanol hydrochloride protonates the hydroxyl group of HMP which is eliminated as a water molecule due to effect of resonance. This results in the formation

of an iminium ion which reacts with the primary alcohol(s) of HEC. The summary of this mechanism is presented in Scheme 3-5.

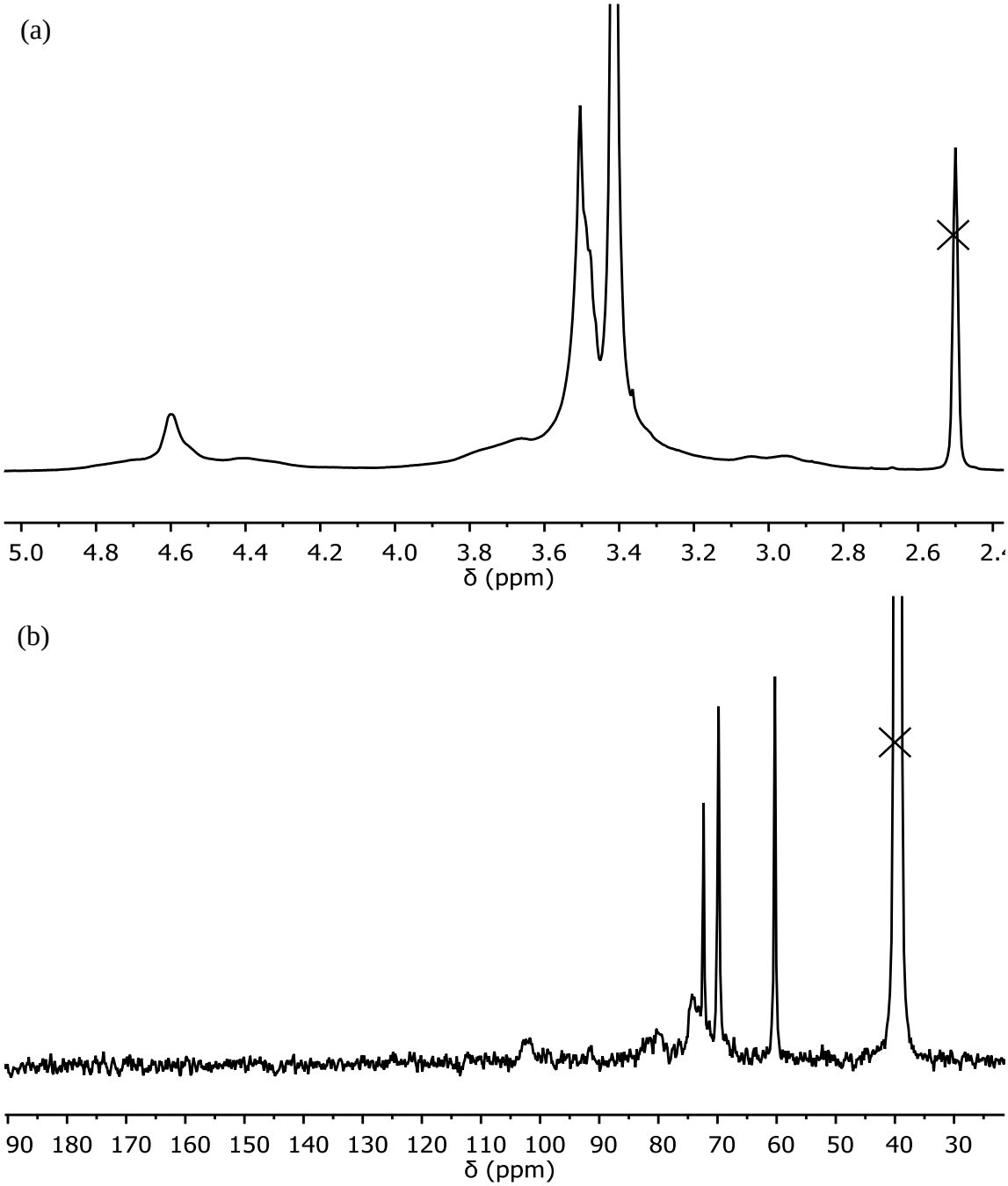


**Figure 3-14:** Solution state NMR spectra of product **6;** (a) $^{1}H$ (400.13 MHz, DMSO-$d_6$) and (b) $^{13}C$ (100.62 MHz, DMSO-$d_6$).

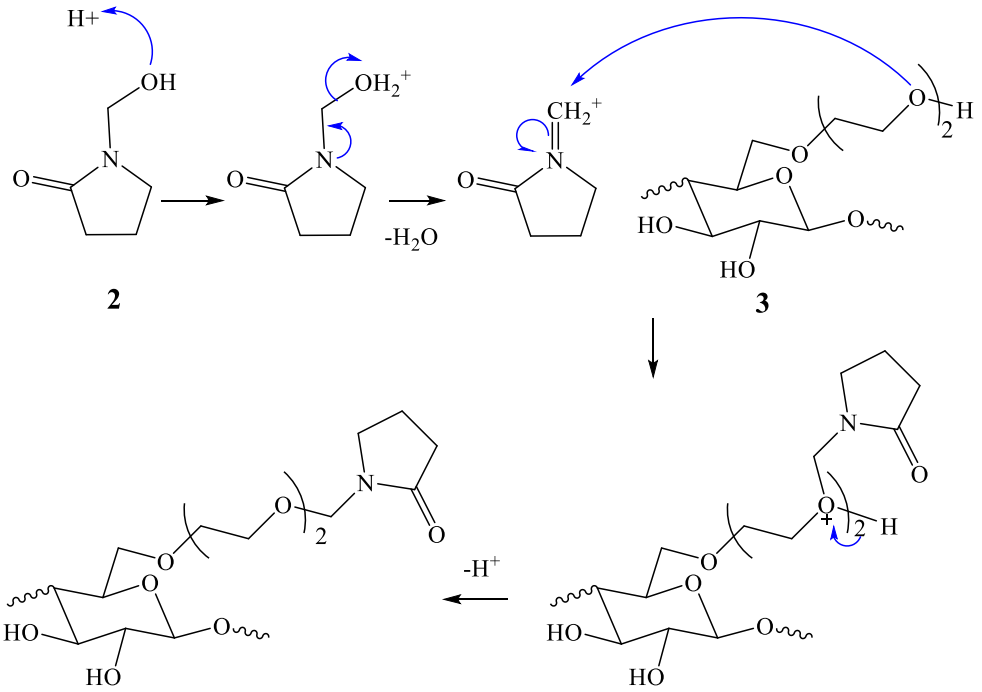


**Scheme 3-5:** Reaction mechanism scheme for the reaction between HMP **2** and HEC **3** (DS =1 at C10 position)

## 3.3.2. Evaluation of physical properties

The physical properties of HMP-functionalized HEC with a $DS_{primary\ alcohol}$ of ~0.9 were evaluated in comparison to unmodified HEC. Solubility, viscosity, thermal stability, dye release and bacteriological effects were investigated.

### 3.3.2.1. Solubility

The solubility of the HMP-functionalized HEC ($DS_{primary\ alcohol}$ ~0.9) was tested and compared to the unfunctionalized material, HEC. A concentration of 10 mg/mL of cellulosic material was chosen. The results of the tests are summarised in Table 3-4.

HEC, which is not soluble in organic solvents, became soluble or swelled in these same organic solvents such as DMF, DCM and EtOH after functionalization with HMP. HMP contains a lactam group which represents the key moiety of poly(N-vinylpyrrolidone) (PVP). PVP is well-known for its solubility in both aqueous and organic solvents due to its amphiphilic character. The introduction of lactam groups onto HEC could lead to the development of an amphiphilic derivative of HEC which could see its uses extended in industrial applications.

**Table 3-4:** Results of the solubility testing for HEC and HMP-functionalized HEC ($DS_{primary\ alcohol}$ ~0.9)

| Solvents | HEC | HMP-functionalized HEC |
|---|---|---|
| **Water** | + | + |
| **dimethyl sulfoxide** | + | + |
| **dimethylformamide** | s | + |
| **cyclohexane** | - | S |
| **Dioxane** | - | S |
| **butanone** | - | - |
| **Ethanol** | - | S |
| **dichloromethane** | - | + |
| **propan-2-ol** | - | S |
| **chloroform** | - | + |
| **Toluene** | s | S |
| **diethyl ether** | - | - |

s, swelling; +, soluble; -, insoluble

### 3.3.2.2. Dye release study

HEC is used in the preparation of pharmaceutical tablets as a binder because of its biocompatibility and biodegradability, however, the modification of HEC with HMP

could affect the release profile of the active molecule from such a tablet. Therefore, the dye-release test was undertaken to simulate the release of a drug from a tablet prepared from HEC and HMP-functionalized HEC ($DS_{primary\ alcohol}$ ~0.9). A water soluble dye, rhodamine B was used as a model drug and tablets were prepared using a KBr press. The dye release was evaluated as a function of time and is shown in Figure 3-15.

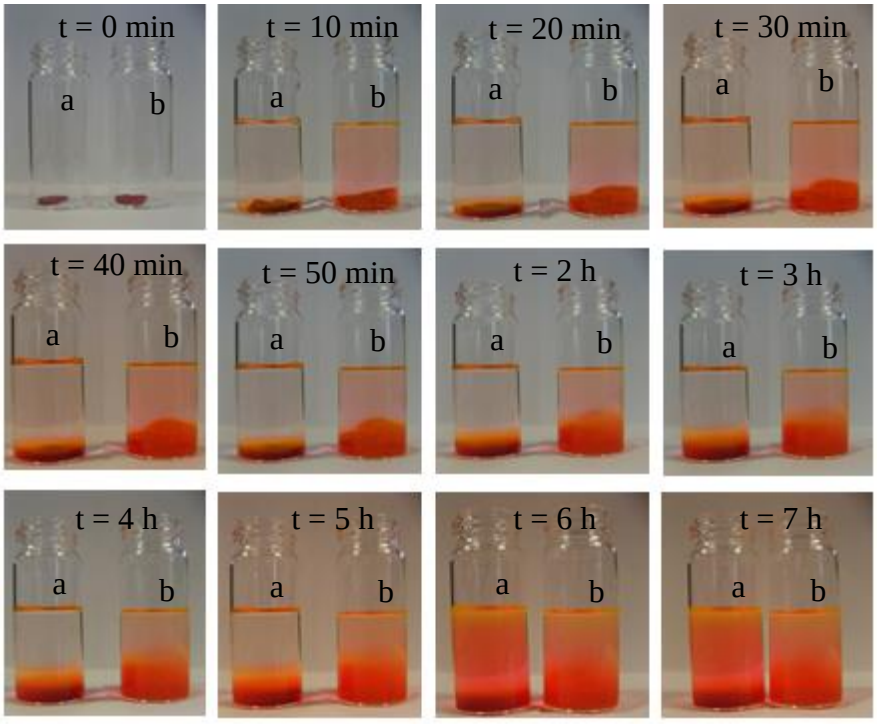


**Figure 3-15:** Results of the swelling test of (a) HEC and (b) HMP-functionalized HEC (DS ~0.9) using rhodamine B

The dye contained in the unmodified HEC disc was released into water, indicating the beginning of the disintegration of the disc. The dye diffusion started from the bottom of the vial where the HEC disc was located, leaving the top of the vial clear. The diffusion of the dye increased slightly during the first hour. Over the following hours, an increase

of the dye diffusion was continuously observed with disc disintegration. After 6 h, the entire aqueous solution contained the dye and the disc had completely disintegrated. However, the colour effect suggests a gradual dye concentration decrease from the bottom to the top of vial. A homogeneous concentration in the vial may be achievable with a longer experiment time or stirring.

Regarding HMP-functionalized HEC, the disc swelled continuously with time in water. The dye contained in the centre of the disc was not released, highlighting the swelling of the disc, however, the dye at the surface was released and diffused completely into the water. The swelling of the disc increased rapidly during the first hour without dye release into the water. After 2 h, the gel-like disc started to release the dye, and, over the following hours, the swollen disc decomposed. The dye was then released and diffused through the water. At 6 h, the observations were similar to the HEC disc with a gradual change in dye concentration through the solution.

HMP functionalization clearly affected the dye release properties of HEC. The introduction of HMP to HEC was expected to interrupt the H-bonding network, resulting in increased water solubility. Furthermore, the polarity of the amide group of HMP may further improve the solubility of functionalized HEC in water as well as in polar organic solvents, compared to HEC. However, HMP also presents a partial hydrophobic character due to the presence of the lactam ring. The bonding of HMP to HEC may cause an increase of HEC hydrophobicity (estimated log P of N-methyl-pyrrolidone ranges from −0.38 to −0.57[71]). The hydrophobic/hydrophilic properties could explain the tendency of the functionalized HEC to swell in water during the first hour and subsequent dissolution.

### 3.3.2.3. Thermal stability

The thermal stability was studied for determining the range of temperatures over which HMP-functionalized HEC can be processed and/or used without any degradation. The weight losses on heating of HMP-functionalized HEC ($DS_{primary\ alcohol}$ ~0.9) and HEC as a function of temperature are recorded in Figure 3.16. HEC (Figure 3-16 a) lost ~5% of weight between 20 °C and 70 °C due to the loss of water after which its weight remained stable from 70 to 200 °C indicating its thermal stability over this temperature range. However, weight loss increased sharply above 210 ºC indicating the beginning of HEC decomposition. At 300 ºC, a weight loss of 40% was measured. Regarding the functionalized HEC (Figure 3-16 b), a slight loss of weight (~3%) was observed from 20 °C to 70 °C indicating the presence of moisture contained in the material, however its weight was relatively stable over the temperature range 70 ºC to 210 ºC. From 250 °C, the functionalized HEC started to show a very slight weight loss, however, at 300 ºC, the functionalized HEC had lost only ~4% of its weight.

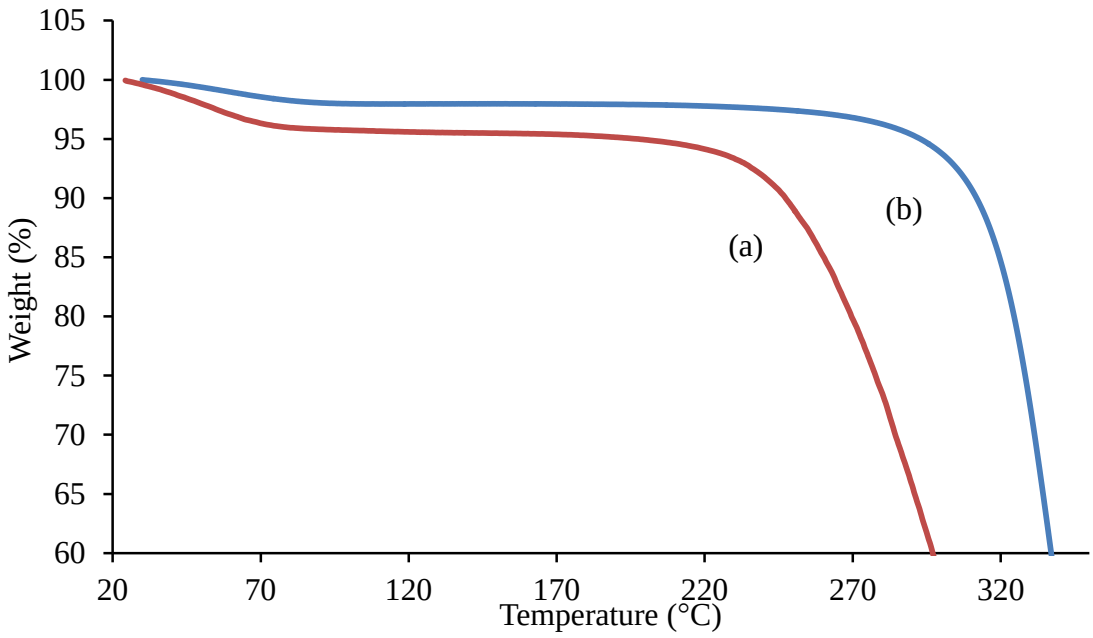


**Figure 3-16:** Evolution of weight loss as a function of temperature by TGA (a) HEC and (b) HMP-functionalized HEC ($DS_{primary\ alcohol}$ ~0.9)

The measured weight loss at 300 ºC of the functionalized HEC was ten times less than that of the HEC material. The functionalization of HEC with HMP therefore generated a more thermally stable polymer compared to unfunctionalized HEC due to the increase of the molecular weight of HMP-functionalized HEC compared to unmodified HEC. This provides another piece of evidence concerning the integrity of the HEC chains, which corroborates with the results of our previous studies. In fact, significant degradation of HEC backbone should result in the loss of thermal stability because of a decrease of the average molecular weight of HEC, however an increase of the thermal stability was demonstrated compared to the parent HEC. HMP-functionalized HEC can be used and/or processed for desirable industrial applications over a broader range of temperature than HEC.

### 3.3.2.4. Viscosity measurement

The measured dynamic (absolute) viscosities for HEC and functionalized HEC were respectively 453.1 and 15.6 mPa.s. The viscosity of functionalized HEC is approximately 30 times lower compared to that for HEC and this cannot due to a possible degradation of HEC backbone. In fact, the integrity of HEC chains remains under the reaction conditions that were used to functionalize HEC with HMP and this was demonstrated using SEC (Figure 3-12). The introduction of the lactam group into HEC causes both the breaking of the H-bonding network and an increase in the distance between HEC chains. As a consequence, the water accessibility into the structure is improved, the solubilisation of functionalized HEC is enhanced, and this, in turn, causes the drastic viscosity reduction.

### 3.3.2.5. Bacteriological testing

Cellulosic materials are widely used in regenerative tissue culture, drug delivery, personal care, cellular immobilization and wound healing applications[72, 73]. The adherence of bacteria to such surfaces can lead to the establishment of infections and the formation of complex biofilms that hinder treatment. A plausible route to reduce the risk of infections is to chemically modify material surfaces, where the modified surfaces could result in the death and/or the reduced adhesion of bacteria. For instance, the presence of cationic molecules such as imidazolium groups is known to kill bacteria[74]. In 2007, Cheng *et al.*[75] investigated the anti-adhesion properties of bacteria on zwitterionic surfaces which are produced via Atom Transfer Radical Polymerisation (ATRP) of N-(3-sulfopropyl)-N-(methacryloxyethyl)-N,N-dimethylammonium betaine from gold particles. The reduction

in bacterial adhesion was most evident with zwiterrionic and hydrophilic/neutral polymers, with both Gram-positive and Gram-negative bacteria behaving in a similar fashion. It was anticipated that the introduction of lactam groups would confer dipolar properties to HEC and thus could enhance its anti-adhesion properties against bacteria. The influence of the HMP-functionalization of HEC on bacterial viability, growth and adhesion was therefore examined using representative Gram-negative (*E. coli*) and Gram-positive (*S. aureus*) strains to investigate bacterial selectivity.

For the viability and growth experiments, a solution in water of HEC and HMP-functionalized HEC was added to a 96-well microplate containing bacteria grown to an $A_{650nm}$ of approximately 0.25. Growth was recorded as a function of time for both *E. coli* and *S. aureus* (Figure 3-17 a & b). For anti-adhesion testing, filter paper was impregnated with a solution containing either HEC or HMP-functionalized HEC; sterile water was used as a control. Cultures of *E. coli* and *S. aureus* in mid-logarithmic phase ($A_{650nm}$ 0.4) were applied to the surface of the paper and the adhered bacteria were recovered after 24 h at 37 °C. Serial ten-fold dilutions of the recovered bacteria were prepared and spotted onto an agar plate (Figure 3-18). The plate was incubated and bacterial recovery was evaluated visually by counting colonies at appropriate dilutions (Table 3-5).

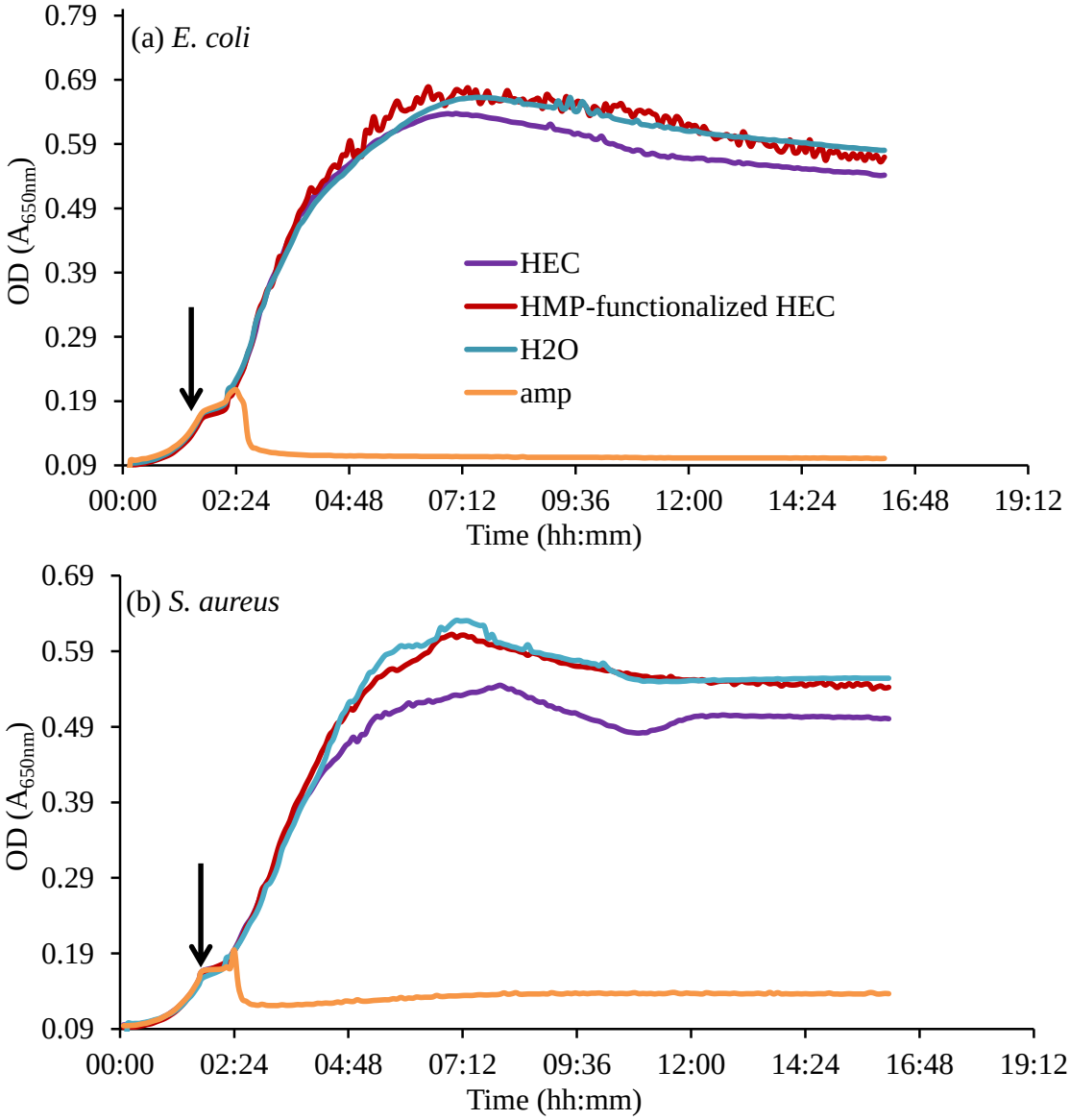


**Figure 3-17:** Growth of *E. coli* and *S. aureus* as a function of time after addition (indicated by arrows) of solutions containing HEC, HMP-functionalized HEC ($DS_{primary\ alcohol}$ ~0.9), water ($H_2O$) and ampicillin (amp)

For *E. coli*, the growth and viability (as judged by optical density) of the bacteria (Figure 3-17 a) were largely unaffected by the presence of HEC and HMP-functionalized HEC solutions indicating that these materials lack bactericidal properties. Regarding anti-adhesion properties (Figure 3-18 a & Table 3-5), the number of recovered bacteria from

the filter paper treated with water (Figure 3-18 i (b)) was slightly lower ($1.0 \times 10^7$ cfu/mL) than that coated with functionalized HEC ($1.36 \times 10^7$ cfu/mL), whereas a significantly larger number of bacteria were recovered from samples treated with HEC ($1.96 \times 10^8$ cfu/mL). *E. coli* therefore adhered most strongly to the control filter paper (treated with water). HEC treatment (Figure 3-18 i (c)) significantly enhanced the bacterial anti-adhesion properties of the paper with a 20-fold increase in recovery of bacteria and enhanced the growth of bacteria with a 2-fold increase of recovered bacteria compared to the control ($7.2\times10^{-7}$ CFU/mL) which represents the number of deposited bacteria on the surface. The functionalized HEC treated paper (Figure 3-18 i (d)) showed considerably reduced anti-adhesion properties, with only a 1.4-fold increase in the number of bacteria recovered relative to the paper treated with water.

For *S. aureus,* the viability and growth (Figure 3-17 b) was unaffected following the addition of a solution containing HMP-functionalized HEC. HEC did reduce the bacterial density as cells entered the stationary phase of growth compared to HMP-functionalized HEC, although the results are similar to those seen with *E. coli* (Figure 3-17 a). In anti-adhesion experiments (Figure 3-18 ii & Table 3-5), the number of recovered bacteria from the paper treated with the solution of HMP-functionalized HEC (Figure 3-18 ii (d)) was the highest ($8.3 \times 10^4$ cfu/mL) compared to those treated with water ($5.4 \times 10^3$ cfu/mL) or with the HEC solution (0 cfu/mL). For the paper treated with HEC (Figure 3-18 ii (c)), bacteria were not recovered indicating complete adhesion of *S. aureus* to the paper since HEC does not show any significant bactericidal effects (Figure 3-17). In the case of *S. aureus*, the chemical modification of HEC with HMP clearly improved the anti-adhesion properties relative to the unfunctionalized HEC.

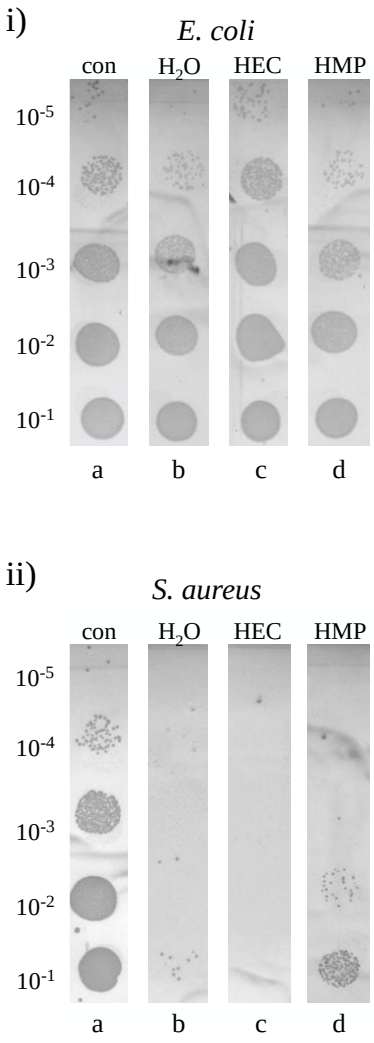


**Figure 3-18:** Adhesion testing of i) *E. coli* ii) *S. aureus* monitoring the recovery of viable bacteria from filter paper pre-treated with (b) $H_2O$, (c) HEC, and (d) HMP-functionalized HEC ($DS_{primary\ alcohol}$ ~0.9). A control sample (a) not exposed to filter paper was also tested.

**Table 3-5:** Recovery of bacteria from filter papers treated with water, HEC and HMP-functionalized HEC ($DS_{primary\ alcohol}$ ~0.9)

| | | cells/mL | SD | fraction recovered |
|---|---|---|---|---|
| ***E. coli*** | control | $7.2 \times 10^7$ | $1.6 \times 10^7$ | 1.0 |
| | $H_2O$ | $1.0 \times 10^7$ | $4.0 \times 10^5$ | 0.14 |
| | HEC | $1.4 \times 10^8$ | $1.2 \times 10^7$ | 1.9 |
| | HMP | $1.9 \times 10^7$ | 0 | 0.27 |
| ***S. aureus*** | control | $2.4 \times 10^8$ | $8.0 \times 10^7$ | 1.0 |
| | $H_2O$ | $5.4 \times 10^3$ | $1.4 \times 10^3$ | $2.2 \times 10^{-5}$ |
| | HEC | 0 | 0 | 0 |
| | HMP | $8.3 \times 10^4$ | $1.0 \times 10^3$ | $3.5 \times 10^{-4}$ |

In summary, the anti-adhesion testing reveals a marked difference in the behaviour of HEC and HMP-functionalized HEC between the two bacterial species. This difference may be due to altered hydrophobicity, one of the criteria influencing bacterial adhesion. In fact, bacterial adhesion depends on surface properties, including roughness, charge, hydrophobicity and chemical composition, the hydrophobicity and charge of the bacterial envelope and other surface structures[76]. Bacteria with a hydrophobic exterior will adhere preferentially to hydrophobic substrates, whereas bacteria with hydrophilic surfaces favour hydrophilic materials[77]. The *E. coli* bacteria used in this study present a predominantly negatively-charged, hydrophilic surface composed of lipopolysaccharides and outer membrane proteins, whereas *S. aureus*, although possessing a negatively-charged surface composed of peptidoglycan, teichoic acids and surface proteins, is radically different in character[78]. The filter paper treated with water presents a more hydrophilic surface with a larger surface area than that treated with HEC, hence the adhesion of *E. coli* increased slightly, whereas almost all of the *S. aureus* cells were retained. Treatment with a solution containing HEC appears to increase the hydrophobicity of the paper and reduces bacterial adhesion by *E. coli* and increases

adhesion by *S. aureus*. Introduction of lactam groups onto HEC decreases its hydrophobic character and improves bacterial adhesion by *E. coli* but significantly decreases bacterial adhesion by *S. aureus*, reflecting the differences in the cell envelope architecture in these bacteria.

## 3.4. CONCLUSION

Our strategy to introduce lactam groups onto a cellulosic material *via* the functionalization of HEC with HMP was found to be highly efficient. The synthesis of the functionalizing agent, HMP **1**, gave reproducibly high yields. The modification of HEC with HMP was investigated in different media. However, the highest degree of functionalization was reached in a solvent free reaction when HMP acted as both functionalizing agent and solvent resulting in the preparation of HMP-functionalized HEC with $DS_{primary\ alcohol}$ of ~0.9. The incomplete functionalization of the primary alcohols of HEC is consistent with the particular structure of the cellulose, notably the presence of intramolecular and intermolecular hydrogen bonding which block the accessibility of the primary alcohols to the functionalizing agent. The conditions of the modification reaction with HMP have been shown not to lead to any significant degradation of the cellulose backbone. The lactam-functionalized HEC gave faster the dye release compared to unfunctionalized HEC. Moreover, the viscosity of the lactam-functionalized HEC decreased while the thermal stability increased compared to unmodified HEC. Furthermore, bacteriological assays revealed an increase in bacterial adhesion by *E. coli* and, reciprocally, a decrease in adhesion of *S. aureus* to lactam-functionalized HEC in comparison to unfunctionalized HEC. This can be explained by both the breakage of the hydrogen bonding network and the introduction of the lactam

groups which enhance the material's hydrophilicity and has contrasting effects depending on the nature of the bacterial envelope surface. The HMP-functionalized HEC could be used as a controlled drug delivery system and as a coating which is more thermally stable than the parent HEC and can prevent the adhesion of bacteria of Gram-positive. Overall, the modification of HEC did not lead to new applications but added a considerable value to the use of a cellulosic material in industry because of the alteration of its properties (solubility, viscosity and thermal stability).

# Chapter 4: "Grafting from" approach for preparing graft-copolymers of hydroxyethyl cellulose

## 4.1. INTRODUCTION

This chapter details the preparation of well-defined graft-copolymers of hydroxyethyl cellulose (HEC) using a "grafting from" approach. During the last decade, the most investigated reversible-deactivation radical polymerisation (RDRP) technique for preparing well-defined cellulose-based graft-copolymers has been Atom Transfer Radical Polymerisation (ATRP) and this has been reviewed by the author in the article entitled "*The Preparation of Graft Copolymers of Cellulose and Cellulose Derivatives Using ATRP Under Homogeneous Reaction Conditions*"[79] which was arranged into sections based on the parent cellulose derivative undergoing chemical modification. Cellulose (Cell), ethyl cellulose (EC) and hydroxypropyl cellulose (HPC) have received most attention as materials for the graft-copolymerisation of various monomers, including methyl methacrylate[80-82], N-isopropylacrylamide[83-85] and styrene[86, 87] (Table 4-1). The graft-copolymerisation process involves principally two steps. The first is the preparation of macro-initiators characterised using DS which determined the graft-density of graft-copolymers. The second step is the use of macro-initiators for initiating the ATRP process of various monomers, resulting in the formation of graft-copolymers of cellulose and cellulose derivatives. The efficiency of the polymerisation was highlighted using the monomer conversion (%) which permitted the determination of the chain length, and the control of the polymerisation was evaluated measuring $Đ_M$. The main purpose of the grafting was to create amphiphilic hybrid materials which could self-assemble into nanoscale species and/or which possess stimuli-responsive properties. These materials

are being considered for applications in biotechnology given their cost effectiveness and their largely renewable origin.

As discussed in Chapter 2 (section 3.1.), the monomer N-vinylpyrrolidone (NVP) has been polymerised onto cellulose and cellulose derivatives using free radical and anionic polymerisation, however, its controlled polymerisation *from* cellulose and derivatives has not been yet reported. ATRP of NVP has been investigated in solution and from surfaces. The ATRP was initiated from modified silicon[88] and gold[89] surfaces and the control of the polymerisation was proven by determining the homogeneity of the surface using surface characterisation technique such as X-ray photoelectron spectroscopy (XPS), reflectance FT-IR and water contact angles. The thickness of the PVP layer was up to 15 nm from the silicon wafers whereas only 5 nm was generated from the gold surface. In solution[90], NVP has been successfully polymerised from methyl-2-propionate chloride with a conversion up to 65% after 3 h, and a narrow molecular weight distribution ($Đ_M$ =1.1-1.2) was obtained. Furthermore, Mishra *et al.*[91] reported the use of glucose which had been prior-modified into an initiator via the derivatization of the alcohol groups with an alkyl bromide for initiating the polymerisation leading to the formation a five-arm star structure.

In order to satisfy Ashland requirements, ATRP of NVP from HEC was investigated as a novel strategy for introducing lactam groups onto cellulosic materials. In parallel, we were also interested in developing the antibacterial properties of cellulose materials because of the use of cellulose in biomedical applications[92, 93]. In Chapter 3 we showed that the introduction of lactam groups onto HEC affected only the adhesion of bacteria, subsequently we were not expecting that the graft-copolymer, HEC-g-PVP, to present any bactericidal properties. However, the introduction of cationic polymers onto HEC should lead to the preparation of bactericidal graft-copolymers. Tatsuo Tashiro[94] and,

more recently, Muñoz-Bonilla[95], reviewed the advances in the preparation of antibacterial polymers which contain, for instance, quaternary ammonium salts, biguanide groups, quaternary pyridinium salts, phosphonium or sulfonium salt, and these functional groups lead to the death of bacteria. A new class of monomers, ionic liquid monomers (IL), which include vinylimidazolium, (methyl)acryloyl and styrene-based ILs (Figure 4-1) have been recently developed and present promising properties such as high thermal stability, high ionic conductivity, low vapour pressure and bactericidal effects[96-98].

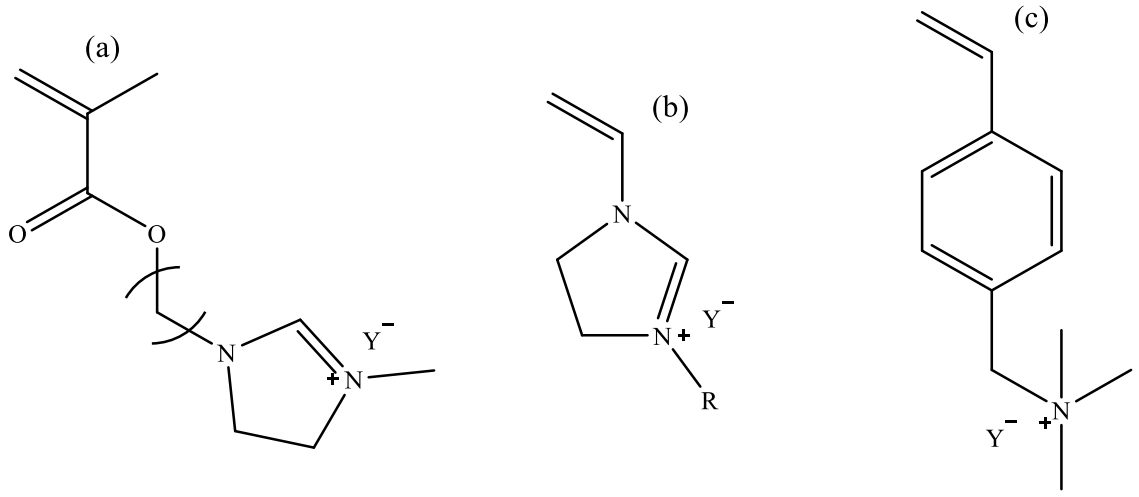


**Figure 4-1:** Ionic liquid monomer structure (a) acryloyl-, (b) vinyl-imidazolium- and (c) styrene- based IL

ILs have been successfully polymerised using conventional free radical polymerisation[99] and RDRP techniques such as ATRP[100-102] and RAFT[103, 104]. Thus, the ATRP of an acryloyl-based IL, 1-(11-acryloyloxyundecyl)-3-methylimidazolium bromide, which has

to be prior-synthesised, was investigated in order to prepare bactericidal HEC-based graft-copolymers.

**Table 4-1:** Graft-copolymers of cellulose and cellulose derivatives arranged in chronological order of date of publication[79]

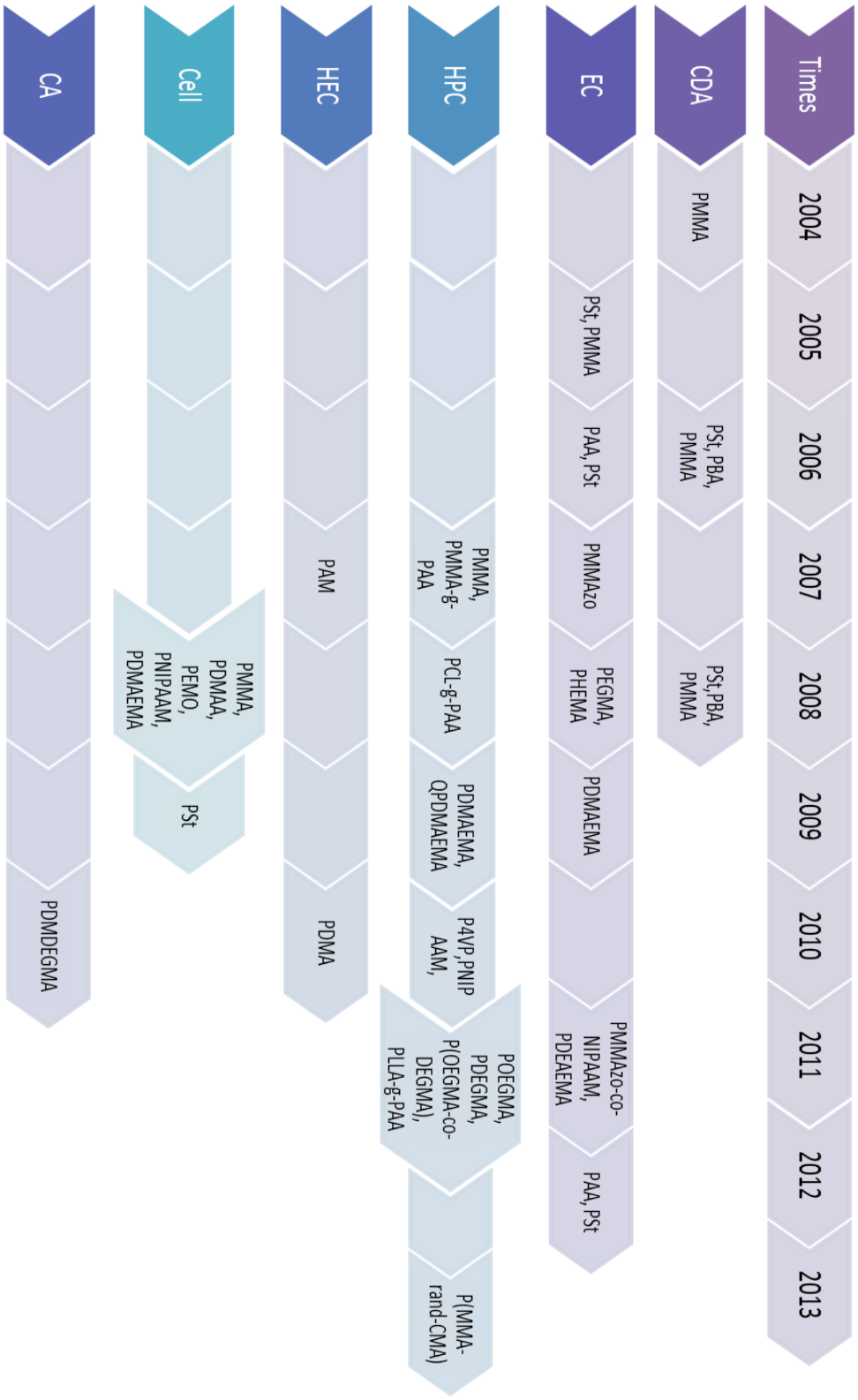

## 4.2. EXPERIMENTAL

### 4.2.1. Materials

2-Hydroxyethyl cellulose (HEC) ($M_w$ =90 kDa, MS =2.5), HEC ($M_w$ =250 kDa, DS =1, MS =2), collidine, triethylamine (TEA), 2-bromoisobutyryl bromide, copper (I) bromide (CuBr), methyl methacrylate (MMA), N,N,N′,N′-tetramethylethylenediamine (TMEDA), N-vinylpyrrolidone (NVP), 11-bromo-1-undecanol, *p*-toluene sufonic acid, monomethyl ether hydroquinone (MEHQ), acrylic acid, 1-methylimidazole, dimethyl sulfoxide (DMSO), potassium hydroxide (KOH) and sodium hydroxide (NaOH) were purchased from Sigma Aldrich. Dichloromethane (DCM), chloroform, tetrahydrofuran (THF), methanol, 1 M solution hydrochloride, toluene, acetone, cyclohexane and diethyl ether were supplied from Fisher Scientific and the deuterated solvent, DMSO-$d_6$ was purchased from Apollo Scientific.

### 4.2.2. Characterisation techniques

For solid state $^{13}C$ NMR spectroscopy, a Varian VNMRS spectrometer with a 9.4 T magnet was used at 100.56 MHz employing the cross polarisation method. Solution state NMR spectroscopy was performed using a Bruker Advance 400 spectrometer at 400.13 MHz ($^1H$) and 100.60 MHz ($^{13}C$). IR spectra were recorded on a Perkin-Elmer 1600 Series FT-IR spectrometer. Elemental analyses were performed using an ULTIMA 2ICP optical emission spectrometer. Size Exclusion Chromatography (SEC) was performed on a Viscotek TDA 302 complete with a GPCmax autosampler where refractive index,

viscosity and light scattering detectors were used to determine the number average molecular weight ($M_n$) and dispersity ($Đ_M$). A value of 0.08 mL/g[105] was used for the d*n*/ d*c* of PMMA, 2 × 300mm PLgel 5 µm mixed C columns were used with a linear range of molecular weight from 200 to 2 000 000 g/mol and THF was used as the eluent with a flow rate of 1.0 mL/min at 35 ºC.

## 4.2.3. Synthesis and characterisation

### 4.2.3.1. Preparation of the macro-initiators: Br-HECs

In a one-necked, round-bottomed flask, 2-hydroxyethyl cellulose (HEC) **1** (4.8 g, 1 eq.) and a base; either collidine or triethylamine (2 eq.) were mixed in dry dichloromethane (DCM) (80 mL). The mixture was cooled to 0 ºC and 2-bromoisobutyryl bromide **2** (2 eq.) was added carefully. The reaction was carried out at room temperature for 24 h. The mixture was filtered and the solid residues were washed with acetone (200 mL). The product was dried overnight under vacuum at 40 °C. Finally, unreacted 2-bromoisobutyryl bromide was removed from the product by Soxhlet extraction using chloroform for 48 h. The product **3** was then dried under vacuum at 40 °C and was obtained as a white powder. The influence of the atmosphere, the molecular weight and molar substitution (MS) of HEC, and the choice of the base on the degree of the substitution (DS) were investigated; Table 4-2 summarises the different reaction conditions, yield (%) and mass recovery (g).

Samples were characterised using solid state $^{13}C$ CP-MAS NMR and FT-IR spectroscopies and the content of bromine was determined using elemental analysis and to estimate the DS.

### 4.2.3.2. Preparation of HEC-graft-poly(methyl methacrylate)

#### 4.2.3.2.1. Synthesis

In a two-necked, round-bottomed flask, CuBr (0.1 g, $6.9\times10^{-4}$ mol, 1 eq.) and a magnetic stirrer bar were degassed three times by freeze-pump-thaw cycling. MMA **4** (125 eq., 30 eq., 15 eq. and 12 eq.), TMEDA (0.2 mL, $1.3\times10^{-3}$ mol, 2 eq.) and DMSO (10 mL) were added and the resulting mixture was degassed three times. Under $N_2$, the mixture was heated to 90 °C and the macro-initiator Br-HEC **3** (DS ~0.3 or 0.7, 0.2 g, 1 eq.) was then added. The reaction was run overnight. Once cooled to room temperature, the polymer **5** was isolated by precipitation using chloroform. The polymer was then dried overnight under vacuum at 40 °C. The polymer was obtained as a light blue powder. Products were characterised using solid state $^{13}C$ CP-MAS NMR and FT-IR spectroscopies.

Different degrees of MMA polymerisation (DP) and DS for the macro-initiator Br-HEC were chosen and these are summarised in Table 4-4.

#### 4.2.3.2.2. Cleavage of PMMA chains

The procedure followed that reported in the literature[106, 107]. In a round-bottomed flask, sample FJ120 (1 g) was mixed in THF (80 mL) and a 1 M KOH solution in methanol (40 mL) was added. The reaction was run for 3 days at room temperature. A 1 M solution of hydrochloric acid (30 mL) was added and the solvents were removed by rotary evaporation. Toluene (30 mL) was added to ensure the dissolution of the PMMA chains. The solution was then filtered. The PMMA grafts were precipitated in to petroleum ether,

solids were collected by filtration and dried overnight under vacuum at 40 °C. The PMMA chains were characterised using SEC.

#### 4.2.3.3. Preparation of HEC-graft-poly(N-vinylpyrrolidone)

In a two-necked, round-bottomed flask, N-vinylpyrrolidone **6** (13.40 mL, 1.2 mol, 400 eq.), CuBr (0.35 g, $2.5\times10^{-3}$ mol, 1 eq.) and TMEDA (370 µl, $3\times10^{-3}$ mol, 2 eq.) were dissolved in a water / methanol mixture (25 mL / 75 mL). The flask was sealed and the solution was degassed three times. Under a $N_2$ atmosphere, the macro-initiator $Br_{0.7}$-HEC **3** (1 g, $2.8\times10^{-3}$ mol, 1 eq.) was added to the solution. The mixture was heated at 60 °C for 4 h under a $N_2$ atmosphere. The mixture was cooled to room temperature and dialysed against water for 2 days. The final aqueous solution was then freeze-dried. The recovered product **7** was obtained as a fine powder in a yield of 0.5% (0.6 g). The product was characterised using solid state $^{13}C$ CP-MAS NMR and FT-IR spectroscopies. Furthermore, elemental analysis C, H and N was performed and the bromine content was determined.

#### 4.2.3.4. Preparation of HEC-graft-poly(1-(11-acryloyloxyundecyl)-3-methylimidazolium bromide)

##### 4.2.3.4.1. Synthesis of 1-(11-acryloyloxyundecyl)-3-methylimidazolium bromide

First step: In two-necked, round-bottomed flask fitted with both a condenser and a dropping funnel, 11-bromo-1-undecanol **8** (2.5 g, $9.95\times10^{-3}$ mol, 1 eq.), *p*-toluene sulfonic acid (0.2 g, $1.16\times10^{-3}$ mol,1 eq.) and monomethyl ether hydroquinone (MEHQ)

(0.02 g, $1.6\times10^{-4}$ mol, 0.02 eq.) were dissolved in 27 mL of cyclohexane and the mixture was refluxed for 1 h. Acrylic acid **9** (0.8 mL, $1.16\times10^{-2}$ mol, 1 eq.) was dissolved in 4 mL of cyclohexane and was dropped into the mixture using the dropping funnel. The final mixture was refluxed overnight. Once cooled to room temperature, the organic solution of product was washed with NaOH (10% w/w, 3×50 mL), dried over $MgSO_4$ and concentrated under vacuum. The product **10** was obtained in a yield of 88% (2.4 g). $^1$H NMR (400 MHz, DMSO-$d_6$): $\boldsymbol{\delta}_H$ (ppm) 1.3-1.8 (m, 18H, Br-$CH_2$-(C**H$_2$)$_9$**-), 3.52 (t, J =6.7 Hz, 2H, Br-C**H$_2$**-), 4.10 (t, J =6.7 Hz, 2H, -O-C**H$_2$**-), 5.94 (dd, J =10.3, 1.6 Hz, 1H, **H**CH=CH-), 6.17 (dd, $J_{ac}$ =17.3, 10.3 Hz 1H, -C**H**-$CH_2$), 6.32 (dd, J =17.3, 1.6 Hz, 1H, HC**H**=CH-); $^{13}$C NMR (100 MHz, DMSO-$d_6$): $\boldsymbol{\delta}_C$ (ppm) 25.3-35.1 (9C, Br-$CH_2$-(**C**$H_2$)$_9$-),40.4 (-**C**$H_2$-Br) 64.0 (-**C**$H_2$-O-), 128.4 (-CH=**C**$H_2$), 131.2 (-**C**H=$CH_2$), 165.4 (-**C**=O).

<u>Second step:</u> Bromoalkylacrylate **10** (2.4 g, $7.96\times10^{-3}$ mol, 1 eq.), and 1-methylimidazole **11** (0.6 mL, $7.96\times10^{-3}$mol, 1eq.) were mixed and heated at 50 °C for 24 h. When the mixture was cooled to room temperature, the product precipitated and was filtered. The product **12** was then washed with diethyl ether (3×50 mL) and dried under vacuum to obtain a white powder in a yield of 85% (2.6 g). $^1$H NMR (400 MHz, DMSO-$d_6$): $\boldsymbol{\delta}_H$ (ppm) 1.24-1.77 (m, 18H, -O-$CH_2$-(C**H$_2$**)$_9$-$CH_2$-), 3.86 (s, 3H, -N-C**H$_3$**), 4.08 (t, J =6.6 Hz, 2H, -O-C**H$_2$**-), 4.16 (t, J =7.2 Hz, 2H, $CH_2$-C**H$_2$**-N-), 5.95 (dd, J =10.3, 1.7 Hz, 1H, **H**CH=CH-), 6.15 (dd, J =20.3, 10.3 Hz, 1H, -C**H**-$CH_2$), 6.30 (dd, J =17.3, 1.6 Hz, 1H, HC**H**=CH-), 7.77 (dd, 2H, J =27.0, 0.97 Hz, -C**H**=C**H**-), 9.22 (s, 1H, -C**H**=$N^+$-); $^{13}$C NMR (100 MHz, DMSO-$d_6$): $\boldsymbol{\delta}_C$ (ppm) 25.3-35.1 (9C, Br-$CH_2$-(**C**$H_2$)$_9$-), 35.7 (N-**C**$H_3$), 48.7 ($CH_2$-**C**$H_2$-N-), 64.0 (-**C**$H_2$-O-), 122.2 (N-**C**H=CH-N) , 123.5 (N-CH=**C**H-N), 128.4 (-CH=**C**$H_2$), 131.2 (-**C**H=$CH_2$), 136.5 (-N-**C**H=N-), 165.4 (-**C**=O).

#### 4.2.3.4.2. ATRP of 1-(11-acryloyloxyundecyl)-3-methylimidazolium bromide

In one-necked, round-bottomed flask equipped with a magnetic stirrer, CuBr (1 eq.) was degassed three times by freeze-pump-thaw cycling and back filled with $N_2$. 1-(11-Acryloyloxyundecyl)-3-methylimidazolium bromide **12** (100 eq. and 10 eq.), TMEDA (2 eq.) and DMSO were added and the mixture then degassed three times and back filled with $N_2$. The mixture was heated at 90 ºC and the macro-initiator, $Br_{0.7}$-HEC **3** ($M_w$ =129 kDa, $M_{w/AGU}$ =406 g/mol, $DS_{Br}$ ~0.7, 1 eq.) was added. The reaction was run overnight at 90 ºC and was quenched by opening the flask to air. Once cooled, the product **13** was precipitated in methanol (10 × volume of DMSO) and was dried overnight at 40 ºC under vacuum. Different concentrations of $Br_{0.7}$-HEC in DMSO and different degrees of polymerisation were chosen. The reaction conditions and yields (%) of each reaction are summarised in Table 4-5. Samples were characterised using solid state $^{13}C$ CP-MAS NMR and FT-IR spectroscopies.

# 4.3. RESULTS AND DISCUSSION

## 4.3.1. Macro-initiators Br-HECs

Macro-initiators Br-HECs **3** were synthesised from under heterogeneous conditions using 2 equivalents of bromoisobutyryl bromide **2** per AGU unit of HEC **1,** and the reactions were performed at room temperature for 24 h (Scheme 4-1). To investigate the influence of the reaction conditions on the degree of functionalization of the hydroxyl groups, the base, atmosphere quality and molecular weight and molar substitution levels of HEC were changed and are reported in Table 4-2.

**Table 4-2:** Summary of reaction conditions for the bromination of HEC

| Exp. Nº | HEC | | | Base | Atm. | Mass (g) | Yield (%) |
|---|---|---|---|---|---|---|---|
| | $M_w$ | DS | MS | | | | |
| **FJ -232** | 90 | .. | 2.5 | TEA | air | 5.1 | 84 |
| **FJ -233** | 90 | .. | 2.5 | collidine | air | 5.3 | 80 |
| **FJ -237** | 90 | .. | 2.5 | TEA | $N_2$ | 5.4 | 81 |
| **FJ -242** | 90 | .. | 2.5 | collidine | $N_2$ | 5.6 | 79 |
| **FJ -245** | 250 | 1 | 2 | collidine | $N_2$ | 5.0 | 84 |

For the experiments FJ-233, FJ-232, FJ-237 and FJ-242, a 90 kDa molecular weight HEC with a molar substitution level of 2.5 was chosen because of its good solubility properties. In fact, 90 kDa HEC is the lowest commercially available molecular weight of HEC resulting in better solubility properties compared to HEC of higher molecular weight. Its use should therefore enhance the degree of functionalization. The importance of the choice of base was investigated in experiments FJ-232 and FJ-233 where triethylamine (TEA) and collidine were used respectively. Furthermore, these two reactions were repeated (FJ-237 and FJ-242) where the air was replaced by nitrogen, permitting the investigation of the influence of the atmosphere quality on the DS. In the last experiment FJ-245, a higher molecular weight of HEC (250 kDa, MS =2) was used leading to investigate the importance of molecular weight on the DS. Due to a lack of solubility in common deuterated solvents, samples of each experiment were characterised using solid state $^{13}C$ CP-MAS NMR and FT-IR spectroscopies and, the bromine content was measured to estimate the DS.

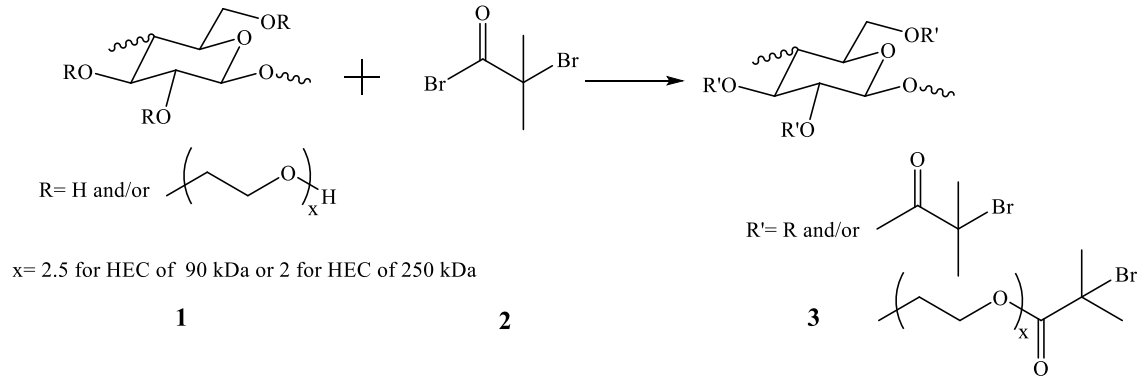


**Scheme 4-1:** Synthesis of the macro-initiator, Br-HEC **3**

In the solid state $^{13}C$ CP-MAS NMR spectrum for the sample of experiment FJ-232 (Figure 4-4 a), the presence of bromoisobutyryl bromide and hydroxyethyl cellulose signals was demonstrated. The set of signals $\boldsymbol{\delta}_C$ ~104 ppm, 83 ppm, 75 ppm, 72 ppm and 62 ppm are assigned to the carbons defining hydroxyethyl cellulose. The peaks $\boldsymbol{\delta}_C$ ~104 ppm and 83 ppm are respectively assigned to anomeric carbon at the position C1 and to the carbon at the position C4 (Figure 4-3). The peak $\boldsymbol{\delta}_C$ ~75 ppm is assigned to the carbons at position C2, C3 and C5 and, the peak $\boldsymbol{\delta}_C$ ~71 ppm is assigned to the carbons defining the ethylene oxide side chain -**C**$H_2$**C**$H_2$O- whereas the peak $\boldsymbol{\delta}_C$ ~62 ppm is assigned to the carbon carrying the primary alcohols, i.e., -**C**$H_2$OH. Meanwhile, the peaks $\boldsymbol{\delta}_C$ ~31 ppm, 57 ppm and 171 ppm are assigned respectively to methyl groups, the tertiary carbon and the carbonyl group of the alkyl bromide. In the spectrum recorded for the sample of the experiment FJ-233 (Figure 4-4 b), the same set of signals was observed, however the intensities of the signals $\boldsymbol{\delta}_C$ assigned to the alkyl bromide increased compared to those of HEC, suggesting a higher degree of functionalization for sample FJ-233 than for FJ-232. The increase of the functionalization resides in the change of base; triethylamine used in experiment FJ-232 was replaced by collidine in the experiment FJ-233. The use of collidine enhanced the degree of functionalization of the hydroxyl groups with bromo-alkyl bromide. The reaction between hydroxyethyl cellulose and bromo-alkyl bromide is

a nucleophilic substitution followed by an elimination reaction. The latter involves the liberation of a proton which will complex with the base forming an aminium which compensate the charge of the release bromide anion (Figure 4-2). The both bases removed acidic protons from HEC backbone, however, triethylamine is much more nucleophilic than collidine resulting in a higher probability of side reactions and thus a slower rate for the functionalization reaction.

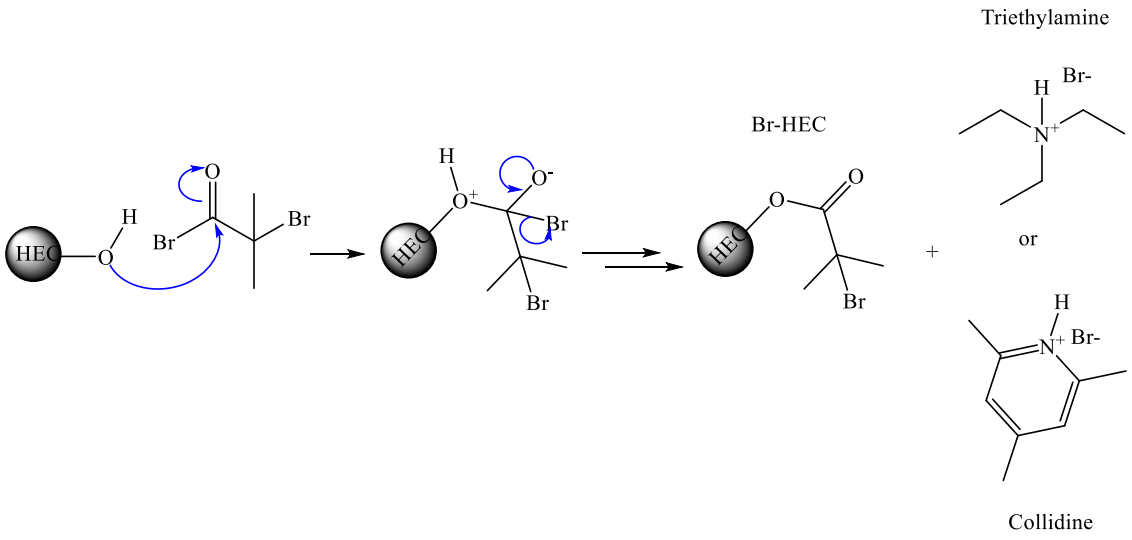


**Figure 4-2:** Nucleophilic substitution/elimination mechanism for preparing Br-HEC

The spectrum of the sample of experiment FJ-237 (Appendix 1), where triethylamine was used as a base and the reaction was carried under positive $N_2$ pressure, is very similar to the spectrum (b) in Figure 4-4 implying a similar degree of functionalization for sample of experiment FJ-233 and a higher DS compared to the sample of experiment FJ-232. The latter could be due to a change of the atmosphere quality. In fact, for experiment FJ-237, the reaction was carried under positive nitrogen pressure whereas FJ-232 was run under atmospheric pressure. The spectrum recorded for the sample of experiment FJ-242

(Figure 4-4 c) showed an increase of the intensity of the peaks $\boldsymbol{\delta}_C$ ~31 ppm, 57 ppm and 171 ppm which are assigned to the alkyl bromide. Furthermore, the intensity of the peak $\boldsymbol{\delta}_C$ ~62 ppm assigned to the carbon of the primary alcohol of HEC decreased and an increase of the intensity of the peak $\boldsymbol{\delta}_C$ ~72 ppm assigned to the ethylene oxide side chain was observed. This suggests that the functionalization reaction takes place preferentially at the primary alcohols, i.e., at C6 and C8 positions where respectively R'=H and R''=H (shown in Figure 4-3). The increase of the signal intensity $\boldsymbol{\delta}_C$ ~72 ppm is attributed to the chemical shift of the carbons at C6 and C8 positions where respectively R'≠H and R''≠H after having reacted with the bromo-alkyl bromide. Overall, the sample of experiment FJ-242 was shown to have the highest degree of substitution of the hydroxyl groups with the alkyl bromide compared to the previous samples because of the use of collidine as base and the use of nitrogen as atmosphere, both reducing the probabilities of side reactions. The spectrum (d) of the sample of experiment FJ-245 in Figure 4-4 showed same set of signals as in (b) and (c), however the intensity of the signals assigned to the alkyl bromide is lower. Spectrum (b) is similar to spectrum (a) suggesting a decrease of the degree of functionalization compared to the samples of experiments FJ-242, FJ-237 and FJ-233. However, a similar degree of functionalization should be observed between samples of experiments FJ-232 and FJ-245. The low DS of the hydroxyl group was explained by the change of the molecular weight of HEC from 90 kDa (MS =2.5) to 250 kDa (MS =2). The use of a higher molecular weight decreased the reactivity of the hydroxyl groups of HEC, resulting in a decrease of degree of functionalization.

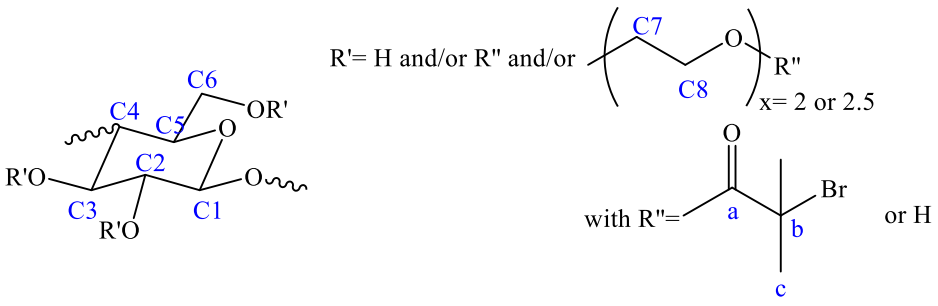


**Figure 4-3:** Numbering of the Br-HEC **3** structure

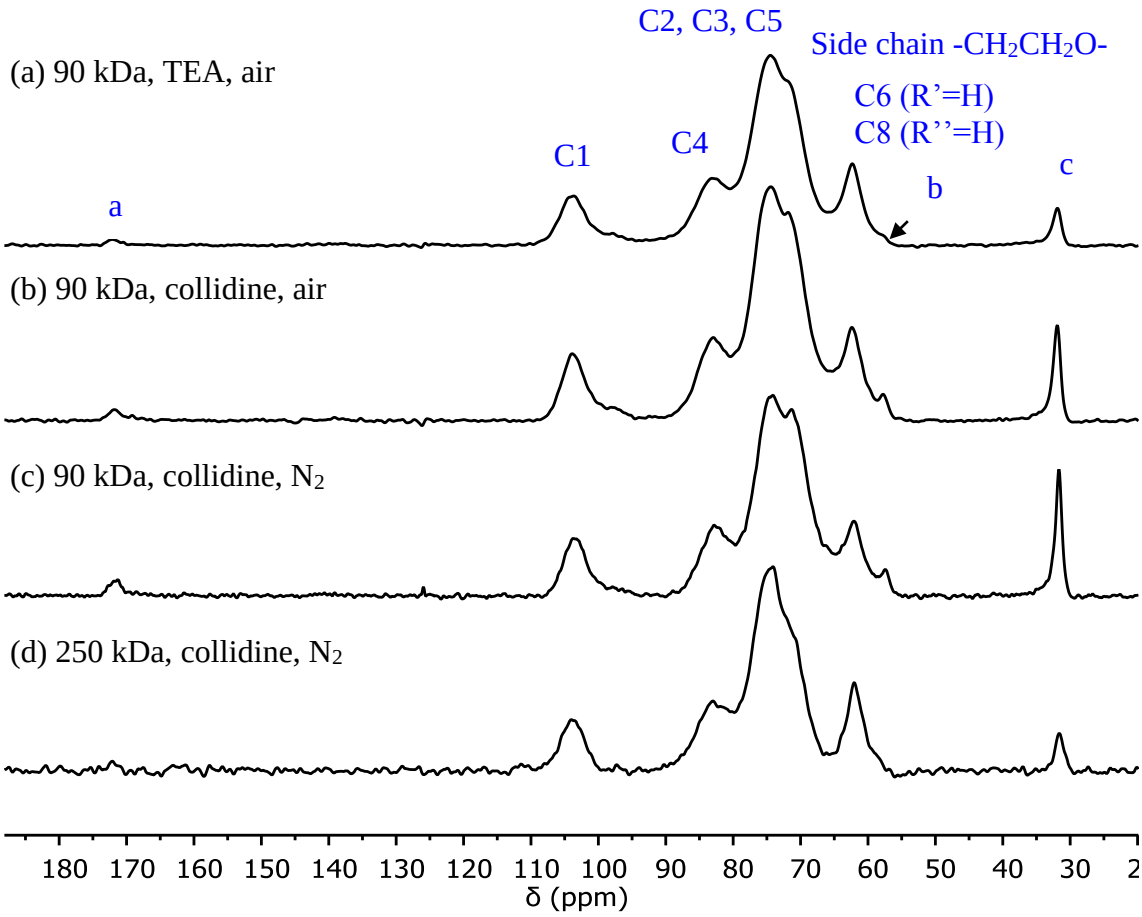


**Figure 4-4:** Solid state $^{13}C$ CP-MAS NMR spectra of Br-HECs **3;** (a) exp. FJ-232, (b) exp. FJ-233, (c) exp. FJ-242 and (d) exp. FJ-245.

The FT-IR spectra of the macro-initiators, Br-HECs are displayed in Figure 4-5. The absorption bands between 1000 $cm^{-1}$ to 1230 $cm^{-1}$ are assigned to the -C-O stretching

vibrations, the band at 1300 $cm^{-1}$ is assigned to the bending vibration of -C-H in the methyl groups, the band at 2900 $cm^{-1}$ is assigned to the -C-H stretching vibrations of the $-CH_2$ and $-CH_3$ groups. Finally, the bands at 3400 $cm^{-1}$ and 1740 $cm^{-1}$ are recorded and are assigned to the hydroxyl group stretching and bending vibrations of HEC backbone and the carbonyl stretching vibration of the bromoisobutyryl group respectively.

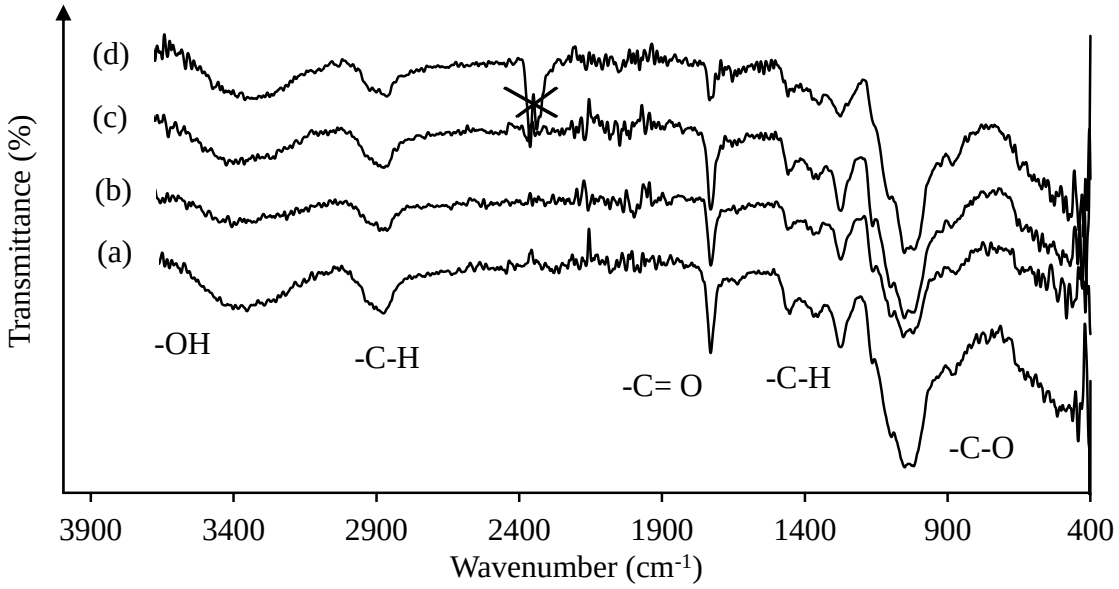


**Figure 4-5:** FT-IR spectra of Br-HECs **3;** (a) FJ-232 (90 kDa, TEA, air), (b) FJ-233 (90 kDa, collidine, air), (c) FJ-242 (90 kDa, collidine, $N_2$) and (d) FJ-245 (250 kDa, collidine, $N_2$).

In the spectrum of sample of experiment FJ-245, the absorption band at 1740 $cm^{-1}$ assigned to the carbonyl group of the bromo-alkyl is the weakest compared to the bands in the spectra of the sample of experiments FJ232, FJ233 and FJ-242, suggesting the sample of experiment FJ-245 has the lowest DS. The spectra of samples of experiments FJ-232, FJ-233 and FJ-245 are similar, suggesting similar $DS_{Br}$ values. To quantify the DS, the content of bromine (%Br) of each sample was measured and there are reported in

Table 4-3. The theoretical relationship between the content of bromine and $DS_{Br}$ is reported in Equation 4-1.

$$\%Br = (DS_{Br} \times M_{Br'}) / (DS_{Br} \times M_{Br} + M_{HEC} - DS_{Br}) \times 100 \quad \textbf{(4-1)}$$

where $M_{Br'}$, $M_{Br}$ and $M_{HEC}$ are constant values and correspond respectively to the molecular weight of the bromine, the bromoisobutyryl group and the molecular weight of the repeating unit of HEC.

The plots of the $DS_{Br}$ values as a function of the theoretical bromine content were processed for the two molecular weights of HEC that have been use to prepare Br-HEC and are shown in Figure 4-6. The $DS_{Br}$ evolutions for a 90 kDa and 250 kDa HEC are non-linear as a function of the % of Br, but are described as polynomial functions of order 4 in Equation 4-2 and 4-3.

$$DS_{Br}\ (90\ kDa) = 2\times10^{-6}\times(\%Br)^4 - 8\times10^{-5}\times(\%Br)^3 + 0.0021\times(\%Br)^2 + 0.0257\times(\%Br) + 0.0108 \quad \textbf{(4-2)}$$

$$DS_{Br}\ (250\ kDa) = 2\times10^{-6}\times(\%Br)^4 - 9\times10^{-5}\times(\%Br)^3 + 0.0022\times(\%Br)^2 + 0.0214\times(\%Br) + 0.0134 \quad \textbf{(4-3)}$$

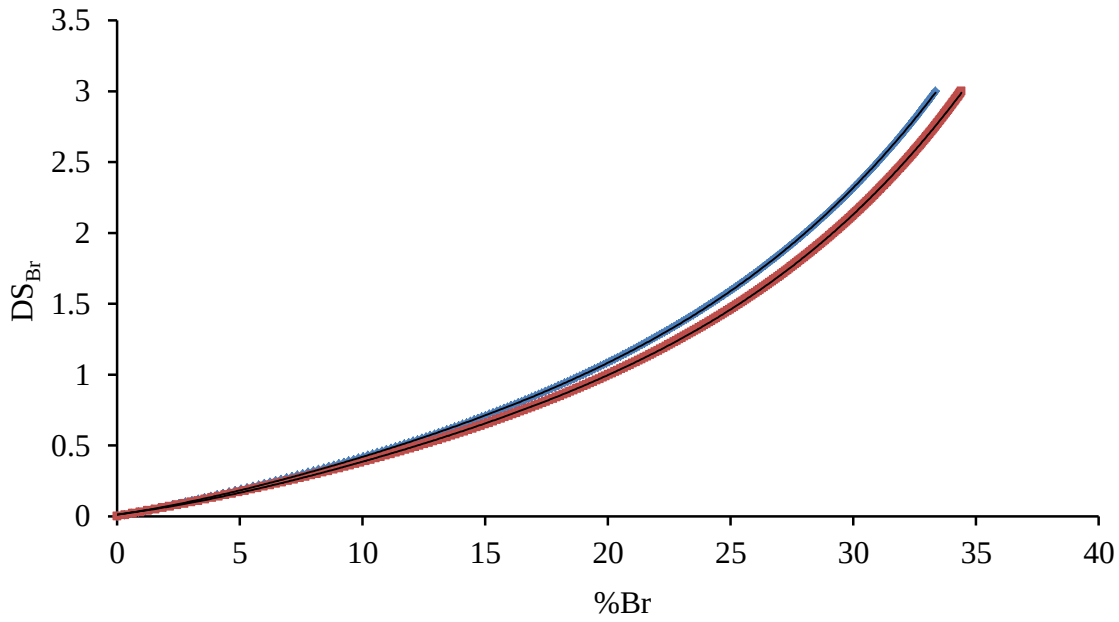


**Figure 4-6:** $DS_{Br}$ evolution as a function of bromine content (%Br) for HEC with $M_w$ of 90 kDa (blue) and 250 kDa (red)

From the equations, the DS of each sample was calculated and is reported in Table 4-3. A DS of 0.5 was calculated for the sample of experiment FJ-232 whereas a higher DS of 0.7 was estimated for samples of experiment FJ-233 and FJ-237. This increase of DS was explained by the replacement of triethylamine by collidine as base or the air substituted by nitrogen. A maximum DS of 0.9 was obtained for sample of experiment FJ-242 because both collidine was used and the reaction was conducted under positive pressure nitrogen. A DS value of 0.3 was found for sample of experiment FJ-245 and the large DS decrease from 0.9 to 0.3 was due to the change of HEC molecular weight. The use of a 250 kDa HEC resulted in a lower reactivity of the hydroxyl groups of HEC with the bromoisobutyryl bromide. Knowing the DS of each sample, the yields (%) were calculated for all experiments and were found relatively high ranging from 79% to 84%.

**Table 4-3:** $DS_{Br}$ determination from the measure of bromine content in Br-HEC

| Exp. | HEC (kDa) | Base | Atm. | Yield (%) | %Br | DS |
|---|---|---|---|---|---|---|
| **FJ -232** | 90 | TEA | air | 84 | 11.3 | 0.5 |
| **FJ -233** | 90 | collidine | air | 80 | 14.8 | 0.7 |
| **FJ -237** | 90 | TEA | $N_2$ | 81 | 14.4 | 0.7 |
| **FJ -242** | 90 | collidine | $N_2$ | 79 | 18.0 | 0.9 |
| **FJ -245** | 250 | collidine | $N_2$ | 84 | 8.6 | 0.3 |

To summarise the preparation of the macro-initiators Br-HECs, the use of solid state $^{13}C$ CP-MAS NMR and FT-IR spectroscopies highlighted the presence of the bromoisobutyryl bromide on the HEC backbone. The selectivity of the functionalization reaction at the primary alcohol in the C6 and C8 positions was demonstrated using NMR spectroscopy. Furthermore, the level of the modification of the hydroxyl groups with bromo-alkyl groups was determined using the measured content of bromine (%Br). The calculated DS values were in agreement with the observations that have been discussed for the NMR spectra. In fact, the DS was influenced by the choice of the base, the quality of the atmosphere and the molecular weight of the starting material HEC. A maximum DS of 0.9 was reached when collidine was used as a base and the functionalization reaction was conducted under positive nitrogen. However, an increase of the molecular weight of HEC (250 kDa) resulted in a decrease of the DS of -OH groups because of the lower reactivity of -OH compared to that in 90 HEC. In fact, the accessibility of the -OH groups was more limited in HEC of 250 kDa because of its higher average chain length. The variation of reaction conditions permitted the creation of Br-HECs which had DS ranging from 0.3 to 0.9 and are obtained in a high yield (~80%). This will further give us opportunities to prepare graft-copolymers of HEC with various graft-densities.

## 4.3.2. Poly(methyl methacrylate) grafted from Br-HEC

Atom Transfer Radical Polymerisation (ATRP) of methyl methacrylate (MMA) **4** was performed to verify the reactivity of the macro-initiator Br-HEC (Scheme 4-2). The graft-copolymers HEC-g-PMMAs **5** were prepared from different macro-initiators Br-HECs **3**. For experiments FJ-120 and FJ-125, a high DS of 0.7 for Br-HEC was chosen in order to produce graft-copolymers with high graft-densities whereas a lower DS of 0.3 was used in experiment FJ-130 and FJ-297 for preparing graft-copolymers with low graft-densities (Table 4-4).

**Table 4-4:** Summary of reaction conditions for the ATRP of MMA onto Br-HEC

| **Exp. Nº** | **Br-HEC** | | | **MMA (g)** | **Ratio*** **[M]/[I]/[C]/[L]** | **Weight (g)** | **Yield (%)** |
|---|---|---|---|---|---|---|---|
| | $DS_{Br}$ | $M_w$ (kDa) | W (g) | | | | |
| **FJ -120** | 0.7 | 129 | 0.20 | 5.20 | 125/1/1/2 | 3.20 | 58 |
| **FJ -125** | 0.7 | 129 | 0.14 | 0.56 | 12/1/1/2 | 0.46 | 61 |
| **FJ -297** | 0.3 | 295 | 0.2 | 0.75 | 30/1/1/2 | 0.56 | 48 |
| **FJ -130** | 0.3 | 295 | 0.2 | 0.34 | 15/1/1/2 | 0.35 | 73 |

*[M]/[I]/[C]/[L] defines the ratio of monomer (M) to initiator (I), catalyst (C) and ligand (L).

For the high graft-density macro-initiator $Br_{0.7}$-HEC, two chains length of 125 and 12 repeating units of MMA were targeted whereas only short chains of 30 and 15 were targeted for the low graft-density. Based on the conventional ATRP of MMA found in the literature[108], the temperature was set at 90 ºC with overnight reaction time and the ratio of initiator to catalyst and ligand was kept constant at 1:1:2. Furthermore, the volume of solvent (DMSO) was adjusted for each experiment to ensure constant concentrations

of AGU in each reaction. The amount of solvent is an important parameter on the ATRP process because it controls the concentration of initiator sites. In fact, a too high concentration of initiator leads to the formation of a gel resulting in a poor control of the polymerisation. In our experiments, a 0.02 g/mL concentration of AGU was chosen to suppress the gelation process. The products were precipitated using chloroform in which HEC-g-PMMAs were found to be insoluble, but, in which PMMA chains are soluble. The monomer conversion based on the weight recovery was estimated to lie between 50 and 60% depending on the experiment (Table 4-4). Due to the poor solubility in common deuterated solvents, the samples were characterised in their solid states using $^{13}C$ CP-MAS NMR and FT-IR spectroscopies. In order to estimate the control of the ATRP process, PMMA chains in the sample of experiment FJ-125 were hydrolyzed from their HEC backbone following a reported procedure[107] and then analyzed using size exclusion chromatography (SEC) to estimate the dispersity ($Đ_M$).

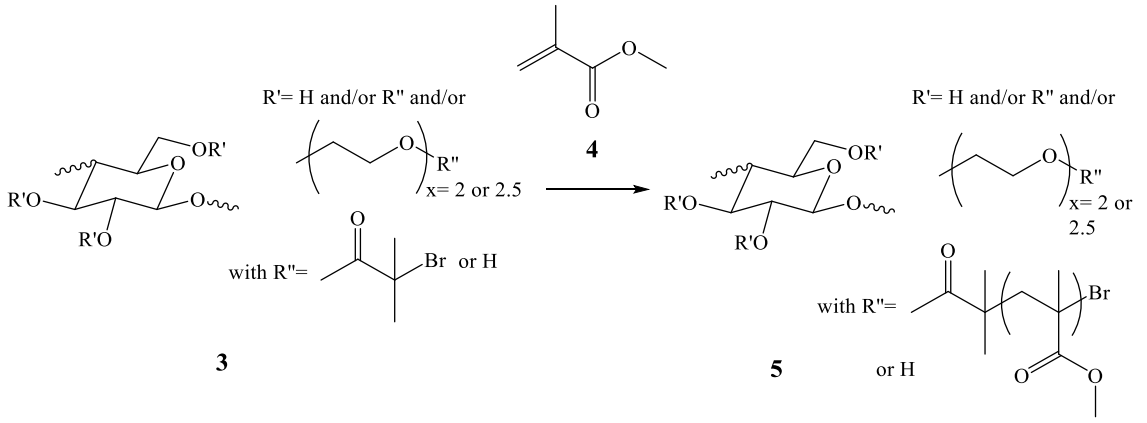


**Scheme 4-2:** Atom Transfer Radical Polymerisation of MMA **4** from Br-HEC **3**

Figure 4-7 displays the FT-IR spectrum of $HEC_{0.7}$-g-$PMMA_{125}$ of experiment FJ-120, but the detected absorption bands indicated mainly the presence of PMMA chains. The

absorption band at 754 $cm^{-1}$ was assigned to the α-methyl group vibrations. Furthermore, the absorption bands from 1150 $cm^{-1}$ to 1200 $cm^{-1}$ were assigned to the –C-O- stretching vibrations whereas from 2900 $cm^{-1}$ to 3000 $cm^{-1}$ to the -C-H stretching vibrations of the $-CH_2$ and $-CH_3$ groups. The -C-H bending vibrations of $-CH_3$ groups appeared at 1250 $cm^{-1}$. The absorption band at 1728 $cm^{-1}$ was assigned to the -C=O group stretching vibrations. However, the FT-IR spectrum of the graft-copolymer $HEC_{0.7}$-g-$PMMA_{12}$ of experiment FJ-125 (Figure 4-8) where a lower degree of polymerisation was targeted showed absorption bands assigned to the HEC structure such as at 3400 $cm^{-1}$ and at 1028 $cm^{-1}$ which were assigned respectively to the alcohol -OH group stretching and bending vibrations and to the -C-O stretching vibration. Furthermore, the band at 2900 $cm^{-1}$ became broader indicating the presence -C-H stretching vibrations of the methylene group of HEC. Decreasing the degree of polymerisation (DP) of MMA onto $Br_{0.7}$-HEC was responsible for the detection of both PMMA and HEC by FT-IR spectroscopy. The FT-IR spectrum of $HEC_{0.3}$-g-$PMMA_{15}$ (Appendix 2) is similar to the spectrum of $HEC_{0.7}$-g-$PMMA_{12}$ where both PMMA and HEC were detected, however, the increased DP of MMA lead to a weaker relative absorption band at 1028 $cm^{-1}$ in the FT-IR spectrum of $HEC_{0.3}$-g- $PMMA_{30}$ (Appendix 3) compared to the spectrum of $HEC_{0.3}$-g-$PMMA_{15}$.

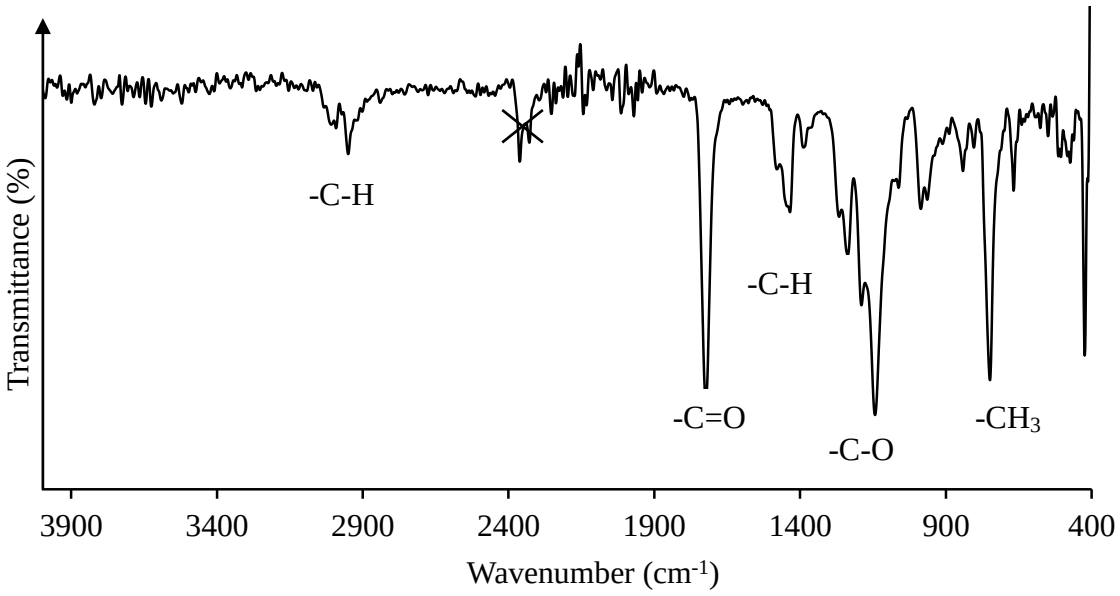


**Figure 4-7:** FT-IR spectrum of $HEC_{0.7}$-g-$PMMA_{125}$ (exp. FJ-120)

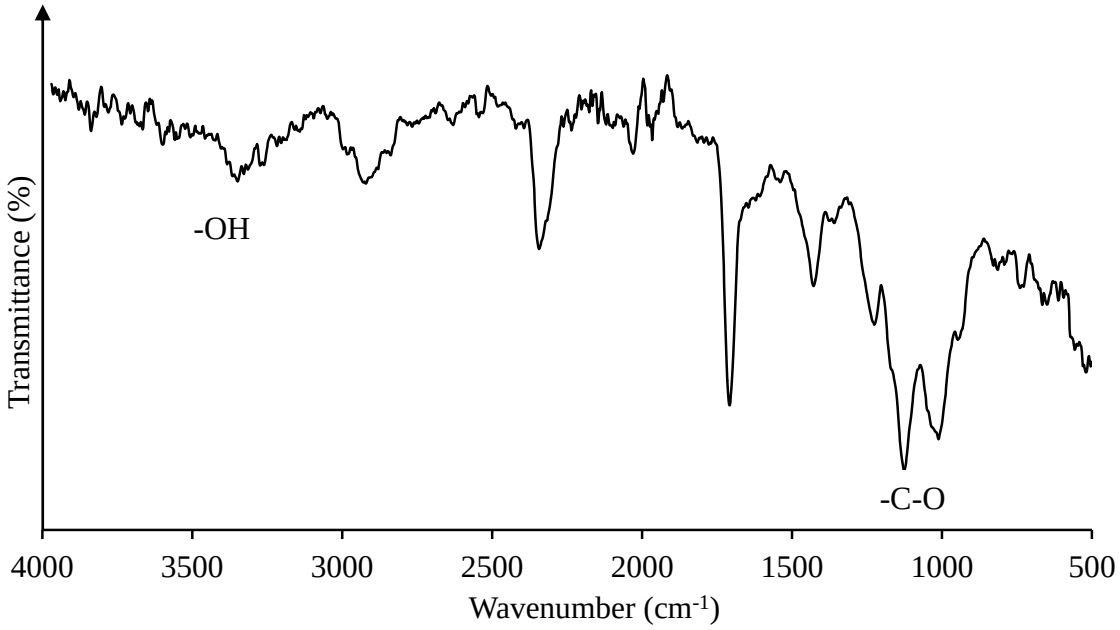


**Figure 4-8:** FT-IR spectrum of $HEC_{0.7}$-g-$PMMA_{12}$ (exp. FJ-125)

For HEC-g-PMMA (numbered structure shown in Figure 4-9), a solid state $^{13}C$ NMR spectrum was recorded and is shown in Figure 4-10. The sets of signals $\boldsymbol{\delta}_C$ ~16 ppm, 45 ppm, 52 ppm, 56 ppm and 178 ppm are respectively assigned to -C-**C**$H_3$, -**C**$H_2$-C, -**C**-

$CH_3$ -O-**C**$H_3$ and -**C**=O group of the PMMA chains, however, the signals of the HEC backbone are absent from the spectrum of $HEC_{0.7}$-g-$PMMA_{125}$. Furthermore, the homopolymerisation of MMA cannot be the reason of the non-detection of HEC because of the use of chloroform for recovering the crude HEC-g-PMMAs. In order to prove the grafting efficiency of PMMA onto HEC, the targeted DP of MMA was reduced for experiment FJ-125. This allowed the detection of a peak $\boldsymbol{\delta}_C$ ~62 ppm and a band $\boldsymbol{\delta}_C$ ~71 ppm in the spectrum of $HEC_{0.7}$-g-$PMMA_{12}$ (Figure 4-10 b). The weak peak $\boldsymbol{\delta}_C$ ~62 ppm is assigned to the carbon of the unmodified primary alcohol of HEC where the broad band at ~71 ppm to the other carbons of HEC. To improve the intensities of HEC signals, a less functionalized $Br_{0.3}$-HEC was used for the ATRP of MMA and the spectrum of $HEC_{0.3}$-g-$PMMA_{15}$ is displayed in Figure 4-10. The peaks of HEC are clearly defined at $\boldsymbol{\delta}_C$ ~71 ppm, 74 ppm, 81 ppm and 104 ppm which are respectively assigned to the -**C**$H_2$**C**$H_2$O- side chains, carbons C2, C3 and C5 positions, carbon C4 and the C1 position. Compared to the spectrum of $HEC_{0.3}$-g-$PMMA_{15}$ the increase of the degree of polymerisation of MMA onto $Br_{0.3}$-HEC in the graft-copolymer $HEC_{0.3}$-g-$PMMA_{30}$ did not affect the detection of HEC using NMR spectroscopy because of the similarity of their NMR spectra (Appendix 4).

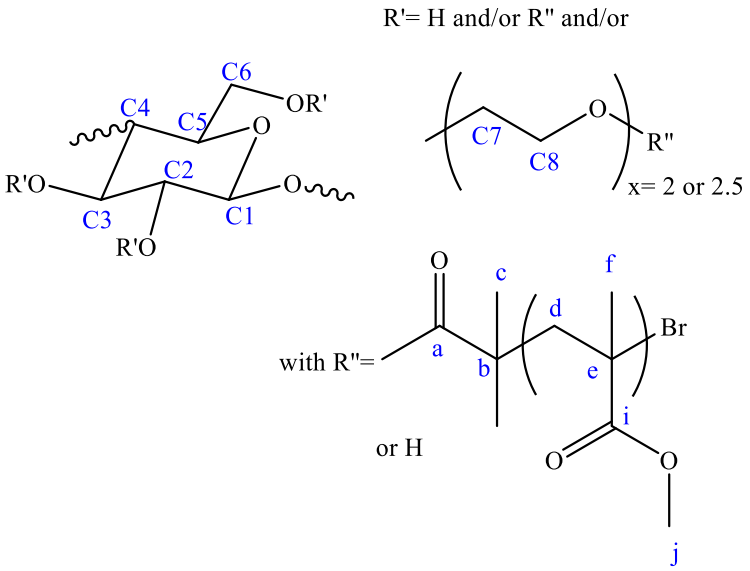


**Figure 4-9:** Numbering of HEC-g-PMMA **5** structure

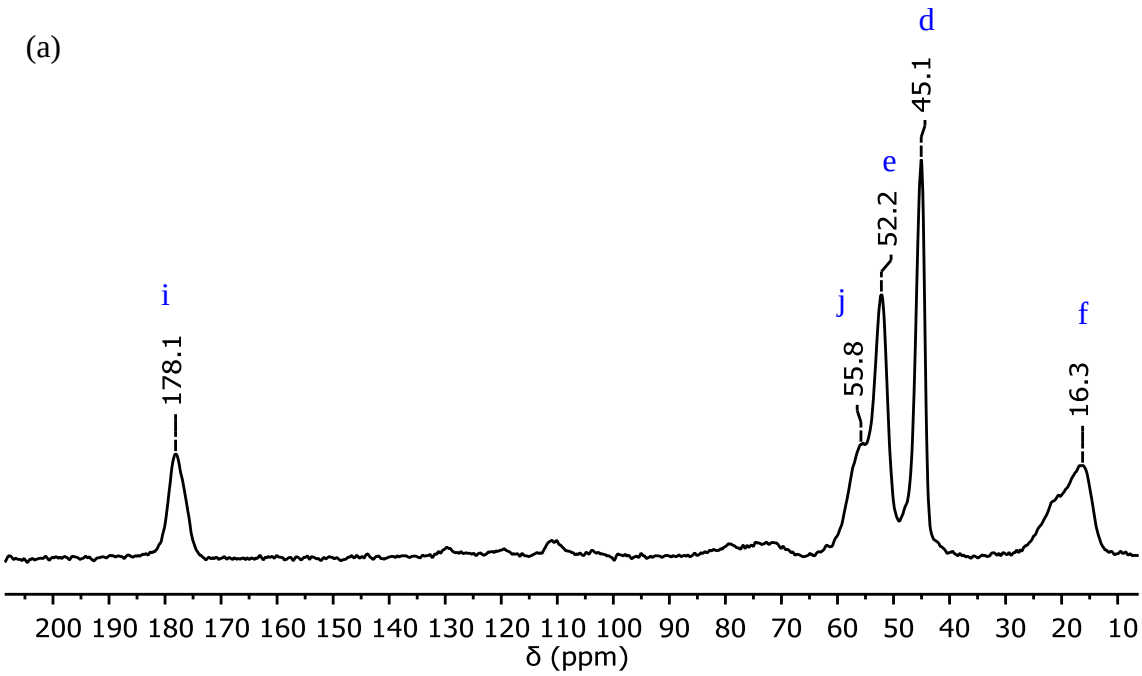

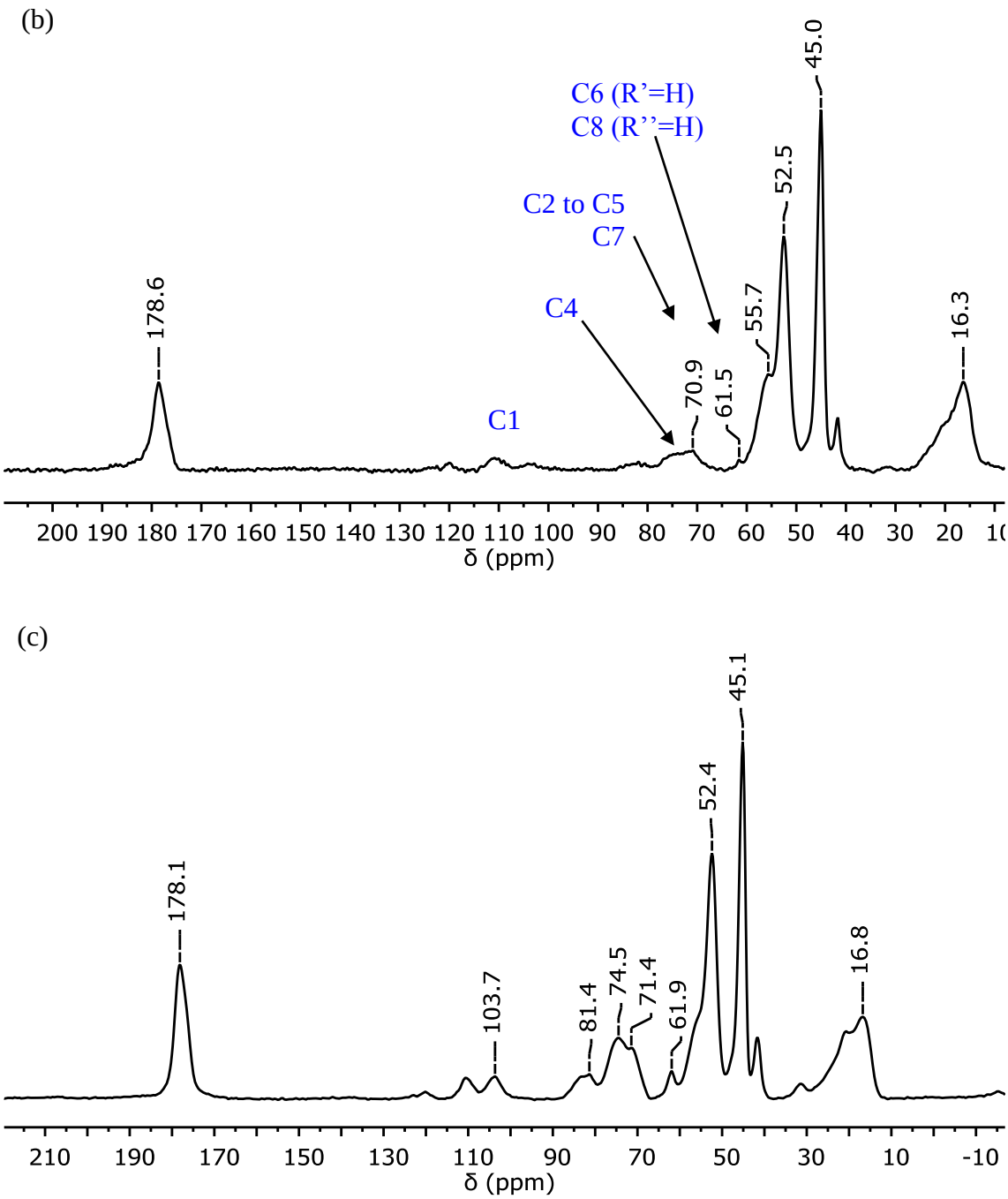


**Figure 4-10:** Solid state $^{13}C$ CP-MAS NMR spectra of HEC-g-PMMAs **5**; (a) $HEC_{0.7}$-g-$PMMA_{125}$, (b) $HEC_{0.7}$-g-$PMMA_{12}$ and (c) $HEC_{0.3}$-g-$PMMA_{15}$.

The NMR and FT-IR spectroscopy results highlighted the grafting efficiency of PMMA from HEC. The preparation of graft-copolymers with low graft-density and/or short length improved the detection of the HEC backbone suggesting a lack of PMMA

homopolymer. However, the question which remains, when using a RDRP technique to produce graft-copolymers by "grafting from", is the determination of the dispersity ($Đ_M$) of the grafts. Due to their insolubility in conventional solvents such as THF, DMF and water, the graft-copolymers HEC-g-PMMAs could not been analysed using SEC. However, procedures have been described in the literature, where grafts are hydrolysed from the main backbone and further analysed using SEC. PMMA chains from the graft-copolymer $HEC_{0.7}$-g-$PMMA_{125}$ were hydrolysed from the HEC backbone permitting the determination of both $Đ_M$ and number average molecular weight ($M_n$) using SEC. The graft-copolymer with the longest chains was chosen to give the strongest light scattering detector signal. The SEC trace of the hydrolysed $HEC_{0.7}$-g-$PMMA_{125}$ is shown in Figure 4-11, $M_n$ of 90 000 g/mol and a $Đ_M$ of 1.2 were estimated using light scattering with dn/dc equal to 0.08 mL/g.

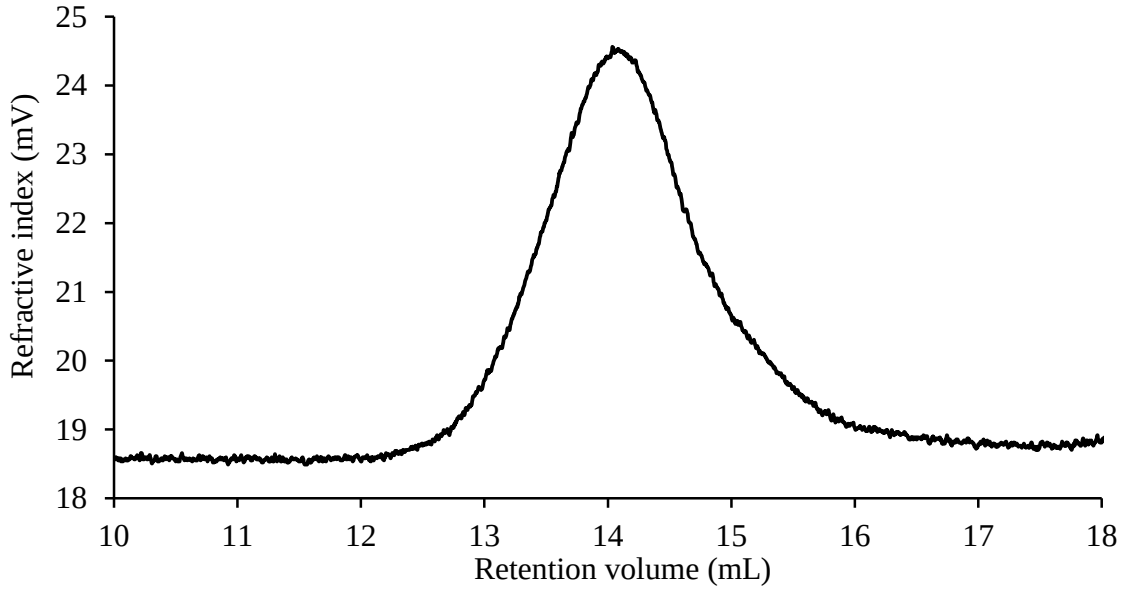


**Figure 4-11:** Result of SEC analysis of PMMA grafts of $HEC_{0.7}$-g-$PMMA_{125}$; plot shown is from RI detection.

The low value of dispersity indicates a narrow molecular weight distribution which confirms the control of the polymerisation process. However, the calculated molecular weight value was high compared to that based on the monomer conversion (7,500 g/mol). This suggests that the ATRP of MMA had been activated by only 1 bromine per 12 initiator sites resulting in the preparation of a graft-copolymer with one PMMA chain with a length of 900 repeating units for every 15 AGU units. The low level of ATRP initiation of MMA onto Br-HEC can be due to a limited accessibility of the activation site by the monomer. Both the steric hindrance and H-bonding networks can affect the reactivity of the macro-initiator Br-HEC.

To summarise, HEC-g-PMMAs have been successfully prepared from macro-initiators Br-HECs with a DS of 0.7 and 0.3, indicating the preparation of graft-copolymers with different graft-densities. Furthermore, the chain length of the HEC-g-PMMAs were varied targeting different degrees of polymerisation i.e. 125, 30 and 15. The use of a low DS for Br-HEC and/or the targeting of short length chains permitted the detection of the HEC backbone by NMR and FT-IR spectroscopies, confirming the grafting efficiency of PMMA from HEC. However, the SEC results showed that the polymerisation was not initiated at all sites for $Br_{0.7}$-HEC resulting in the preparation of a graft-copolymer defined by both a low graft-density and long grafts with a narrow molecular weight distribution. The partial activation of the bromine in $Br_{0.7}$-HEC may be due to the inaccessibility of MMA to some initiation sites of the HEC backbone.

## 4.3.3. Poly(N-vinylpyrrolidone) grafted from Br-HEC

The macro-initiator Br-HEC **3** with a DS of 0.7 described in part 4.3.1 was used to initiate the ATRP of N-vinylpyrrolidone **6** (Scheme 4-3) because the reactivity of Br-HEC was demonstrated with the initiation of the ATRP of MMA from the HEC backbone (part 4.3.2). For the ATRP of NVP, a higher degree of polymerisation (DP ~600) was chosen compared to that for the ATRP of MMA (DP ~125) because of the anticipation of a low monomer conversion which will still produce long chain length. However, the ratio of initiator to catalyst and ligand was the same as that for the ATRP of MMA. The reaction was run overnight at 60 ºC under an oxygen-free environment. Based on the product **7** weight recovery, a 0.5% of monomer conversion was calculated and a graft chain length of 3 repeat units of NVP was estimated. Due to the lack of solubility in common deuterated solvents, the graft-copolymer was characterised using solid state $^{13}C$ CP-MAS NMR and FT-IR spectroscopies. Furthermore, the grafts were not hydrolysed from the backbone because SEC is not suitable for such short chain lengths. However, the determination of the content of nitrogen provided an estimation of the chain length.

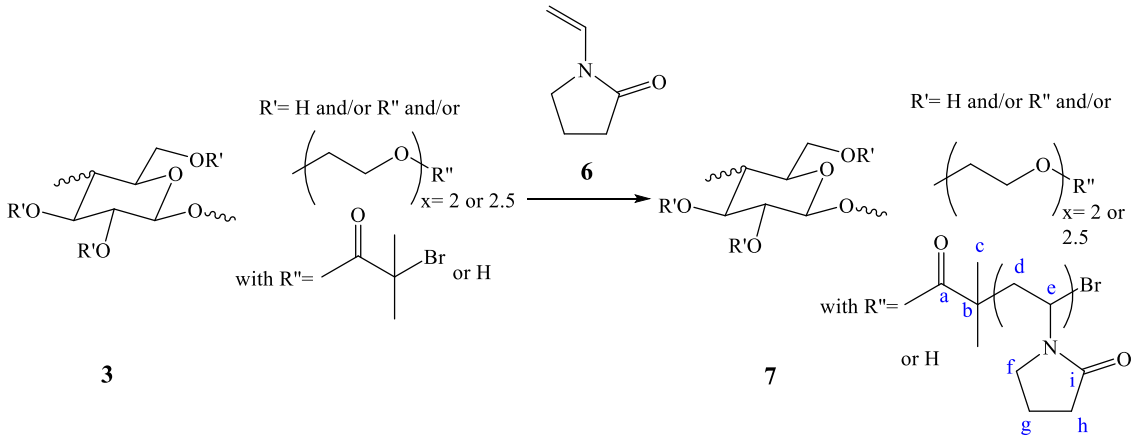


**Scheme 4-3:** Atom Transfer Radical Polymerisation of N-vinylpyrrolidone **6** from $Br_{0.7}$-HEC **3**

The solid state $^{13}C$ CP-MAS NMR spectrum was recorded and is shown in Figure 4-12. The set of signals from $\delta_C$ ~62 ppm to 104 ppm is assigned to carbons of the HEC backbone. The peak $\delta_C$ ~62 ppm is assigned to the carbon of primary alcohols -**C**$H_2$OH; $\delta_C$ ~72 ppm to carbons constituting the side chain -**C**$H_2$**C**$H_2$O-; $\delta_C$ ~75 ppm to the group of carbons at C2, C3 and C5 positions; $\delta_C$ ~83 ppm to the carbon at C4 position; $\delta_C$ ~104 ppm to the anomeric carbon. Furthermore, the set of signals $\delta_C$ ~19 ppm, 32 ppm and 43 ppm are assigned to the pyrrolidone ring. More precisely, the peak $\delta_C$ ~19 ppm is assigned to the -$CH_2$-**C**$H_2$-$CH_2$- group; $\delta_C$ ~32 ppm to the -**C**$H_2$-C=O group; $\delta_C$ ~43 ppm to the -**C**$H_2$-N- group. The peak $\delta_C$ ~177 ppm is assigned to both carbonyl groups from the pyrrolidone ring and the macro-initiator. The weak peak $\delta_C$ ~23 ppm is assigned to the methyl groups of the bromoisobutyryl group residue in the macro-initiator, Br-HEC. Furthermore, the weakness of the carbon signals assigned to poly(N-vinylpyrrolidone) compared to those of HEC suggests a relatively low degree of polymerisation.

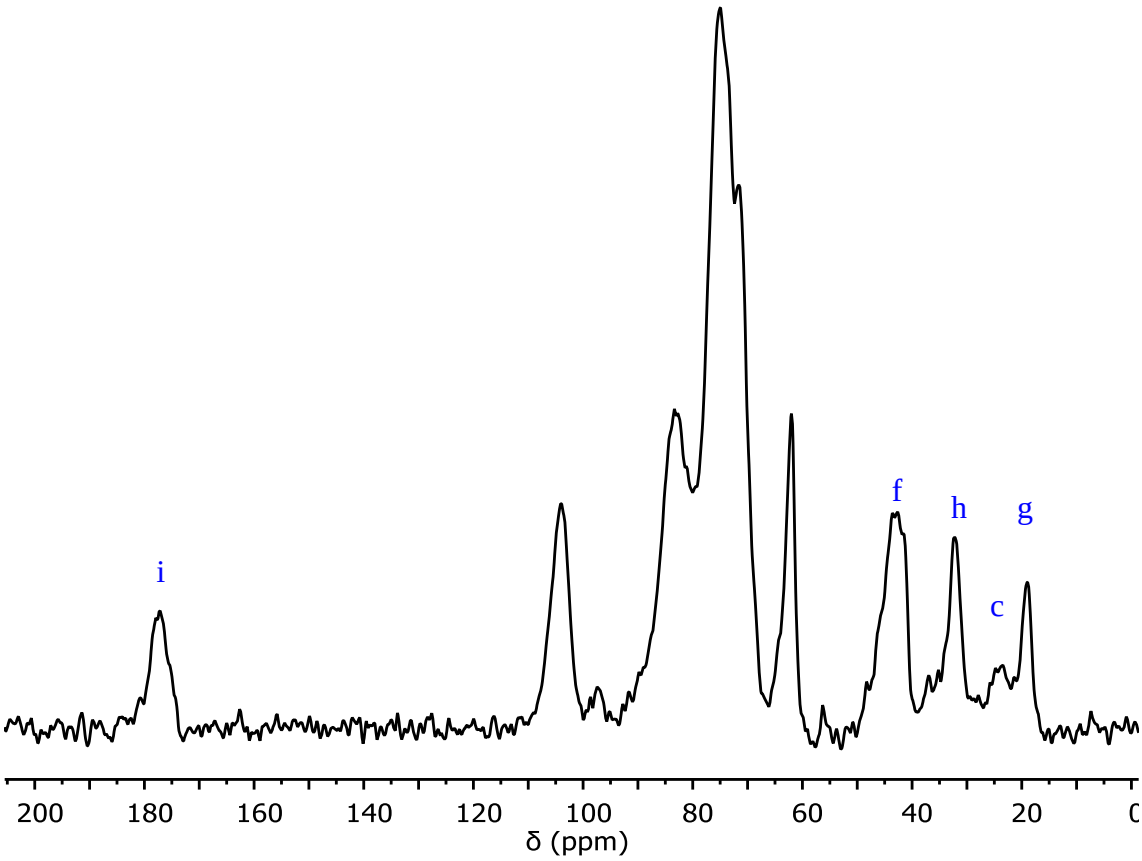


**Figure 4-12:** Solid state $^{13}C$ CP-MAS NMR spectrum of HEC-g-PVP **7**

Figure 4-13 displays the FT-IR spectrum of HEC-g-PVP. The absorption bands between 800 $cm^{-1}$ to 1230 $cm^{-1}$ are assigned to the -C-O stretching vibrations. Furthermore, the absorption band at 1300 $cm^{-1}$ is assigned to the bending vibration of -C-H in the methyl groups. The absorption band at 2900 $cm^{-1}$ is assigned to the -C-H stretching vibrations of the $-CH_2$ and $-CH_3$ groups. Furthermore, an absorption band at 3400 $cm^{-1}$ was recorded and was respectively assigned to the -OH group stretching and bending vibrations of the HEC backbone. Two absorption bands are detected at 1670 $cm^{-1}$ and 1726 $cm^{-1}$ which are assigned to the stretching vibration of carbonyl -C=O groups. In fact, one carbonyl group is involved in the pyrrolidone ring and another from the bromoisobutyryl group. However, a much stronger carbonyl absorption band was expected for the carbonyl group

of the pyrrolidone ring as the targeted DP was ~600, this then suggested a drastically low degree of polymerisation.

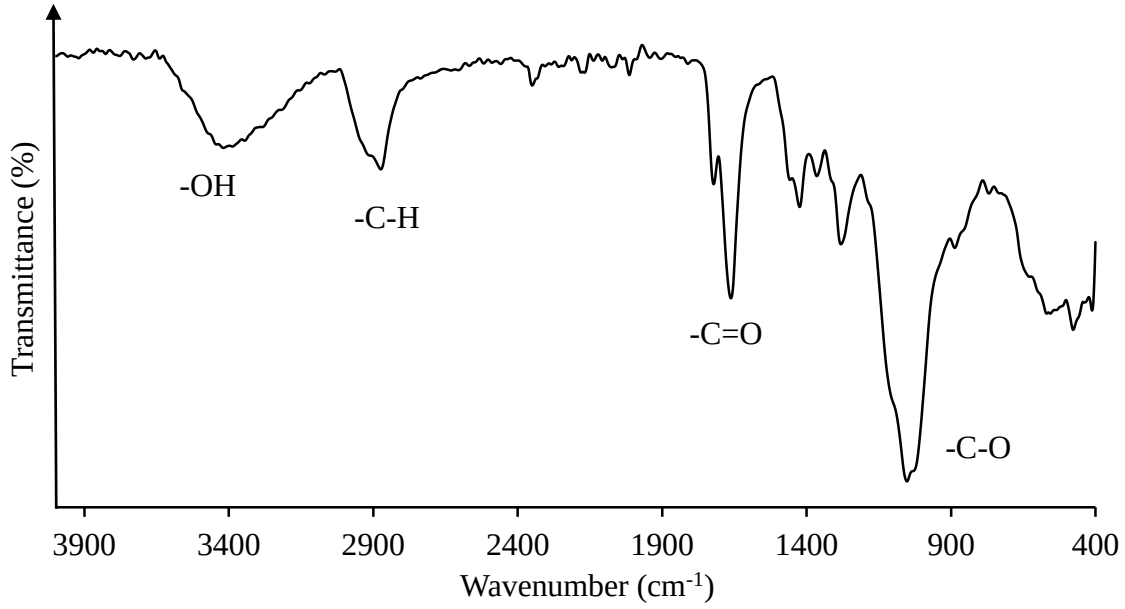


**Figure 4-13:** FT-IR spectrum of HEC-g-PVP **7**

In order to quantify the DP of NVP ($DP_{NVP}$) per repeat unit of HEC, the content of N was modelled as a function of the $DP_{NVP}$ which was ranged from 0 to 600 by increments of 1 and the model is represented in Equation 4-4.

$$\%N = (DP_{NVP} \times M_N) / (DS_{Br} \times (M_{Br} + DP_{NVP} \times M_{NVP}) + M_{HEC} - DS_{Br}) \times 100 \quad \textbf{(4-4)}$$

where $M_N$, $M_{Br}$, $M_{NVP}$, $M_{HEC}$ and $DS_{Br}$ are constant values and correspond respectively to atomic weight of nitrogen, molecular weight of the bromoisobutyryl group, the repeat unit in PVP, the repeat unit in HEC and the DS of Br-HEC.

$DP_{NVP}$ values were then plotted as a function of the theoretical content of nitrogen values (Appendix 5). A mathematical model cannot be fitted to the entire curve, however, a model can be performed on a segment of the data between a nitrogen content of 0% to 12% and the model is described in Equation 4-5.

$$DP_{NVP} = 7\times10^{-5} \times (\%N)^5 - 0.0017 \times (\%N)^4 + 0.0172 \times (\%N)^3 - 0.0532 \times (\%N)^2 + 0.3503 \times (\%N) - 0.0001 \quad \textbf{(4-5)}$$

The recorded %N from elemental analysis is 1.69% which gives a $DP_{NVP}$ less than 1 (0.7) per bromine. Considering the discussion in part 4.3.2, the reactivity of the bromine in $Br_{0.7}$-HEC was partial and only 1 bromine from 12 activated the ATRP of MMA. This suggests that $DP_{NVP}$ is 12 times more than 0.7 resulting in a chain length of PVP of approximately 8 repeating units.

To summarise, HEC-g-PVP was prepared and the presence of the repeating unit NVP was demonstrated by NMR and FT-IR spectroscopies, however the signals of PVP were weaker compared to those of HEC, indicating a poor polymerisation efficiency. Furthermore, the weight recovery and the amount of %N confirmed the low grafting efficiency with a degree of NVP polymerisation varying from 1 to 8 per bromine depending on the calculation. A possible reason for the low DP is due to deactivation of the catalyst because of its binding to the amine containing in the monomeric species. Other plausible reasons for the problems of performing ATRP of NVP are reported in the literature[109, 110], including substitution of the halide by of the propagating chain ends by the amide and the low values of the ATRP equilibrium constant for amide monomers. Thus, ATRP of NVP remains a highly challenging particularly on a cellulosic material.

Further work may need necessary to develop a catalyst system which is not deactivated by the monomer species.

### 4.3.4. Poly(1-(11-acryloyloxyundecyl)-3-methylimidazolium bromide) grafted from Br-HEC

An acryloyl-based ionic liquid (IL) monomer, 1-(11-acryloyloxyundecyl)-3-methylimidazolium bromide **5** was synthesised following a 2-step procedure (Scheme 4-4) found in the literature[111]. The first step consisted of reaction of bromo-11-undecanol **1** with acrylic acid **2** forming the acrylate **3** in a yield of 88%, and the second step, substitution of the bromine with 1-methylimidazole **4** forming thus the imidazolium salt **5** which was obtained in a yield of 85%.

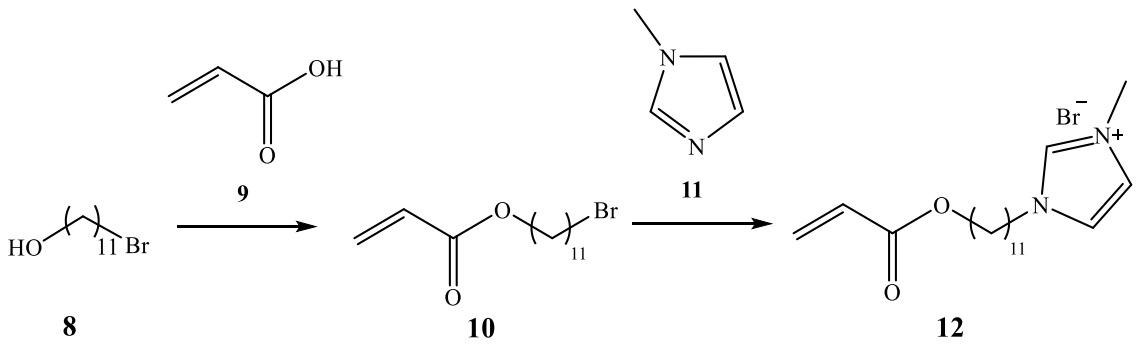


**Scheme 4-4:** Preparation of 1-(11-acryloyloxyundecyl)-3-methylimidazolium bromide **12**

IL **12** was graft-copolymerised from macro-initiator $Br_{0.7}$-HEC **3** with 0.7 DS (Scheme 4-5). The ratio of initiator to catalyst and ligand was equal to 1:1:2 and is the same as that

used for the ATRP of MMA and NVP. The polymerisation proceeded at 90 ºC overnight under oxygen-free environment and the graft-copolymer was isolated by precipitation in methanol, in which IL and P(IL) are both soluble. Different degrees of polymerisation and concentration of initiator were chosen and are summarised in Table 4-5.

**Table 4-5:** Reaction conditions for the graft-copolymerisation of 1-(11-acryloyloxyundecyl)-3-methylimidazolium bromide onto $Br_{0.7}$-HEC

| Exp. N° | $Br_{0.7}$-HEC | | IL | | DMSO (mL) | Ratio [M]:[AGU]:[C]:[L] | Concentration of AGU (g/mL) | Yield (%) |
|---|---|---|---|---|---|---|---|---|
| | g | mol ($\times10^{-4}$) | g | mol ($\times10^{-2}$) | | | | |
| **FJ - 230** | 0.08 | 2.0 | 8.0 | 2 | 20 | 100/1/1/2 | $4\times10^{-3}$ | 5 |
| **FJ - 248** | 0.05 | 1.2 | 5.0 | 1.3 | 6 | 100/1/1/2 | $8.3\times10^{-3}$ | 11 |
| **FJ - 282** | 0.50 | 12 | 4.7 | 1.2 | 5 | 10/1/1/2 | 0.1 | 30 |

A DP of 100 was aimed for experiment FJ-230 and FJ-248 whereas a DP of 10 was targeted for the experiment FJ-282. The decrease of the DP permitted the easier detection of the graft-copolymer's HEC backbone by both NMR and FT-IR spectroscopies as previously demonstrated by the HEC-g-PMMAs discussed in part 4.3.2. The influence of the concentration of initiator on the grafting efficiency was also studied. For experiment FJ-230, a $4\times10^{-3}$ g/mol concentration was chosen whereas this was increased by a factor 2 for the experiment FJ-248 followed by an increase of a factor 10 for experiment FJ-282. Due to insolubility in common deuterated solvents, the graft-copolymers were characterised in the solid state using NMR and FT-IR spectroscopies.

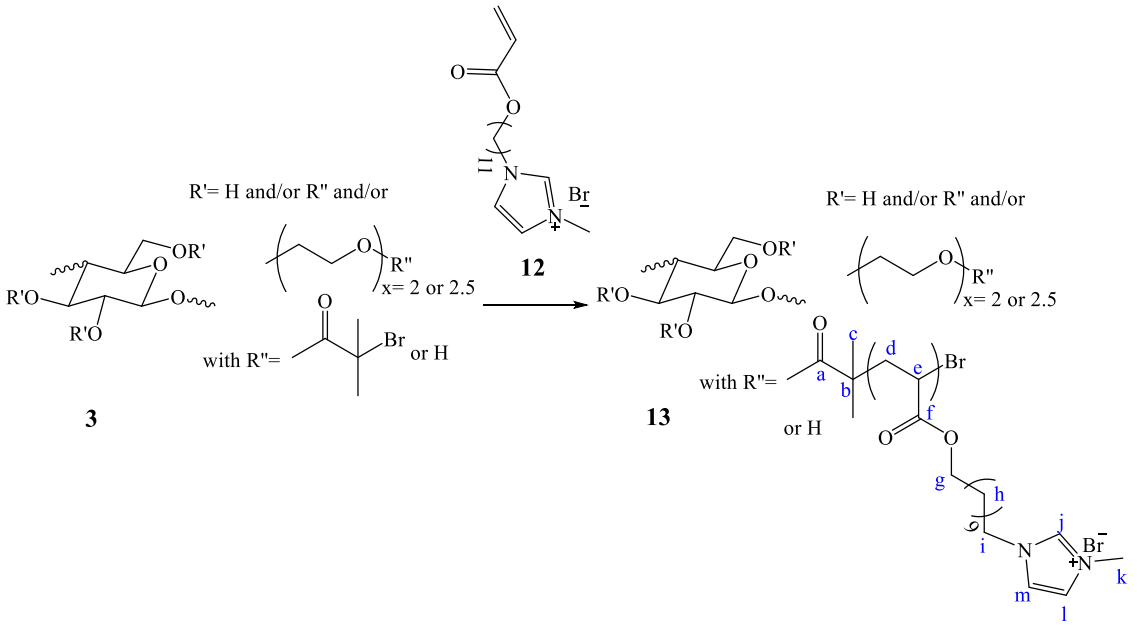


**Scheme 4-5:** Atom Transfer Radical Polymerisation of 1-(11-acryloyloxyundecyl)-3-methylimidazolium bromide **12** onto $Br_{0.7}$-HEC **3**

The solid state $^{13}C$ CP-MAS NMR spectrum of the HEC-g-P(IL)s from experiment FJ-230 (Figure 4-14 a) showed signals related to the presence of the P(IL) grafts. The peak $\boldsymbol{\delta}_C$ ~27 ppm is assigned to the methyl groups from the bromoisobutyryl group; $\boldsymbol{\delta}_C$ ~31 ppm is assigned to the methylene and methine groups; $\boldsymbol{\delta}_C$ ~37 ppm is assigned to the methyl groups carried by the tertiary amine and $\boldsymbol{\delta}_C$ ~51 ppm is assigned to the methylene groups next to the oxygen and nitrogen present in the grafts. The carbons contained in the imidazolium ring were detected at $\boldsymbol{\delta}_C$ ~124 ppm and 138 ppm. The signals of P(IL) are narrow indicating a short length chain and this explains the lack of detection of the carbonyl groups of P(IL). Although the chain length of the grafts is expected to be short, the HEC backbone was not detected because of the high molecular weight of the monomer. In the spectrum (Figure14 b) of the graft-copolymers from experiment FJ-248 where the concentration of initiating site was higher, the same signals are detected; however they become broader and then overlapped suggesting an increased chain length.

Furthermore, the detection of the peak $\delta_C$ ~175 ppm assigned to the carbonyl group of the acrylate monomer corroborated with the increase of the molecular weight of the grafts. The spectrum of HEC-g-P(IL) from experiment FJ-282 (Figure 14 c) shows signals assigned to P(IL), however weak and broad signals appeared between $\delta_C$ ~60 ppm and 110 ppm which are commonly assigned to the carbons of the HEC backbone. The detection of HEC suggests that the chain length chain was shorter compared to that of HEC-g-P(IL) of experiment FJ-230 and FJ-248.

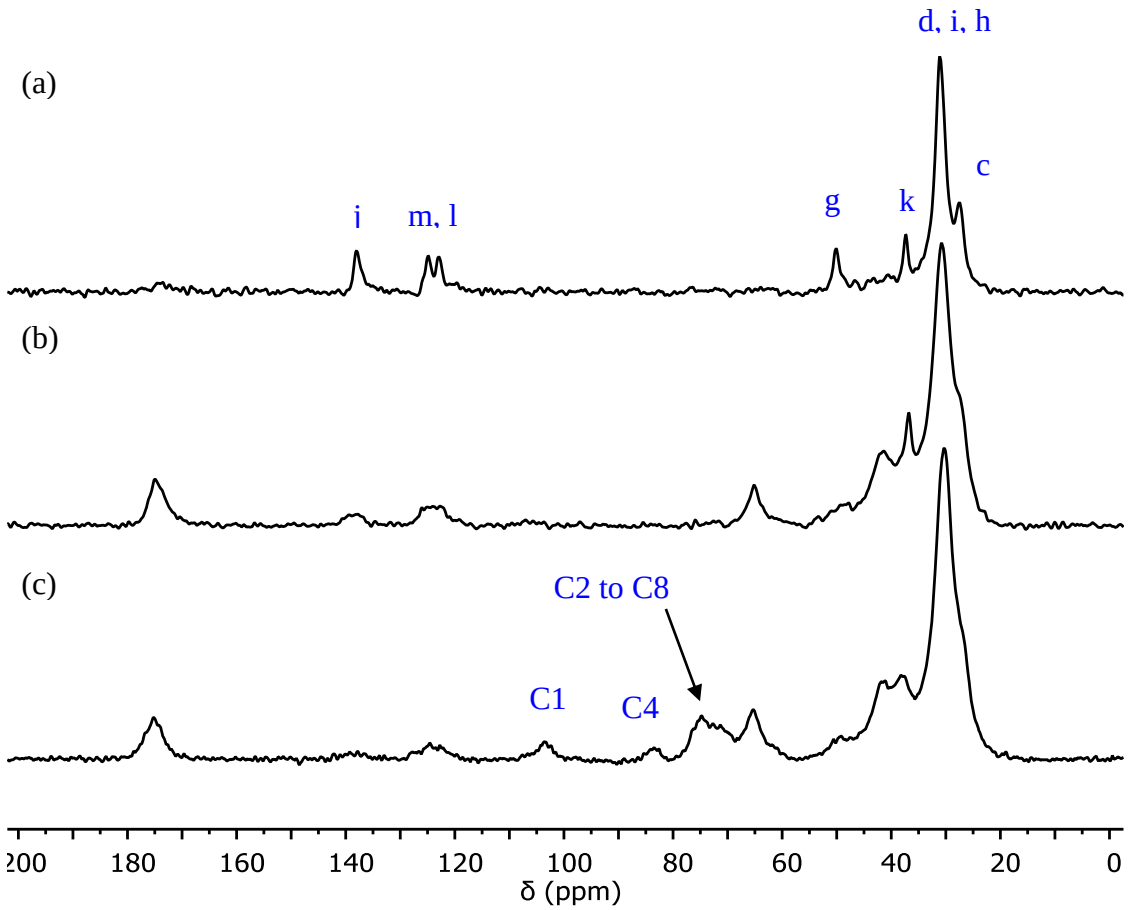


**Figure 4-14:** Solid state $^{13}C$ CP-MAS NMR spectra of HEC-g-P(IL)s **13;** (a) FJ-230, (b) FJ-248 and (c) FJ-282.

The FT-IR spectra of the graft-copolymers are displayed in Figure 4-15. Each spectrum shows the same set of absorption bands which are principally assigned to the P(IL) grafts.

The absorption band at 620 $cm^{-1}$ is assigned to the stretching vibration of the -C-Br. The absorption bands at 1082 and 1170 $cm^{-1}$ are both assigned to -C-O- stretching vibration, however, the former (1082 $cm^{-1}$) is related to the ester group in the P(IL) and the latter (1170 $cm^{-1}$) to the ester contained in the macro-initiator Br-HEC. The weak absorption band at 1264 $cm^{-1}$ is assigned to the -C-O stretching vibration of the ether group in Br-HEC. The absorption bands at 1468 and 1574 $cm^{-1}$ are assigned to the double bond stretching vibration in the imidazolium ring and the strong absorption band at 1732 $cm^{-1}$ is assigned to the carbonyl group. The absorption band at 2854 and 2924 $cm^{-1}$ is assigned to the stretching vibration of -C-H in alkanes and the absorption band at 3400 $cm^{-1}$ to the -O-H stretching and bending vibration in HEC. However, some difference were observed between spectra, more precisely in the relative intensity of the band at 1082 $cm^{-1}$ which decreased in the spectrum of HEC-g-P(IL) (Figure 4-15 c) of experiment FJ-282 compared to that of the two other graft-copolymers (Figure 4-15 a & b). Furthermore, an increase of the relative intensity is observed between the spectrum of HEC-g-P(IL) of experiment FJ-230 (Figure 4-15 a) and FJ-248 (Figure 4-15 b). Due to the assignment of the band to the ester group in the P(IL), the increase in the spectra translates to an increase of the length chain of the grafts.

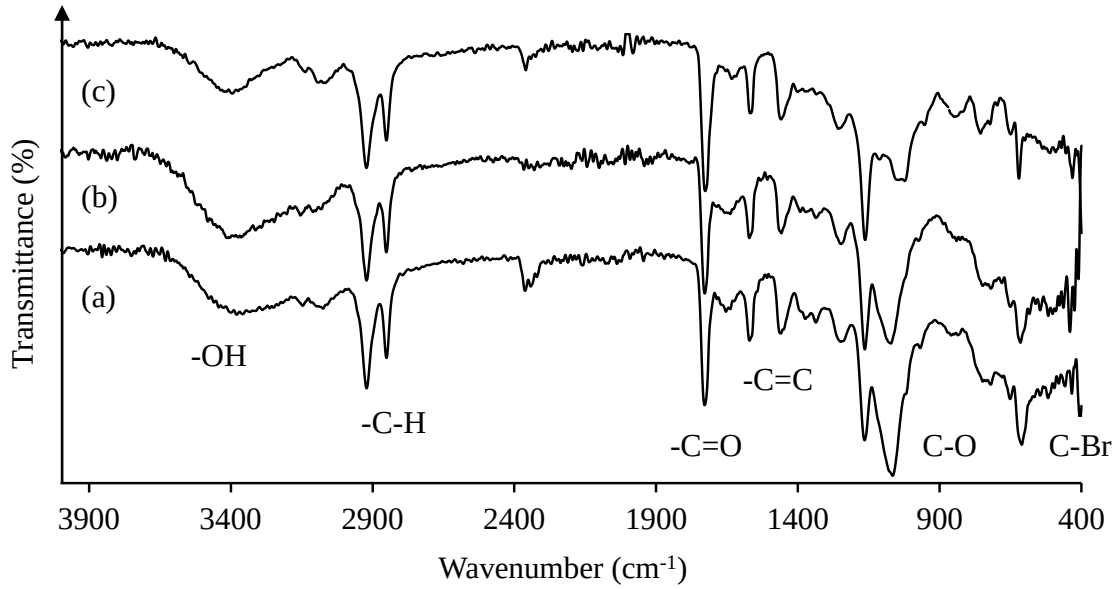


**Figure 4-15:** FT-IR spectra of HEC-g-P(IL)s **13;** (a) FJ-248, (b) FJ-230 and (c) FJ-282.

Based on the weight recovery, monomer conversion was estimated for each experiment and the chain length of each graft-copolymer was determined. For experiment FJ-230, 5% of monomer conversion was calculated whereas for experiment FJ-248, the monomer conversion was increased by a factor 2 due to the increase by 2 of the concentration of initiation sites. The HEC-g-P(IL)s of experiment FJ-230 and FJ-248 had a length chain of 5 and 11 repeating units respectively. For experiment FJ-282, a 30% monomer conversion was obtained leading to grafts of 3 repeating units because of the low targeted DP. This increase arises from the increase of the concentration of initiating sites, enhancing the rate of polymerisation.

To summarise, characterisation using NMR and FT-IR spectroscopies highlighted the presence of the P(IL) instead of the backbone due to the rigidity of the HEC structure and

the number of monomer species per AGU unit. Both FT-IR and NMR spectra indicated a difference of chain length between the graft-copolymers and this is corroborated by the weight recovery which was used to determine the monomer conversion. Assuming that the molecular weight distribution was narrow, DP was estimated from the monomer conversion determined for each experiment and ranged from 3 to 11 depending on the concentration of AGU in the solvent. The dispersity was not measured using SEC because P(IL) were not hydrolysed from the backbone due to a very low value of DP.

## 4.4. CONCLUSION

The macro-initiator, Br-HEC has been successfully prepared with a DS ranging from 0.3 up to 0.9, in a yield of ~80%. To verify its activity for the ATRP process, Br-HEC was used to polymerise a well-known acrylate monomer, methyl methacrylate which is readily homo-polymerised using ATRP. The polymerisation lead to monomer conversion up to 61% and a narrow molecular weight distribution of the PMMA grafts with $Đ_M$ of ~1.2. However, polymerisation of MMA was not activated by each bromine suggesting a limited accessibility of the monomer to the initiation site due to the steric hindrance and /or H-bonding networks. Although the "grafting from" approach limited the graft-density of the polymeric chains onto HEC, the graft-copolymerisation of N-vinylpyrrolidone onto Br-HEC was investigated for the first time. However it has been unsuccessful presumably because of the deactivation of the catalyst in the presence of amide. In order to prepare a bactericidal graft-copolymer, an acrylate containing an imidazolium ring, 1-(11-acryloyloxyundecyl)-3-methylimidazolium bromide was also graft-copolymerised onto Br-HEC leading to 30% of monomer conversion. Although graft-copolymers of HEC can be prepared using the ATRP method, this approach involves important difficulties and

there are limitations in the characterisation. For instance, hybrid materials could not be studied in the liquid phase due to their insolubility in common solvents and the detection of the HEC backbone was extremely challenging using standard spectroscopy analysis. The chain length of the grafts was estimated using the weight recovery, however, the dispersity was unknown as the grafts were not hydrolysed from the HEC backbone. Because of the difficulties in characterisation, the relatively poor level of grafting, and the limited solubility of the graft-copolymers, the physical properties such as viscosity, thermal stability and bacteriological effects were not evaluated.

# Chapter 5: "Grafting to" approach for preparing graft-copolymers of hydroxyethyl cellulose

## 5.1. INTRODUCTION

Due to the unsuccessful preparation of well-defined graft-copolymers using the "grafting from" approach in Chapter 4, our strategy changed to the "grafting to" approach which has received much less attention (see Chapter 1, Section 1.1.3.2.3.). The "grafting to" permits both the preparation of well-defined synthetic polymers and the control of the graft-density along the cellulose backbone, determined by the DS of the hydroxyl groups. Comparing to the "grafting from" approach, "grafting to" allows the full characterisation of both the grafts and the cellulose backbone using conventional instruments prior to "clicking" and there is no need to hydrolyse the grafts after coupling to permit analyses.

Atom transfer Radical Polymerisation (ATRP)[53, 112] and Reversible Addition-Fragmentation Chain-Transfer (RAFT)[48, 54] polymerisation were used previously for "grafting to" cellulosic materials, however, RAFT polymerisation has been chosen for preparing synthetic polymers because of the wider number of monomers that can be polymerised compared to ATRP. Furthermore, the required conditions for RAFT polymerisations are less constrained than those for ATRP (e.g., no need for a rigorously oxygen-free environment or the use of a copper catalyst). For instance, N-vinylpyrrolidone (NVP) was poorly polymerised *from* hydroxyethyl cellulose (HEC) using ATRP (Chapter 4, Section 4.3.3.) because of the deactivation of the catalyst by the amide, however NVP can be polymerised efficiently using RAFT polymerisation, with an appropriate chain transfer agent. In the literature[113-117], both xanthate and dithiocarbamate chain transfer agents were shown to be good candidates for polymerising

NVP, a monomer that is a member of the "less activated monomers" (LAM) class described by Keddie *et al.*[5]. The presence of the double bond next to a nitrogen leads to conjugation between the C=C and the nitrogen lone pair which leads to the low activity of such monomers, thus their RAFT polymerisation requires the use of less active RAFT agents such as xanthates or dithiocarbamates which have high transfer constants. This also explains why Mori *et al.*[103] used a xanthate-type transfer agent to RAFT polymerise vinylimidazolium salt-based ionic liquid (IL) monomers leading to a monomer conversion up to 78% and dispersity ($Đ_M$) ranging from 1.2 to 1.4. Vijayakrishna *et al.*[104], however, used dithiocarbonate to RAFT polymerise meth(acryloyl)-based IL monomers such as 2-(1-methylimidazolium-3-yl)ethyl methacrylate bromide and 2-(1-ethylimidazolium-3-yl)ethyl methacrylate bromide and a lower monomer conversion was obtained after a longer reaction time. $Đ_M$ was not determined using size exclusion chromatography (SEC), but the degree of polymerisation was estimated using $^1$H NMR spectroscopy and was in agreement with the monomer conversion determined using $^1$H NMR spectroscopy.

A new range of RAFT agents[118] was developed for preparing clickable polymers, including alkyne-terminated chain transfer agents which have been used to RAFT polymerise vinyl acetate, styrene or butyl acrylate[119-123]. For instance, Patel *et al.*[124] and Akeroyd *et al.*[119] reported the preparation of alkyne-terminated xanthate RAFT agents which were used for preparing clickable PVP or "macro-RAFT agents" which were subsequently used to RAFT polymerise NVP. Furthermore, alkyne-terminated trithiocarbonate was successfully prepared and were used to polymerise "more activated monomers" (MAMs), another class of monomer described by Keddie *et al.*[5] such as NIPAAM[125-127].

Huisgen azide-alkyne cycloaddition (CuAAC) was chosen to click poly(NVP), prepared using alkyne-terminated xanthate, to HEC which was prior-functionalized with sodium azide. Evidence of the coupling was provided using a partially labelled $N_3$-HEC. In order to confirm the versatility of our method, PNIPAAM that was polymerised using an alkyne-terminated trithiocarbonate chain transfer agent, was coupled to $N_3$-HEC. This proves that coupling can be promoted between other synthetic polymers, presenting attractive properties such as stimuli-responsiveness or bactericidal properties leading to broadened uses of cellulose in industrial applications. The preparation of a bactericidal-based HEC from an acryloyl-based ionic liquid (IL) monomer was discussed in Chapter 4, however, the "grafting from" technique was not efficient. Thus, we decided to use this straightforward method to prepare well-defined graft-copolymers HEC-g-P(IL)s and variants containing different chain lengths which were tested against both bacteria and human cells determining the cytotoxicity.

## 5.2. EXPERIMENTAL

### 5.2.1. Materials

2-Hydroxyethyl cellulose (HEC) ($M_w$ =90 kDa, MS =2.5), sodium azide ($NaN_3$), $^{15}N$-labelled sodium azide ($Na^{15}N$), tetrabromide, triphenylphosphine, propargyl bromide solution (80% wt. in toluene), potassium ethyl xanthogenate, N-(3-dimethylaminopropyl)-N'-ethylcarbodiimide (EDC), 4-(dimehylamino)pyridine (DMAP), 2-(dodecylthiocarbonothioylthio)-2-methylpropionic acid (trithiocarbonate CTA), propargyl alcohol, 2,2′-azobis(2-methylpropionitrile) (AIBN), N-vinylpyrrolidone (NVP), N-isopropyl acrylamide (NIPAAM), sodium L-ascorbate, copper (II) sulphate pentahydrate, N,N,N′,N′-tetramethylethylenediamine (TMEDA), dimethylformamide

(DMF), pentane, sodium chloride, 1,4-dioxane, ampicillin sodium salt, Luria broth and deuterated chloroform ($CDCl_3$) were purchased from Sigma Aldrich. Iso-sensitest broth was obtained from Oxoid$^{TM}$. Toluene, diethyl ether, acetone, tetrahydrofuran (THF), dichloromethane (DCM), 1 M solution hydrochloride, hexane and chloroform were supplied from Fisher Scientific and deuterated DMSO-$d_6$ was purchased from Apollo Scientific. Both bacteria, *Escherichia coli* K-12 wild-type strain (W3110 / ATCC27325, F-, λ-, rpoS(Am), rph-1, Inv(rrnD-rrnE)) and *Staphylococcus aureus* (3R7089 strain Oxford / ATCC9144) were prepared in the laboratory. A549 immortalized lung alveolar cell line was provided from the American tissue culture collection (ATCC). Dulbecco's Modified Eagle Medium (DMEM), Fetal Calf Serum (FCS) and Almar blue were purchased from Life Technologies Limited (UK).

## 5.2.2. Characterisation techniques

Solution state NMR spectra were recorded using a Bruker Advance 400 spectrometer at 400.13 MHz ($^1$H) and 100.60 MHz ($^{13}$C). For solid state NMR spectroscopy, a Varian VNMRS spectrometer with a 9.4 T magnet was used and $^{13}$C (100.562 MHz) and $^{15}$N (40.527 MHz) experiments were run using the cross polarisation method. IR spectra were recorded on a Perkin-Elmer 1600 Series FT-IR spectrometer. For PVP and PNIPAAM, molecular weight data and the dispersity ($Đ_M$) were obtained using triple detection size exclusion chromatography (SEC) on a Viscotek TDA 302 with refractive index, viscosity and light scattering detectors and 2 × 300mL PLgel 5 μm mixed C columns. Dimethylformamide (DMF) was used as the eluent at a flow rate of 1.0 mL/min and at a constant temperature of 70 ºC. For ionic liquid polymers, molecular weight data and the

dispersity ($Đ_M$) were obtained using triple detection SEC on a Viscotek TDA 301 with refractive index, viscosity and light scattering detectors and 2 × 300mL PL HFIPgel 9 µm columns. 1,1,1,3,3,3-Hexafluoropropan-2-ol with 25mM NaTFAc was used as the eluent at a flow rate of 0.8 mL/min and at a constant temperature of 40 ºC.

## 5.2.3. Synthesis and characterisations

### 5.2.3.1. Preparation of $N_3$-HEC

In a round-bottomed flask fitted with a condenser, 2-hydroxyethyl cellulose **1** ($M_w$ =90 000 g/mol, MS =2.5, 2.5 g, $9.19\times10^{-3}$ mol, 1 eq), sodium azide (3.8 g, $5.85\times10^{-2}$ mol, 6 eq.) and $^{15}$N-labelled sodium azide $Na^{15}N_3$ (0.1 g, $1.54\times10^{-3}$ mol, 0.1 eq) were dissolved in DMF (100 mL). The mixture was heated to 80 °C for 1 h in order to dissolve HEC. The mixture was cooled to room temperature and carbon tetrabromide (14.3 g, $4.31\times10^{-2}$ mol, 5 eq) was added. Triphenylphosphine (11.8 g, $4.50\times10^{-2}$ mol, 5 eq) dissolved in DMF (12.5 mL) was added carefully to the HEC mixture. The reaction was then left for 24 h at room temperature under magnetic stirring. The product was precipitated by addition of toluene (500 mL) and collected by filtration. The solid was dissolved in DMF (50 mL) and re-precipitated using diethyl ether (500 mL). After being filtered, the solid was washed with acetone (100 mL) and dried under vacuum at 50 °C overnight. The product **2** was obtained as a light yellow solid in quantitative yield (3.1 g). The product was characterised using solid state $^{13}$C, $^{15}$N CP-MAS NMR and FT-IR spectroscopies.

## 5.2.3.2. Preparation of the chain transfer agents

### 5.2.3.2.1. O-ethyl S-prop-2-ynyl carbonodithiolate

In a one-necked, round-bottomed flask, propargyl bromide solution **3** (80% wt. in toluene, 1.02 g, $8.57\times10^{-3}$ mol) and potassium ethyl xanthogenate **4** (1 g, $6.24\times10^{-3}$ mol) were dissolved in THF (10 mL). The flask was covered with aluminium foil and the reaction was run overnight at room temperature. THF (100 mL) was added and the mixture was filtered to remove KOH. The excess solvent was evaporated and distilled water (10 mL) was added to the residues. The product was extracted with diethyl ether (3×30 mL). The diethyl ether was removed under vacuum and the final product **5** was purified *via* column chromatography using pentane as eluent and dried under vacuum overnight. The product was obtained as pale yellow oil in a yield of 48% (0.48 g). $^{1}$H NMR (400 MHz, DMSO-$d_6$): $\delta_H$ (ppm) 1.4 (t, J =7.0 Hz, 3H, C**H**$_3$-$CH_2$-O), 3.2 (t, J =2.6 Hz, 1H, C**H**≡C-), 4.0 (d, J =2.6 Hz, 2H, CH≡C-C**H**$_2$-), 4.6 (q, J =7.0 Hz, 2H, -C**H**$_2$-O); $^{13}$C NMR (400 MHz, DMSO-$d_6$): $\delta_C$ (ppm) 13.5 (**C**$H_3$-$CH_2$-O-), 23.5 (-**C**$H_2$-S-), 70.6 (-**C**$H_2$-O-), 74.1 (**C**H≡C-), 78.6 (CH≡**C**-), 211.8 (-**C**=S).

### 5.2.3.2.2. Alkyne-terminated trithiocarbonate

In a one-necked, round-bottomed flask, trithiocarbonate CTA **6** (1 g, $2.74\times10^{-3}$ mol, 1 eq.), N-(3-dimethylaminopropyl)-N′-ethylcarbodiimide (EDC) (0.783 g, $5.04\times10^{-3}$ mol, 2 eq.) and 4-(dimethylamino)pyridine (DMAP) (0.5 g, $4.09\times10^{-3}$ mol, 2 eq.) were dissolved in dichloromethane (10 mL) and the mixture was purged with nitrogen for 10 min. Propargyl alcohol **7** (0.5 mL, $8.59\times10^{-3}$ mol, 3 eq.) was added and the mixture was stirred

overnight at room temperature under a positive $N_2$ pressure. The flask was opened to air and the product **8** was extracted by washing with each of the following solvents (3×30 mL); dilute aqueous HCl, distilled water and brine solution (3.5% w/w NaCl). After concentration of the organic layer under vacuum, the product **8** was obtained as a viscous yellow liquid in a yield of 87% (0.95 g). $^1$H NMR (400 MHz, $CDCl_3$): $\delta_H$ (ppm) 0.8 (t, 3H, J =7.0 Hz, C**H**$_3$-$CH_2$-), 1.19-1.66 (m, 20H, $CH_3$-(C**H**$_2$)$_{10}$-), 1.6 (s, 6H, -S-C(C**H**$_3$)$_2$-), 2.4 (t, 1H, J =2.4 Hz, -C≡C**H**), 3.2 (t, 2H, J =7.5, -C**H**$_2$-S-), 4.6 (d, 2H, J =2.5 Hz, -O-C**H**$_2$-); $^{13}$C NMR (100 MHz, $CDCl_3$): $\delta_C$ (ppm) 14.3 (**C**$H_3$-), 22.8 ($CH_3$-**C**$H_2$-), 25.4 (C-(**C**$H_3$)$_2$-), 28-32 (9C, $CH_3$-$CH_2$-(**C**$H_2$)$_9$-), 37.1 (-**C**$H_2$-S-), 53.5 (-O-**C**$H_2$-), 55.7 (-**C**$(CH_3)_2$-), 75.2 (-C≡**C**H) , 77.4 (-**C**≡CH), 172.5 (-**C**=O).

## 5.2.3.3. RAFT polymerisations

### 5.2.3.3.1. Synthesis of poly(N-vinylpyrrolidone)

In a one-necked, round-bottomed flask, O-ethyl S-prop-2-ynyl carbonodithiolate **5** (0.50 g, $3.05\times10^{-3}$ mol, 1 eq.), AIBN (0.35 g, $2.13\times10^{-3}$ mol, 0.7 eq.) and N-vinylpyrrolidone **9** (3.44 g, $3.09\times10^{-2}$ mol, 10 eq.) were dissolved in toluene (20 mL). The mixture was purged with $N_2$ for 10 min. The flask was sealed and the reaction was run overnight at 70 °C. The mixture was then cooled to room temperature and the product was precipitated using diethyl ether (200 mL). The product was collected by filtration and dried overnight under vacuum at 40 °C. The product **10** was obtained as a white powder in quantitative yield (3.30 g). The polymer was characterized using solution state $^1$H NMR spectroscopy and SEC. NMR spectra were recorded in $CDCl_3$ and the number average molecular weight ($M_n$) and the dispersity ($Đ_M$) were determined using SEC with conventional

calibration (PMMA standards). Solid state $^{15}$N CP-MAS NMR (40.52 MHz): $\delta_N$ (ppm) ~-253.8.

#### 5.2.3.3.2. Synthesis of poly(N-isopropyl acrylamide)

In a one-necked, round-bottomed flask, alkyne-terminated CTA **8** (0.4 g, $9.93\times10^{-4}$ mol, 1 eq.), N-isopropyl acrylamide **11** (1.12g, $9.90\times10^{-3}$ mol, 10 eq.), and AIBN (0.02 g, $1.21\times10^{-4}$ mol, 0.12 eq.) were dissolved in 1,4-dioxane (10 mL). The flask was purged with $N_2$ for 15 min and, once sealed, the polymerisation was run overnight at 60 °C. The polymer was precipitated in hexane (100 mL) and recovered by filtration. The product **12** was dried overnight under vacuum at 40 °C and was obtained as a white powder in a yield of 87% (1.12 g). The polymer was characterised using solution state $^1$H NMR spectroscopy and SEC. NMR spectra were recorded in $CDCl_3$ and the $M_n$ and $Đ_M$ were determined using SEC with conventional calibration (PMMA standards).

#### 5.2.3.3.3. Synthesis of poly(1-(11-acryloyloxyundecyl)-3-methylimidazolium bromide)

1-(11-acryloyloxyundecyl)-3-methylimidazolium bromide (IL) **13** (10, 50 or 100 eq.), xanthate **5** (1 eq.) and AIBN (0.3 eq.) were dissolved in DMF (10 mL) and the mixture was purged with $N_2$ for 10 min. The flask was sealed and the reaction was heated at 70 °C for 17 h. The mixture was dialysed against water for 2 days using a dialysis tubing of MWCO of 500-1,000 g/mol for $P(IL)_{10}$ and 3,500 for $P(IL)_{50}$ and $P(IL)_{100}$. Subsequently,

the dialysed material was freeze-dried overnight and the polymer **14** was obtained as sticky white solid in a yield of 70-80% (Table 5-1). The polymer was characterised using solution state NMR spectroscopy and SEC. NMR spectra were recorded in DMSO-$d_6$ and the $M_n$ and $Đ_M$ were determined using SEC with conventional calibration (PMMA standards).

## 5.2.3.4. Copper-catalysed azide-alkyne cycloaddition (CuAAC)

### 5.2.3.4.1. CuAAC between $N_3$-HEC and O-ethyl S-prop-2-ynyl carbonodithiolate

In a one-necked, round-bottomed flask, $N_3$-HEC **2** (0.5 g, $1.7\times10^{-3}$ mol, 1 eq.), O-ethyl S-prop-2-ynyl carbonodithiolate (0.7 g, $4.4\times10^{-3}$ mol, 3 eq.) **5**, sodium L-ascorbate (0.24 g, $3.3\times10^{-4}$ mol, 0.2 eq.)**,** copper (II) sulfate pentahydrate (0.15 g, $1.7\times10^{-4}$ mol, 0.1 eq.) and N,N,N′,N′-tetramethylethylenediamine (0.07 g, $1.7\times10^{-4}$ mol, 0.1 eq) were dissolved in DMF (10 mL). The flask was heated at 30 °C for 24 h, the mixture was cooled to room temperature and the products were precipitated with chloroform (100 mL). The solid was then filtered and was washed with acetone (~20 mL) under stirring in order to remove the unreacted RAFT agent. The product **15** was then filtered and dried overnight under vacuum at 50 °C. The product was obtained in near quantitative yield (0.7 g). The macro-CTA was characterised using solid state ($^{13}C$ and $^{15}N$) CP-MAS NMR spectroscopies and FT-IR spectroscopy.

The same procedure has been repeated without the use of copper sulfate pentahydrate in order to investigate the regioselectivity of the reaction. The resulting material obtained in

a yield of 66% (0.33 g) was characterised using solid state $^{13}C$ and $^{15}N$ CP-MAS NMR and FT-IR spectroscopies.

#### 5.2.3.4.2. CuAAC between $N_3$-HEC and alkyne-terminated polymers

In a round-bottomed flask fitted with a drying tube, $N_3$-HEC **2** (0.5 g, $1.7\times10^{-3}$ mol, 1 eq.), alkyne-terminated poly(N-vinylpyrrolidone) **10** (2 eq, 0.3 eq and 0.5 eq), sodium L-ascorbate (0.57 g, $2.88\times10^{-3}$ mol, 2 eq.)**,** copper (II) sulfate pentahydrate (0.36 g, $1.44\times10^{-3}$ mol, 1 eq.) and N,N,N′,N′-tetramethylethylenediamine (0.17 g, $1.46\times10^{-3}$ mol, 1 eq) were dissolved in DMF (20 mL). The flask was heated at 30 °C for 24 h. The mixture was cooled to room temperature and polymeric materials were precipitated with diethyl ether (200 mL). The solid was then collected by filtration and was washed for 24 h in water (~20 mL) under stirring in order to remove the unreacted PVP chains. The product **16** was then collected by filtration and dried overnight under vacuum at 50 °C. The product was obtained in a yield of approximately 40% by mass. The graft-copolymers were characterised using solid state ($^{13}C$ and $^{15}N$) CP-MAS NMR and FT-IR spectroscopies.

The following procedure was adopted for coupling PNIPAAM **12** (1.06 g, $6.91\times10^{-4}$ mol, 3 eq.) to $N_3$-HEC **2** (0.06 g, $2.02\times10^{-4}$ mol, 1 eq.) and the resulting product **17** was obtained in quantitative yield (0.47 g). The polymer was characterised using solid state ($^{13}C$ and $^{15}N$) CP-MAS NMR and FT-IR spectroscopies.

The same procedure was also used for coupling P(IL)s **14** (70 mg of $P(IL)_{10}$, 50 mg of $P(IL)_{50}$, 685 mg of $P(IL)_{100}$, $3.4\times10^{-5}$ mol, 2 eq.) to $N_3$-HEC **2** (4 mg, $1.7\times10^{-5}$ mol, 1 eq.), except that at the end of the reaction, the mixture was dialysed for 3 days using a 50,000 Da MWCO membrane against milli-Q water. HEC-g-P(IL)s **18** were further lyophilized

and were obtained in quantitative yield (36 mg of HEC-g-P(IL)$_{10}$, 284 mg of HEC-g-P(IL)$_{50}$, 533 mg of P(IL)$_{100}$). HEC-g-P(IL)s were characterised using solid state ($^{13}$C and $^{15}$N) CP-MAS NMR and FT-IR spectroscopies.

## 5.2.4. Biological study of HEC-g-P(IL)s

### 5.2.4.1. Bacteriological testing

The effect of the HEC-g-P(IL)$_n$s **18** (with n =10, 50 and 100) on bacteria was investigated using *Escherichia coli* K-12 wild-type strain (W3110, $F^-$, $\lambda^-$, *rpoS(Am), rph-1, Inv*(*rrnD-rrnE*))[62] and *Staphylococcus aureus* (3R7089 strain Oxford)[63] which were selected as representative Gram-negative (*E. coli*) and Gram-positive (*S. aureus*) species.

#### 5.2.4.1.1. Bacterial growth inhibition assay on agar plates

HEC-g-P(IL)$_n$s were dissolved in Oxoid$^{TM}$ iso-sensitest broth with a concentration of 10 mg/mL and 6 sequential 2-fold dilutions were prepared in the same medium. 10 µL of each dilution was spotted onto a Luria-Bertani (LB) agar plate containing bacteria in a soft agar overlay (5 mL) and the plates were incubated overnight at 30 °C. A zone of growth inhibition was observed due to the presence of the HEC-g-P(IL)$_n$s.

#### 5.2.4.1.2. Determination of minimum inhibitory concentration (MIC)

MIC determination followed the protocol described by Andrews[128]. 10 mg/mL dilution of HEC-g-P(IL)$_n$s in iso-sensitest broth were prepared and 11 sequential 2-fold dilutions were made using the medium as diluent. The inoculum was prepared from bacteria grown on agar plates and inoculation of 5 mL of iso-sensitest broth with a single colony cultures and incubated overnight at 37 °C. 20-50 µL of overnight culture was inoculated into 1 mL of iso-sensitest broth and incubated at 37 °C with aeration until an inoculum density of approximatively $10^4$ cfu/spot was reached as determined by an optical density $A_{650nm}$ of 0.07, equivalent to a 0.5 MacFarland standard (240 µM $BaCl_2$ in 0.18 M $H_2SO_{4\ aq.}$). This inoculum was diluted 10-fold in iso-sensitest broth for use in MIC determination.

In a 96-well microtiter plate, 50 µl of each dilution of HEC-g-P(IL)$_n$ was mixed with 50 µl of inoculum for each dilution. Ampicillin was diluted in a similar manner as HEC-g-P(IL)$_n$s and was used as a positive antibacterial control. The plate was incubated at 37 °C overnight with shaking and the optical density $A_{650nm}$ of each well was recorded using a Biotek Synergy HT Multi-Mode Microplate Reader. Samples were analysed in duplicate.

### 5.2.4.2. Measurement of the cytotoxicity

A549, an immortalized lung alveolar cell line[129], was cultured in DMEM (Dulbecco's Modified Eagle Medium, GIBCO) supplemented with 10% FCS (Fetal Calf Serum). Approximately $5\times10^3$ cells in a volume of 100 µL per well were used to seed a 96 well plate. Cells were allowed to grow in a humidified incubator with an atmosphere of 5% $CO_2$ at 37 °C until 70% confluency was achieved. HEC-g-P(IL)$_n$s (n =10, 50, 100) to be tested were dissolved in culture medium to a concentration of 1 mg/mL and 100 µL was

added to each well of the first column of wells to give a final concentration of 500 μg/mL. Subsequently 2-fold serial dilutions were performed from columns 1-11 with the final column left as a negative control. After further incubation the effect of the treatment was determined by a cell viability assay using Almar Blue[130] (GIBCO) and analysed on a fluorescent plate reader (BioTek, FL500) using the GEN5 software package. The fluorescence was read using a fluorescence excitation and emission wavelength of 540–570 nm (peak excitation is 570 nm) and 580–610 nm (peak emission is 585 nm) respectively. The evolution of the fluorescence intensity as a function of the concentration of HEC-g-P(IL) permitted the graphically determination of $LD_{50}$ (Lethal Dose that kills 50% of cells).

## 5.3. RESULTS AND DISCUSSION

### 5.3.1. Synthesis of $N_3$-HEC

$N_3$-HEC was prepared from HEC using a one-step procedure (Scheme 5-1)[131] In order to aid the detection of nitrogen by $^{15}N$ NMR spectroscopy, sodium azide was doped with $Na^{15}N_3$.

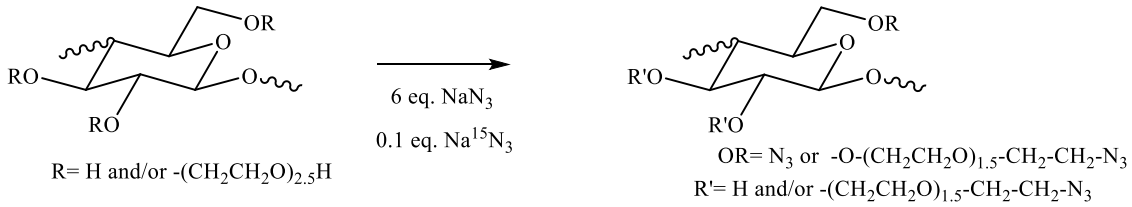


**1** **2**

**Scheme 5-1:** Synthesis of partially $^{15}N$-labelled $N_3$-HEC **2**

The solid state $^{13}C$ NMR spectrum (Figure 5-1 b) shows signals at ~103 ppm, 83 ppm, 74 ppm, 71 ppm and 52 ppm. The signals at ~103 ppm and 81 ppm are typical of HEC and are assigned respectively to the anomeric carbon (C1) and the carbon at the C4 position. The signals $\boldsymbol{\delta}_C$ ~74 ppm are assigned to the set of carbons at C2, C3 and C5 positions and the signal $\boldsymbol{\delta}_C$ ~71 ppm is assigned to the inner carbon of the ethylene oxide side chain. The signal at ~52 ppm is assigned to the -**C**$H_2$-$N_3$ and the loss of the signal at ~62 ppm commonly assigned to the C6 (R=H) and the final carbon of the ethylene oxide side chain (Figure 5-1 a) indicates a complete functionalization of the primary alcohol of HEC with $NaN_3$.

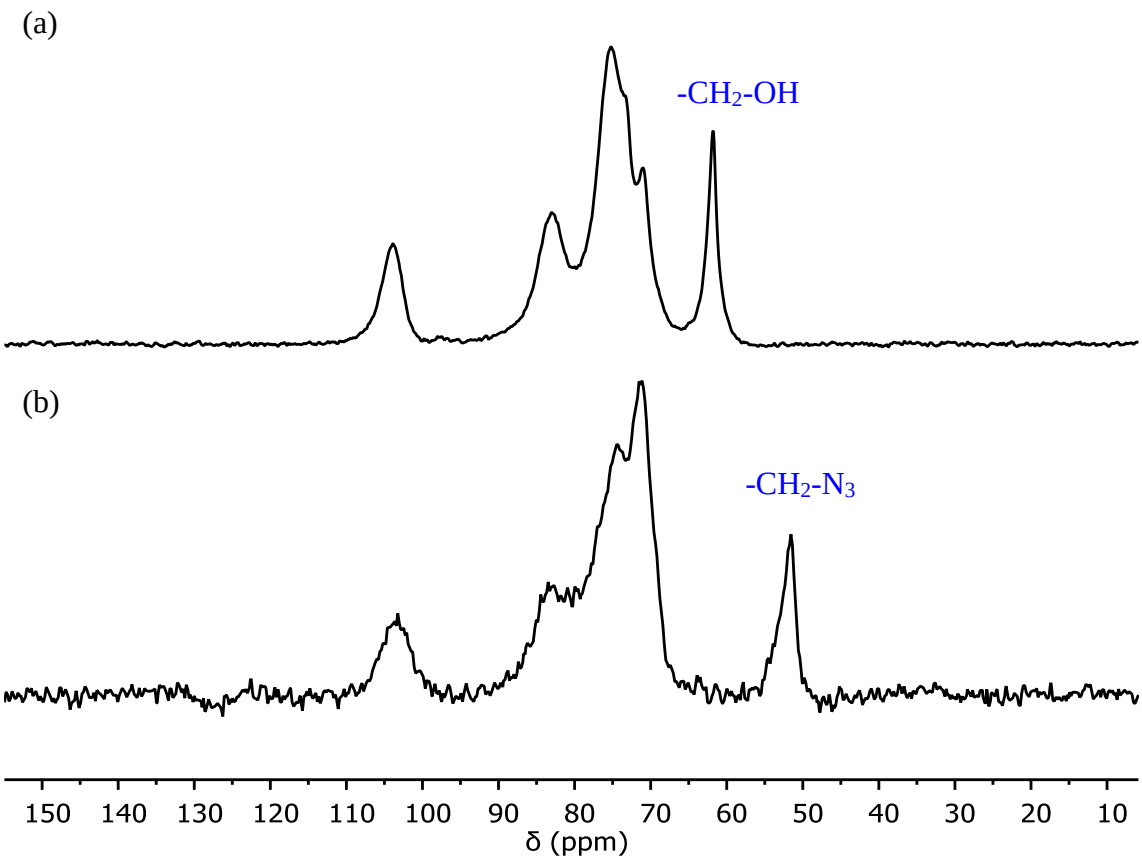


**Figure 5-1:** Solid state $^{13}C$ CP-MAS NMR spectra of (a) HEC **1** and (b) $N_3$-HEC **2**

The solid state $^{15}N$ NMR spectrum (Figure 5-2) shows two signals at ~-310 and -170 ppm which are characteristic respectively of -$CH_2$-**$N_\alpha$**=$N_\beta$=$N_\gamma$ and -$CH_2$-$N_\alpha$=$N_\beta$=**$N_\gamma$**[132]. The labelled $NaN_3$ is labelled at $N_\alpha$ and $N_\gamma$ only, and this explains why $N_\beta$ was not detected. In the cross polarisation method, the detection of nitrogen is obtained from the transfer of energy from protons to the nitrogen. Thus, the more protons environments, there are near to the nitrogen and the closer these protons are to the nitrogen, the easier will be their detection. In $N_3$-HEC, $N_\alpha$ is directly attached to a methylene group which represents also the closest source of protons for $N_\gamma$. The excitation energy received by $N_\alpha$ is greater than that received by $N_\gamma$, resulting in an easier detection of $N_\alpha$ which is demonstrated by a higher intensity of the signal $\boldsymbol{\delta}_N$ ~-310 ppm assigned to $N_\alpha$.

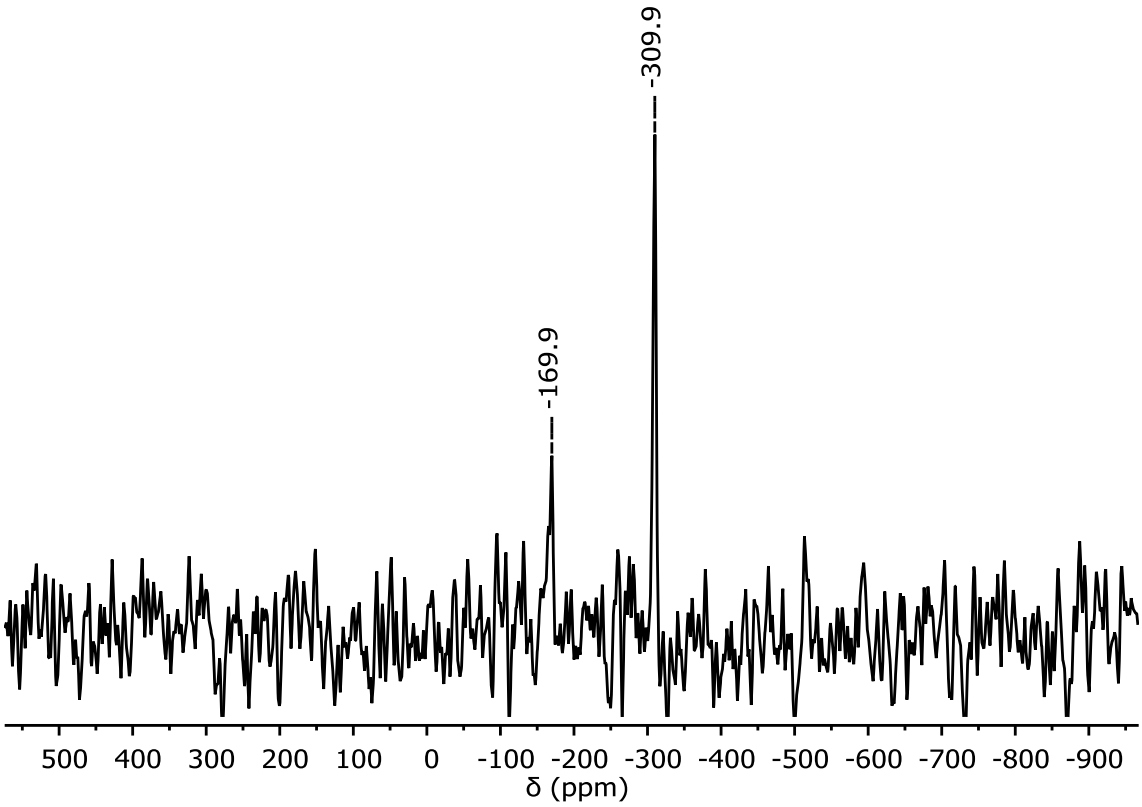


**Figure 5-2:** Solid state $^{15}N$ CP-MAS NMR spectrum of $N_3$-HEC **2**

The FT-IR spectrum of $N_3$-HEC (Figure 5-3) shows a strong absorbance band at ~2100 $cm^{-1}$, characteristic of the presence of an azide group and a relative decrease of the absorbance band at 3400 $cm^{-1}$ indicating the loss of some hydroxyl groups, reinforcing the evidence of the functionalization of the primary alcohol with sodium azide.

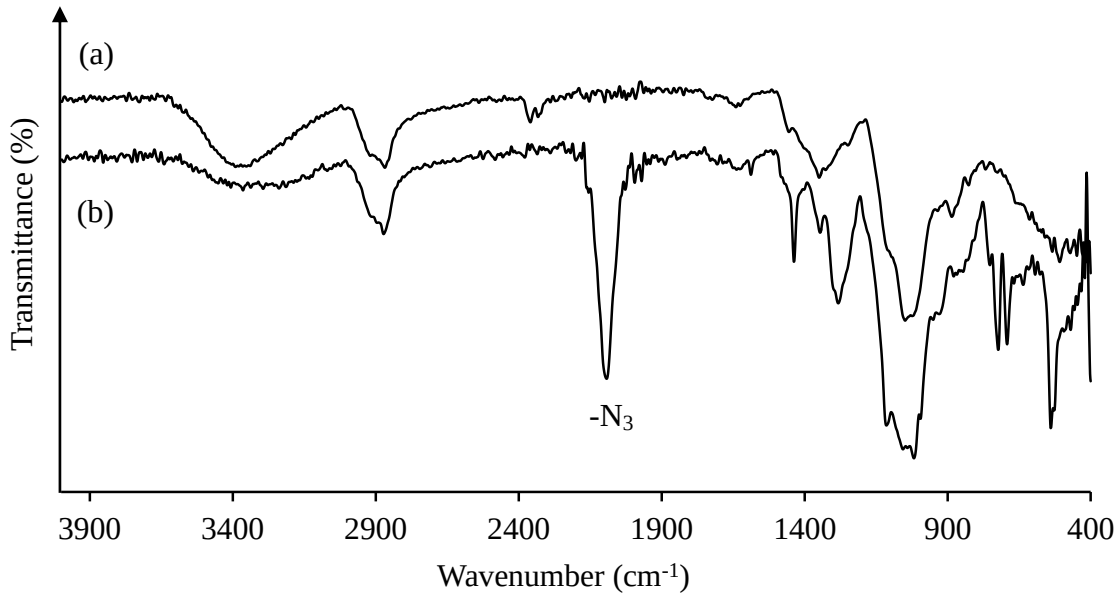


**Figure 5-3:** FT-IR spectra of (a) HEC **1** and (b) $N_3$-HEC **2**

## 5.3.2. Preparation of alkyne-terminated polymers

### 5.3.2.1. RAFT polymerisation of NVP

The transfer agent was prepared following a reported procedure[119]. Propargyl bromide **3** was reacted with potassium ethyl xanthogenate **4** overnight at room temperature to obtain O-ethyl-S-prop-2-ynyl carbonodithiolate **5** (Scheme 5-2) in a yield of 50%.

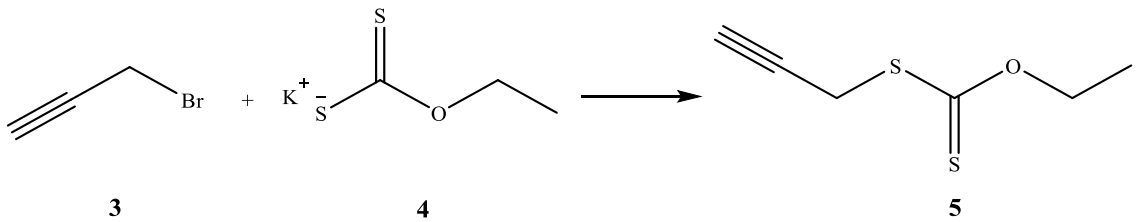


**Scheme 5-2:** Preparation of O-ethyl S-prop-2-ynyl carbonodithiolate **5**

The O-ethyl-S-prop-2-ynyl carbonodithiolate **5** was then used to polymerise NVP **6** in a controlled manner (Scheme 5-3). The ratio RAFT agent:initiator (AIBN) was optimised to obtain relatively high conversion and good control of the polymerisation, and we found that 1:0.7 was a good compromise, with a monomer conversion and a $Đ_M$ of 80% and 1.4 respectively. The degree of polymerisation ($DP_{targeted}$ =10) was kept low in order to facilitate the spectroscopic detection of the HEC backbone and PVP in the graft-copolymer HEC-g-PVP, thus highlighting the grafting between the two polymers. At the end of the reaction, 80% monomer conversion was determined using $^1$H NMR spectroscopy. PVP **7** was isolated by precipitation with diethyl ether in near-quantitative yield. The polymer was then characterised using NMR spectroscopy and SEC.

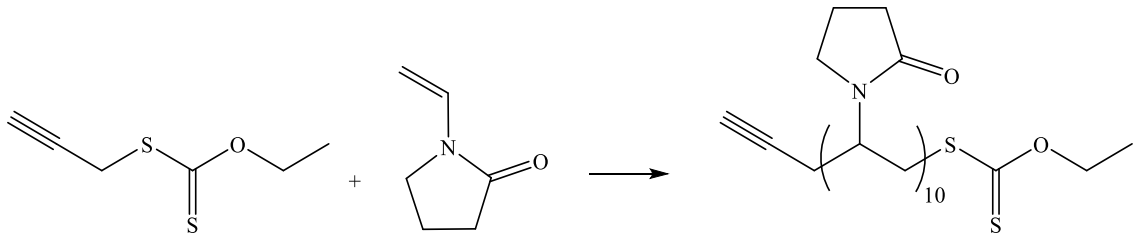


**5** **9** **10**

**Scheme 5-3:** RAFT polymerisation of NVP **9**

The $^1$H NMR spectrum of PVP (Figure 5-4) shows signals at $\delta_H$ ~2.0 ppm, 2.4 ppm and 3.2 ppm which are characteristic of the protons of the pyrrolidone ring. The complex signal at $\delta_H$ ~1.4-1.7 ppm is assigned to the chain end -C**H**$_3$ and methylene groups of both polymer chain and protons of -C**H**$_2$-C≡. Furthermore, the signal at $\delta_H$ ~3.7-3.9 ppm is assigned to methine groups of the polymer chain and the signal at $\delta_H$ ~4.6 ppm is assigned

to methylene of the end group, i.e., the protons of -C**H**$_2$-O. The DP was estimated using the integral of the signal at $\boldsymbol{\delta}_H$ ~4.6 ppm, normalised to 2H against the integrals of the signal $\boldsymbol{\delta}_H$ between 3.7 ppm and 3.9 ppm (12H). From the resulting DP value, a molecular weight ($M_{n\ NMR}$) of 1,500 g/mol was estimated. This is in good agreement with the targeted DP of 10.

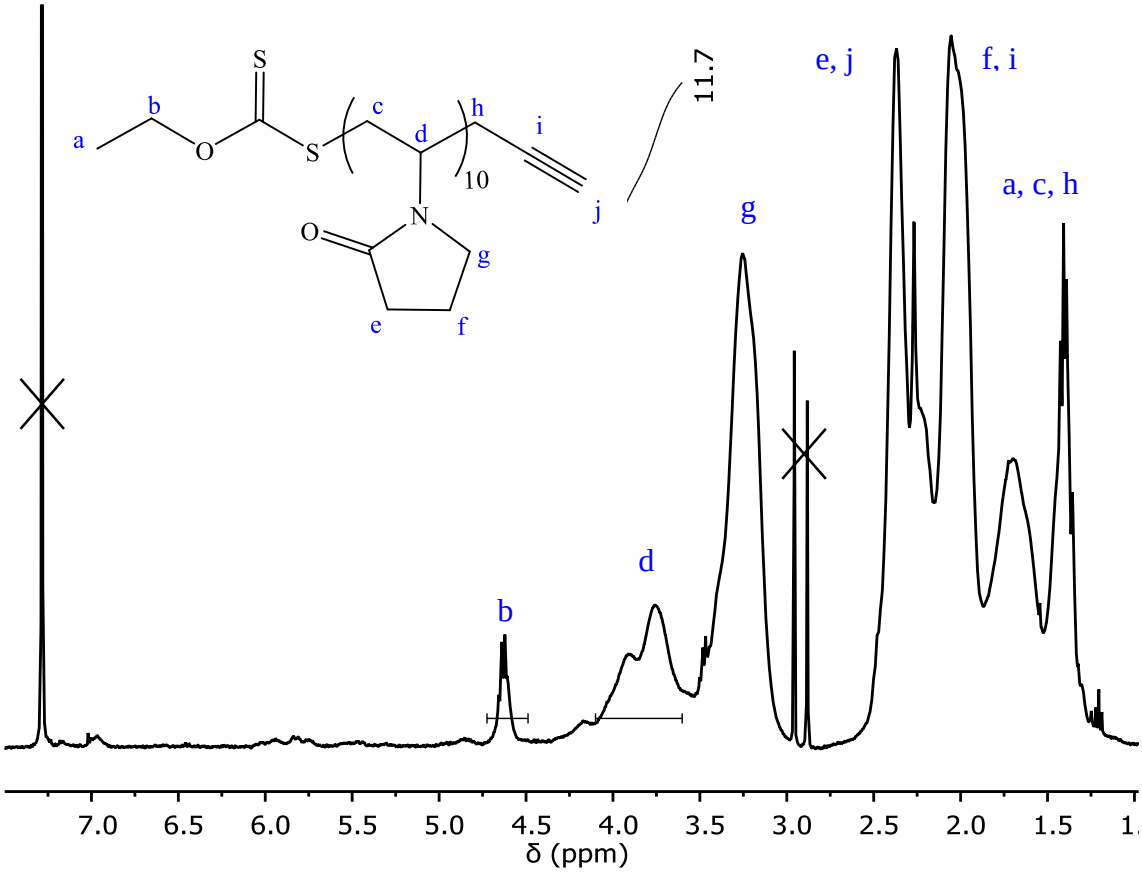


**Figure 5-4:** Solution state $^1$H NMR (400 MHz, $CDCl_3$) spectrum of poly(N-vinylpyrrolidone) ($DP_{targeted}$ =10) **10**

The SEC results (Figure 5-5) indicate a number average molecular weight ($M_{n\ SEC}$) of 1,180 g/mol and a dispersity ($Đ_M$) of 1.4, calculated with conventional calibration using

PMMA standards. The $M_{n\ SEC}$ value is not representative of the true value because of a non-negligible difference of the hydrodynamic volume of PMMA standards and PVP chains. However, the $Đ_M$ value is measured independently of the method used for determining the molecular weight and is characteristic of the molecular weight distribution. A $Đ_M$ below 1.2 indicates a controlled polymerisation while a value above 1.5 indicates a loss of control. The $Đ_M$ value of 1.4 therefore indicates some evidence of control of the polymerisation, especially given the low DP. In fact, a low degree of polymerisation results in broader molecular weight distribution because of retardation effects of the propagation step. In theory, the chains should start their growth at the same time resulting in the preparation of chains of the same length. However this is rarely the case, as there are always some retardation effects because all chains do not start their growth at same time. For a high degree of polymerisation such as 100, this retardation will not significantly influence the dispersity, however for a low DP such as 10, the value of $Đ_M$ is expected to be higher compared to a DP of 100 because the detection of the retardation phenomenon is amplified for a such low DP.

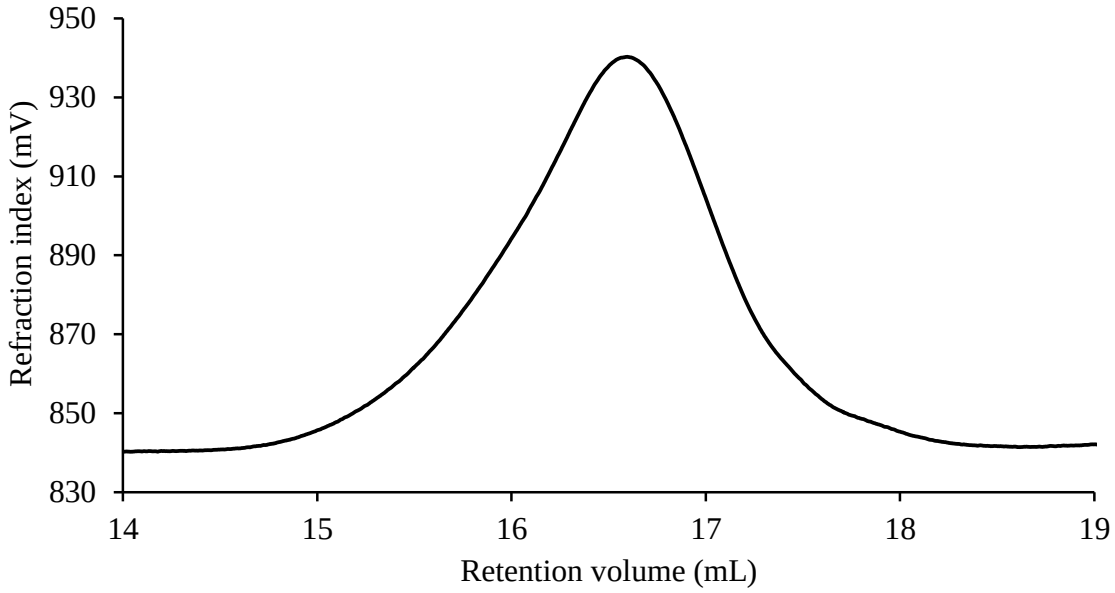


**Figure 5-5:** Results of SEC analysis of PVP ($DP_{targeted}$ =10) **10**; plot shown is from RI detection.

### 5.3.2.2. RAFT polymerisation of NIPAAM

From a procedure developed by Ranjan and co-worker[121], an alkyne-terminated trithiocarbonate **8** (Scheme 5-4) was synthesised from CTA **6** and propargyl alcohol **7** in a yield of 87% and was fully characterised using NMR spectroscopy.

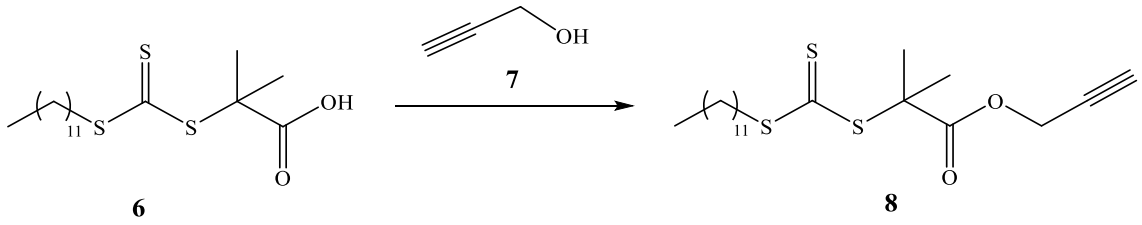


**Scheme 5-4:** Synthesis of alkyne-terminated trithiocarbonate **8**

NIPAAM **11** was successfully polymerised overnight under mild conditions using **8** at a 0.12:1 ratio of initiator to chain transfer agent. The alkyne-ended PNIPAAM **12** (Scheme 5-5) was obtained in a monomer conversion of 90% determined by $^{1}$H NMR spectroscopy. The polymer was further characterised by NMR spectroscopy and SEC.

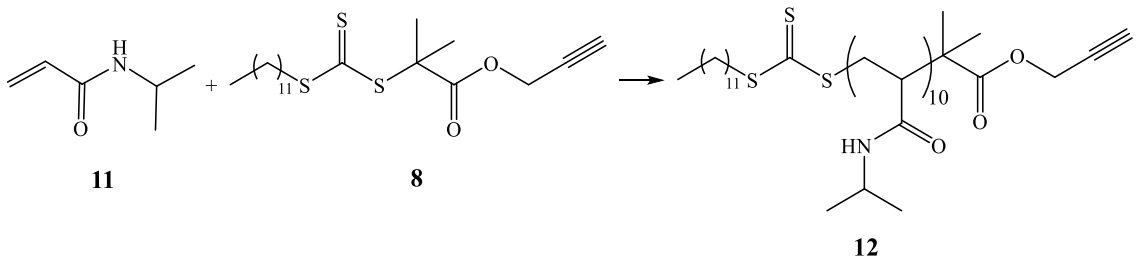


**Scheme 5-5:** RAFT polymerisation of NIPAAM **11**

In the $^{1}$H NMR spectrum (Figure 5-6), the set of signals at $\delta_H$ ~1.1, 1.6, 2.1 and 3.9 ppm are characteristic of PNIPAAM where the peak at $\delta_H$ ~1.1 ppm is assigned to the methyl groups, $\delta_H$ ~1.6 and 2.1 ppm respectively to the -C**H**$_2$- and -C**H**- group of the polymeric chain and $\delta_H$ ~3.9 ppm to the -N-C**H**- group. Some of the transfer chain signals are detected with the peak at $\delta_H$ ~0.8 ppm assigned to the methyl group of the chain end, $\delta_H$

~1.2 ppm to the gem-dimethyl groups, $\delta_H$ ~1.8 ppm to the -C≡C**H**, $\delta_H$ ~3.2 ppm to the -C**H**$_2$-S-, $\delta_H$ ~4.6 ppm to the -O-C**H**$_2$- and $\delta_H$ ~6 ppm to the -N**H** group. From the integration of the signal of the end group at $\delta_H$ ~4.6 ppm compared to the methine group at $\delta_H$ ~3.9 ppm characteristic of PNIPAAM, a degree of polymerisation ($DP_{NMR}$) of ~10 was estimated and this corroborated the calculated monomer conversion.

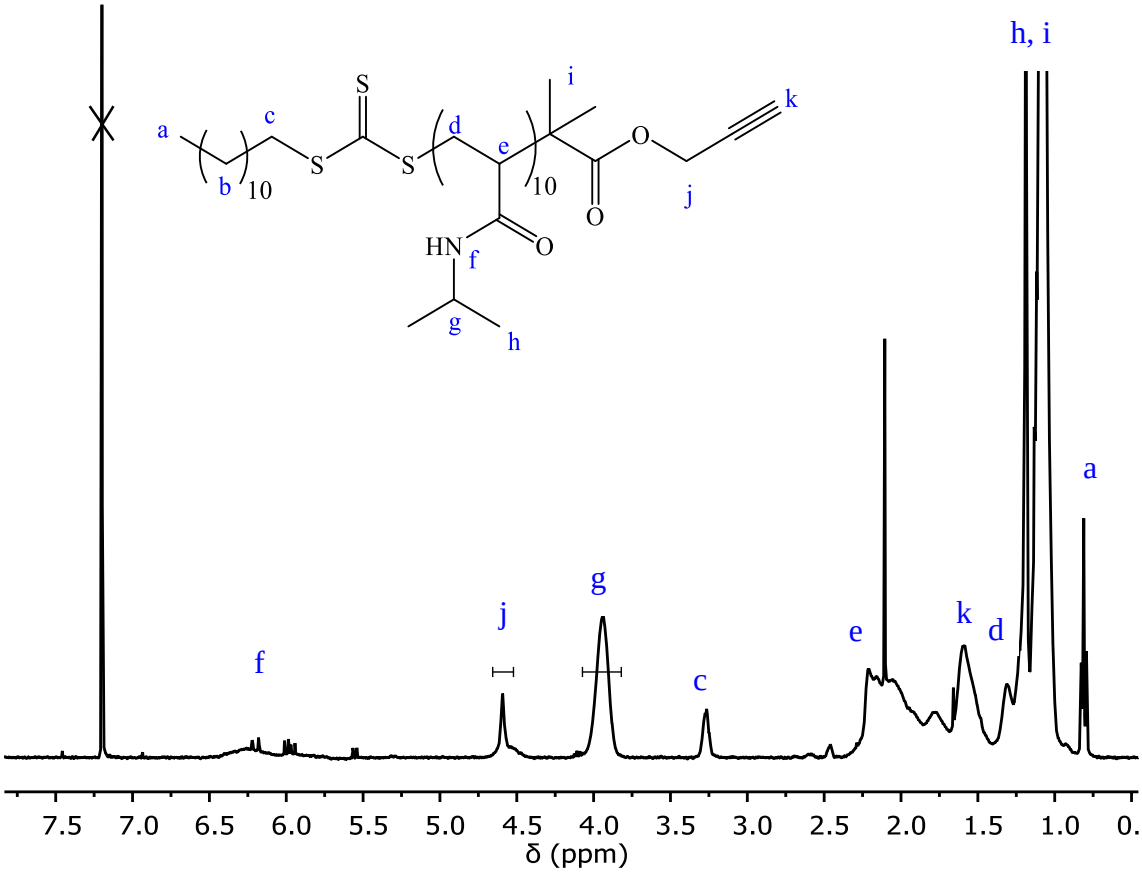


**Figure 5-6:** Solution state $^1$H NMR (400 MHz, $CDCl_3$) spectrum of PNIPAAM **12** ($DP_{targeted}$ =10)

The $Đ_M$ measured by SEC (Figure 5-7) was found to be 1.2 confirming the control of the polymerisation. Because of a very low targeted DP, the calculation of the molecular

weight using SEC was not reliable regardless of the detector used. However, the confirmation of a narrow molecular weight distribution permitted the use of the calculated $DP_{NMR}$ to give an approximation of the molecular weight as ~1,400 g/mol.

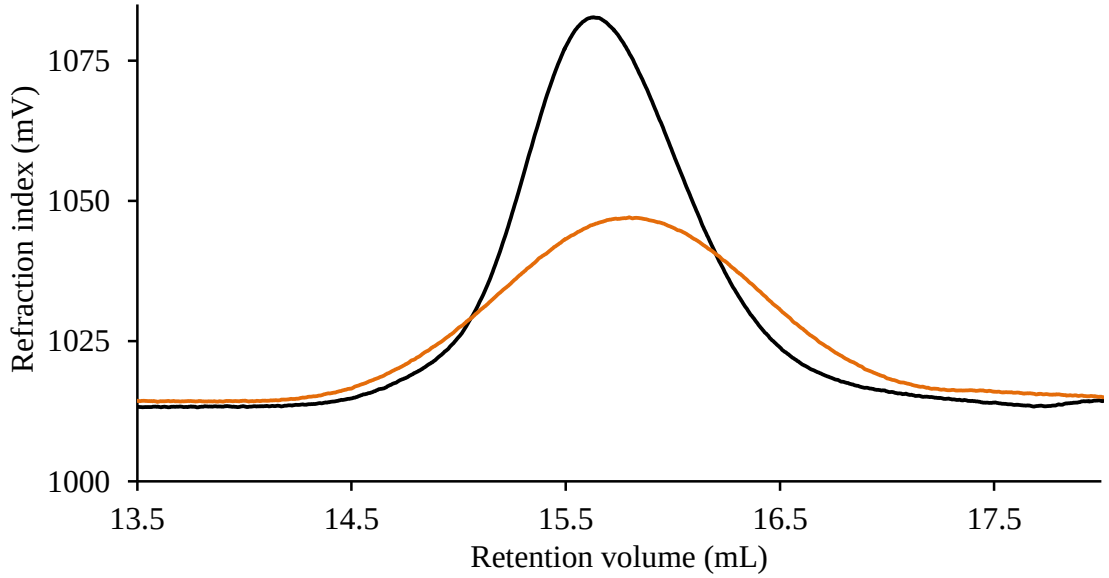


**Figure 5-7:** Results of the SEC analysis of PNIPAAM ($DP_{targeted}$ =10) **12** polymerised using trithiocarbonate **8** (black) and xanthate **5** (orange) as chain transfer agent; plot shown is from RI detection.

The xanthate that was used to polymerise NVP (**5**) was also used to polymerise NIPAAM. However, only 60% monomer conversion was obtained after overnight reaction and the molecular weight distribution (Figure 6 b) was broader compared to that obtained with the trithiocarbonate ($Đ_M$ =1.5 vs. 1.2). Since our aim is to prepare well-defined graft-copolymers of hydroxyethyl cellulose, only PNIPAAM polymerised using alkyne-terminated trithiocarbonate CTA was further coupled to $N_3$-HEC.

### 5.3.2.3. RAFT polymerisation of 1-(11-acryloyloxyundecyl)-3-methylimidazolium bromide

1-(11-acryloyloxyundecyl)-3-methylimidazolium bromide **13** was prior-synthesised (see part 4.2.2.4.1.) and was polymerised using a xanthate **5** as transfer agent (Scheme 5-6). The polymerisation of IL was performed at 70 °C in DMF using a ratio of xanthate to initiator (AIBN) of 1:0.3. Different degrees of polymerisation (10, 50 and 100) were targeted in order to produce graft-copolymers of HEC with different chain length. After 17 h of polymerisation, the monomer conversion was determined using $^{1}$H NMR spectroscopy and was found to be approximatively 70-80% (Table 5-1). Subsequently, the P(IL)s **14** were characterised using NMR spectroscopy and SEC.

**Table 5-1:** Reaction conditions for the preparation of P(IL)s

| $DP_{targeted}$ | IL | | Xanthate | | AIBN | | P(IL) | | |
|---|---|---|---|---|---|---|---|---|---|
| | g | mmol | mg | mmol | mg | mmol | Conv. (%) | mg | Yield (%) |
| **10** | 1.13 | 2.92 | 46.0 | 0.287 | 12 | 0.079 | 70 | 672 | 57 |
| **50** | 1.56 | 4.03 | 13.0 | 0.081 | 4 | 0.024 | 80 | 880 | 56 |
| **100** | 1.83 | 4.73 | 7.6 | 0.047 | 2 | 0.012 | 75 | 973 | 53 |

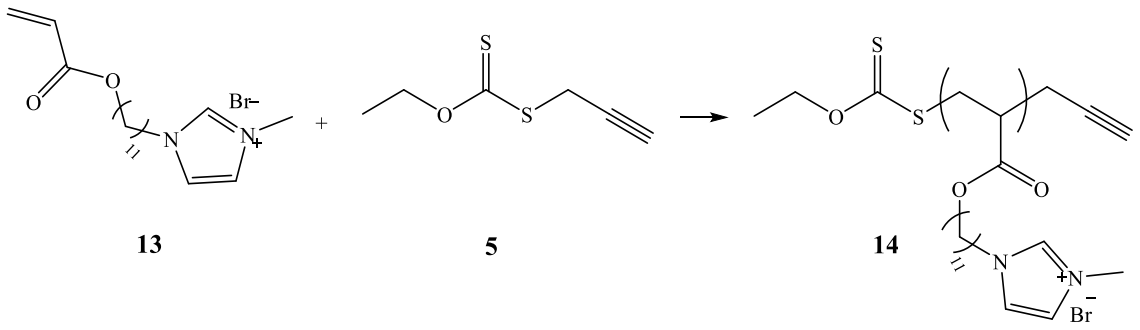


**13** **5** **14**

**Scheme 5-6:** RAFT polymerisation of 1-(11-acryloyloxyundecyl)-3-methylimidazolium bromide (IL) **13**

In the $^{1}$H NMR spectrum of $P(IL)_{100}$ (Figure 5-8), signals $\boldsymbol{\delta}_H$ ~1.2-1.8 ppm are assigned to protons -C**H**$_2$**s** along the side chain and the backbone of P(IL). The signal $\boldsymbol{\delta}_H$ ~2.2 ppm is assigned to the methine group of the backbone and the signal $\boldsymbol{\delta}_H$ ~3.9 ppm is assigned to the -$CH_3$ group which is the substituent group of the ring. The signal $\boldsymbol{\delta}_H$ ~4 ppm is assigned to -C**H**$_2$- next to the tertiary amine and the signal $\boldsymbol{\delta}_H$ ~4.2 ppm is assigned to the protons –C**H**$_2$ next to the acrylate group. The signal $\boldsymbol{\delta}_H$~ 7.7-7.8 and 9.4 ppm are assigned to the protons defining the imidazolium ring. The signals of the end groups were not found, perhaps, because they are most likely to be hidden by the signals of P(IL). The spectra of the $P(IL)_{50}$ and $P(IL)_{10}$ did not exhibit any new signals corroborating the proposed overlap between the polymer and end groups signals. Thus, the estimation of the chain length, based on the ratio of integrals between protons of the polymers and end groups, was not feasible using NMR spectroscopy.

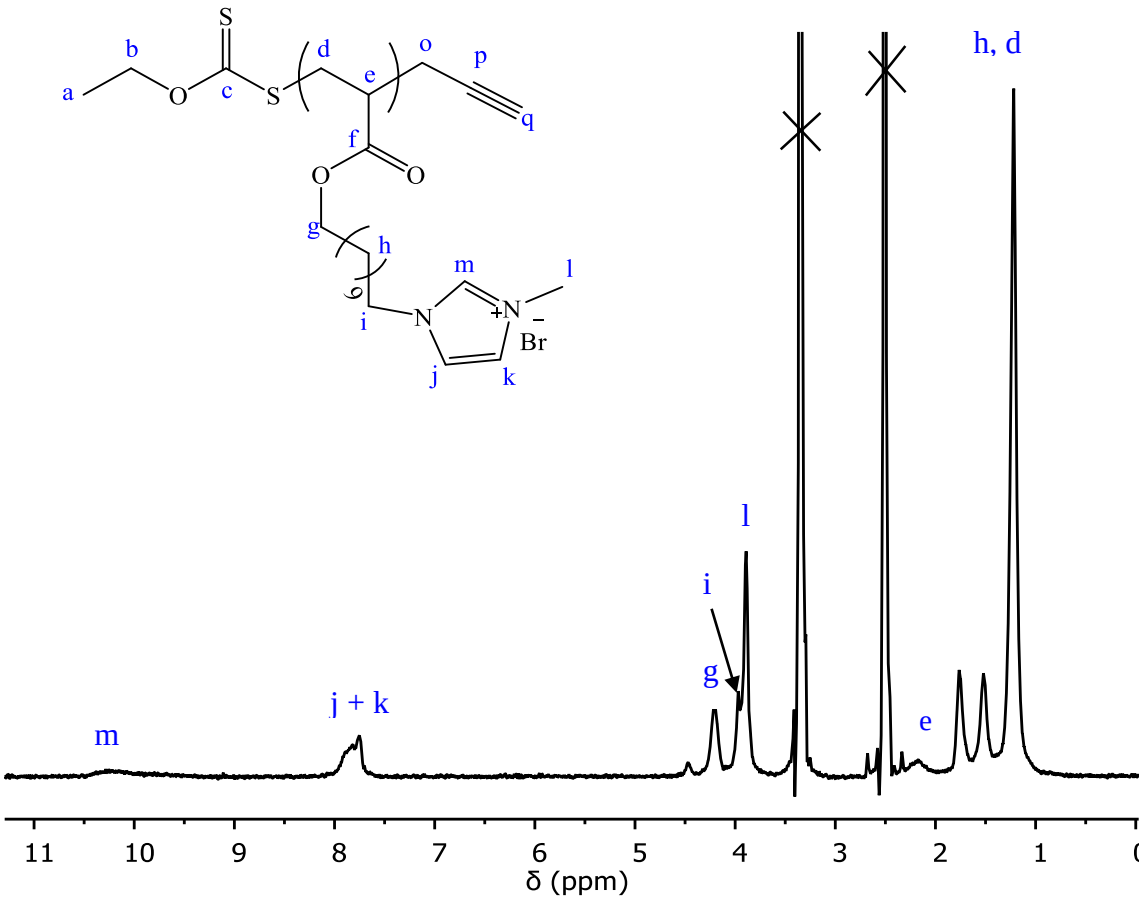


**Figure 5-8:** Solution state $^{1}$H NMR (400 MHz, DMSO-$d_6$) spectrum of poly(1-(11-acryloyloxyundecyl)-3-methylimidazolium bromide) ($DP_{targeted}$ =100) **14**

The molecular weight and dispersity of P(IL) were determined using SEC where the experiments were done by Smithers Rapra in Shawbury, UK. Due to the cost of the analyses, only $P(IL)_{100}$ was analysed and the result is displayed in Figure 5-9. Conventional calibration with PMMA standards was used to determine the average molecular weight $M_n$ and was found to be 26,600 g/mol. This is in good agreement with the 71% monomer conversion (27,600 g/mol) considering a low $Đ_M$. Effectively, $Đ_M$ of 1.5 was measured indicating some control of the polymerisation. In fact, a value $Đ_M$ of inferior of 1.2 demonstrates the full control of the polymerisation, however a value

between 1.2 to 1.5 indicates still some control of the polymerisation. A value superior to 1.5 means the loss of control resulting in broader molecular weight distribution. Typically polymers produced *via* conventional free radical polymerisation have $Đ_M$ value higher than 1.5. The dispersity value of 1.5 for $P(IL)_{100}$ was borderline for a polymer which was prepared from a RDRP process. Regarding P(IL)s with shorter chain length (10 and 50 DP) $Đ_M$ values were expected to be similar or slightly higher due to the amplification of the detection of the retardation effects when polymerising shorter chain length.

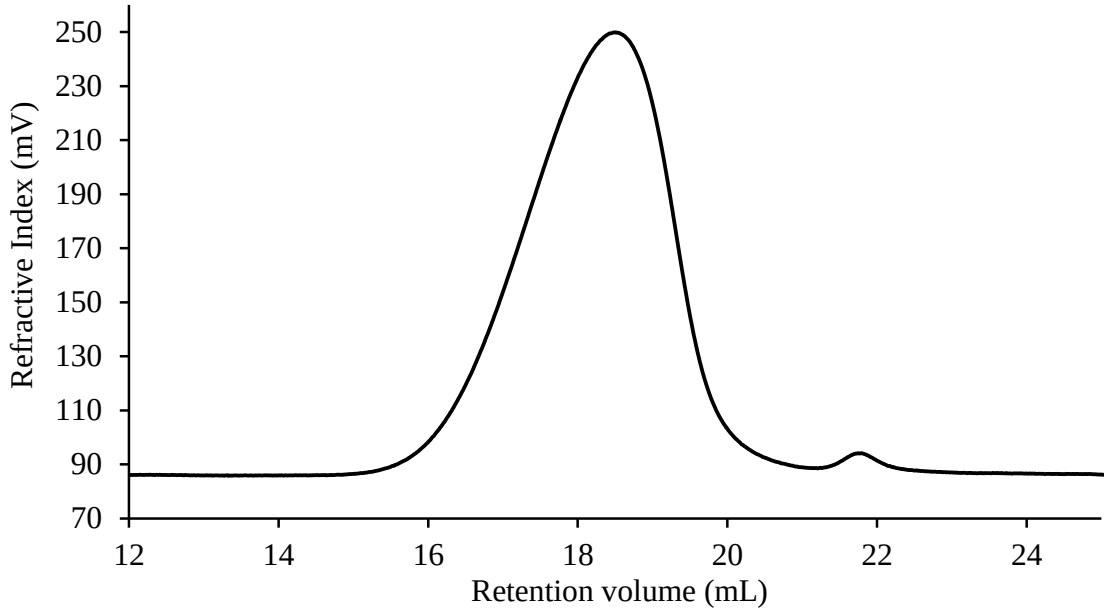


**Figure 5-9:** Results of the SEC analysis of P(IL) ($DP_{targeted}$ =100) **14**; plot shown is from RI detection.

## 5.3.3. Copper catalysed azide-alkyne cycloaddition (CuAAC)

### 5.3.3.1. $N_3$-HEC with transfer agent O-ethyl S-prop-2-ynyl carbonodithiolate: Macro-CTA

O-Ethyl-S-prop-2-ynyl carbonodithiolate-functionalized HEC **15** was prepared *via* click chemistry using copper sulfate pentahydrate, sodium ascorbate and TMEDA (Scheme 5-7). After 24 h at 30 °C, the macro-CTA **15** was isolated in 100% yield assuming complete coupling. Due to a lack of solubility in common deuterated NMR solvents, the product was characterised using FT-IR and solid state NMR spectroscopies.

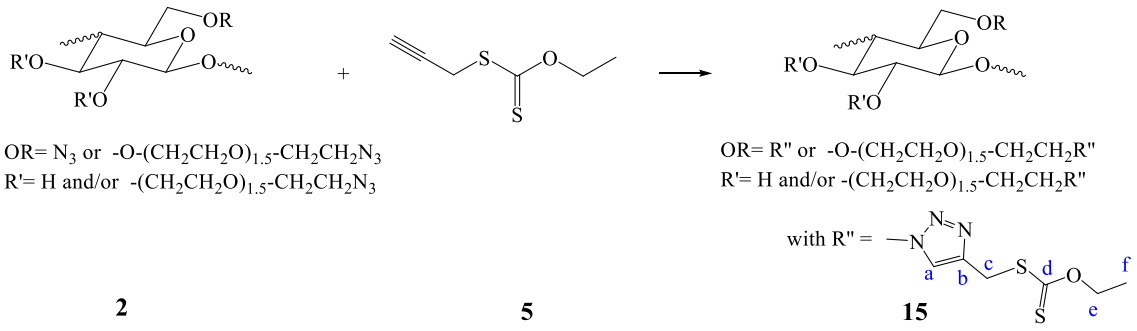


**2** **5** **15**

**Scheme 5-7:** CuAAC between partially $^{15}N$-labelled $N_3$-HEC **2** and transfer agent **5**

The preparation of macro-CTA **15** was performed to demonstrate the click reaction between HEC and a RAFT agent, and help in the assignment of the NMR spectra of the graft-copolymers. This reaction was thus a key point in our work towards the preparation of HEC-g-$PVP_{10}$ graft-copolymers.

The $^{13}C$ NMR spectrum (Figure 5-10) showed a large band of peaks between 71 and 81 ppm which are assigned to the carbons of the HEC backbone. The peak at 103.2 ppm is

assigned to the carbon at the C1 position, and the peak at 51.9 ppm is assigned to the carbon directly attached to the nitrogen of the triazole ring. Comparing the product to the $N_3$-HEC spectrum (Figure 5-1), the chemical shift of this carbon is the same as that of -**C**$H_2$-$N_3$. However, the click reaction is demonstrated by the presence of peaks at 124.0 and 123.2 ppm which are assigned to the carbons in the triazole ring. Furthermore, the peak at 15.0 ppm and the broad peak at 32.4 ppm are assigned respectively to the methyl and methylene of the RAFT agent.

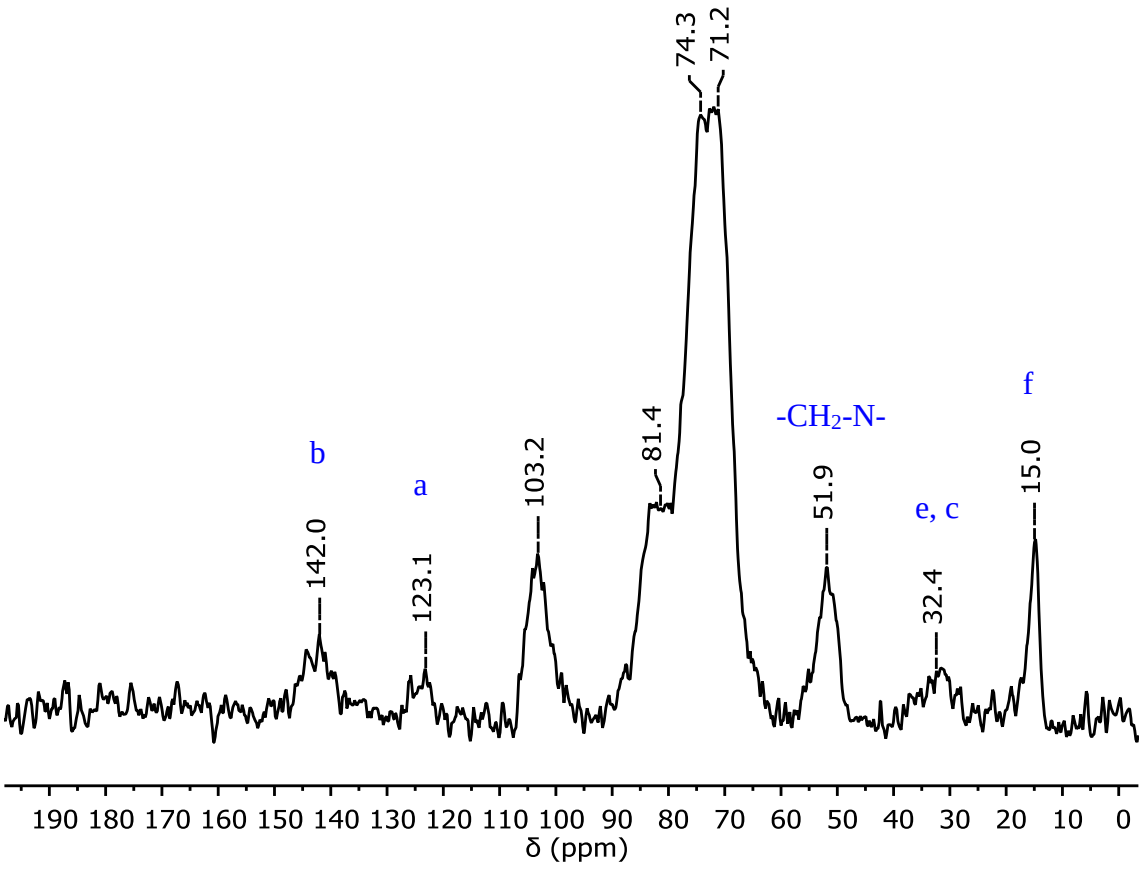


**Figure 5-10:** Solid state $^{13}C$ CP-MAS NMR spectrum of the macro-CTA **15**

In order to further confirm the coupling, FT-IR and $^{15}N$ NMR spectroscopies were performed. The FT-IR spectra (Figure 5-11) showed a strong relative decrease of the absorption band at 2100 $cm^{-1}$ assigned to the azide groups, indicating the near-complete consumption of the azide.

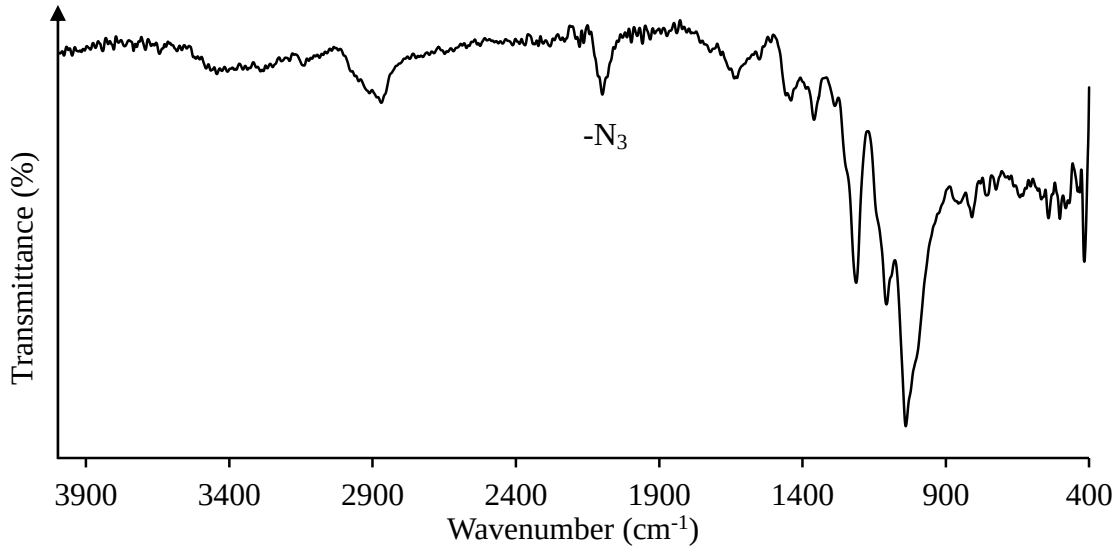


**Figure 5-11:** FT-IR spectrum of the macro-CTA **15**

In the $^{15}N$ NMR spectrum (Figure 5-12), only one peak at $\delta_N$ ~ -134 ppm is present and is assigned to the $N_\alpha$ after cycloaddition with the RAFT agent. The large change in the chemical shift of $N_\alpha$ from -310 ppm to -134 ppm suggests complete reaction of $N_3$ with the alkyne group of the transfer agent, however, because the FT-IR spectrum showed the presence of unreacted $N_3$, we propose that the expected peak at -310 ppm corresponding to unreacted $N_\alpha$ was too weak and thus was undetectable by NMR. Comparing to the spectrum of $N_3$-HEC (Figure 5-2), the ratio of the signal of $N_\alpha$ to noise is lower due to the

change of the environment in terms of protons and the change in the symmetry of the environment. The peak present at -170 ppm in the $^{15}N$ spectrum of N-HEC (Figure 5-2) and assigned to $N_\gamma$ is absent from the $^{15}N$ spectrum of the macro-CTA because the ratio of signal $N_\gamma$ to noise decreased, resulting in an inability to detect it. This peak was expected to shift to approximately -20 ppm according to studies carried by Corredor *et al.*[133].

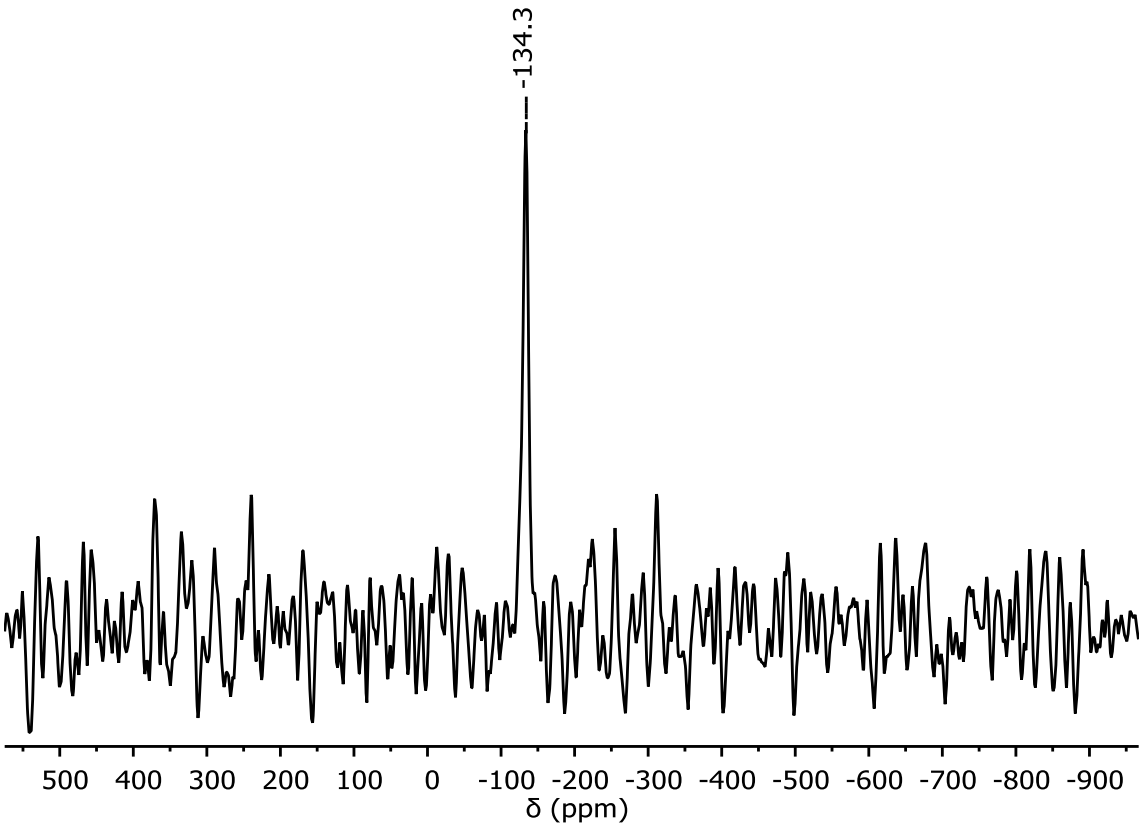


**Figure 5-12:** Solid state $^{15}N$ CP-MAS NMR spectrum of the macro-CTA **15**

Copper catalysed azide-alkyne cycloaddition (CuAAC) is a regioselective reaction that takes place under mild conditions without special requirements (e.g., exclusion of

oxygen), resulting in the preparation of 1,4- isomer. In contrast, Huisgen 1,3-cycloaddition is conducted without copper, typically at much higher temperature, and leads to a mixture of 1,4- and 1,5-regioisomers[134]. In order to demonstrate that our reaction was indeed a CuAAC process and not a Huigsen cycloaddition, the reaction between $N_3$-HEC and the alkyne-terminated xanthate was repeated without copper sulphate pentahydrate. The NMR spectrum of the resulting product (not shown) does not contain any signals attributable to a cycloaddition product from the two materials. This indicates that Huisgen 1,3- cycloaddition did not occur under these experimental conditions. The macro-CTA was obtained following the CuAAC process alone and thus is expected to constrain the outcome of the 1,4-disubstituted 1,2,3-triazole exclusively.

To summarise, $N_3$-HEC functionalization was near-complete with the RAFT agent using a selective 1,4- click reaction resulting in the formation of a macro-CTA from an HEC backbone. This could be used for the preparation of graft-copolymers of cellulose, such as in the work by Perrier and co-workers[43]. In our case, the preparation of the macro-CTA allows us to identify the correct conditions for the click reaction and also to determine the chemical shift of the product in the $^{15}N$ NMR experiments. This information assisted in identifying the grafting of the alkyne ended PVP to $N_3$-HEC and in the characterisation of HEC-g-PVP confirming the triazole formation.

#### 5.3.3.2. $N_3$-HEC and alkyne-terminated PVP

The CuAAC reaction (Scheme 5-8) was used to couple $PVP_{10}$ **7** to $N_3$-HEC **2**, forming the graft-copolymer **16**. A chain length of 10 repeat units of the synthetic polymer was

chosen because this aided the characterisation of the graft-copolymer and the properties of HEC should be retained. To examine the scope of the grafting process, ratios of PVP chain to AGU units (in other words to azide groups) equal to 1:5, 1:3 and 2:1 were chosen. The coupling reaction was carried out for 24 h at 30 °C. The graft-copolymers HEC-g-$PVP_{10}$s and possibly some unreacted $PVP_{10}$ chains were precipitated with diethyl ether. HEC-g-$PVP_{10}$s were then separated from ungrafted $PVP_{10}$ chains through differences in solubility in water ($PVP_{10}$ chains are water soluble whereas HEC-g-$PVP_{10}$s are not). Based on the theoretical ratio of PVP chains to AGU units, the HEC-g-$PVP_{10}$s were obtained in a yield of ~40%.

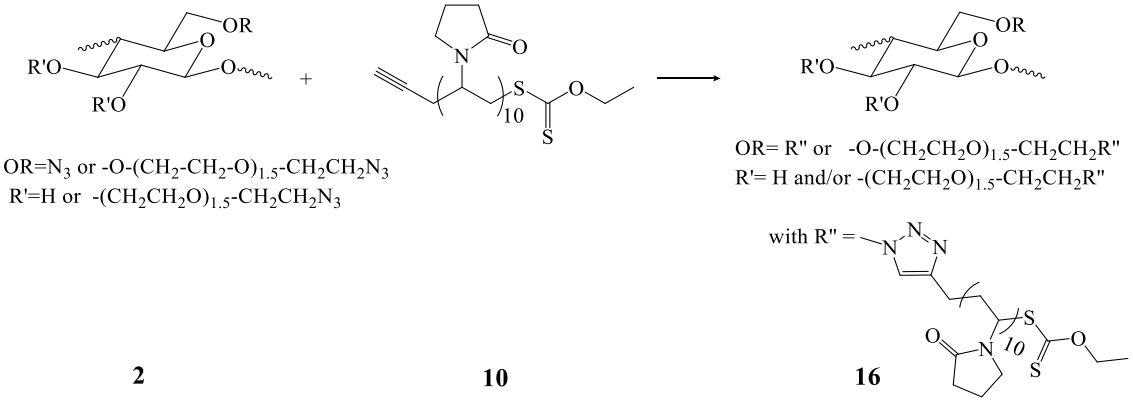


**Scheme 5-8:** CuAAC reaction between partially $^{15}N$-labelled $N_3$-HEC **2** and alkyne-terminated $PVP_{10}$ **10**

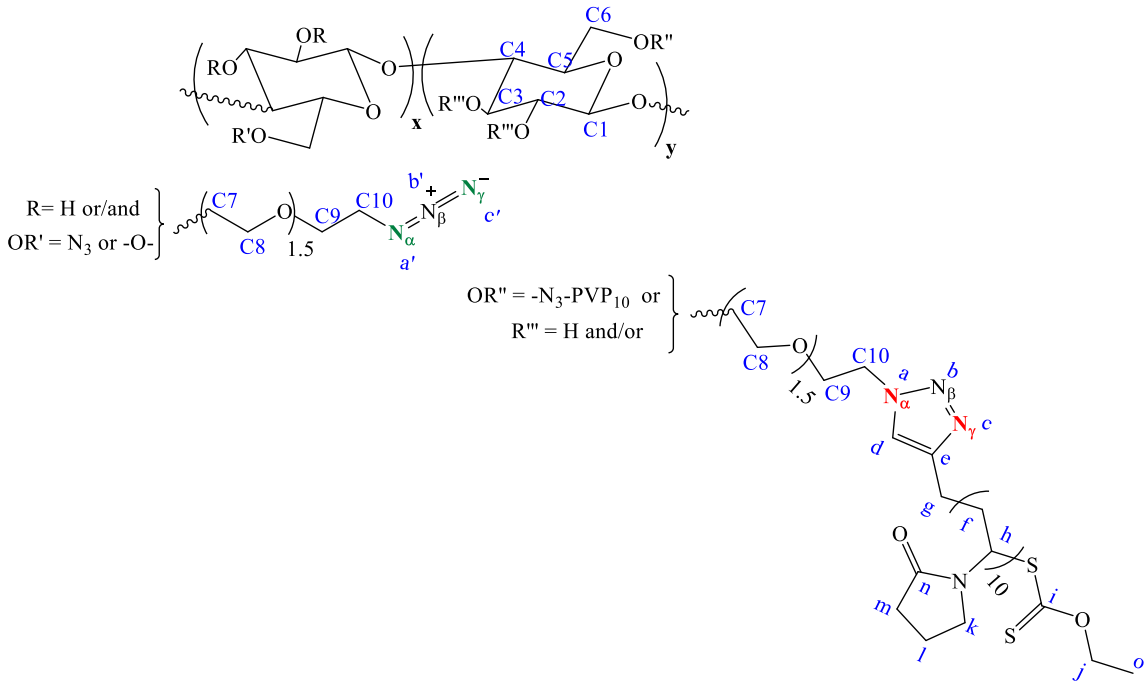


**Figure 5-13:** Numbering of the molecular structure of HEC-g-$PVP_{10}$ **16**, where x and y the degree of functionalization

In the $^{13}C$ NMR spectrum of HEC-g-$PVP_{10}$ with a ratio of PVP to AGU equal to 1:5 (y =1, x =4) (Figure 5-14 b), peaks characteristic of HEC were detected. The peak at 51 ppm is assigned to the carbon at the C10 position (Figure 10), the large band between 60 ppm to 90 ppm is assigned to the carbons of the HEC ring and the ethylene oxide side chain and the peak at 104 ppm is assigned to the anomeric centre (C1). The presence of PVP is demonstrated by the peaks at 19.3 ppm, 32.6 ppm, 43.8 ppm and 176.7 ppm which are assigned respectively to the pyrrolidone ring and the carbonyl group. In the spectrum of HEC-g-$PVP_{10}$ (Figure 5-14 c) where the ratio PVP to -$N_3$ increased to 1:3, signals of HEC and $PVP_{10}$ are detected. The intensity of the peaks assigned to PVP has increased whereas the intensity of the peaks characteristic of HEC decreased, due to the increase of the graft-

density of HEC with $PVP_{10}$. Increasing the graft-density to attempt to achieve complete functionalization of $N_3$-HEC with PVP resulted in an almost complete disappearance of HEC signals in the $^{13}C$ NMR experiment (Figure 5-14 d). Furthermore, the carbons responsible for the cycloaddition between $PVP_{10}$ and $N_3$-HEC were not detected because of their low concentration within the structure and/or an insufficient relaxation time between the pulses. In fact, these carbons could potentially relax much more slowly than the others limiting their detection using solid state CP-MAS NMR[135]. The NMR experiments indicated the presence of PVP and HEC in the structure. The signals of the HEC backbone decreased with increasing grafting density. However, definitive evidence of the coupling is not demonstrated using these NMR experiments.

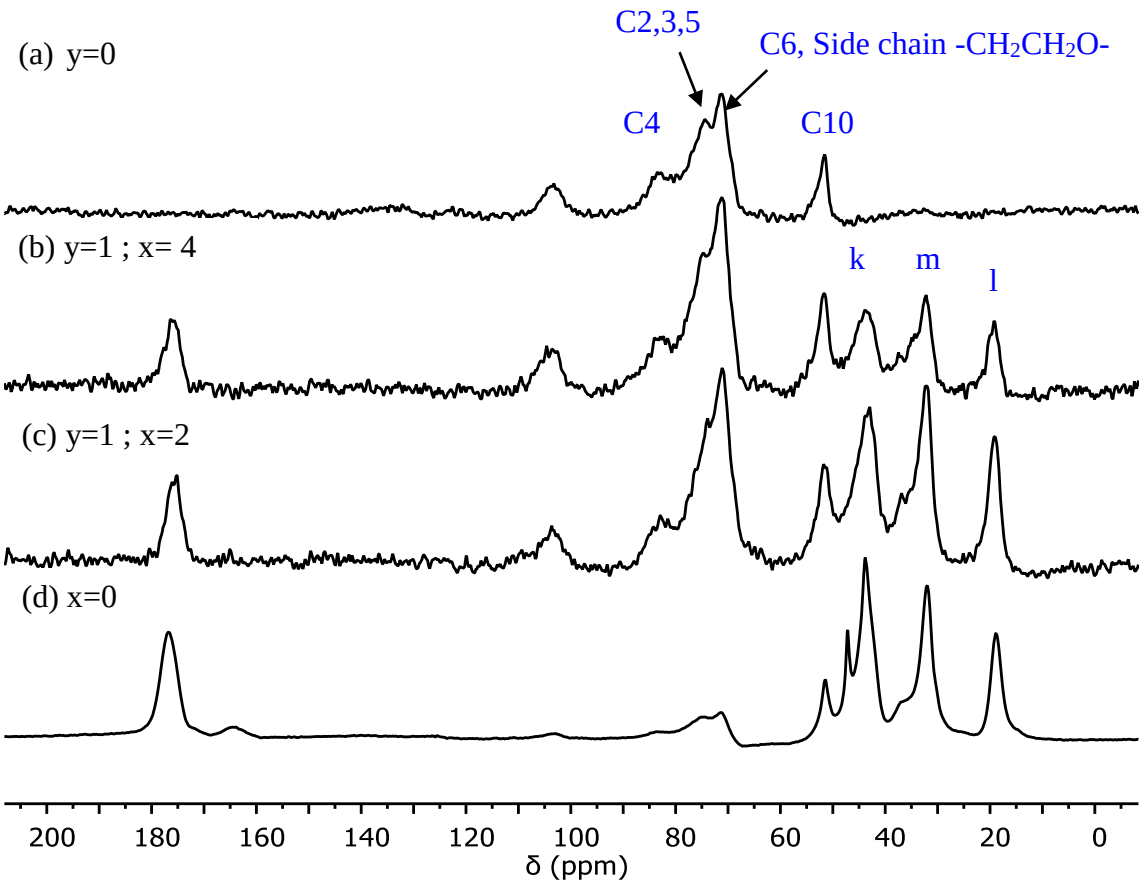


**Figure 5-14:** Solid state $^{13}C$ CP-MAS NMR spectra of (a) $N_3$-HEC **2**, (b) HEC-g-$PVP_{10}$ (1:5), (c) HEC-g-$PVP_{10}$ (1:3) and (d) HEC-g-$PVP_{10}$ (2:1). Numbering shown in Figure 5-13; x and y defines in Figure 5-13.

In the FT-IR spectrum of $N_3$-HEC (Figure 5-15 a), an absorption band at ~2100 $cm^{-1}$ typical of azide groups is present. Coupling $PVP_{10}$ with $N_3$-HEC at a ratio PVP:$N_3$ of 1:5 caused the relative intensity of the band at 2100 $cm^{-1}$ (Figure 5-15 b) to decrease and a band at ~1700 $cm^{-1}$ appears which is assigned to the carbonyl group in $PVP_{10}$. Increasing the graft-density of PVP to $N_3$-HEC, the band at 2100 $cm^{-1}$ decreases whereas the band at 1700 $cm^{-1}$ increases and the total disappearance of the band at 2100 $cm^{-1}$ in the spectrum

of HEC-g-PVP where the ratio PVP:$N_3$ was 2:1 indicates the complete consumption of the azide of $N_3$-HEC which probably reacted with $PVP_{10}$.

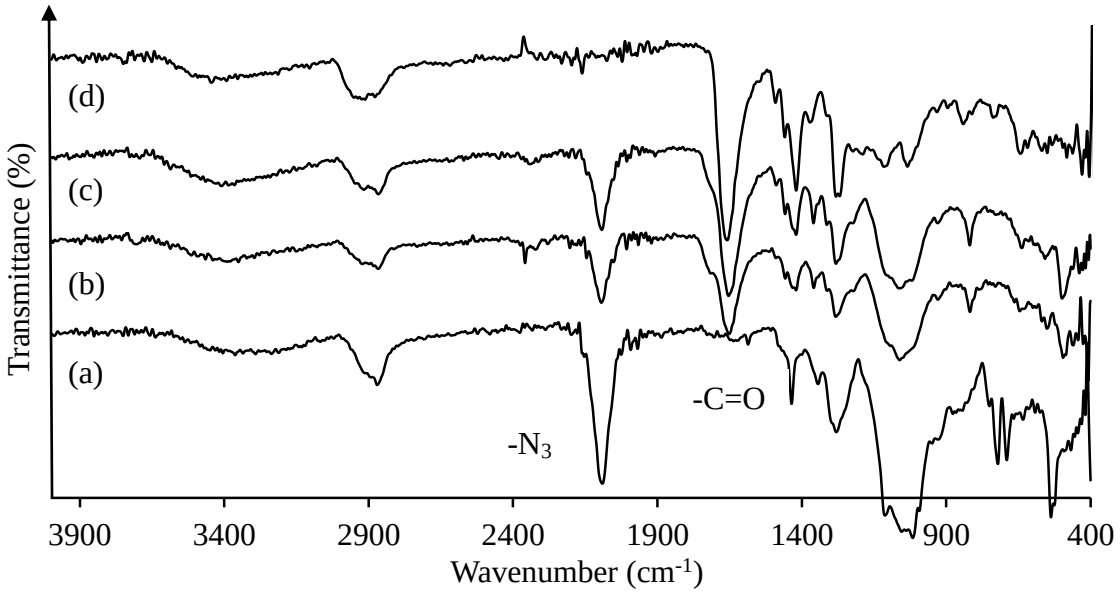


**Figure 5-15:** FT-IR spectra of (a) $N_3$-HEC 2, (b) HEC-g-$PVP_{10}$ (1:5), (c) HEC-g-$PVP_{10}$ (1:3) and (d) HEC-g-$PVP_{10}$ (2:1)

To try to demonstrate more clearly the coupling between the $PVP_{10}$ and $N_3$-HEC, partially $^{15}N$-labelled $N_3$-HEC was prepared. In the $^{15}N$ NMR spectrum of $N_3$-HEC (Figure 5-16 a), two peaks at ~-310 and -170 ppm are assigned to $N_\alpha$ and $N_\beta$. When $PVP_{10}$ was coupled to $N_3$-HEC at a ratio PVP:$N_3$ equal to 1:5 (Figure 5-16 b), a peak at -256.3 ppm appeared which is assigned to the amine present in the pyrrolidone ring (the $^{15}N$ signal for $PVP_{10}$ is ~-253.8 ppm) which was not doped with an extra $^{15}N$. Increasing the PVP:$N_3$ ratio to 1:3 (Figure 5-16 c) resulted in the detection of an additional signal at ~-140 ppm which is assigned to $N_\alpha$ after its cyclisation with $PVP_{10}$. The peaks of unfunctionalized $N_\alpha$ and

$N_\gamma$ are still present in the spectrum but their intensities are decreased relative to the signal of nitrogen in PVP, indicating an increase in the functionalization of $N_3$-HEC with $PVP_{10}$.

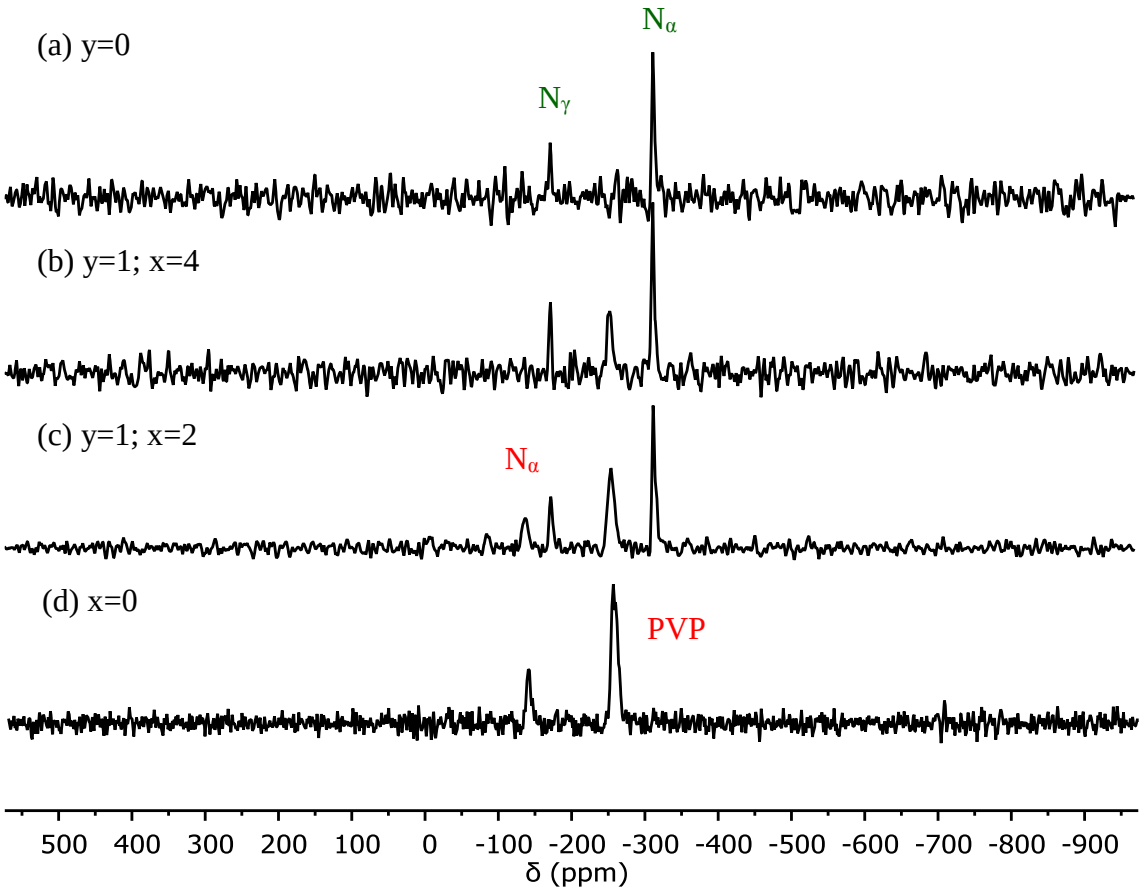


**Figure 5-16:** Solid state $^{15}N$ CP-MAS NMR spectra of (a) $N_3$-HEC 2, (b) HEC-g-$PVP_{10}$ (1:5), (c) HEC-g-$PVP_{10}$ (1:3) and (d) HEC-g-$PVP_{10}$ (2:1)

For the spectrum of HEC-g-$PVP_{10}$ prepared from a ratio PVP:$N_3$ equal to 2:1 (Figure 5-16 d), two signals at -256.3 ppm and -140.4 ppm are detected and are assigned respectively to the nitrogen in the pyrrolidone ring and the $N_\alpha$ after the cycloaddition process. The intensity of the PVP signal is much higher than that of $N_\alpha$ due to the high ratio of nitrogen of PVP to $N_3$-HEC. In fact, 10 nitrogens of PVP are present per each $N_\alpha$ of $N_3$-HEC

resulting in a higher intensity of the peak assigned to PVP compared to that of $N_\alpha$. Furthermore, the intensity of the signal of $N_\gamma$ in $N_3$-HEC decreased when the graft-density of $N_3$-HEC with $PVP_{10}$ increased, however no signal for $N_\gamma$ after cyclisation with $PVP_{10}$ is detected. This was also the case in the spectrum of the macro-CTA where the reasons are identical namely lack of nearby protons for excitation. Because of the total loss of both signals at -310 ppm and -170 ppm assigned respectively to $N_\alpha$ and $N_\beta$ in $N_3$-HEC and the appearance of the signal at ~-140.4 ppm assigned to $N_\alpha$ after the cycloaddition, a complete coupling between $N_3$-HEC and $PVP_{10}$ was thus proved and this is corroborated by the FT-IR spectra of HEC-g-$PVP_{10}$s where the consumption of the azide increased with the increase of the graft-density.

#### 5.3.3.3. $N_3$-HEC and alkyne-terminated $PNIPAAM_{10}$

In order to highlight the versatility of our grafting method, $PNIPAAM_{10}$ **12** was successfully synthesised with an alkyne-terminated trithiocarbonate CTA and coupled to $N_3$-HEC **2** using identical conditions to those described in the previous section (Scheme 5-9). Solid state $^{13}C$, $^{15}N$ NMR and FT-IR spectroscopies were used to characterise the graft-copolymer, HEC-g-$PNIPAAM_{10}$ **17**.

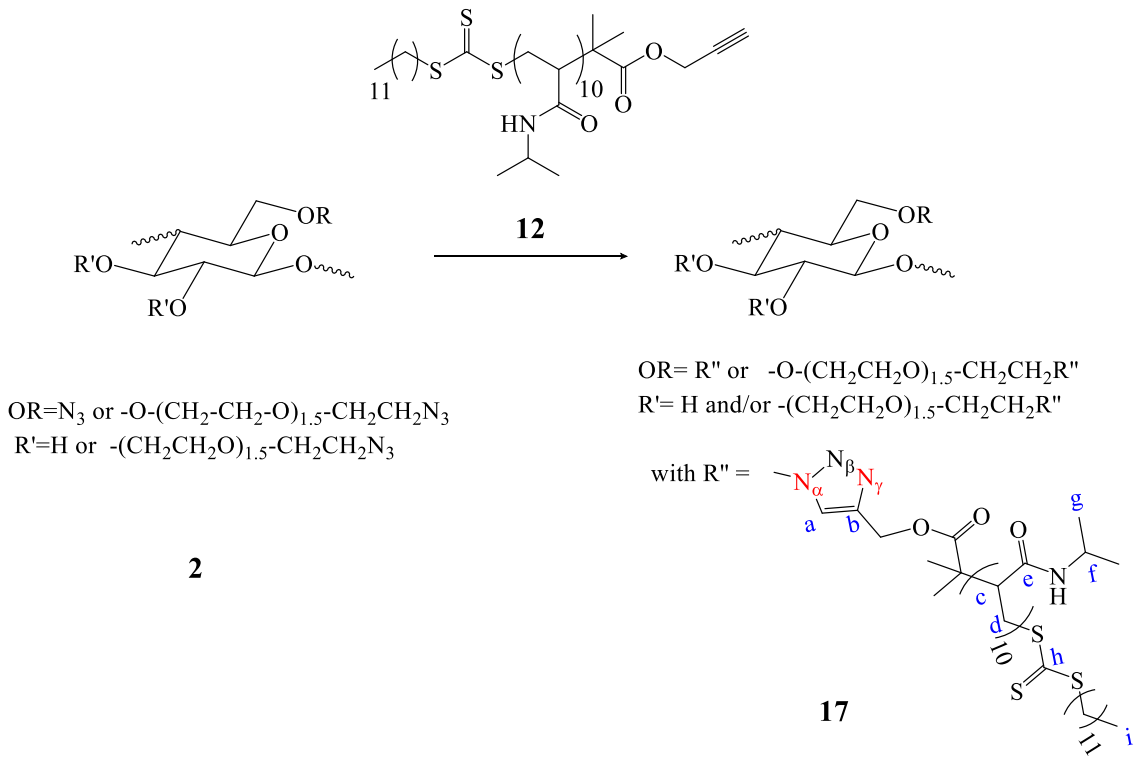


**Scheme 5-9:** CuAAC between alkyne-ended PNIPAAM$_{10}$ **12** and partially $^{15}$N-labelled $N_3$-HEC **2**

In the solid state $^{13}$C CP-MAS NMR spectrum (Figure 5-17 a), detection of PNIPAAM was confirmed with peaks at 23.1, 30.1, 41.7 and 175.1 ppm which are assigned respectively to the methyl, methylene, methine and the carbonyl group. However, additional weak peaks (Figure 5-17 a inset) are observed and these are assigned either to the cellulose backbone or the chain transfer agent. The peaks at 14.7 ppm and 242.4 ppm are assigned to the methyl and the thiocarbonate group of the RAFT agent. Furthermore, bands at ~71 and ~107 ppm are characteristic of the NMR signals commonly observed for cellulosic materials, which were assigned respectively to the set of carbons at C2 to C6 positions and to the anomeric centre (C1). The cycloaddition between PNIPAAM and

$N_3$-HEC was highlighted due to the presence of signals at ~125 and 143 ppm which are assigned to the carbons responsible for the formation of the ring.

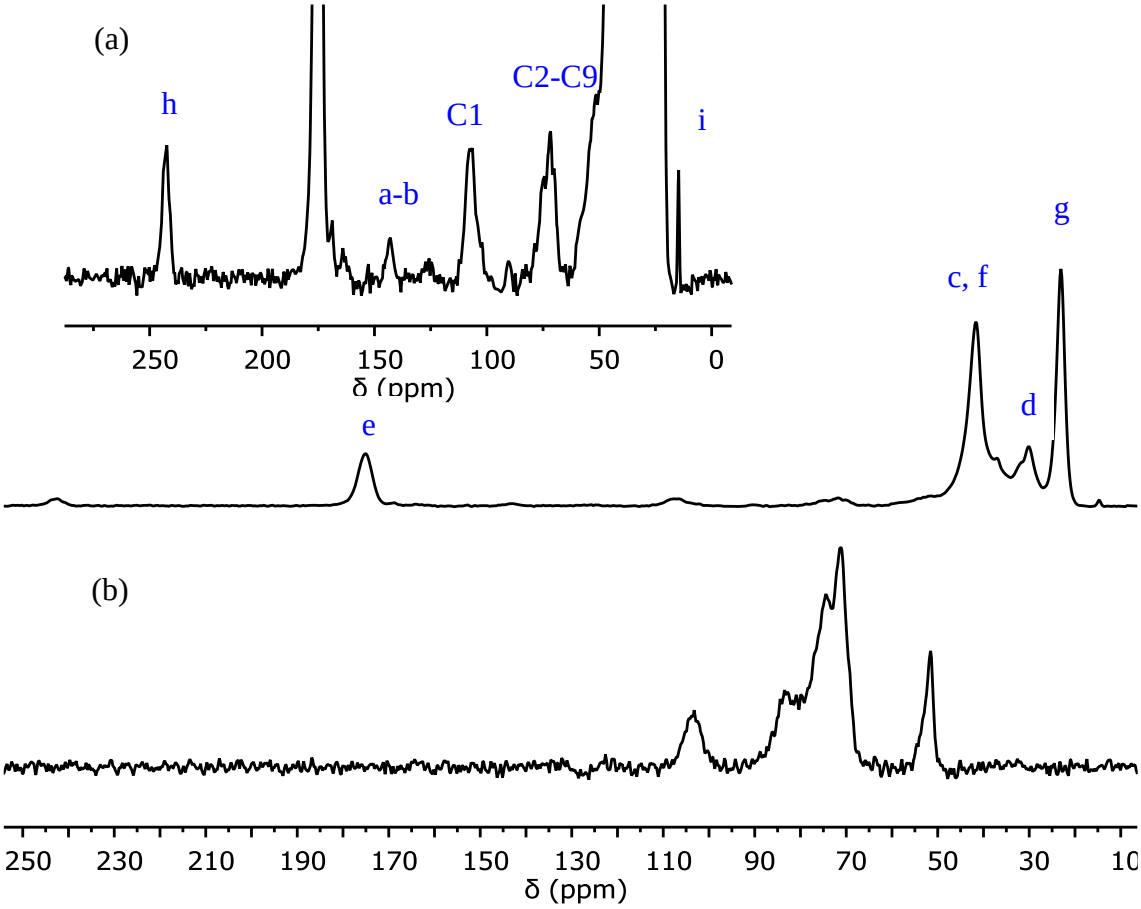


**Figure 5-17:** Solid state $^{13}C$ CP-MAS NMR spectra of (a) HEC-g-PNIPAAM$_{10}$ **17** and (b) $N_3$-HEC **2**. Numbering as in Figure 5-13 and Scheme 5-9.

The FT-IR spectrum of HEC-g-PNIPAAM$_{10}$ (Figure 5-18 a) showed complete disappearance of the band at 2100 cm$^{-1}$ indicating an full consumption of azide *via* the reaction of $N_3$-HEC with the alkyne group at the end chain of the PNIPAAM$_{10}$ chains. Furthermore, bands at 1646 and 1538 cm$^{-1}$ are assigned to -C=O and -N-C groups in

PNIPAAM and the band at 2900 $cm^{-1}$ is representative of -C-H present in the synthetic polymer.

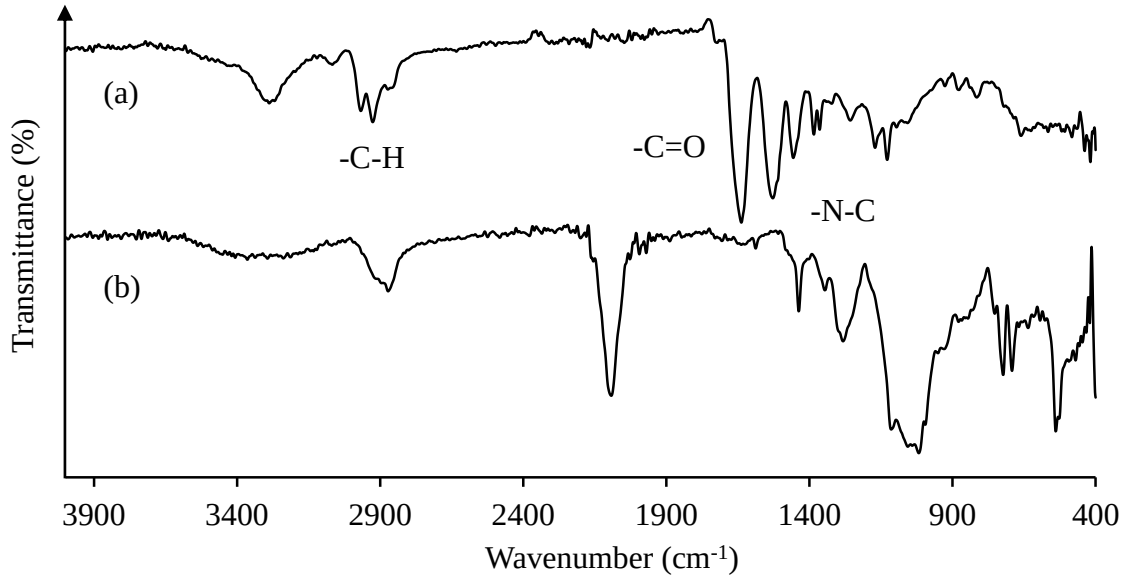


**Figure 5-18:** FT-IR spectra of (a) HEC-g-$PNIPAAM_{10}$ **17** and (b) $N_3$-HEC **2**

The solid state $^{15}N$ CP-MAS NMR spectrum (Figure 5-19 a) of the graft-copolymers showed two signals -134.8 ppm and -244 ppm which are respectively assigned to the labelled nitrogen $^{15}N_\alpha$ of $N_3$-HEC after the cycloaddition and the nitrogen of PNIPAAM. The difference in intensities between the two peaks was explained by the concentration of each within the structure; there is only one partially labelled $N_\alpha$ per 10 nitrogens of PNIPAAM in the structure, resulting in a low intensity of the signal of $N_\alpha$. Furthermore, the signals of $N_\alpha$ and $N_\gamma$ of $N_3$-HEC disappeared after the cycloaddition, indicating a complete coupling between the azide and the alkyne-terminated $PNIPAAM_{10}$.

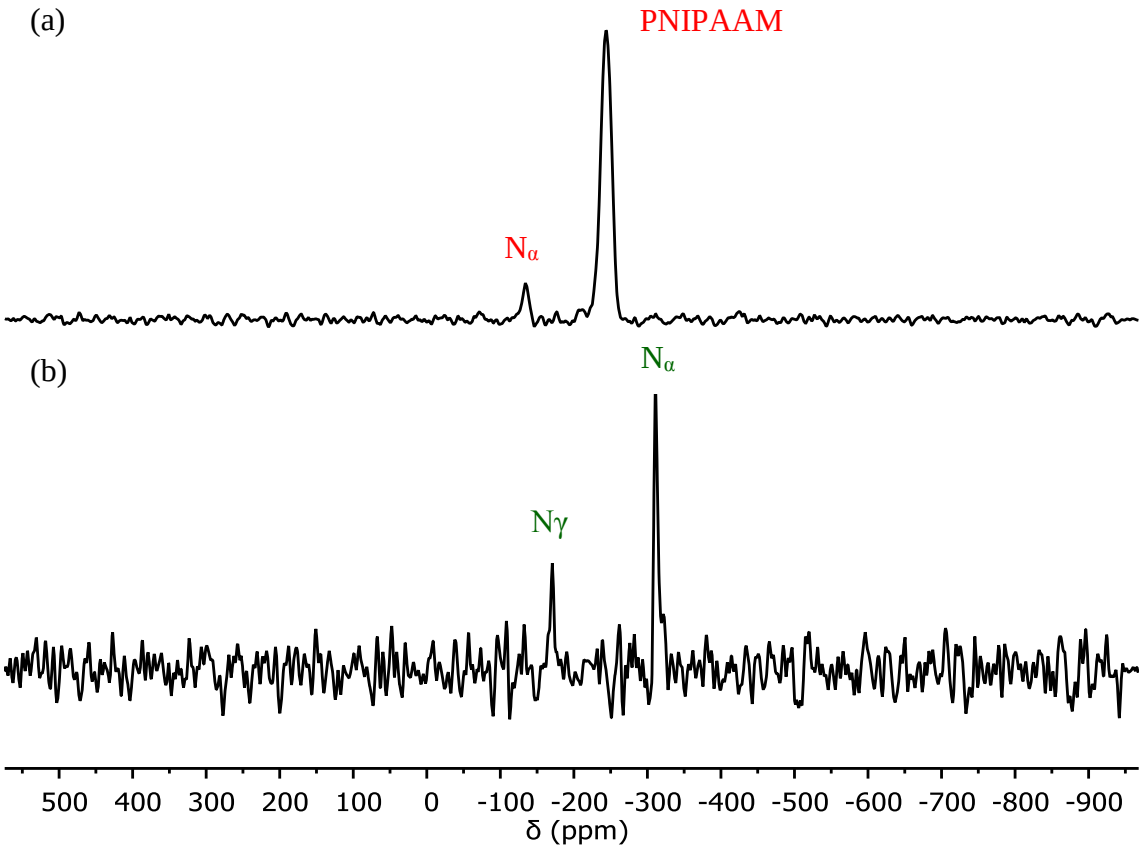


**Figure 5-19:** Solid state $^{15}$N CP-MAS NMR spectra of (a) HEC-g-PNIPAAM$_{10}$ **17** and (b) $N_3$-HEC **2**

### 5.3.3.4. $N_3$-HEC and alkyne-terminated P(IL)s

Ionic Liquid polymers P(IL)$_n$ **14** of different chain length (n =10, 50 or 100) were coupled to $N_3$-HEC **2** and this resulted in the preparation of graft-copolymers HEC-g-P(IL)s **18** (Scheme 5-10) where the grafts were composed of 10, 50 or 100 repeated units of ionic liquid monomers. In order to remove homopolymer, P(IL)$_n$, the reaction mixture was dialysed against water using a dialysis tubing of a MWCO of 50,000 g/mol ensuring the recovery of only HEC-g-P(IL)$_n$s. The graft-copolymers were characterised using solid state $^{13}$C and $^{15}$N CP-MAS NMR and FT-IR spectroscopies. Furthermore, their solubility

permits characterisation using solution state NMR spectroscopy, unfortunately the resulting spectra showed only the presence of P(IL) and no evidence of the coupling can be demonstrated. We decided that the characterisations of HEC-g-P(IL)$_n$s in their solid state was more appropriate to be reported here. Furthermore, the chain length (defined by "n") of P(IL) did not affect the detection, thus only the characterisation of HEC-g-P(IL)$_{50}$ is reported here.

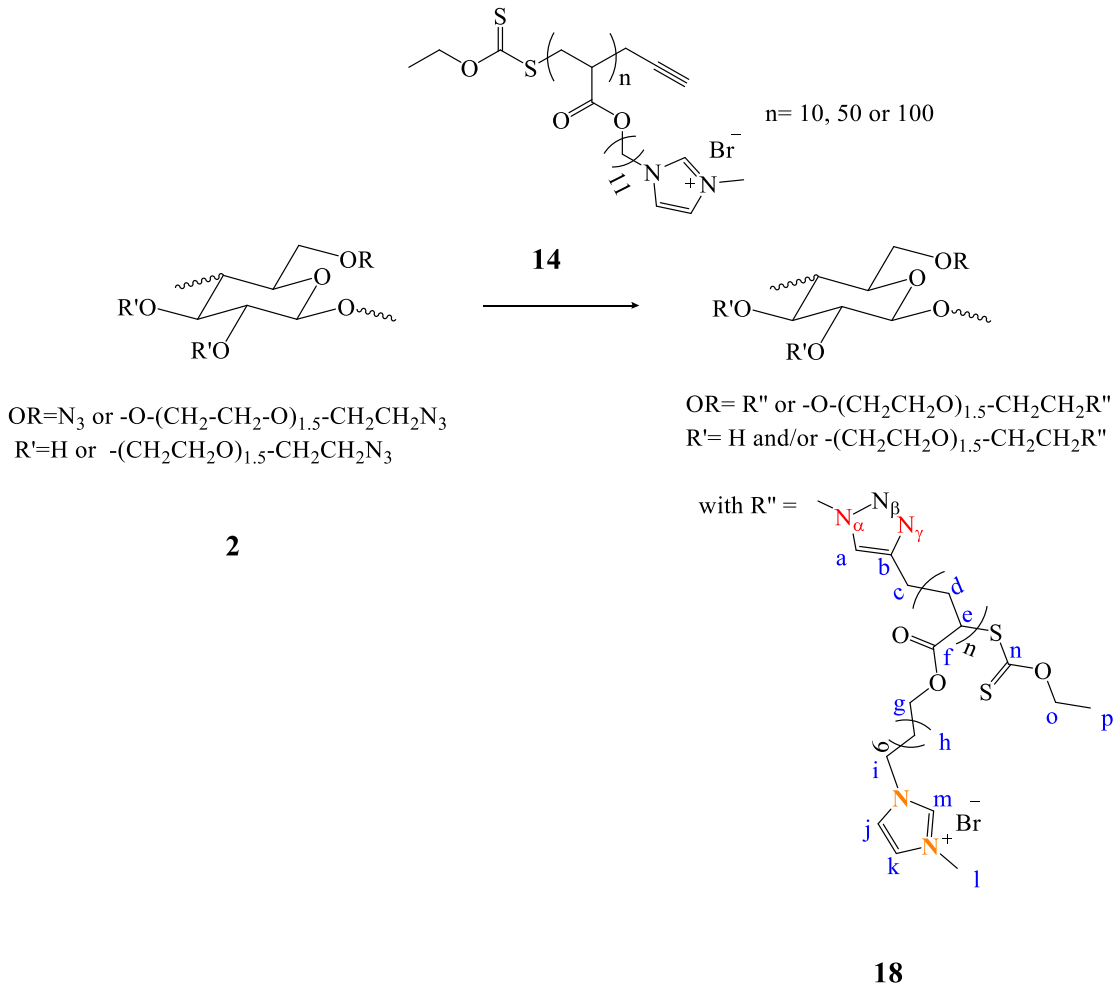


**Scheme 5-10:** CuAAC between alkyne-ended P(IL)$_n$ **14** and partially $^{15}$N-labelled $N_3$-HEC **2**

FT-IR spectra of $N_3$-HEC, $P(IL)_{50}$ and HEC-g-$P(IL)_{50}$ are displayed in Figure 5-20, and the total loss of the azide signal at 2136 $cm^{-1}$ in the spectrum of HEC-g-$P(IL)_{50}$ (Figure 5-20 c) indicated the complete consumption of the azide group of $N_3$-HEC due to the formation of the triazole with the alkyne-terminated $P(IL)_{50}$. This is the unique evidence of the grafting because, otherwise, the IR spectrum of HEC-g-$P(IL)_{50}$ is the same of that of $P(IL)_{50}$ (Figure 5-20 b), and no absorption band of HEC were detected because they are probably hidden by those of $P(IL)_{50}$. The band at 3400 $cm^{-1}$ are assigned to -OH groups, at ~3142 $cm^{-1}$ to the -CH groups of the ring, at 2856-2926 $cm^{-1}$ to the alkyl -CH groups, at 1734 $cm^{-1}$ to the carbonyl group, at 1676 $cm^{-1}$ to the -C=C- and -C=N- groups, at 1576 $cm^{-1}$ to the -C-C- and -C-N- groups, at 1468 $cm^{-1}$ to the -CH alkyl groups and at ~1170 $cm^{-1}$ to the alkyl -CH groups.

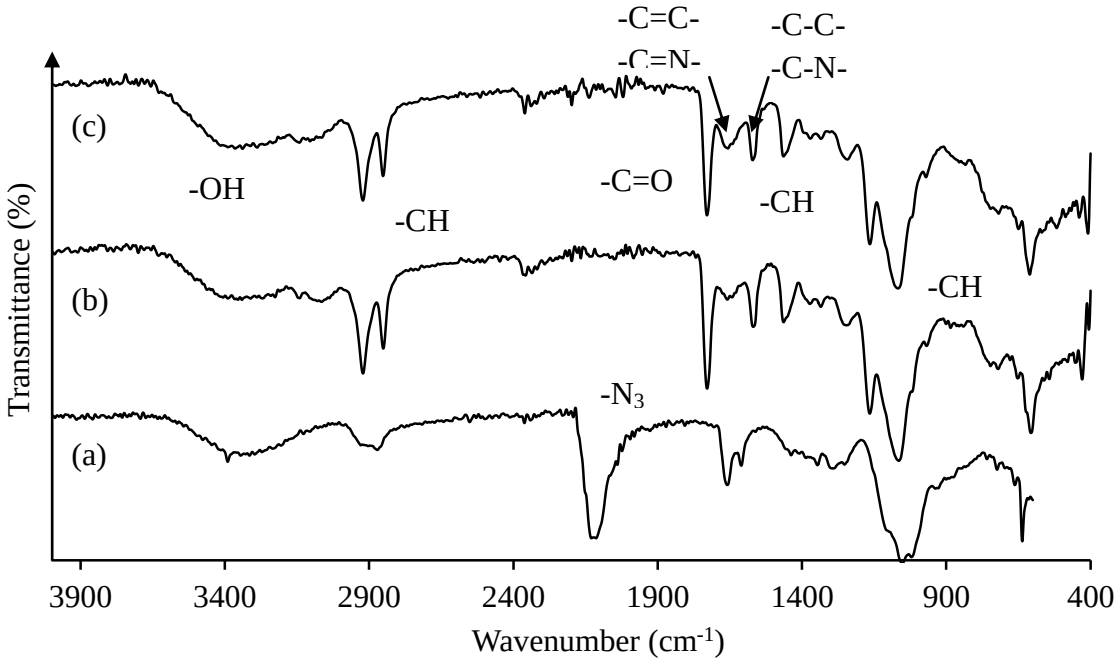


**Figure 5-20:** FT-IR spectra of (a) $N_3$-HEC **2**, (b) $P(IL)_{50}$ **14** and (c) HEC-g-$P(IL)_{50}$ **18**

Solid state $^{13}C$ CP-MAS NMR spectrum of HEC-g-$P(IL)_{50}$ (Figure 5-22) showed only signals of the grafts $P(IL)_{50}$. The signal $\boldsymbol{\delta}_C$ ~174.4 ppm is assigned to the carbonyl group, $\boldsymbol{\delta}_C$ ~139.5 and ~123.6 ppm are assigned to the alky -**C**H groups of the ring, $\boldsymbol{\delta}_C$ ~64.9 ppm to the -**C**$H_2$-O group, $\boldsymbol{\delta}_C$ ~49.1 ppm to the -**C**$H_2$-N group, $\boldsymbol{\delta}_C$ ~41.4 ppm to the methine group and the signals $\boldsymbol{\delta}_C$ ~36.0-30.6 ppm to the methylene and methyl groups. The absence of signals for the HEC backbone was predictable because of the high molecular weight of the grafts, $P(IL)_{50}$. In the previous couplings with $N_3$-HEC, the molecular weight of the grafts ($PVP_{10}$ or $PNIPAAM_{10}$) did not exceeded 1,000 g/mol and weak signals assigned to HEC backbone were detected in the solid state $^{13}C$ NMR spectra of the resulting graft-copolymers. Thus, an increase in the molecular weight of the grafts will result in the disappearance of signals of HEC. This is what we observed here with the shortest $P(IL)_n$ chains having a molecular weight of approximately 4,000 g/mol.

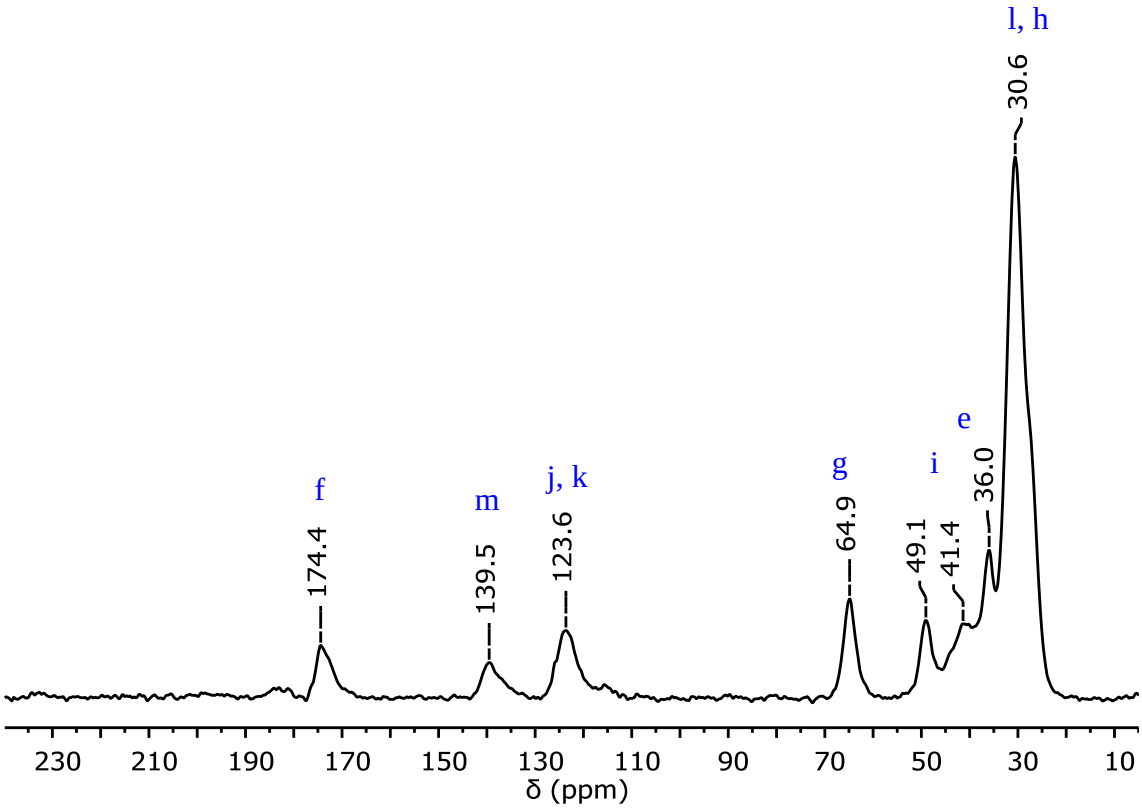


**Figure 5-21:** Solid state $^{13}C$ CP-MAS NMR spectrum of HEC-g-P(IL)$_{50}$ **18**

The solid state $^{15}N$ spectrum of HEC-g-P(IL)$_{50}$ (Figure 5-21) showed two signals $\boldsymbol{\delta}_N$ ~-208.0 and ~-194.3 ppm which are assigned to the imidazolium ring based on the literature[136]. More precisely, the former is assigned to -N-$CH_3$ group and the latter to the N-$CH_2$- group. The absence of the signal $\boldsymbol{\delta}_N$ ~-134 ppm assigned to the $N_\alpha$ after the cycloaddition is caused by the presence of high molecular weight of the grafts P(IL)$_n$.

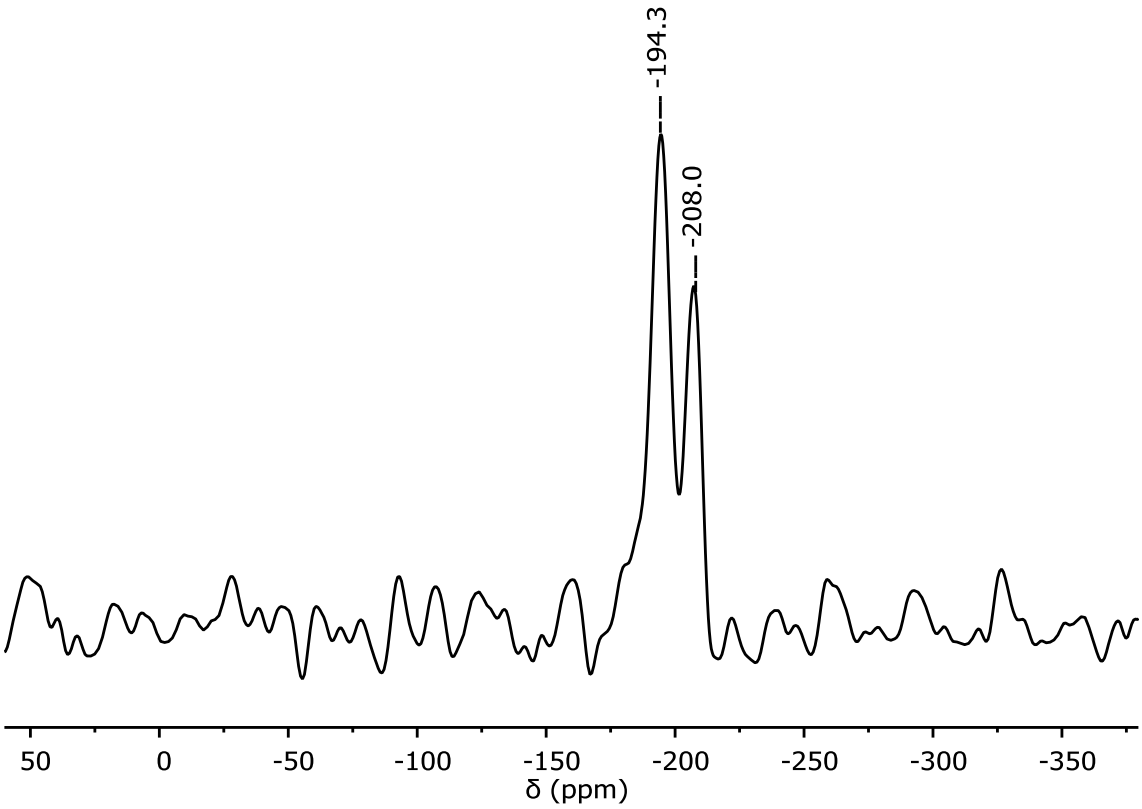


**Figure 5-22:** Solid state $^{15}N$ CP-MAS spectrum of HEC-g-P(IL)$_{50}$ **18**

To summarise, the characterisation of the graft-copolymers highlighted the presence of P(IL)$_n$, however, the presence of HEC could not been proven using NMR and FT-IR spectroscopies. The only evidence of coupling between P(IL)s and $N_3$-HEC is the disappearance of the azide band at 2100 $cm^{-1}$ in the FT-IR spectrum of the graft-copolymers. Although HEC backbone was not detected using spectroscopic techniques, P(IL) chains of different chain length were probably coupled to HEC backbone because the use of a dialysis tubing of a 50,000 g/mol MWCO would not retain P(IL) chains ($M_n$ ranged from 4,000 to 39,000 g/mol) without the presence of a HEC backbone ($M_W$ =90,000 g/mol). Furthermore, a quantitative yield for each coupling reaction proved complete functionalization of the azide in $N_3$-HEC, resulting in the preparation of three

HEC based graft-copolymers, HEC-g-P(IL)$_{10}$, HEC-g-P(IL)$_{50}$ and HEC-g-P(IL)$_{100}$. The lack of detection of HEC in the characterisation processes was presumably due to the too high molecular weight of the grafts per AGU units.

## 5.3.4. Biological study of HEC-g-P(IL)s

### 5.3.4.1. Introduction

The successful preparation of HEC-g-P(IL)s **18** allowed us to study their biological effects against bacteria and an immortalized lung alveolar cell line (A549) to determine potential applications. Furthermore, the importance of the chain length of P(IL) in the graft-copolymers was investigated.

### 5.3.4.2. Evaluation of antibacterial effects

Two tests were performed to evaluate the bacteriological effects of the HEC-g-P(IL)s and were carried out in collaboration with Dr. Gary J. Sharples at Durham University. The first was a qualitative test to visualise any effects on growth inhibition, whereas the second was a quantitative test permitting a determination of the minimum inhibition concentration (MIC) which is the lowest concentration of a compound which inhibits bacterial growth. *E. coli* (Gram-negative) and *S. aureus* (Gram-positive) were chosen as representative of the difference cell wall architectures of these bacteria.

In order to proceed to these tests, 10 mg/mL solutions of each HEC-g-P(IL) (n =10, 50 and 100) were prepared using iso-sensitest broth and series of eleven 2-fold dilutions were

prepared resulting in concentrations ranging from 10 mg/mL to 2 μg/mL. In the first test, which shall be referred to as the zone inhibition assay, 10 μL of each solution of the first 6 dilutions were spotted onto an agar plate containing an overlay of *E. coli* or *S. aureus* bacteria. The plates were incubated overnight to allow the lawn of bacteria to grow (Figure 5-23). To determine the MIC ($2^{nd}$ test), 50 μL of each graft-copolymer solution was pipetted into a 96-well plate containing 50 μL of bacteria solution (both in iso-sensitest broth). The 96-well plate was incubated overnight and the optical density (OD) at $A_{650nm}$ was determined in each well (Figure 5-24). A 10 mg/mL dilution series of ampicillin was used as a positive control.

For *S. aureus* (Figure 5-23 a), zones of growth inhibition were observed at 10 mg/mL concentration for each of the graft-copolymers and the size of zones were similar suggesting that there is not a strong influence of the chain length on the growth of Gram-positive bacteria. A decrease in the HEC-g-P(IL) concentration resulted in a reduction in the inhibitory effect as the size of the zones decreased, however at 2.5 mg/mL concentration, HEC-g-$P(IL)_{10}$ still showed a slight growth inhibition, whereas HEC-g-$P(IL)_{50}$ and HEC-g-$P(IL)_{100}$ did not. Increased chain length grafts of HEC-g-$P(IL)_n$ (n =50 and 100) showed a similar modest reduction in their effect on the growth of *S. aureus* bacteria. A MIC value (Figure 5-24 a) for HEC-g-$P(IL)_{10}$ was estimated to be 20 μg/mL whereas a MIC value of 39 μg/mL was determined for HEC-g-$P(IL)_{50}$ and HEC-g-$P(IL)_{100}$. Compared to ampicillin, which is well-known for its antibiotic properties against bacterial infections, the MICs of both HEC-g-$P(IL)_{100}$ and HEC-g-$P(IL)_{50}$ were similar, however, the MIC of HEC-g-$P(IL)_{10}$ was lower, suggesting a potentially stronger efficacy of this graft-copolymer against Gram-positive bacteria. The anti-bacterial activity against S. aureus was slightly stronger using graft-copolymers with shorter chains and one plausible explanation can be the accessibility of the cationic charges. In fact, the cationic

charge interferes with the cell wall envelope of the bacteria resulting in its death. Graft-copolymers with long grafts can undertake different conformations limiting the accessibility of the cationic charge for the bacteria and thus the antibacterial power.

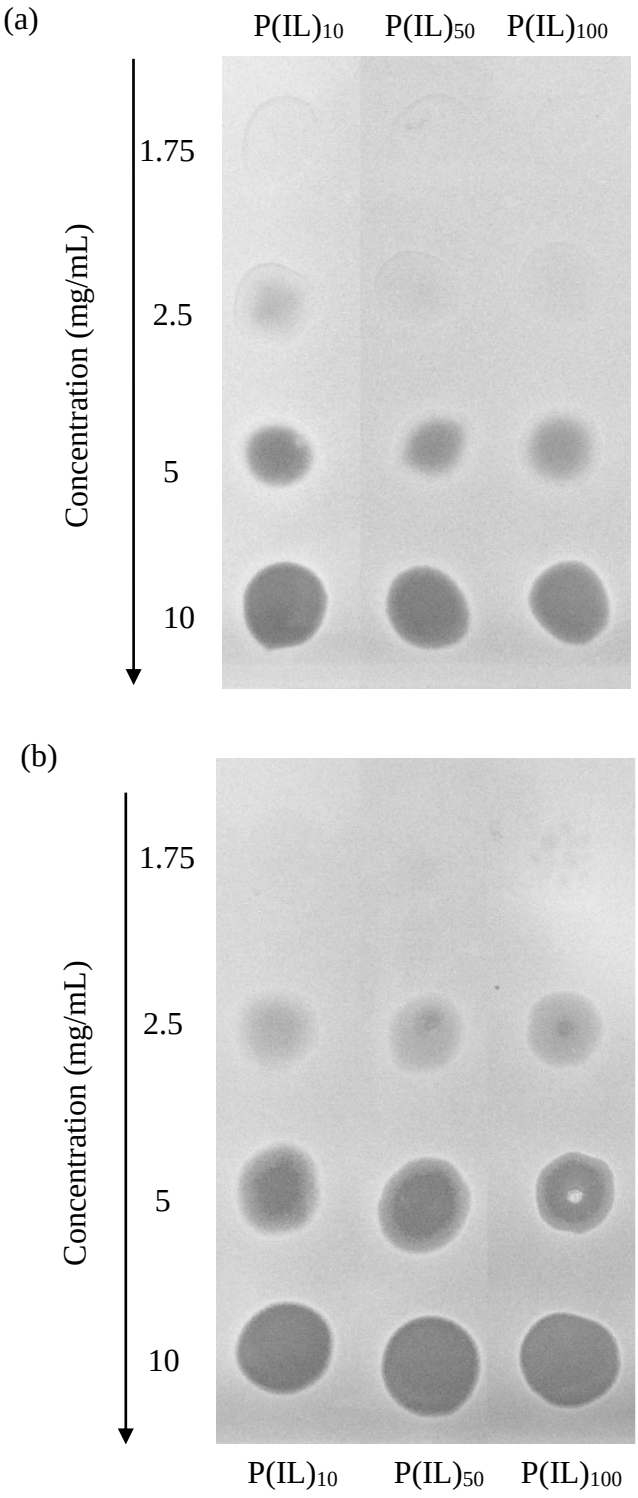


**Figure 5-23:** Results of the growth inhibition assays for the graft-copolymers HEC-g-P(IL)s **18** against (a) *S. aureus* and (b) *E. coli*

Regarding the Gram-negative bacterium, *E. coli,* growth inhibition (Figure 5-23 b) was obtained from solutions of HEC-g-P(IL)$_n$s with concentrations ranging from 10 to 2.5 mg/mL. For each graft-copolymer, the size of the zone of inhibition decreased with decreasing concentrations of the cellulosic material. At a 1.75 mg/mL HEC-g-P(IL)$_n$ concentration, inhibition was not observed indicating the loss of antibacterial effect at this concentration. At 2.5 mg/mL, the size of the inhibition zones for the three graft-copolymers HEC-g-P(IL)$_n$s were similar indicating there was no major influence of the chain length on antibacterial properties. In order to corroborate these observations, MICs were determined and found to be 20 µg/mL for each of the graft-copolymers (Figure 5-24). Furthermore, a 39 µg/mL MIC was measured for ampicillin which is higher than that determined for HEC-g-P(IL)s demonstrating a stronger inhibition effect against Gram-negative bacteria of the graft-copolymers. Surprisingly, the chain length did not influence the anti-bacterial activity against *E. coli* suggesting that the density of charge didn't influence the anti-bacterial properties. The anti-bacterial activity results from the presence of the cationic charge at the outer surface and did not rely on the number of the charges that contains the graft-copolymers.

To summarise, inhibitory effects of the graft-copolymers were observed for both Gram-positive and Gram-negative bacteria and were comparable to those produced by antibiotics such as ampicillin. The cationic charge which defines the imidazolium ring, where the charge disrupts the membrane of the bacteria is likely to be responsible for this effect[94]. The chain length of the grafts, which determines the number of charges, did not influence the antibacterial properties of HEC-g-P(IL)s against *E. coli* with a constant MIC of 20 µg/mL, however in the case of *S. aureus*, a lower MIC (20 µg/mL) for HEC-g-P(IL)$_{10}$ was noted compared to those of HEC-g-P(IL)$_{50}$ and HEC-g-P(IL)$_{100}$ (39 µg/mL).

This was also indicated in the growth inhibition assay on agar plates. The anti-bacterial activity seems to be independent of the charge density but depends most likely on the accessibility of the positive charge at the outer surface of the graft-copolymers by the bacteria[137]. In fact, the short grafts for HEC-g-P(IL)$_{10}$ have less option of chain conformation and thus the charge is probably more accessible to affect the bacteria cell envelope while for longer grafts, the cationic charge can be hidden from the bacteria because of the different possible chain conformations. Furthermore, HEC-g-P(IL)$_n$s (n =50 and 100) were slightly more resistant to *E. coli* than *S. aureus*. The mechanism of the inhibitory effects resides in the interaction between the cationic charge and the bacterial membrane which is different for Gram-positive and -negative bacteria in terms of permeability and density of charge. Although more permeable, *S. aureus* membrane is slightly negatively-charge and permits the adhesion of graft-copolymers on the bacteria surface. In order to destabilise the *S. aureus* membrane the concentration in HEC-g-P(IL)$_n$ (n =50 and 100) had to be higher compared to that for *E. coli* where its membrane is neutral. However, HEC-g-P(IL)$_{10}$ has similar antibacterial effects against both bacteria (*E. coli* and *S. aureus*) and this can be due to relatively good accessibility of the cationic charge to destabilise readily Gram-positive bacteria. The three graft-copolymers display promising antibacterial properties which could extend the use of cellulose in industrial applications.

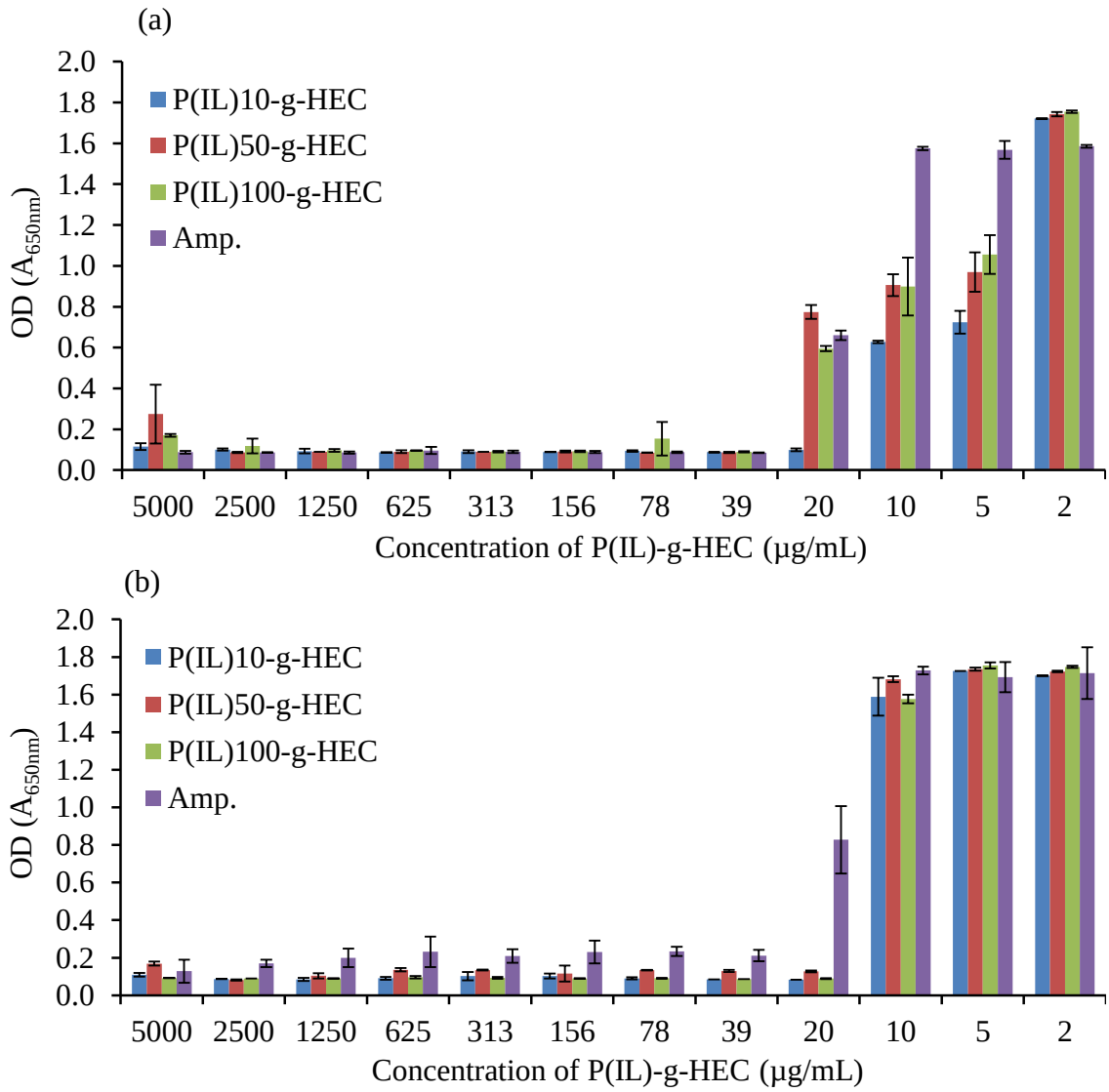


**Figure 5-24:** Determination of the MIC of HEC-g-P(IL)s **18** for (a) *S. aureus* and for (b) *E. coli*

### 5.3.4.3. Evaluation of cytotoxicity against an immortalized lung alveolar cell line (A549)

To evaluate the possible uses of HEC-g-P(IL)s in medical applications, an estimation of the cytotoxicity against A549, an immortalized lung alveolar cell line was essential and

this study was carried by Dr. Paul Yeo at Durham University. The cytotoxicity is measured using $LD_{50}$, the lethal dose that kills 50% of cells. A 500 µg/mL concentration solution was prepared of each graft-copolymer followed by eleven 2-fold serial dilutions. Each solution was spotted into 96-well plate containing the cells. After incubating overnight, Almar blue solution was added and the fluorescence of each well containing both cells line and HEC-g-P(IL) was read using a fluorescence excitation and emission wavelength of 540–570 nm (peak excitation is 570 nm) and 580–610 nm (peak emission is 585 nm) respectively. The evolution of its intensity as a function of the concentration of each graft-copolymer is displayed in Figure 5-25.

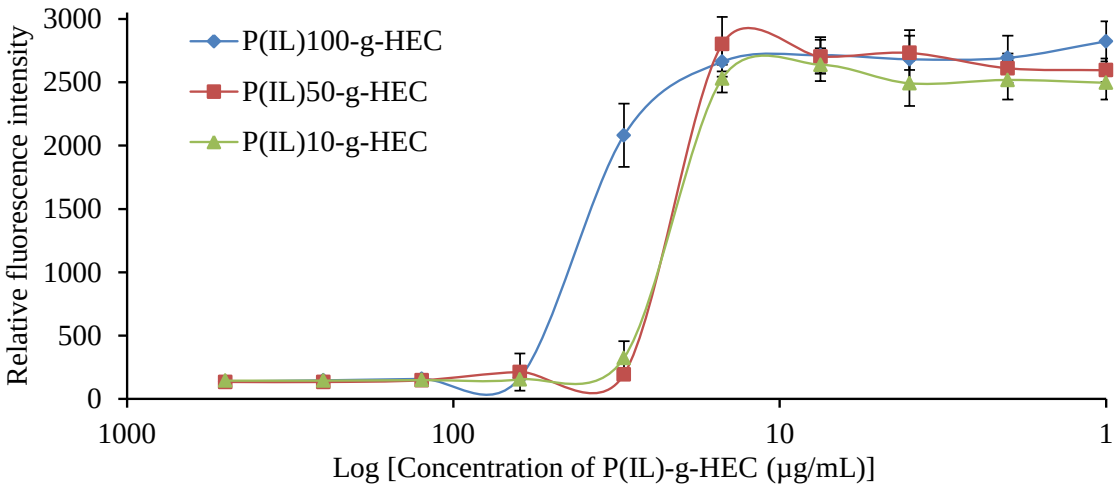


**Figure 5-25:** Determination of $LD_{50}$ for HEC-g-P(IL)s **18**

The fluorescence decreases with the death of cells and approaches zero when all cells have died, however $LD_{50}$ corresponds to the concentration in HEC-g-P(IL) at which half of the fluorescence was lost. For HEC-g-$P(IL)_{10}$ and HEC-g-$P(IL)_{50}$, $LD_{50}$ was ~20 µg/mL whereas ~40 µg/mL $LD_{50}$ was measured for HEC-g-$P(IL)_{100}$. The increase of the

length chain of P(IL) grafts reduced by a factor 2 the toxicity of the graft-copolymers HEC-g-P(IL) against the lung cells. The cationic charge is responsible for the attachment between the cell membrane and the graft-copolymers resulting in the necrosis of the cell, i.e. their death[137, 138]. One plausible reason of the difference of toxicity observed between chain lengths is the accessibility of the cation on the outer surface of the graft-copolymers which depends on the conformational flexibility.

#### 5.3.4.4. Summary

HEC-g-P(IL) materials showed promising antibacterial properties against both *E. coli* and *S. aureus*. For Gram-negative bacteria (*E. coli*), the chain length of the grafts did not influence the MIC of the graft-copolymer (20 µg/mL). For Gram-positive (*S. aureus*), a decrease in the chain length to 10 repeated IL units decreased the MIC by a factor of two (20 µg/mL) probably due to the conformational flexibility of the cationic charge for a shorter chain length of the grafts. The graft-copolymers of 50 repeated IL units and above had lower MICs against *E. coli* (20 µg/mL) than against *S. aureus* (39 µg/mL) resulting in the higher sensitivity of these graft-copolymers against *E. coli* because of the differences in electrostatic properties of the two bacterial surfaces, whereas HEC-g-$P(IL)_{10}$ did not present a sensitivity criteria for bacteria of Gram-positive or negative with a common 20 µg/mL MIC because the cationic charge has a limited conformational flexibility compared to graft-copolymers containing longer grafts. Although possessing antibacterial properties at a 20 µg/mL concentration, HEC-g-P(IL)s is also toxic against an immortalized lung alveolar cell line, A549, at that concentration resulting in the impossibility of its use as an antibiotic, however it could be of great interest as an

antibacterial compounds which could be included, for instance, in the formulation of paints and antiseptics.

## 5.4. CONCLUSION

Azide-functionalised HEC, $N_3$-HEC **2**, in which all the primary alcohols were placed with azide groups, was prepared successfully. Alkyne-terminated RAFT agents for polymerising NVP and NIPAAM were also prepared. A xanthate, O-ethyl S-prop-2-ynyl carbonodithiolate **5**, was used to polymerise NVP whereas a trithiocarbonate **8** was chosen for NIPAAM, targeting degrees of polymerisation of 10 in each case. Both polymers were synthesised successfully with monomer conversions up to 80-90% and $Đ_M$ values of 1.2 (PNIPAAM) and 1.4 (PVP). Prior to the cycloaddition of $N_3$-HEC with alkyne-ended $PVP_{10}$, the transfer agent was successful coupled to $N_3$-HEC. This permitted the validation of the click chemistry between the alkyne and the azide *via* the NMR chemical shifts ($^{13}C$ and $^{15}N$) of the products of the click reaction. Furthermore, HEC-g-$PVP_{10}$ hybrid materials with different PVP graft-densities were made by varying the ratio of PVP to $N_3$. A decrease in the ratio of $PVP_{10}$ to $N_3$ provided evidence of the grafting between $PVP_{10}$ and $N_3$-HEC. The use of $^{15}N$-labelled $N_3$-HEC unequivocally demonstrated the successful coupling of $PVP_{10}$ and HEC. In order to demonstrate the versatility of our method, $PNIPAAM_{10}$ polymerised in the presence of a trithiocarbonate transfer agent was also successfully coupled to $N_3$-HEC. Our strategy for preparing graft-copolymers of cellulose is efficient and produces well-defined hybrid materials by combining RAFT polymerisation and CuAAC. Subsequently, novel graft-copolymers of HEC with promising antibacterial properties were prepared. The ionic liquid (IL) monomer, 1-(11-acryloyloxyundecyl)-3-methylimidazolium bromide **13** was chosen

because of the presence of the imidazolium ring, which probably damages the bacterial membrane causing the death of the bacteria. IL was polymerised using the xanthate as transfer agent **5** with monomer conversion up to 80% and $Đ_M$ of 1.5. DPs of 10, 50 and 100 were targeted in order to produce graft-copolymers of HEC containing different lengths of chain grafts. The graft-copolymers HEC-g-P(IL)$_n$s (n =10, 50 and 100) were characterised using NMR and FT-IR spectroscopies and their biological effects were study against bacteria (Gram-positive and -negative) and an immortalized lung alveolar cell line (A549). The results showed antibacterial effects against both bacteria *E. coli* and *S. aureus* and were comparable to those of ampicillin which is a powerful antibiotic, however HEC-g-P(IL)$_n$s were toxic against A549 at the same dose that was required to inhibit the bacterial growth. These findings suggested the possible use of HEC-g-P(IL)s as an antiseptic rather than an antibiotic, in industrial areas such as the paint industry.

# Chapter 6: Conclusion

Three methods for modifying hydroxyethyl cellulose (HEC) have been described in this thesis. The main focus was the introduction of lactam groups due to the desire of Ashland (our sponsor) to combine the properties of poly(N-vinylpyrrolidone) (PVP), such as its solubility in aqueous and organic solvents, with a cellulosic material. Additionally, an interest regarding the introduction of ionic liquid polymers containing imidazolium groups onto HEC was demonstrated in order to develop antibacterial HEC-based materials.

The first method relied on the functionalization of the hydroxyl groups of HEC with 1-(hydroxymethyl)-2-pyrrolidone (HMP) (Chapter 3) which was prepared readily and reproducibly. The functionalization reaction was optimised in order to obtain the highest degree of substitution (DS), which is defined by the number of hydroxyl groups of HEC that have been modified. The first investigations of the reaction were carried in dimethyl sulfoxide (DMSO) to determine an appropriate reaction temperature. A temperature of 155 °C was necessary for HEC to react with HMP and the coupling was confirmed using a 2D NMR experiment. Furthermore, the DS was determined using $^{13}C$ NMR spectroscopy and was found to be 0.1. The NMR analysis highlighted also the selectivity of the reaction for towards the primary alcohols of HEC. In order to increase the degree of functionalization, the solvent was changed to N-methyl-pyrrolidone (NMP) because of its better thermal stability at 155 °C compared to that of DMSO. The change of solvent did not result in increased DS, however, the decrease of the reaction time from 17 h to 2 h increased the degree of functionalization up to a value of 0.2. Furthermore, increased the molar ratio of HMP to AGU did not influence the degree of functionalization and the

remaining question about possible degradation of HEC under the reaction conditions was supressed using size exclusion chromatography (SEC). Subsequently, a solvent free reaction was suggested for promoting increased DS, and thus HMP was used as both the functionalizing agent and the solvent. The resulting HEC-based material displayed near-complete functionalization of the primary alcohol with HMP, with a DS of up to 0.9 after 1 h of reaction time. Furthermore, the functionalization was found to be reversible because DS decreased after a 5 h reaction time. The unsuccessful reaction of 1-(hydroxyethyl)-2-pyrrolidone (HEP) with HEC suggested a specific reaction mechanism for the functionalization of HEC with HMP. The physical properties of HMP-functionalized HEC such as solubility, viscosity, thermal stability, capacity of dye release and anti-adhesion properties against bacteria were investigated and were altered compared to those of the parent material. For instance, the thermal stability of HMP-functionalised HEC increased whereas the viscosity decreased compared to that of HEC. Such changes were also reported in the literature where PVP was grafted onto cellulose or cellulose derivatives using conventional radical polymerisation, however the production of graft-copolymers of HEC having a controlled length chain of PVP grafts were reported here for the first time.

The second method to chemically modify hydroxyethyl cellulose with lactam groups used the most popular approach for preparing well-defined graft-copolymers of cellulose and cellulose derivatives which is the "grafting from" approach used in combination with Atom Transfer Radical Polymerisation (ATRP) (Chapter 4). The macro-initiator Br-HEC was successful prepared in an 80% yield and the influence of the atmosphere, HEC molecular weight and the choice of the base on the DS were discussed. DS values ranged from 0.3 to 0.9 and a 0.7 DS for Br-HEC was chosen to avoid the formation of a gel due to the high concentration of radical species on the backbone. To verify the activity of the

macro-initiator, methyl methacrylate (MMA) was polymerised in a controlled manner, with a 61% monomer conversion. The grafts of the graft-copolymers were hydrolysed from the backbone and analysed using SEC to determine a $Đ_M$ of 1.2, however the molecular weight of the grafts indicated a lack of reactivity of the alkyl bromide which can be caused by the steric hindrance and H-bonding networks of HEC. Subsequently, the polymerisation of N-vinylpyrrolidone (NVP) was investigated, but it did not work efficiently because the catalyst was rapidly deactivated due to the presence of the amide group within the monomer species. 1-(11-acryloyloxyundecyl)-3-methylimidazolium bromide (IL) was a good candidate for ATRP because it is an acrylate-based monomer. The introduction of imidazolium groups onto HEC was promising for the development of graft-copolymers with antibacterial activity. Unfortunately, the ATRP of IL from Br-HEC showed a limited success with only 30% monomer conversion. Instead of evaluating the physical properties of these graft-copolymers, which cannot be described as well-defined, a more versatile method was developed based on the "grafting to" approach (Chapter 5).

The "grafting to" approach permitted the preparation of a well-defined synthetic polymers which were coupled to HEC backbone using a "click" reaction. Reversible Addition-Fragmentation Chain-Transfer (RAFT) polymerisation was chosen for the synthesis of polymers because of its versatility towards monomer structure compared to ATRP. Alkyne-terminated RAFT agents were used in order to set up azide-alkyne Huisgen cycloaddition (CuAAC) with HEC that has been prior-functionalized with a partially labelled $^{15}N$ sodium azide. NVP and IL were successfully polymerised using an alkyne-terminated xanthate whereas N-isopropylacrylamine (NIPAAM) was polymerised with alkyne-ended trithiocarbonate. In each case, the monomer conversion was high (70-90%) and acceptable molecular weight distributions were obtained for such RDRP process. For

the polymerisation of NIPAAM and NVP, a low degree of polymerisation (DP) of 10 was targeted whereas IL was polymerised with three different targeted DPs (10, 50 and 100). $PVP_{10}$ and $PNIPAAM_{10}$ were used to unequivocally establish the method because of the use of different RAFT agent structure for the polymerisation of NVP and NIPAAM. $PVP_{10}$ was grafted to HEC to produce graft-copolymers with different graft-densities and prove the attachment between $PVP_{10}$ and HEC using spectroscopic techniques. Furthermore the use of partially labelled $^{15}N_3$-HEC proved the effectiveness of the "click" chemistry using $^{15}N$ NMR spectroscopy. The coupling between $PNIPAAM_{10}$ and HEC demonstrated the versatility of the method by way of the change from a RAFT agent to an alkyne-terminated trithiocarbonate for the polymerisation of NIPAAM. Once the method was well-established, $P(IL)_n$ (n =10, 50 and 100) were successfully grafted to HEC and the biological effects of the resulting graft-copolymers HEC-g-P(IL)s were investigated. The introduction of P(IL) onto HEC allowed the development of antibacterial properties with minimum inhibition concentrations (MICs) against bacteria of Gram-positive (*S. aureus*) and Gram-negative (*E. coli*) similar to those of ampicillin which is well-known as an antibiotic. The influence of graft length on these properties was investigated. For Gram-negative bacteria (*E. coli*), no influence was observed indicating a poor influence of the density of charge. However, for Gram-positive bacteria (*S. aureus*), the graft-copolymers HEC-g-$P(IL)_{10}$ with the shortest length chain had a stronger antibacterial effect compared to those with longer chain length (n =50 and 100) and this can be due to the conformational flexibility of the grafts containing the cationic charge which is responsible for the disruption of the bacterial cell wall. Furthermore, a stronger sensitivity of HEC-g-P(IL)s against *E. coli* was observed, with a lower MICs against *E. coli* than that against *S. aureus*, potentially, due to the electrostatic effects engendering by *S. aureus* bacteria on their outer surface. To evaluate the potential of the

graft-copolymer in the medical field, the cytotoxicity was measured using $LD_{50}$ corresponding to the lethal dose that kills 50% of cells. HEC-g-P(IL)s became toxic at the same concentrations that inhibited bacterial growth and thus its applications as an antibiotic is limited, however, its use as an antibacterial agent in the formulation of paint and personal care products is promising.

To summarise, three methods have been used to introduce mainly lactam groups onto HEC. The first method consisted of the functionalization of nearly all AGU units of HEC with a single lactam group. The resulting bio-based material presented different properties compared to those of the parent HEC and these differences, such as the change of solubility, decrease of the viscosity, and improvement of the thermal stability could extend the use of HEC in industry. The other two methods aimed to prepare well-defined graft-copolymers of HEC using grafting approaches to produce materials such as HEC-g-PVP. One variant is based on the "grafting from" approach using ATRP to control the length of the grafts whereas the other, based on the "grafting to approach", combines RAFT polymerisation with the CuAAC reaction. The "grafting from" approach was not as successful as the "grafting to" approach because of the poor polymerisation of NVP and IL from the HEC backbone using ATRP. However, alkyne-terminated PVP and P(IL) were obtained with high monomer conversions using RAFT polymerisation and, subsequently were clicked to the partially $^{15}N_3$-HEC forming well-defined graft-copolymers. This method is promising for developing hybrid materials of HEC with well-defined properties. The advantage of this method resides mainly in the use of RAFT process which polymerises a wider number of monomers compared to ATRP and the "click" process which takes place readily under mild-conditions. For instance, a promising antibacterial HEC-based material was developed in this thesis.

# Chapter 7: Future work

In the immediate future, work should be mainly based on the evaluation of the physical properties of the graft-copolymers which have already been successful prepared in this thesis. For HEC-g-$PVP_{10}$, the study of its viscosity, thermal stability, capacity to release dye, solubility and anti-adhesion properties against bacteria should be prioritised in order to compare to those of HMP-functionalized HEC. These findings will determine the influence of the number of lactams on the physical properties of the hybrid material. Regarding the graft-copolymer, HEC-g-$PNIPAAM_{10}$, the thermo-responsiveness should be studied, because, the introduction of $PNIPAAM_{10}$ chains onto HEC should provide thermo-responsiveness properties. This is because PNIPAAM has a lower critical solution temperature (LCST) at 32 °C. First, solubility testing of the graft-copolymers should be assessed, where, the LCST of HEC-g-$PNIPAAM_{10}$ could be determined using UV-Vis spectrophotometer coupled with a temperature controller. Second, the morphology and size of HEC-g-$PNIPAAM_{10}$ aggregates should be studied above and below its LCST using scanning electron microscopy (SEM) and dynamic light scattering (DLS). Based on these results, the use of HEC-g-$PNIPAAM_{10}$ as drug delivery vesicle could be considered because of the biocompatibility and biodegradability of HEC, however, further experiments concerning the loading capacity and the kinetics of the release should be made. Regarding HEC-g-P(IL), the influence of the graft-density on the antibacterial effect should be studied. Because of a minor influence of the length chain (10, 50 and 100 of IL repeated units) of HEC-g-P(IL) on the inhibitory effects, the preparation of hybrid materials, HEC-g-P(IL)s, containing different graft-densities of $P(IL)_{10,}$ should be investigated. For instance, one $P(IL)_{10}$ chain per three and per six repeated units of HEC could be coupled, and these could be tested against bacteria and

against immortalized lung alveolar cell line (A549) to determine their cytotoxicity. Furthermore, the structure-activity relationship between HEC-g-P(IL) and bacteria should be explored to determine the cause of the inhibitory effects which can be due to a bactericidal and/or bacterio-statistical effect of HEC-g-P(IL). The work could be extended with the preparation of more complex graft-copolymers of HEC. For instance, HEC-g-P(IL) contains an imidazolium ring which could be readily functionalized with silver acetate (AgOAc) forming a silver carbene (Figure 7-1). There could be two strategies to introduce silver carbene on HEC. The first would be the formation of the carbene by functionalizing the synthetic polymer P(IL) with the silver acetate, and thus, silver-functionalized P(IL) will be coupled onto HEC. The second will be the functionalization of the graft-copolymer HEC-g-P(IL) with the AgOAc. The former method should be easier in terms of characterisation, however, CuAAC of silver-functionalised P(IL) with $N_3$-HEC may result in the loss of the silver complex under the reaction conditions.

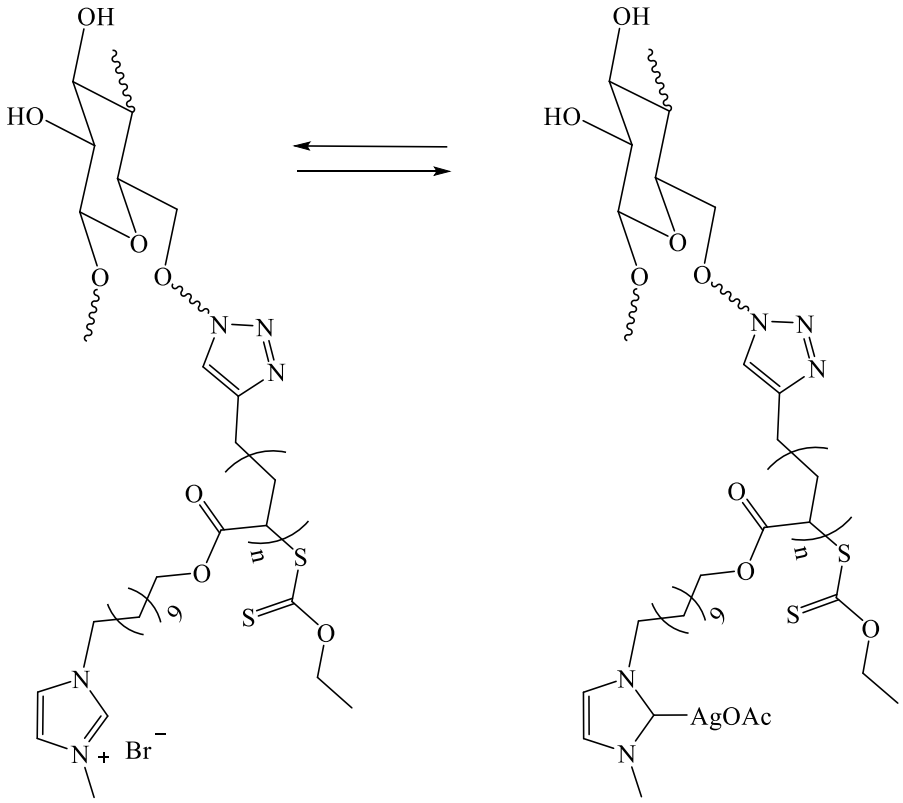


**Figure 7-1:** Silver-functionalized HEC-g-P(IL)

The silver-functionalized graft-copolymer of HEC should present enhanced antibacterial properties due to the presence of the silver which has been known as a disinfectant since antiquity. In fact, the graft-copolymers should possess a dual antibacterial action. The first antibacterial action consists of the detachment of silver and its drilling in to the membrane of bacteria leading to their death. The second one is the re-formation of the imidazolium ring which will cause also the inhibition of the bacterial growth due to the presence of the cationic charge. For instance, this hybrid material could possibly be used as an "auto-sterile" coating in some biomedical applications.

The straightforward strategy of combining RAFT polymerisation and CuAAC should be extended to preparing combined graft-copolymer of HEC possessing dual-responsiveness properties. PNIPAAM and P(IL) which are a thermoresponsive and

antibacterial polymers respectively could be combined to form an innovative graft-copolymer of HEC. The preparation of such a material would require two coupling steps to ensure the grafting of the two synthetic polymers onto HEC. For instance, the first step could consist of functionalizing one azide group with PNIPAAM per two AGU units of HEC, and subsequently ($2^{nd}$ step), the residual $N_3$ could be cyclised with alkyne-terminated P(IL) forming HEC-g-PNIPAAM-comb-P(IL) (Figure 7-2). The graft-density of the each polymer could be easily modulated by varying the ratio of number of polymer chains to the number of $N_3$ in $N_3$-HEC.

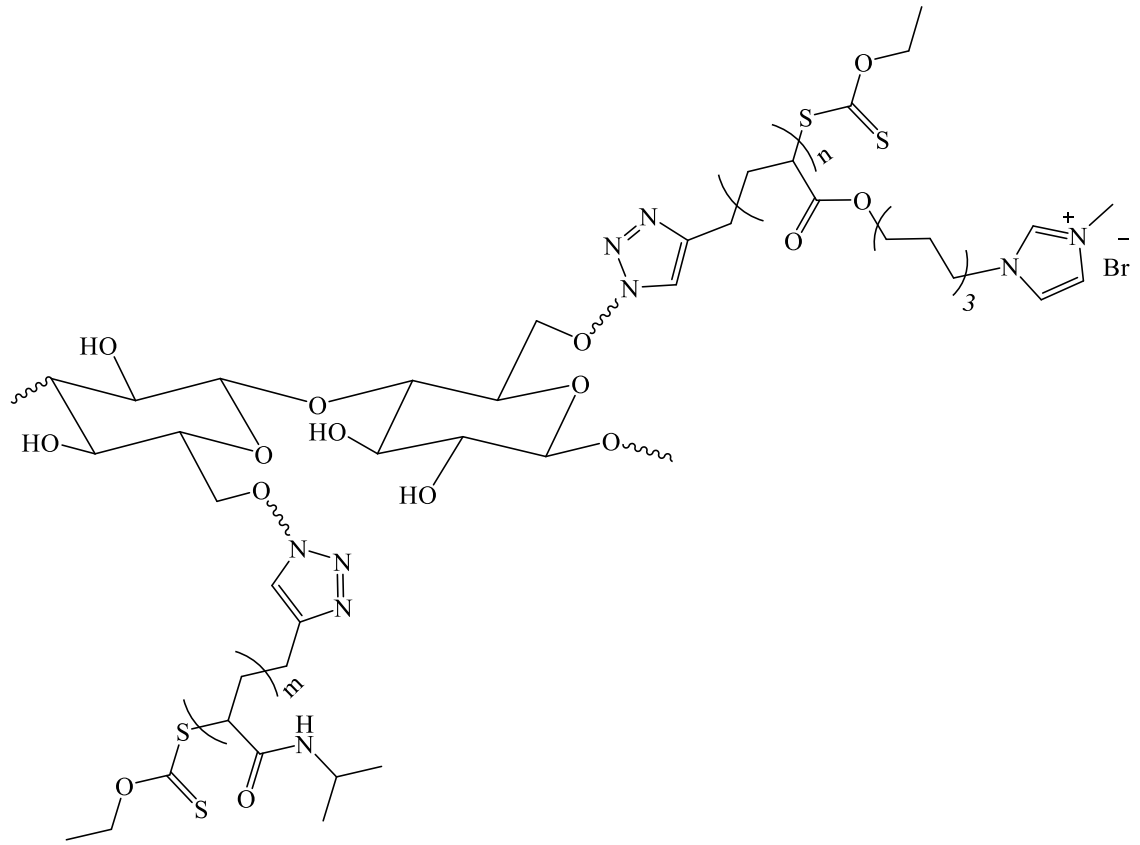


**Figure 7-2:** HEC-g-PNIPAAM-comb-P(IL)

HEC-g-PNIPAAM-comb-P(IL) should possess both thermo-responsiveness and antibacterial properties. In fact, PNIPAAM chains will collapse above 32 °C whereas P(IL) chains would maintain antibacterial properties independently of the temperature. This complex system may find potential applications as an antibacterial nanocontainer in the biomedical field.

# Appendices

**Appendix 1:** Solid state $^{13}C$ CP-MAS NMR spectrum of $Br_{0.7}$-HEC (exp. FJ-237)

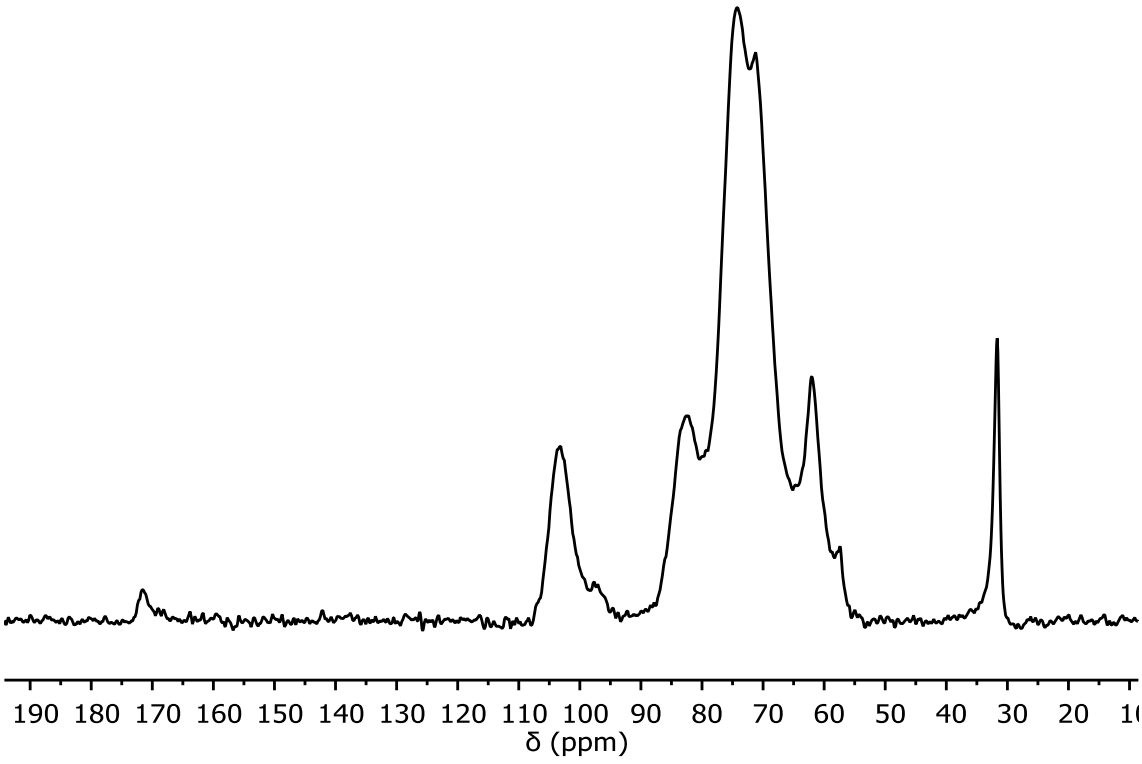

**Appendix 2:** FT-IR spectrum of $HEC_{0.3}$-g-$PMMA_{15}$ (exp. FJ-130)

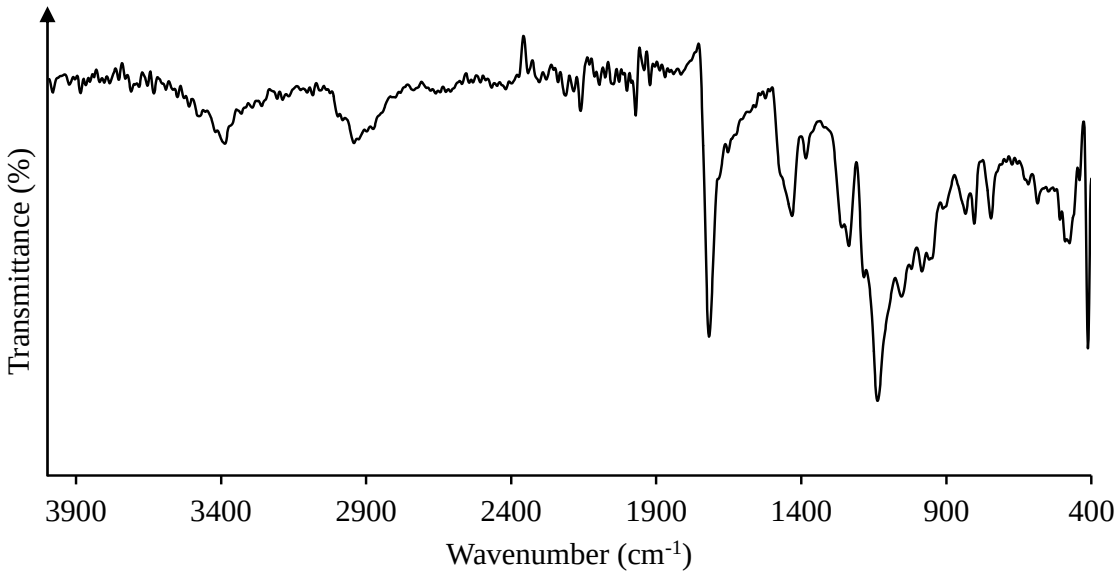


**Appendix 3:** FT-IR spectrum of $HEC_{0.3}$-g-$PMMA_{30}$ (exp. FJ-297)

**Appendix 4:** Solid state $^{13}C$ CP-MAS NMR spectrum of $HEC_{0.3}$-g-$PMMA_{30}$ (exp. FJ-297)

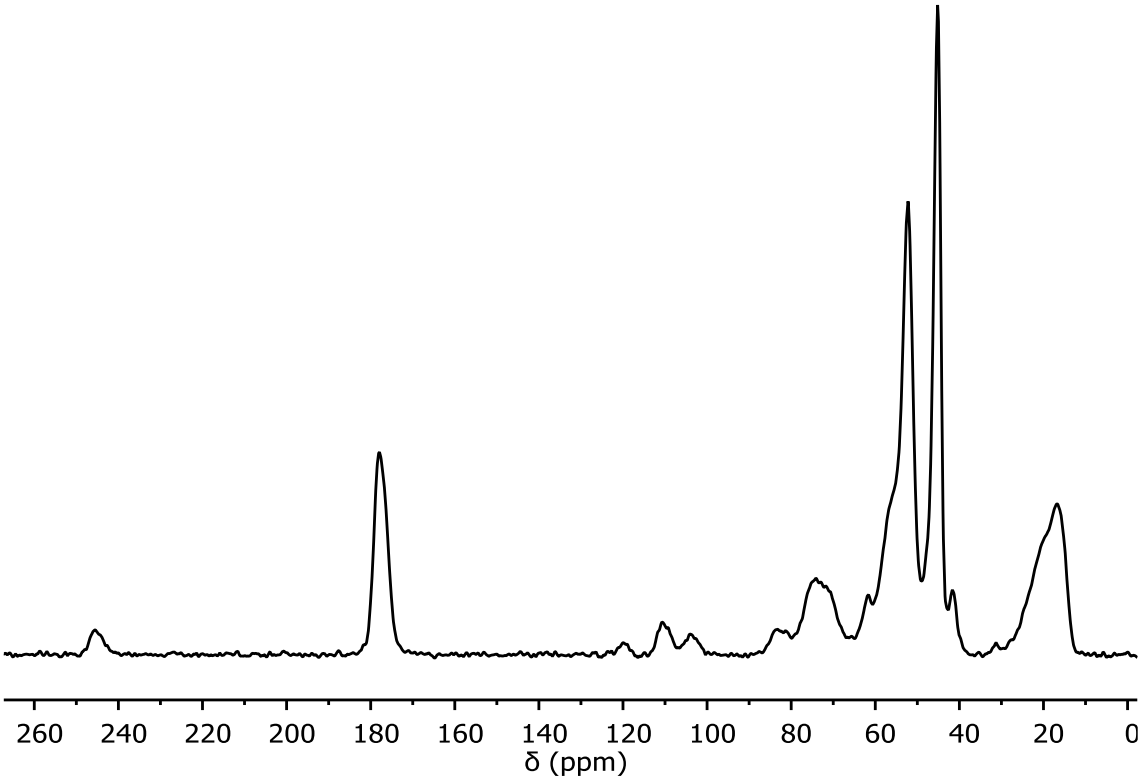


**Appendix 5:** Model of the evolution of $DP_{NVP}$ as a function of %N

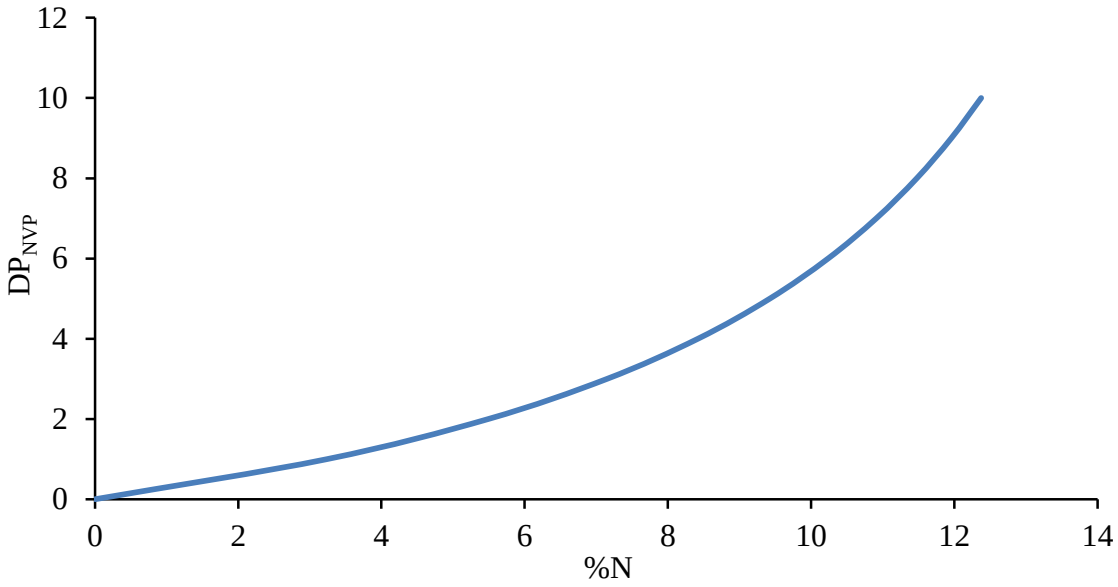

# References


1. J. M. G. Cowie and V. Arrighi, *Polymers : Chemistry and Physics of Modern Materials*, CRC Press, 2008.

2. J. Qiu, B. Charleux and K. Matyjaszewski, *Polimery*, 2001, 46, 453-460.

3. K. Matyjaszewski, *Macromolecules*, 2012, 45, 4015-4039.

4. G. Odian, *Principles of Polymerization*, John Wiley & Sons Inc., 2004, 10.1002/047147875X.ch3, 198-349.

5. D. J. Keddie, G. Moad, E. Rizzardo and S. H. Thang, *Macromolecules*, 2012, 45, 5321-5342.

6. D. J. Keddie, *Chem. Soc. Rev.*, 2014, 43, 496-505.

7. S. Dumitriu, *Polysaccharides: Structural Diversity and Functional Versatility*, Marcel Dekker, 2005.

8. D. Klemm, H.-P. Schmauder and T. Heinze, *Biopolymers Online*, Wiley-VCH Verlag GmbH & Co. KGaA, 2005, 10.1002/3527600035.bpol6010.

9. D. R. Nobles and R. M. Brown, *Cellulose*, 2008, 15, 691-701.

10. D. Klemm, *Comprehensive Cellulose Chemistry: Fundamentals and Analytical Methods*, Wiley-VCH, 1998.

11. K. Kamide, *Cellulose and Cellulose Derivatives: Molecular Characterization and Its Applications*, Elsevier, 2005.

12. J.-L. Wertz and J. P. Mercier, *Cellulose Science and Technology*, EPFL Press, 2008.

13. A. O'Sullivan, *Cellulose*, 1997, 4, 173-207.

14. D. Plackett, *Biopolymers: New Materials for Sustainable Films and Coatings*, John Wiley & Sons, 2011.

15. S. Kamel, N. Ali, K. Jahangir, S. M. Shah and A. A. El-Gendy, *Express Polym. Lett.*, 2008, 2, 758-778.

16. H. Pereira, *Cork: Biology, Production and Uses*, Elsevier, 2007.

17. R. Myers, *The Basics of Chemistry*, Greenwood Press, 2003.

18. T. Heinze, H. Barsett and A. Ebringerová, *Polysaccharides I: Structure, Characterisation and Use*, Springer, 2005.

19. D. Roy, M. Semsarilar, J. T. Guthrie and S. Perrier, *Chem. Soc. Rev.*, 2009, 38, 2046-2064.

20. A. W. T. King, J. Jalomäki, M. Granström, D. S. Argyropoulos, S. Heikkinen and I. Kilpeläinen, *Anal. Methods*, 2010, 2, 1499-1505.

21. F. F. L. Ho, R. R. Kohler and G. A. Ward, *Anal. Chem.*, 1972, 44, 178-181.

22. C. Vaca-Garcia, M. E. Borredon and A. Gaseta, *Cellulose*, 2001, 8, 225-231.

23. A. Reza Fareghi, P. Najafi Moghaddam, A. Akbar Entezami and M. Ensafi Avval, *Iran. Polym. J.*, 2013, 22, 361-367.

24. A. Carlmark and E. Malmström, *J. Am. Chem. Soc.*, 2002, 124, 900-901.

25. P.-S. Liu, Q. Chen, S.-S. Wu, J. Shen and S.-C. Lin, *J. Membr. Sci.*, 2010, 350, 387-394.

26. N. Singh, Z. Chen, N. Tomer, S. R. Wickramasinghe, N. Soice and S. M. Husson, *J. Membr. Sci.*, 2008, 311, 225-234.

27. G. Morandi, L. Heath and W. Thielemans, *Langmuir*, 2009, 25, 8280-8286.

28. J. Majoinen, A. Walther, J. R. McKee, E. Kontturi, V. Aseyev, J. M. Malho, J. Ruokolainen and O. Ikkala, *Biomacromolecules*, 2011, 12, 2997-3006.

29. C. Olsson and G. Westman, *Cellulose - Fundamental Aspects*, InTech, 2013, 10.5772/2705

30. G. F. Stewart, *Advances in Food Research*, Academic Press, 1963.

31. A. A. Tracton, *Coatings Materials and Surface Coatings*, CRC Press, 2006.

32. C. G. Wilson and P. J. Crowley, *Controlled Release in Oral Drug Delivery*, Springer, 2011.

33. A. Bhattacharya and B. N. Misra, *Prog. Polym. Sci.*, 2004, 29, 767-814.

34. M. B. K. Horie , R. B. Fox, J. He, M. Hess, J. Kahovec, T. Kitayama, P. Kubisa, E. Maréchal, W. Mormann, R. F. T. Stepto, D. Tabak, J. Vohlídal, E. S. Wilks and W. J. Work, *Pure Appl. Chem.*, 2004, 76, 889-906.

35. E. M. Flefel, M. M. Ibrahim, W. K. El-Zawawy and A. M. Ali, *Polym. Adv. Technol.*, 2002, 13, 541-547.

36. M. Yigitoglu, N. Isiklan and R. Ozmen, *J. Appl. Polym. Sci.*, 2007, 104, 936-943.

37. M. M. Ibrahim, E. M. Flefel and W. K. El-Zawawy, *Polym. Adv. Technol.*, 2002, 13, 548-557.

38. G. S. Chauhan, B. Singh and S. Kumar, *J. Appl. Polym. Sci.*, 2005, 98, 373-382.

39. E. Takács, H. Mirzadeh, L. Wojnárovits, J. Borsa, M. Mirzataheri and N. Benke, *Nucl. Instrum. Methods Phys. Res., Sect. B*, 2007, 265, 217-220.

40. N. Inagaki and K. Katsuura, *J. Polym. Sci., Part A: Polym. Chem.*, 1980, 18, 441-448.

41. J.-S. Wang and K. Matyjaszewski, *J. Am. Chem. Soc.*, 1995, 117, 5614-5615.

42. J.-S. Wang and K. Matyjaszewski, *Macromolecules*, 1995, 28, 7901-7910.

43. M. Semsarilar, V. Ladmiral and S. Perrier, *J. Polym. Sci., Part A: Polym. Chem.*, 2010, 48, 4361-4365.

44. J. Chiefari, Y. K. Chong, F. Ercole, J. Krstina, J. Jeffery, T. P. T. Le, R. T. A. Mayadunne, G. F. Meijs, C. L. Moad, G. Moad, E. Rizzardo and S. H. Thang, *Macromolecules*, 1998, 31, 5559-5562.

45. A. Postma, T. P. Davis, G. Moad and M. S. O'Shea, *Macromolecules*, 2005, 38, 5371-5374.

46. H. Willcock and R. K. O'Reilly, *Polym. Chem.*, 2010, 1, 149-157.

47. G.-L. Zhao, J. Hafren, L. Deiana and A. Cordova, *Macromol. Rapid Commun.*, 2010, 31, 740-744.

48. A. S. Goldmann, T. Tischer, L. Barner, M. Bruns and C. Barner-Kowollik, *Biomacromolecules*, 2011, 12, 1137-1145.

49. T. Tischer, A. S. Goldmann, K. Linkert, V. Trouillet, H. G. Boerner and C. Barner-Kowollik, *Adv. Funct. Mater.*, 2012, 22, 3853-3864.

50. G. J. Chen, L. Tao, G. Mantovani, V. Ladmiral, D. P. Burt, J. V. Macpherson and D. M. Haddleton, *Soft Matter*, 2007, 3, 732-739.

51. I. Filpponen, E. Kontturi, S. Nummelin, H. Rosilo, E. Kolehmainen, O. Ikkala and J. Laine, *Biomacromolecules*, 2012, 13, 736-742.

52. M. Krouit, J. Bras and M. N. Belgacem, *Eur. Polym. J.*, 2008, 44, 4074-4081.

53. S. Hansson, V. Trouillet, T. Tischer, A. S. Goldmann, A. Carlmark, C. Barner-Kowollik and E. Malmström, *Biomacromolecules*, 2013, 14, 64-74.

54. C. Xiao and C. Xia, *Int. J. Biol. Macromol.*, 2013, 52, 349-352.

55. F. Haaf, A. Sanner and F. Straub, *Polym. J.*, 1985, 17, 143-152.

56. Schur H.B. , 2007, *Non-Irritating Formulation and Method for the Intradermal Delivery of Substances*, United States, 20070092571.

57. ISP Investments Inc. (Wilmington, DE), 1993, *Pharmaceutical Tablet with Pvp Having Enhanced Drug Dissolution Rate*, United States, 5262171.

58. BEIERSDORF AG (Unnastrasse 48, Hamburg, DE), 2007, *Care System Constituted of PVP and Acrylate Polymers*, United States, 20070212320.

59. Societe L'Oréal S.A. (Paris, FR), 2002, *Enhanced Spf Sunscreen (Sprayable) Formulations Comprising Interpolymers of PVP/Dimethiconylacrylate/Polycarbamyl/Polyglycol Ester*, United States, 6436377.

60. J. N. Moss, R. Brendel, J. M. Beiler and G. J. Martin, *Am. J. Pharm.*, 1952, 124, 94-97.

61. IND BIOLOGY LAB INC, 1965, *Water-Insoluble Polyvinylpyrrolidone Composition*, United States, 3216579.

62. K. Hayashi, N. Morooka, Y. Yamamoto, K. Fujita, K. Isono, S. Choi, E. Ohtsubo, T. Baba, B. L. Wanner, H. Mori and T. Horiuchi, *Mol. Syst. Biol.*, 2006, 10.1038/msb4100049.

63. F. I. Rosenbach, *Mikroorganismen Bei Den Wund-Infections- Krankheiten Des Menschen*, J. F. Bergmann, 1884.

64. T. J. Wood, G. A. Hurst, W. C. E. Schofield, R. L. Thompson, G. Oswald, J. S. O. Evans, G. J. Sharples, C. Pearson, M. C. Petty and J. P. S. Badyal, *Journal of Materials Chemistry*, 2012, 22, 3859-3867.

65. GAF Corporation (New York, NY), 1979, *Herbicidal N-(Haloacetyl)-N-(N'-Methylenepyrrolidonyl)-2-Alkoxyanilines Useful as Herbicides*, United States, 4178167.

66. GAF CORP, 1969, *Modification of Textile Material with Methylolated Lactams*, United States, 3486838.

67. Q. Zhou, L. N. Zhang, M. Li, X. J. Wu and G. Z. Cheng, *Polym. Bull.*, 2005, 53, 243-248.

68. J. R. DeMember, L. D. Taylor, S. Trummer, L. E. Rubin and C. K. Chiklis, *J. Appl. Polym. Sci.*, 1977, 21, 621-627.

69. E. H. Cordes and H. G. Bull, *Chem. Rev.*, 1974, 74, 581-603.

70. E. Hartwell, D. R. W. Hodgson and A. J. Kirby, *J. Am. Chem. Soc.*, 2000, 122, 9326-9327.

71. http://logkow.cisti.nrc.ca/logkow/display?OID=1077, Accessed 28/08/13, 2013.

72. A. Sannino, C. Demitri and M. Madaghiele, *Materials*, 2009, 2, 353-373.

73. S. Yang, S. Fu, X. Li, Y. Zhou and H. Zhan, *BioResources*, 2010, 5, 1114-1125.

74. D. Campoccia, L. Montanaro and C. R. Arciola, *Biomaterials*, 2006, 27, 2331-2339.

75. G. Cheng, Z. Zhang, S. Chen, J. D. Bryers and S. Jiang, *Biomaterials*, 2007, 28, 4192-4199.

76. C. Sousa, P. Teixeira and R. Oliveira, *Int. J. Biomater.*, 2009, Article ID 718017, 9 pages.

77. Y. H. An and R. J. Friedman, *J. Biomed. Mater. Res.*, 1998, 43, 338-348.

78. T. J. Silhavy, D. Kahne and S. Walker, *Cold Spring Harbor Perspect. Biol.*, 2010, 10.1101/cshperspect.a000414.

79. F. Joubert, O. M. Musa, D. R. W. Hodgson and N. R. Cameron, *Chem. Soc. Rev.*, 2014, 43, 7217-7235.

80. L. Chun-xiang, Z. Huai-yu, L. Ming-hua, F. Shi-yu and Z. Jia-jun, *Carbohydr. Polym.*, 2009, 78, 432-438.

81. E. Östmark, S. Harrisson, K. L. Wooley and E. E. Malmström, *Biomacromolecules*, 2007, 8, 1138-1148.

82. D. Shen, H. Yu and Y. Huang, *J. Polym. Sci., Part A: Polym. Chem.*, 2005, 43, 4099-4108.

83. S. Ifuku and J. F. Kadla, *Biomacromolecules*, 2008, 9, 3308-3313.

84. G. Cui, Y. Li, T. Shi, Z. Gao, N. Qiu, T. Satoh, T. Kakuchi and Q. Duan, *Carbohydr. Polym.*, 2013, 94, 77-81.

85. F. J. Xu, Y. Zhu, F. S. Liu, J. Nie, J. Ma and W. T. Yang, *Bioconjugate Chem.*, 2010, 21, 456-464.

86. D. Shen, H. Yu and Y. Huang, *Cellulose*, 2006, 13, 235-244.

87. P. Vlček, M. Janata, P. Látalová, J. Kríž, E. Čadová and L. Toman, *Polymer*, 2006, 47, 2587-2595.

88. Z. Q. Wu, H. Chen, X. L. Liu, Y. X. Zhang, D. Li and H. Huang, *Langmuir*, 2009, 25, 2900-2906.

89. X. L. Liu, K. Sun, Z. Q. Wu, J. H. Lu, B. Song, W. F. Tong, X. J. Shi and H. Chen, *Langmuir*, 2012, 28, 9451-9459.

90. X. Lu, S. Gong, L. Meng, C. Li, S. Yang and L. Zhang, *Polymer*, 2007, 48, 2835-2842.

91. V. Mishra and R. Kumar, *Carbohydr. Polym.*, 2011, 83, 1534-1540.

92. N. A. Hoenich, *BioResources*, 2007, 1, 270-280.

93. W. K. Czaja, D. J. Young, M. Kawecki and R. M. Brown, *Biomacromolecules*, 2006, 8, 1-12.

94. T. Tashiro, *Macromol. Mater. Eng.*, 2001, 286, 63-87.

95. A. Muñoz-Bonilla and M. Fernández-García, *Prog. Polym. Sci.*, 2012, 37, 281-339.

96. B. F. Gilmore, G. P. Andrews, G. Borberly, M. J. Earle, M. A. Gilea, S. P. Gorman, A. F. Lowry, M. McLaughlin and K. R. Seddon, *New J. Chem.*, 2013, 37, 873-876.

97. D. Demberelnyamba, K.-S. Kim, S. Choi, S.-Y. Park, H. Lee, C.-J. Kim and I.-D. Yoo, *Bioorg. Med. Chem.*, 2004, 12, 853-857.

98. M. R. Cole, M. Li, B. El-Zahab, M. E. Janes, D. Hayes and I. M. Warner, *Chem. Biol. Drug Des.*, 2011, 78, 33-41.

99. J. Yuan and M. Antonietti, *Polymer*, 2011, 52, 1469-1482.

100. S. Ding, H. Tang, M. Radosz and Y. Shen, *J. Polym. Sci., Part A: Polym. Chem.*, 2004, 42, 5794-5801.

101. H. He, M. Zhong, D. Luebke, H. Nulwala and K. Matyjaszewski, *J. Polym. Sci., Part A: Polym. Chem.*, 2014, 52, 2175-2184.

102. X. Ma, M. Ashaduzzaman, M. Kunitake, R. Crombez, J. Texter, L. Slater and T. Mourey, *Langmuir*, 2011, 27, 7148-7157.

103. H. Mori, M. Yahagi and T. Endo, *Macromolecules*, 2009, 42, 8082-8092.

104. K. Vijayakrishna, S. K. Jewrajka, A. Ruiz, R. Marcilla, J. A. Pomposo, D. Mecerreyes, D. Taton and Y. Gnanou, *Macromolecules*, 2008, 41, 6299-6308.

105. M. J. Leamen, N. T. McManus and A. Penlidis, *J. Appl. Polym. Sci.*, 2004, 94, 2545-2547.

106. V. Raus, M. Stepanek, M. Uchman, M. Slouf, P. Latalova, E. Cadova, M. Netopilik, J. Kriz, J. Dybal and P. Vlcek, *J. Polym. Sci., Part A: Polym. Chem.*, 2011, 49, 4353-4367.

107. L. Dupayage, M. Save, E. Dellacherie, C. Nouvel and J.-L. Six, *J. Polym. Sci., Part A: Polym. Chem.*, 2008, 46, 7606-7620.

108. A. Limer and D. M. Haddleton, *Macromolecules*, 2006, 39, 1353-1358.

109. M. Teodorescu and K. Matyjaszewski, *Macromol. Rapid Commun.*, 2000, 21, 190-194.

110. D. Neugebauer and K. Matyjaszewski, *Macromolecules*, 2003, 36, 2598-2603.

111. J. Harmand, M. Rogalski, M. Sindt and J.-L. Mieloszynski, *Environ. Chem. Lett.*, 2009, 7, 255-260.

112. W. Yuan, J. Zhang, H. Zou, T. Shen and J. Ren, *Polymer*, 2012, 53, 956-966.

113. V. Mishra and R. Kumar, *J. Appl. Polym. Sci.*, 2012, 124, 4475-4485.

114. G. Pound-Lana and B. Klumperman, *Controlled/Living Radical Polymerization: Progress in RAFT, DT, NMP & OMRP*, American Chemical Society, 2009, 1024, 167-179.

115. D. C. Wan, K. Satoh, M. Kamigaito and Y. Okamoto, *Macromolecules*, 2005, 38, 10397-10405.

116. R. Devasia, R. L. Bindu, R. Borsali, N. Mougin and Y. Gnanou, *Macromol. Symp.*, 2005, 229, 8-17.

117. V. K. Patel, A. K. Mishra, N. K. Vishwakarma, C. S. Biswas and B. Ray, *Polym. Bull.*, 2010, 65, 97-110.

118. U. Mansfeld, C. Pietsch, R. Hoogenboom, C. R. Becer and U. S. Schubert, *Polym. Chem.*, 2010, 1, 1560-1598.

119. N. Akeroyd, R. Pfukwa and B. Klumperman, *Macromolecules*, 2009, 42, 3014-3018.

120. R. Ranjan and W. J. Brittain, *Macromol. Rapid Commun.*, 2008, 29, 1104-1110.

121. R. Ranjan and W. J. Brittain, *Macromol. Rapid Commun.*, 2007, 28, 2084-2089.

122. A. J. D. Magenau, N. Martinez-Castro, D. A. Savin and R. F. Storey, *Macromolecules*, 2009, 42, 8044-8051.

123. T. Zhang, Y. Wu, X. Pan, Z. Zheng, X. Ding and Y. Peng, *Eur. Polym. J.*, 2009, 45, 1625-1633.

124. V. K. Patel, N. K. Vishwakarma, A. K. Mishra, C. S. Biswas, P. Maiti and B. Ray, *J. Appl. Polym. Sci.*, 2013, 127, 4305-4317.

125. G.-Y. Shi, X.-Z. Tang and C.-Y. Pan, *J. Polym. Sci., Part A: Polym. Chem.*, 2008, 46, 2390-2401.

126. J. Chen, M. Liu, C. Chen, H. Gong and C. Gao, *ACS Appl. Mater. Interfaces*, 2011, 3, 3215-3223.

127. X. Liu, X. Feng, J. Chen and Y. Cao, *J. Macromol. Sci., Part A: Pure Appl.Chem.*, 2012, 50, 65-71.

128. J. M. Andrews, *J. Antimicrob. Chemother.*, 2001, 48, 5-16.

129. M. Lieber, B. Smith, A. Szakal, W. Nelsonrees and G. Todaro, *Int. J. Cancer*, 1976, 17, 62-70.

130. B.R.A.H.M.S. Diagnostica GmbH (Berlin, DE) 1993, *Immunological Test for the Presence of Antibodies in Biological Fluids* United States, 5501955.

131. A. M. Eissa, E. Khosravi and A. L. Cimecioglu, *Carbohydr. Polym.*, 2012, 90, 859-869.

132. R. N. Butler, J. M. Hanniffy, J. C. Stephens and L. A. Burke, *J. Org. Chem.*, 2008, 73, 1354-1364.

133. M. Corredor, J. Bujons, A. Messeguer and I. Alfonso, *Org. Biomol. Chem.*, 2013, 11, 7318-7325.

134. V. V. Rostovtsev, L. G. Green, V. V. Fokin and K. B. Sharpless, *Angew. Chem., Int. Ed.*, 2002, 41, 2596-2599.

135. D. C. Apperley, R. K. Harris and P. Hodgkinson, *Solid State NMR: Basic Principles & Practice*, Momentum Press, 2012.

136. A. Lyčka, R. Doleček, P. Šimûnek and V. Macháček, *Magn. Reson. Chem.*, 2006, 44, 521-523.

137. G. Lu, D. Wu and R. Fu, *React. Funct. Polym.*, 2007, 67, 355-366.

138. D. Fischer, Y. Li, B. Ahlemeyer, J. Krieglstein and T. Kissel, *Biomaterials*, 2003, 24, 1121-1131.